Technische Universität München
TUM School of Computation, Information and Technology

Biosensor-Based Multimodal Intent Detection for Wearable Myocontrol

Mathilde Connan

Vollständiger Abdruck der von der TUM School of Computation, Information and Technology der Technischen Universität München zur Erlangung des akademischen Grades einer

Doktorin der Ingenieurwissenschaften (Dr.-Ing.)

genehmigten Dissertation.

Vorsitz:

Prof. Dr. Cristina Piazza

Prüfer*innen der Dissertation:

1. Prof. Dr.-Ing. Alin Albu-Schäffer
2. Prof. Claudio Castellini, Ph.D.,
   Friedrich-Alexander-Universität (FAU)
3. Prof. Dr. Carlo Menon,
   Eidgenössische Technische Hochschule Zürich (ETHZ)

Die Dissertation wurde am 23.02.2023 bei der Technischen Universität München eingereicht und durch die TUM School of Computation, Information and Technology am 16.07.2023 angenommen.

Abstract

The anatomy of the human hand is incredibly complex. With 27 bones and 33 muscles, it provides a total of 22 degrees of freedom. Scientists, therapists, and engineers have been trying for decades to comprehend and artificially reproduce the versatility of the human hand. This is all the more critical when losing hand functionality following a trauma such as an amputation. From browsing through the pages of a book to simply waving at someone, hand function is essential in activities of daily living or social communication.

For the purpose of intent detection, body signals need to be acquired via sensors. In the case of hand amputation, electromyography is the standard non-invasive method to acquire muscular information. However, one of the major drawbacks of these sensors is the variability of their signals. Indeed, they are significantly influenced by sweat, muscular fatigue, electrode cross-talk, or electrode shift, among others. As a result, simultaneous and proportional control of multiple degrees of freedom is still unreliable and laborious. According to the research community, one of the keys to improving the situation is multimodal sensing. It consists in using different sensor modalities to interpret the user's intent and therefore enhance the reliability and functionality of the control in daily-living activities.

This thesis presents alternative and complementary methods to the standard electromyography, such as: both low and high- density force myography, ultrasound, electroimpedance tomography, and inertial tracking. These modalities are evaluated individually, concurrently, and jointly for myocontrol. The main contribution of this thesis is to identify viable myocontrol modalities, which could contribute to advancing intent detection. This was accomplished by performing user studies, recording sensor data while participants executed different gestures, or while involving them in target achievement tests. Offline and online data could therefore be analyzed to compare modalities, features, and machine learning methods. This thesis also introduces different fusions of modalities, including a fusion of surface and deep recording methods, which resulted in a promising approach for improving muscular intent detection.

Zusammenfassung

Die Anatomie der menschlichen Hand ist ungeheuer komplex. Mit 27 Knochen und 33 Muskeln verfügt sie über insgesamt 22 Freiheitsgrade. Wissenschaftler, Therapeuten und Ingenieure versuchen seit Jahrzehnten, die Vielseitigkeit der menschlichen Hand zu verstehen und künstlich zu reproduzieren. Dies ist umso wichtiger, wenn wir nach einem Trauma, z. B. einer Amputation, die Funktion der Hand verlieren. Ob man in einem Buch blättert oder jemandem einfach nur zuwinkt, die Handfunktion ist für die Aktivitäten des täglichen Lebens und die soziale Kommunikation unerlässlich.

Für die Absichtserkennung müssen Körpersignale über Sensoren erfasst werden. Im Falle einer Handamputation ist die Elektromyografie die nicht-invasive Standardmethode zur Erfassung von Muskelinformationen. Einer der Hauptnachteile dieser Sensoren ist jedoch die Variabilität ihrer Signale. Sie werden u. a. durch Schweiß, Muskelermüdung, Elektrodenübersprechen oder Elektrodenverschiebung erheblich beeinflusst. Infolgedessen ist die gleichzeitige und proportionale Steuerung mehrerer Freiheitsgrade nach wie vor unzuverlässig und mühsam. Nach Ansicht der Forscher ist einer der Schlüssel zur Verbesserung der Situation die multimodale Sensorik. Sie besteht darin, verschiedene Sensormodalitäten zu verwenden, um die Absicht des Benutzers zu interpretieren und somit die Zuverlässigkeit und Funktionalität der Steuerung bei Aktivitäten des täglichen Lebens zu verbessern.

In dieser Arbeit werden alternative und ergänzende Methoden zur Standard Elektromyografie vorgestellt, wie z. B.: Kraftmyografie mit niedriger und hoher Dichte, Ultraschall, Elektroimpedanztomografie und Inertialtracking. Diese Modalitäten werden einzeln, gleichzeitig und gemeinsam für die Myokontrolle bewertet. Der Hauptbeitrag dieser Arbeit besteht darin, praktikable Myokontrollmodalitäten zu identifizieren, die zur Verbesserung der Absichtserkennung beitragen könnten. Dies wurde durch die Durchführung von Nutzerstudien erreicht, bei denen Sensordaten aufgezeichnet wurden, während die Teilnehmer verschiedene Gesten ausführten, oder während sie an Tests zur Zielerreichung teilnahmen. Offline- und Online-Daten konnten so analysiert werden, um Modalitäten, Merkmale und maschinelle Lernmethoden zu vergleichen. In dieser Arbeit werden auch verschiedene Ansätze zur Fusion von Modalitäten vorgestellt, darunter eine Fusion von Oberflächen- und Tiefenaufzeichnungsmethoden, die zu einem vielversprechenden Ansatz zur Verbesserung der Erkennung von Muskelabsichten führte.

Acknowledgments

First and foremost, I would like to thank all the people who supported me in any way: without your help, this work would not have been possible.

This work was performed during my employment at the German Aerospace Center (DLR) - Robotics and Mechatronics Institute and I would like to especially thank Prof. Dr. Alin Albu-Schäffer, the director of this institute and my supervisor, for his advice and support and who provided the best research environment possible. Furthermore, I am extremely grateful to my work supervisor Prof. Claudio Castellini, who offered me the possibility to work in his group, for his guidance, advice and constant positive motivation throughout the years, and without whom this dissertation simply could not have been. I would also like to thank my head of department, Dr. Freek Stulp, who offered me the opportunity to work in his department in the first place and provided me with his support and helpful advice.
I want to thank everyone from the electronics lab, the IT team, the mechanical lab, and the tech lab, without all of whom building the different prototypes and designing experiments would not have been possible and whom it was always a pleasure to meet and discuss with. As well, many thanks to all the co-authors of my publications and the participants in my studies, without whom this thesis would not be. I would also like to extend my gratitude to Prof. Dr. Carlo Menon for accepting to join my dissertation committee, as well as to Prof. Dr. Cristina Piazza for accepting to be the Chair of this committee.

I am grateful for the advice of those who proofread (entirely or parts of) my dissertation: Alin Albu-Schäffer, Claudio Castellini, Bernhard Vodermayer, Andrea Gigli, Markus Nowak, Freek Stulp, and Charles Bernier.

I would like to thank my friends and colleagues of the Adaptive Bio-Interface group, with whom I had the pleasure of working. Especially, I deeply thank Markus Nowak, Andrea Gigli, Christian Nissler, and Konrad Fründ. It has been amazing to work with you and we have made memories that I will cherish. I am very grateful for all of your invaluable help, constructive advice, our discussions, and the fun we have had working together. Without your support, this work would not have been possible either.
Special thanks also go to my friends and officemates Bernhard, Cynthia and Annette. Thanks to you, it is always a pleasure to come to the office (or meet outside), chat and share. I really enjoyed the fruitful discussions with Bernhard, who was my internship's co-supervisor and became a good friend, who has always provided me with great advice and guidance ever since then.

I also want to thank my friends, colleagues, and former colleagues whom I have not yet mentioned: Ribin, Korbi, Thomas, the french crew Antonin and Gabriel, Severin, Seba, Katharina, Karan, and Tanja. As well, our "Girls office" where it all started: Bea, Annette, Carla, later on joined by Imran, Tamara, and Marius. You all made DLR an even nicer place to work at.

To all my friends, whether you were in Brittany, France, Germany, Canada, Italy, Spain, or Morocco, without you, your support, your laugh, your advice, and your fun, this would not have been possible. A proverb says: "Know your roots to know where you are going". Although everyone who knows me knows that Brittany is a rather large root, I want to say that each of you is also part of these roots that gave me the courage and strength to follow my goals (dare I say dreams?) even across the globe.

Most importantly, and the biggest part of these roots, I want to express my deepest gratitude to my family. I am and will be forever immensely grateful to my parents for their endless support and love in every aspect of life, to my sisters Anne and Elodie for always believing in me, and to my grandparents simply for having always been there for me.
Finally, my deepest gratitude goes to my beloved Charles, who crossed an ocean to join me on this adventure. Without his love, patience, support, and laughs, this work would never have been completed.

Munich, February 2023

Mathilde Connan

Publication List

Core publications

The contributions of this cumulative dissertation are based on the following publications, which can be found in Appendix A:

Peer-reviewed Journal Articles

[1] M. Connan, E. R. Ramírez, B. Vodermayer, and C. Castellini, "Assessment of a wearable force- and electromyography device and comparison of the related signals for myocontrol," *Frontiers in Neurorobotics*, vol. 10, no. 17, pp. 1–13, nov 2016, doi: 10.3389/fnbot.2016.00017. A.1

[2] M. Connan, R. Kõiva, and C. Castellini, "Online natural myocontrol of combined hand and wrist actions using tactile myography and the biomechanics of grasping," *Frontiers in Neurorobotics*, vol. 14, no. 11, pp. 1–16, feb 2020, doi: 10.3389/fnbot.2020.00011. A.2

[3] M. Connan, M. Sierotowicz, B. Henze, O. Porges, A. Albu-Schäffer, M. A. Roa, and C. Castellini, "Learning to teleoperate an upper-limb assistive humanoid robot for bimanual daily-living tasks," *Biomedical Physics & Engineering Express*, vol. 8, no. 1, pp. 1–17, dec 2021, doi: 10.1088/2057-1976/ac3881. A.4

Peer-reviewed Conference Publications

[4] M. Connan, B. Yu, C. Gibas, R. Brück, E. A. Kirchner, and C. Castellini, "Deep and surface sensor modalities for myo-intent detection," in *Proceedings of MEC - Myoelectric Control Symposium*, 2022. A.3

Further related co-contributed publications

Additional co-contributed articles were published in relation with this thesis. Their abstracts can be found in Appendix B.

Peer-reviewed Journal articles

[5] N. Jaquier, M. Connan, C. Castellini, and S. Calinon, "Combining electromyography and tactile myography to improve hand and wrist activity detection in prostheses," *Technologies*, vol. 5, no. 4, pp. 1–16, oct 2017, doi: 10.3390/technologies5040064. B.2

[6] C. Nissler, M. Nowak, M. Connan, S. Büttner, J. Vogel, I. Kossyk, Z.-C. Márton, and C. Castellini, "VITA—An everyday virtual reality setup for prosthetics and upper-limb rehabilitation," *Journal of Neural Engineering*, vol. 16, no. 2, p. 026039, mar 2019, doi: 10.1088/1741-2552/aaf35f. B.4

[7] M. Sierotowicz, M. Connan, and C. Castellini, "Human-in-the-loop assessment of an ultralight, low-cost body posture tracking device," *Sensors*, vol. 20, no. 3, p. 890, feb 2020, doi: 10.3390/s20030890. B.5

[8] M. Sierotowicz, D. Brusamento, B. Schirrmeister, M. Connan, J. Bornmann, J. Gonzalez-Vargas, and C. Castellini, "Unobtrusive, natural support control of an adaptive industrial exoskeleton using force-myography," *Frontiers in Robotics and AI*, vol. 9, p. 223, sep 2022, doi: 10.3389/frobt.2022.919370. B.7

Peer-reviewed Conference Publications

[9] C. Nissler, M. Connan, M. Nowak, and C. Castellini, "Online tactile myography for simultaneous and proportional hand and wrist myocontrol," in *MEC2017 - Myoelectric Control Symposium*, 2017 B.1

[10] O. Porges, M. Connan, B. Henze, A. Gigli, C. Castellini, and M. A. Roa, "A wearable, ultralight interface for bimanual teleoperation of a compliant, whole-body-controlled humanoid robot," in *Proceedings of ICRA-International Conference on Robotics and Automation*, vol. 35, no. 12, p. 2289, 2019. URL `www.youtube.com/watch?v=YLEUBFu5qgI`. B.3

[11] B. W. Hallworth, A. W. Shehata, M. R. Dawson, F. Sperle, M. Connan, W. Friedl, B. Vodermayer, C. Castellini, J. S. Hebert, and P. M. Pilarski, "A transradial modular adaptable platform for evaluating prosthetic feedback and control strategies," in *MEC-Myoelectric Control Symposium*, pp. 1–4, 2020. B.6

[12] M. Connan, M. Sierotowicz, B. Henze, O. Porges, A. Albu-Schäffer, M. A. Roa, and C. Castellini, "Learning teleoperation of an assistive humanoid platform by intact and upper-limb disabled users," in *Converging Clinical and Engineering Research on Neurorehabilitation IV. ICNR 2020. Biosystems & Biorobotics*, vol. 28, pp. 165–169, Springer. Springer International Publishing, oct 2020, doi: 10.1007/978-3-030-70316-5_27. B.8

Patent

[13] D. Brusamento, M. Connan, C. Castellini, B. Schirrmeister, J. Bornmann, and J. González-Vargas, "Verfahren zum Kontrollieren eines Exoskeletts, Exoskelett und Computerprogrammprodukt. DE Patent No 102021116202. Dec. 29, 2022," Patent

Nomenclature

a	Scalar. Scalars are denoted by regular characters, such as a, α, β.
$\mathbf{a}$	Vector, e.g. $\mathbf{a} \in \mathbb{R}^n$. Vectors are denoted by bold lower case characters, such as $\mathbf{a}$, $\boldsymbol{\beta}$.
$\boldsymbol{A}$	Matrix, e.g. $\boldsymbol{A} \in \mathbb{R}^{m \times n}$. Matrices are denoted by bold italic upper case characters, such as $\boldsymbol{A}$, $\boldsymbol{\Phi}$.
$\mathbb{R}$	Real numbers.
$\mathbb{N}$	Natural numbers.
$\mathbb{R}^n$	n-dimensional Euclidian space.
$\|\|.\|\|$	Euclidian norm.
$^\mathsf{T}$	denotes the transpose of a matrix or vector.
$\mathcal{O}$	asymptotic upper complexity bound.

Contents

List of Figures

List of Tables

Acronyms

ADC	Analog to Digital Converter
ADLs	Activities of Daily Living
BLE	Bluetooth Low Energy
BSN	Body Sensor Network
ca.	Circa (*Latin.* approximately)
cf.	Confer (*Latin.* compare)
CNN	Convolutional Neural Network
CT	X-ray Computed Tomography
DAC	Digital to Analog Converter
DLR	Deutsches Zentrum für Luft- und Raumfahrt (*German.* German Aerospace Center)
DoF	Degree of Freedom
e.g.	Exempli gratia (*Latin.* for example)
EIM	Electro Impedance Myography
EIT	Electro Impedance Tomography
EMG	Electromyography
FFT	Fast Fourier Transform
FMG	Force Myography
FSR	Force Sensitive Resistor
GPR	Gaussian Process Regression
HD-sEMG	High-Density surface Electromyography
HD-FMG	High-Density Force Myography
HMI	Human Machine Interface
i.e.	Id est (*Latin.* that is)
I2C	Inter-Integrated Circuit
IMU	Inertial Measurement Unit
KRR	Kernel Ridge Regression

LMER	Linear Mixed-Effects Regression
MAPP	Modular-Adaptable Prosthetic Platform
MAV	Mean Absolute Value
MDT	Microsoft Desirability Toolkit
MKL	Multiple Kernel Learning
MMG	Mechanomyography
MRI	Magnetic Resonance Imaging
MUAP	Motor Unit Action Potential
MVC	Maximum Voluntary Contraction
N.B.	Nota bene (*Latin.* note well)
NIDAQ	National Instruments Data Acquisition
NIRS	Near InfraRed Spectroscopy
nRMSE	normalized Root Mean Square Error
PCA	Principal Component Analysis
PPG	Photoplethysmography
px	pixels
RBF	Radial Basis Function
RFF	Random Fourier Features
RMS	Root Mean Square
ROI	Region Of Interest
ROIG	Region Of Interest Gradient
RQ	Research Question
RR	Ridge Regression
RR-ROIG	Ridge Regression with Region Of Interest Gradient
RR-RFF	Ridge Regression with Random Fourier Features
RTLX	Raw Task Load Index
sEMG	surface Electromyography
SI	Separateness Index
SPC	Simultaneous and Proportional Control
SPP	Serial Port Profile
SQUID	Superconducting Quantum Interference Device
SR	Success Rate
SUS	System Usability Scale
SVM	Support Vector Machine
TAC	Target Achievement Control
TCP	Transmission Control Protocol

TCT	Task Completion Time
TIT	Time In Task
TLX	Task Load Index
TMG	Tactile Myography, i.e. HD-FMG
TMR	Targeted Muscle Reinervation
TORO	TOrque-controlled humanoid RObot
UART	Universal Asynchronous Receiver/Transmitter
US	Ultrasound
VR	Virtual Reality

Chapter 1

Introduction

People ignore designs that ignore people.

(Frank Chimero)

Table of Contents

1.1 Motivation

The world around us has been designed in our image. Every object to grasp, every action to undertake often require functioning bimanual dexterity. People suffering from hand amputation are usually strongly impaired in their everyday life, and even the most straightforward task of opening a bottle becomes a challenge. In order to help them regain some mobility, the **intent** of hand movement, i.e. the action that the person wishes to perform, should be correctly detected and interpreted.

For a long time, limb replacement options were mainly cosmetic or passive prostheses, such as unactuated hooks or iron prostheses [18]. The idea of body-powered upper-limb prostheses appeared for the first time in 1818 with the German dentist Peter Baliff, with shoulder and arm movements operating the hand [18]. Myoelectric control with surface Electromyography (sEMG), on the other hand, gained interest with researchers worldwide in the years beginning ca. 1957 [19] and has been a clinically effective option for about 40 years [20]. However, it was as early as 1948 that Reinhold Reiter, a physics student at the Ludwig Maximilian University of Munich, created the first myoelectric

prosthesis [21]. The technology has considerably evolved in 60 years, starting from a single Degree of Freedom (DoF) prosthesis controlled via one muscle to multi-actuated hand prostheses controlled with several groups of muscles. However, levels of abandonment remain relatively high [22–24], with mean rejection rates of 26% for body-powered and 23% for electric prostheses in adult populations [22], and the numbers do not seem to improve with recent innovations [24] In particular, the main reasons for abandonment remain comfort, weight and function [24, 25]. In the case of myoelectric prostheses, although there is a need for up-to-date research on current devices, the principal causes are non-intuitive control, insufficient functionality, and lack of sufficient feedback [23].

In assistive robotics, the term **myocontrol** refers to the control of a mechatronic system or a virtual one by a person via the activation of muscles or, in case of amputation, remnant muscles. Surface electromyography, measuring electrical activity in the muscles, is the standard for acquiring signals for myocontrol, and it has been used for several decades in prosthetics. While it is enough for controlling a few DoFs as required for lower limb prostheses, it seems insufficient for upper limbs as the control of multi-DoF robotic hands is still unreliable [23]. This unreliability is due to multiple factors, including the fact that sEMG sensors have several drawbacks: sweat, electrode shifts, motion artifacts, muscular fatigue, and cross-talk between deep adjacent muscles are some of the complications hindering the control of hand prostheses by sEMG [26–29]. Several researchers propose multimodality as one of the solutions to improve myocontrol [30–32]. Inspired by multisensory learning, which is the assumption that individuals learn more effectively when taught using several senses, the same principle could be applied to machine learning [33]. The term **multimodality** designates the use of different sensors for a specific purpose, in this case, myocontrol. They can be used independently of one another, i.e. each controlling a different function or DoF, or in a more specific fused approach. The sensors used in this framework are placed on the body and can detect bio-phenomena, such as electrical activity in the case of electromyography. They will be referred to as **bio-sensors**. For each type of bio-sensor, their signals and potential for myocontrol must be evaluated before combining them.

Several methods, such as Computed Tomography (CT) scans or Magnetic Resonance Imaging (MRI), can be used to visualize the inner body and thus potentially identify muscular movements. Despite their high precision, these methods are not wearable and will not be considered here. The focus will be on non-invasive approaches, as they bring many advantages: not only would the user not need a surgical procedure or uncomfortable needles, but the method can be tested on a larger pool of potential users. Such a **non-invasive and wearable** interface could not only be used for prosthetics but also for other purposes such as teleoperation, virtual reality, augmented reality, or any future technology requiring a human-machine interface (HMIs). Accordingly, the preferred approach in this framework would be wearable, non-invasive bio-sensors that can detect muscular intent and may eventually be integrated into prostheses. Intent detection HMIs need to meet several criteria in addition to being wearable, such as data acquisition speed

or spatial resolution. While this thesis will often discuss interfaces in terms of prosthetic applications, if such integration is successful in such a constrained setting, it will be a fortiori successful for more straightforward development of HMIs.

1.2 Problem Statement and Objectives

The main objective of this thesis is to identify sensor modalities for myocontrol and to propose an efficient approach to fuse the different sensor information. From this objective, the following research questions can be derived:

Research Question 1

What sensor modalities are viable alternatives or complements to surface electromyography?

In order to answer this first research question, a list of potential modalities should be selected from the state of the art according to defined inclusion and exclusion criteria. The requirements derived from these criteria need to be identified for selecting modalities. For instance, one important aspect of the sensor modality is that it must be non-invasive. Other requirements, such as wearability/portability or data acquisition speed, will need to be determined.

Building on this research question, another aspect to consider is: **How to compare the modalities?** There are several ways to compare modalities, and sensor placement is an important factor. This involves different topics, including the selection of data acquisition devices that may allow for the integration of co-located sensors to enable a more accurate comparison. Another factor is the experimental design, which can be either within-subjects, where all participants engage in every condition, or between-subjects, where separate groups of participants engage in different conditions. The risk of interference between active and passive sensors is also another parameter to take into account. These different settings will need to be defined for the various comparisons of modalities.

Another important question should be addressed: **How to determine if certain modalities are viable alternatives to sEMG?** To assess this, the modalities should enhance the prediction output of machine learning models, ensuring greater stability and robustness. In order to effectively compare the modalities, it is necessary to establish various evaluation criteria and methodologies for testing them using different metrics, as described in Section 3.4. Some metrics are intended for offline analyses, aiding for instance in the development of new methods. Other metrics would be established expressly for online assessments, which more closely reflect real-life conditions. These comprehensive evaluations will help in understanding the advantages and drawbacks of these modalities compared to sEMG.

Research Question 2

What pipelines are beneficial for the alternative modalities?

In myocontrol, a typical **pipeline** consists in feeding raw or pre-processed sensor data to a machine learning model, which identifies patterns and then generates a prediction (cf. Section 2.3). Each of these steps is important for comparing the modalities. While it was previously established that the assessment and comparison of the different modalities required evaluation metrics, it is also necessary to have comparable **machine-learning** algorithms. Several studies involve classification [23], which provides a sequential output [34]. Regression, on the other hand, allows for independent simultaneous and proportional control (SPC) and is, therefore, the method of choice in this thesis for evaluating the different modalities. Whether to apply linear or non-linear regression will need to be determined: depending on the sensors used and their density, it will be part of this work to assess whether a linear or a non-linear approach is better.

Moreover, for each modality, different **features** can be used. While the features for myocontrol with sEMG are known [35, 36], those of other modalities still need to be evaluated. In particular, for high-density modalities, feature extraction or feature selection algorithms (cf. Section 2.3) might be necessary in order to be able to embed the pipeline on a microcontroller for future prosthesis integration. High dimensional data can be represented as a matrix / image, allowing for additional image feature extraction methods. As some features might introduce non-linearity in the process, these should be carefully chosen if the linear character of the machine learning algorithm is desired.

Another issue with myocontrol is that the output of the model becomes increasingly unstable when more patterns are introduced to the machine-learning process. Having combined actions, such as power grasp and wrist supination, usually requires training on each of the individual actions as well as the combined ones, which consequently introduces instability. One question is whether one algorithm or pipeline could simplify this; for instance: **Does a linear model allow for combined actions without training on them for the different modalities?**

Research Question 3

Does a multimodal approach contribute to improving myocontrol?

Different approaches exist when discussing multimodality: using combined independent modalities or fusing them by using concatenation or specific algorithms as described in Section 2.4.

The first approach could enhance myocontrol by using sensors providing dissimilar information, such as vision or angular values that can be computed into body kinematics. This raises the question: **Which conditions would allow a combined use of sensors to improve myocontrol?**

The second approach appears interesting when comparing the different modalities, as each of them present advantages and limitations: **Does a fused approach of different modalities enhance the control?** Surface electromyography, for example, has difficulties identifying wrist rotation movements, as these involve deeper muscles that are not easily detected by the surface sensors. Using force myography, for instance, might solve this problem as, although it is also a surface modality, the movements of underlying muscles might still be detected by morphological changes. Thus, would a fusion of force and surface myography improve intent detection?

Moreover, deep modalities, such as ultrasound or electro-impedance tomography, could provide the deeper insights that are currently lacking. Given that the sensors yield different kind of information, the question arises: **Does fusing deep and surface modalities enhance myocontrol?** Several fusion approaches exist and would need to be compared according to evaluation metrics previously established. Fusing modalities also results in an increased number of features. Therefore, feature selection might be necessary in order to keep reasonable time complexity and ensure embeddability.

1.3 State of the Art[1]

There are several non-invasive approaches as alternatives or complements to sEMG [*37*]. Among them, force myography (FMG) [*38–41*] uses pressure-based sensors (most often Force Sensitive Resistors, or FSRs) to measure the counter-pressure exerted by the muscle bulge at the surface of the forearm. Some studies also evaluated the use of high-density force myography (HD-FMG) with 126 FSR sensors, for instance, in [*42*]. Another modality, near-infrared spectroscopy (nIRS) [*43–45*], has been used for more than 40 years in-vivo. It uses multiple wavelengths of light to penetrate deeply into the tissue and measure functional information, such as the oxygen concentration in the blood that absorbs these specific wavelengths. It is typically used in modern smartwatches to measure blood flow, providing heart-rate estimation. Mechanomyography (MMG) [*46, 47*] uses an accelerometer or a microphone to measure low-frequency vibrations that the muscle emits when contracted. Ultrasound imaging [*48, 49*], also known as sonomyography (SMG), uses sound waves that are reflected by the tissues with different reflection properties in order to recreate an image. EIT [*50, 51*] measures the equipotentials across a section of the body. Its simplest form relies on several electrodes placed on the skin, with a current being passed between two of them, while the voltage induced is

[1] For a better understanding of the state of the art before the start of this thesis, the references' numbers anterior to it (i.e. anterior to the date of publication of the first core article of this thesis) will be *italicized* in this section only.

measured on the other electrodes. Repeating this process across several pairs results in the creation of an image by using back-propagation algorithms. Human arm kinematics, often computed from data of inertial measurement units (IMUs), while not directly a myography technique, has also been used to complement sEMG [*52*, 53].

Researchers have already started to investigate the multimodalities of some of these sensors [54, 55]. Some studies showed that FMG obtained better offline classification accuracies than sEMG [56]. Others also evaluated the combined use of the two modalities [57, 58]. While using the same number of FMG and sEMG electrodes results in a better performance of a hybrid system compared to the single modalities [57], another study showed that using only two sEMG and 78 FMG sensors shows no significant improvement in adding the two sEMG sensors compared to using FMG only [58].

Some research groups also evaluated the combined use of kinematics and sEMG. Several studies showed that the combined use of sEMG and IMUs improved the offline classification accuracy compared to the single modalities [53, *59*]. The combination of these two modalities was further tested by Krasoulis et al. in an offline and online experiment, concluding as well that the joint use of sEMG and IMU improved the classification [60].

Up to now, the mentioned combinations of modalities involved only surface modalities. It is important to note that combining a deep modality (e.g. ultrasound or EIT) with a surface modality would hypothetically bring better results than with surface modalities only. In [61], the results from an offline experiment showed that the fused data of sEMG with A-mode ultrasound outperforms sEMG alone in terms of accuracy and performs slightly better than ultrasound alone. However, a statistical analysis would be necessary to evaluate if this difference was significant. In an online experiment, the same research group also compared ultrasound and sEMG, showing that A-mode ultrasound outperforms sEMG on gesture recognition accuracy in an online experiment without combining the two [62].

While the fusion studies often used a concatenated vector of the different modalities to fuse the multimodal data, several fusion-targeted machine learning algorithms have been evaluated. For instance, [61] extracted the features of sEMG and ultrasound (US) and performed a doubled principal component analysis (PCA) before and after concatenating the two feature vectors and by feeding the remaining features to a classifier. Accelerometers and sEMG were used in a study investigating the use of multistream formalism to effectively combine the information from different sources using cooperative Markov models [*63*]. Ju et al. evaluated the use of Fuzzy Gaussian Mixture Models (FGMM) for use with multisensory information obtaining better results than with Support Vector Machine (SVM) and Gaussian Mixture Models (GMM) [*64*]. In [65], the same research group compared the use of Adaptive Directed Acyclic Graph with classical Neural Network and Fuzzy C-means clustering with successful results.

1.4 Contributions and Overview

The contributions of this cumulative dissertation are based on the publications listed in the Publication List. The full text of the core publications can be found in Appendix A, and the abstracts of co-contributed works are listed in Appendix B.

1.4.1 Overview and Summary of the Contributions

The following list provides an overview of the main contributions of this dissertation and the research questions and publications it refers to:

- Development of devices and methods to compare the modalities. [RQ1]
  in A.1, A.3, B.6
- Identification of surface and deep modalities that best improve the hand/wrist action recognition for prosthetic myocontrol by evaluating them offline and online concurrently with analysis of user studies. [RQ1]
  in A.1, A.2, A.3, A.4, B.1, B.2, B.5
- Design of modality-specific machine learning pipelines, including feature extraction, selection, model training and evaluation. [RQ2]
  in A.1, A.2, A.4, B.2
- Development of fusion approaches between potentially complementary modalities. [RQ3]
  in A.1, A.3 (additional results), B.2
- Design of a multimodal device and platform allowing comparison of performance between people with and without limb difference, as well as an alternative option allowing more functionality than prostheses and the possibility of remote working for users with disability. [RQ3]
  in A.4, follow-up from B.3

1.4.2 Contributions

While some studies have assessed alternative modalities to sEMG, the majority of these evaluations used classification. In contrast, this work will focus on regression as this provides an independent simultaneous and proportional control to prosthesis users [34]. This thesis will initially analyze individual modalities such as sEMG, FMG, HD-FMG, also called tactile myography (TMG), ultrasound, and EIT. The analysis will involve both offline and online experiments in user studies, specifically using regression-based approaches. This research will also investigate how linear algorithms such as ridge regression can harness the inherent linear characteristics within our muscular system for controlling combined hand and wrist movements. By training on individual actions only, the linearity of the algorithm enables combined movements without requiring direct

training on the combined actions themselves. Finally, this research will merge surface and deep modalities in an experiment where a regression-based fusion algorithm will be evaluated to enhance intent detection.

Development of devices and methods for comparison [RQ1]:

For the comparison of modalities, different sensors, with different sampling rates and bandwidths must be used, which makes it difficult to compare or fuse them. To address that, an **innovative wearable multimodal device** was developed and evaluated in a user study **comparing** force and electromyography sensors, as presented in A.1. Since its development, this device has had a considerable impact in the field by raising interest in several international groups and leading to 10 publications listed in Section 1.4.3.

Moreover, it can be challenging to involve prosthesis users in user studies and compare them with non-users on tasks inspired by Activities of Daily Living (ADLs). It often requires the use of two setups: a custom socket for each prosthesis user and an adaptive splint to wear the prosthesis and replace the socket for participants without limb impairment. The setup presented in A.4 allows a **performance comparison** between the two groups of participants under the **same initial conditions**: e.g., no influence of the weight of the grasped object or the prosthesis, and the same sensors are used without the need of custom orthoses.

A similar idea was developed in B.6, in which a **modular multimodal adaptable prosthetic platform** was developed, this time to wear the prosthesis. The setup allows for both FMG and sEMG sensors and could be adapted to other modalities.

In terms of evaluation metrics for comparison, standard types from the literature were considered. These are described in Section 3.4.1. The developed devices and off-the-shelf modalities also needed to be evaluated as user interfaces, and adapted metrics were therefore selected in Sections 3.4.2 and 3.4.3.

Identification and evaluation of modalities [RQ1]:

Force myography and surface electromyography were initially compared in an offline study in A.1. The results showed that **FMG yields a more stable signal across time than sEMG**, as well as a **better separability of the clusters**.

HD-FMG was then evaluated online for **combined gestures** in A.2, showing that by **training on single actions** only and using linear regression, combined 3-DoF hand/wrist actions can be performed. HD-FMG and sEMG were compared **online** in B.1, showing a **better performance of HD-FMG over sEMG**. This was further proven in B.2,

with different regression approaches.

For the **first time, force myography, ultrasound, and electro-impedance tomography** were recorded **simultaneously** in a user study in order to compare the modalities evaluated in A.3. **Ultrasound showed overall better performance**, while EIT was limited. FMG, despite its lower resolution, still had comparable results to deep HD modalities, with overall results even better than EIT.

Body tracking via inertial sensors was also evaluated in B.5 in terms of static and dynamic tracking with high precision, providing, therefore, a complementary modality used in A.4.

Design of pipelines [RQ2]:

While HD modalities are becoming increasingly available, the question of their **integration** into an algorithm optimized for embedded hardware also comes into play. Indeed the capacity of embedded hardware should be considered when implementing machine-learning pipelines for prosthesis use, as developed in Shreyas Waichal's thesis [66]. For this reason, two different **pipelines for the HD-FMG modality** were compared in A.2, with and without **ROIG feature extraction**, with similar results.

From the results of A.2, showing that **combined** hand/wrist **gestures** can be obtained **by training on single actions** only **using linear regression**, future pipelines involving **HD-FMG** should take that into consideration. Not only should linear regression algorithms be favored as they diminish the complexity of the trained actions and therefore increase stability, but if such a linear algorithm is chosen, **features** should be carefully selected to **avoid** introducing any **non-linearity**.

Alternative regression pipelines have been evaluated in B.2. Although Gaussian Process Regression (GPR) forgoes advantageous linearity, it outperformed Ridge Regression for single actions involving hand, wrist, and finger movements. GPR was, however, not tested for combined actions.

Considering the high dimensionality of **ultrasound and EIT**, several **feature selection and extraction methods** were evaluated and **compared** in A.3. For ultrasound, the downsampling providing the highest number of features performed best, followed by ROIG. For EIT, a linear tomographic reconstruction with added artificial data performed best. A specific pipeline for fusion was also implemented, as developed below.

As much as an ideal algorithmic pipeline can improve myocontrol, the human factor and its learning ability should not be removed from the equation. A.4 has shown the ability of humans to adapt and learn to compensate for eventual weaknesses in the control, underlining the fact that co-adaptation is essential in HMIs.

Multimodal approaches [RQ3]:

An application of **inertial motion capture tracking combined with surface electromyography** was presented in A.4 in order to teleoperate a bimanual humanoid robot by involving a pool of participants with and without disabilities to perform complex daily tasks. The platform is proposed as an alternative to prostheses in complex tasks, allowing more functionality due to the embedding constraints of prostheses. It also offers a new assistive solution to people with disabilities, which can be additionally used as an option for them to remote work. The IMU-based tracking device developed specifically for the purpose of this thesis has led to the publication of 4 papers and one patent referenced in Section 1.4.3.

While such an application was a combined use of different modalities to serve a specific purpose, **fusions of different modalities** have also been evaluated in other experiments. The study presented in A.1 offered, **for the first time, an offline fusion of sEMG and FMG** for upper-limb myocontrol. The results showed, unfortunately, no difference with the single modalities. **HD-FMG and sEMG** were also **combined offline** in B.2 with different regression algorithms without further success. This led to thinking that surface modalities might provide too similar information to be able to complete each other. Deep modalities might therefore succeed where surface ones failed.

For the first time, force myography, ultrasound, and electro-impedance tomography were combined in an offline multimodal fusion algorithm from the experiment of A.3. The multimodal algorithm provided overall better results than the single modalities.

1.4.3 Retrospective State of the Art

Since its development, the multimodal data-acquisition device developed in A.1 has led to the publication of the following papers and patent:

M. Connan, E. R. Ramírez, B. Vodermayer, and C. Castellini, "Assessment of a wearable force- and electromyography device and comparison of the related signals for myocontrol," *Frontiers in Neurorobotics*, vol. 10, no. 17, pp. 1–13, nov 2016, doi: 10.3389/fnbot.2016.00017

M. Nowak, T. Eiband, and C. Castellini, "Multi-modal myocontrol: Testing combined force-and electromyography," in *2017 International Conference on Rehabilitation Robotics (ICORR)*, pp. 1364–1368. IEEE, jul 2017, doi: 10.1109/icorr.2017.8009438

M. Nowak, R. M. Bongers, C. K. van der Sluis, and C. Castellini, "Introducing a novel training and assessment protocol for pattern matching in myocontrol: case-study of a trans-radial amputee," in *Proceedings of the Myoelectric Control Symposium (MEC)*,

2017, doi: 10.13140/RG.2.2.28846.61768

C. Nissler, M. Connan, M. Nowak, and C. Castellini, "Online tactile myography for simultaneous and proportional hand and wrist myocontrol," in *MEC2017 - Myoelectric Control Symposium*, 2017

N. Jaquier, M. Connan, C. Castellini, and S. Calinon, "Combining electromyography and tactile myography to improve hand and wrist activity detection in prostheses," *Technologies*, vol. 5, no. 4, pp. 1–16, oct 2017, doi: 10.3390/technologies5040064

R. Meattini, M. Nowak, C. Melchiorri, and C. Castellini, "Automated instability detection for interactive myocontrol of prosthetic hands," *Frontiers in Neurorobotics*, vol. 13, p. 68, aug 2019, doi: 10.3389/fnbot.2019.00068

M. Nowak, T. Eiband, E. R. Ramírez, and C. Castellini, "Action interference in simultaneous and proportional myocontrol: Comparing force- and electromyography," *Journal of Neural Engineering*, vol. 17, no. 2, p. 026011, mar 2020, doi: 10.1088/1741-2552/ab7b1e

B. W. Hallworth, A. W. Shehata, M. R. Dawson, F. Sperle, M. Connan, W. Friedl, B. Vodermayer, C. Castellini, J. S. Hebert, and P. M. Pilarski, "A transradial modular adaptable platform for evaluating prosthetic feedback and control strategies," in *MEC-Myoelectric Control Symposium*, pp. 1–4, 2020

M. Sierotowicz, D. Brusamento, B. Schirrmeister, M. Connan, J. Bornmann, J. Gonzalez-Vargas, and C. Castellini, "Unobtrusive, natural support control of an adaptive industrial exoskeleton using force-myography," *Frontiers in Robotics and AI*, vol. 9, p. 223, sep 2022, doi: 10.3389/frobt.2022.919370

M. Connan, B. Yu, C. Gibas, R. Brück, E. A. Kirchner, and C. Castellini, "Deep and surface sensor modalities for myo-intent detection," in *Proceedings of MEC - Myoelectric Control Symposium*, 2022

M. Nowak, R. M. Bongers, C. K. van der Sluis, A. Albu-Schäffer, and C. Castellini, "Simultaneous assessment and training of an upper-limb amputee using incremental machine-learning-based myocontrol: A single-case experimental design," dec 2022, doi: 10.21203/rs.3.rs-2357029/v1

D. Brusamento, M. Connan, C. Castellini, B. Schirrmeister, J. Bornmann, and J. González-Vargas, "Verfahren zum Kontrollieren eines Exoskeletts, Exoskelett und Computerprogrammprodukt. DE Patent No 102021116202. Dec. 29, 2022," Patent

Since its development, the IMU-based tracking device developed for the purpose of A.3 has led to the publication of the following papers:

M. Connan, M. Sierotowicz, B. Henze, O. Porges, A. Albu-Schäffer, M. A. Roa, and C. Castellini, "Learning teleoperation of an assistive humanoid platform by intact and upper-limb disabled users," in *Converging Clinical and Engineering Research on Neurorehabilitation IV. ICNR 2020. Biosystems & Biorobotics*, vol. 28, pp. 165–169, Springer. Springer International Publishing, oct 2020, doi: 10.1007/978-3-030-70316-5_27

M. Sierotowicz, M. Connan, and C. Castellini, "Human-in-the-loop assessment of an ultralight, low-cost body posture tracking device," *Sensors*, vol. 20, no. 3, p. 890, feb 2020, doi: 10.3390/s20030890

M. Sierotowicz, N. Lotti, R. Rupp, L. Masia, and C. Castellini, "A comprehensive framework for the modelling of cartesian force output in human limbs," in *2022 International Conference on Rehabilitation Robotics (ICORR)*, pp. 1–6. IEEE, jul 2022, doi: 10.1109/ICORR55369.2022.9896547

Chapter 2

Fundamentals

> The most profound technologies are those that disappear. They weave themselves into the fabric of everyday life until they are indistinguishable from it.
>
> *(Mark Weiser)*

Table of Contents

2.1 Amputation and Anatomy

2.1.1 Amputation Levels and Prevalence

Although there is no clear consensus on numbers, in 2017, about 57.7 million people worldwide were living with limb amputation from traumatic causes, of which an estimated 19.6% had a unilateral upper-limb amputation and 19.1% a bilateral [73]. This prevalence varies, of course, in terms of cause, age, and geographical region. The areas with the highest prevalence were East and South Asia, high-income North America, and Western Europe. Furthermore, it is estimated that congenital upper-limb anomaly has an incidence of 15 per 100,000 individuals live birth [74]. Among them, 8% have a deformation that is considered to be major, i.e. beyond finger loss [75]. Levels of upper-limb absence (as shown in Fig. 2.1), traumatic and congenital, are estimated as follows: 2% forequarter, 3% shoulder disarticulation, 16% trans-humeral, 1% elbow disarticulation, 12% transradial, 2% wrist disarticulation, and 61% transcarpal in Italy and United Kingdom [76], but can strongly vary depending on the country and year as reported in [77].

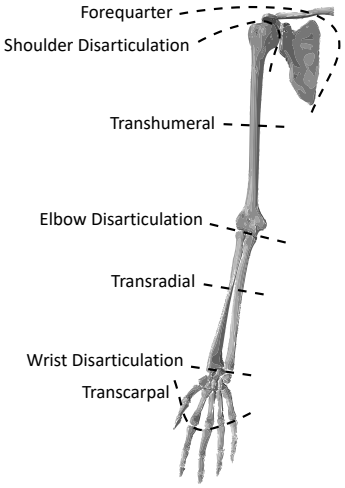

Figure 2.1: Illustration of the different levels of upper limb absence.

2.1.2 Anatomy of the Forearm

In order to understand the principle of deep and surface modalities, a brief explanation of the different muscles, their location, and functionality needs to be established. The cross-section depicted in Fig. 2.2 is at the level of the muscle bulge, since it is where the sensors are usually placed, in particular in the case of a transradial amputation, which is the level studied in this thesis.

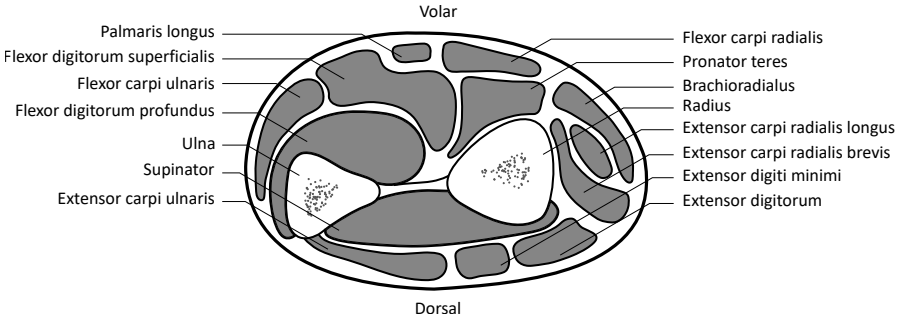

Figure 2.2: Illustration of a cross-section of the forearm at the level of the muscle bulge.

The functions of the muscles illustrated in Fig. 2.2 are listed in Table 2.1 in their order of appearance clockwise from the top:

Muscle	Function
Flexor carpi radialis (FCR)	Flexes and abducts the wrist.
Pronator teres	Pronates the forearm[(1)] (turns it face down)
Brachioradialis	Its main function is to flex the forearm, but it also assists in supination and pronation depending on the position of the forearm [78]. For instance, when the elbow is flexed, the brachioradialis semi-pronates the lower arm. This already shows how the problem of the limb position effect can affect myoelectric prosthesis users.
Extensor carpi radialis longus (ECRL) & Extensor carpi radialis brevis (ECRB)	Their primary function is to extend and abduct the wrist.
Extensor digiti minimi (EDM)	Extends the little finger and the wrist.
Extensor digitorum (ED)	Its role is to extend the phalanges. It also tends to separate (abduct) the fingers as it extends them.
Extensor carpi ulnaris (ECU)	Extends and adducts the wrist.
Supinator	Supinates the forearm (turning face up).
Flexor digitorum profundus (FDP)	Flexes wrist and fingers at both interphalangeal joints.
Flexor carpi ulnaris (FCU)	Flexes and adducts the wrist.
Flexor digitorum superficialis (FDS)	Its primary function is to flex the four fingers (excluding the thumb).
Palmaris longus (PL)	Weak wrist flexor. It is absent in ca. 14% of the people, depending on the population [79]. Its absence does not affect grip strength [80] but decreases pinch strength with the fourth and fifth fingers [81].

[(1)] Forearm pronation/supination is often qualified as wrist pronation/supination by abuse of language, as along this thesis.

Table 2.1: Muscles within the forearm and their function.

As shown in Fig. 2.2, the pronator and supinator are deep muscles at this level of the forearm. Therefore, their activity is difficult to detect with surface electromyography, and other modalities might be more able to do so.

This representation needs to be taken with some considerations in case of amputation as the operation depends on the surgeon as well as the trauma and can change the configuration of the muscles. In addition, the anatomy of the muscles may vary slightly from person to person: for instance, the Gantzer muscle, accessory head of FPL or FDP, depending on the variant, is present in 48% of the population [82].

2.2 Non-Invasive Sensor Modalities

2.2.1 Pre-selection Criteria of Modalities

As explained in the previous section, most muscles controlling the hand and wrist are extrinsic muscles situated in the forearm. The sensors chosen for hand movement's intent detection will need to be placed on the forearm, which also allows a possible application in prosthetics and provides the advantage of leaving the hands free, in contrast to datagloves.

This thesis focuses on non-invasive modalities, i.e. that do not require to be implanted inside the forearm, as they could be applied to prosthesis users without the need for a surgical operation. Even though invasive modalities might give a better signal-to-noise ratio, the invasive character of the sensors greatly complicates the research. Indeed, as the different sensors, algorithms, or features should be evaluated by performing user studies, the necessity of surgical insertion of sensors would drastically limit subject recruitment and applicability. On the contrary, using non-invasive modalities allows the evaluation of the sensors for prosthetic use and potential future HMIs.

Surface modalities are the most studied form of myocontrol input in the literature due to the gold-standard sEMG, their relative ease of use, their market availability, and the alleviated process for subject recruitment. Although not often portable, alternatives to surface modalities also exist for measuring deeper muscular activity. Despite being called deep modalities due to their depth of measurement, these sensing techniques remain non-invasive because they do not need skin perforation or surgery. However, all the ones presented in this section involve sending a signal into the body, be it a micro-current or a sound wave. The following sections will describe the different surface and deep modalities used in this thesis as well as some additional interesting modalities not evaluated in the underlying publications.

As surface modalities, this thesis evaluates FMG by comparing it to the gold-standard sEMG in A.1. Its promising results in this study led to the evaluation of an improved version of FMG, namely HD-FMG, providing a pressure map of the forearm in A.2. While their categorization as bio-sensors is arguable as they are evolving at a macro-level

compared to the previously mentioned modalities, IMUs have also been used to determine upper-body kinematics to lessen the burden of sEMG by, for instance, estimating wrist rotation without the need of machine learning in A.4. In terms of deep modalities, the core publication A.3 evaluated the two on-body deep modalities existing, namely EIT and ultrasound. Ultrasound B-mode, which is the standard mode providing an image, was used in this thesis as it provides a higher resolution than ultrasound A-mode, which is only a few single transducers, and has already been used successfully for single-finger detection [49]. The device used is one of the first portable research prototypes, and researchers are actively working on making it fully wearable [83].

2.2.2 Surface Modalities

2.2.2.1 Surface Electromyography

The human body is composed of a network of over 650 muscles. It comprises three main muscle types: skeletal muscles attached via tendons to our bones, cardiac muscles for the heart, and smooth muscles lining blood vessels and specific organs. They are all made of muscle cells, i.e. fibers (composed of myofibril), bundled tightly together. These bundles receive signals from the neural system, as shown in Fig. 2.3, contracting the fibers and therefore generating force and motion. There are three types of muscle contraction. The first two, shortening and lengthening muscle fibers, generate opposite forces and are involved, for example, in flexing the elbow by shortening the biceps and lengthening the triceps. The third type of contraction creates a stabilizing force, keeping the muscle rigid without any change in length. This is the type of contraction that maintains our posture upright.

Skeletal muscles, the ones we are interested in, are all connected to the somatic nervous system. In order to move the arm, the brain sends an action potential along the motor neuron to its synapses, chemically transforming it into a motor unit action potential (MUAP), which is the sum of the action potentials generated by depolarization and repolarization at the muscle fiber membrane.

Surface electromyography is often defined as the gold standard in prosthetic control. Electromyography is a technique measuring electrical activity in the muscles (cf. Fig. 2.3) when they are activated by a nerve or by electrostimulation.

An example of sEMG electrode is the *Myobock 13E200* from *Ottobock* (cf. Fig. 2.4), a standard type used in prosthetic control. Considering the expensiveness of such electrodes, alternatives have quickly been investigated in the research community, and a possible option was the *Myoband* from *Thalmic lab*. Despite not being a medically certified device and not being the standard in prosthetics, it is sufficient for many research studies, and available at a much lower price [84, 85].

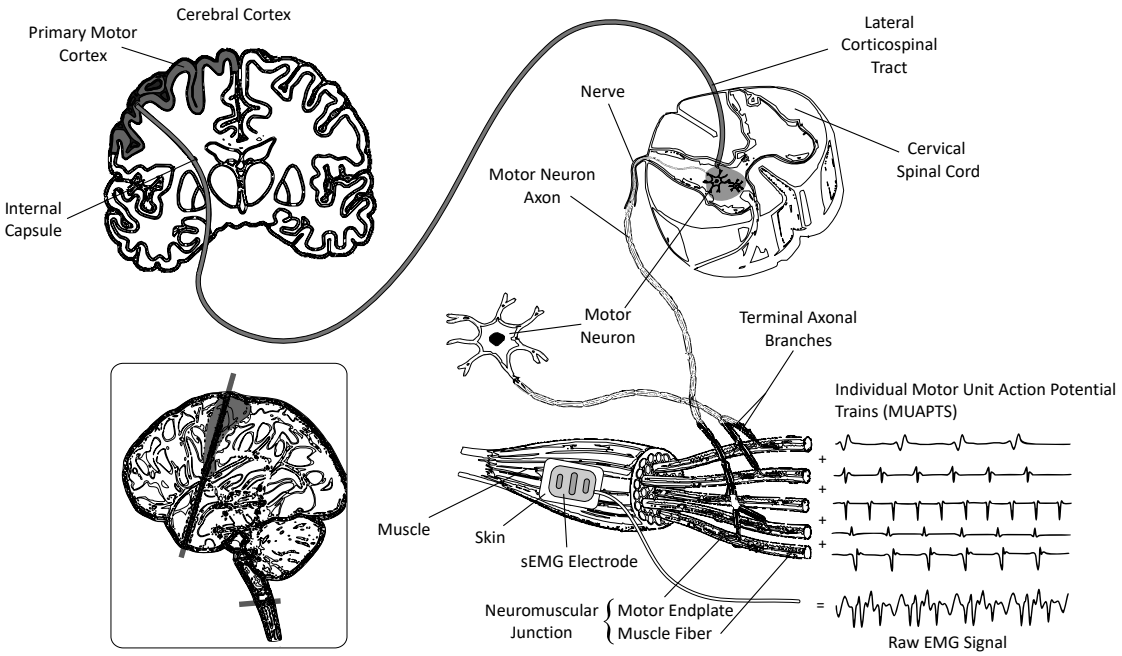

Figure 2.3: Illustration of the working principle of electromyography, from the cerebral cortex down to the neuromuscular junction, showing how individual motor unit action potential trains creates the raw electromyographic signal of a typical double-differential electrode. Inspired from [14, 15].

Several acquisition modes exist for sEMG signals: monopolar, single-differential, and double-differential, as depicted in Fig. 2.5. For sEMG electrodes, the standard one is double-differential, as it allows a stronger pre-filtering of the signal and is less prone to signal cancellation if placed on the muscle's zone of innervation. Indeed, at the neuromuscular junction (cf. Fig. 2.3), the electrical signal propagates in both directions and could thus be canceled out in a single-differential electrode if placed on the junction. Monopolar signals are used in the case of High-Density surface Electromyography (HD-sEMG) in order to have a matrix of electrodes.

The industry standard for controlling hand prostheses consists in placing two electrodes on each side of the stump and using co-contraction of antagonistic muscles to produce two to three different signals, which in turn control the same number of actions (generally, open and close). In order to control more actions more intuitively, researchers have focused on employing machine learning, which requires additional electrodes. But due to the bulkiness of the wearable sEMG electrodes, the research community was constrained to a limited number: in general, eight as in the *Myoband* or ten, which is approximately the maximum that fits around the forearm. As previously mentioned, independent and proportional control of each prosthesis' DoF according to the user's intent would bring a more intuitive control for the user and has been evaluated in several

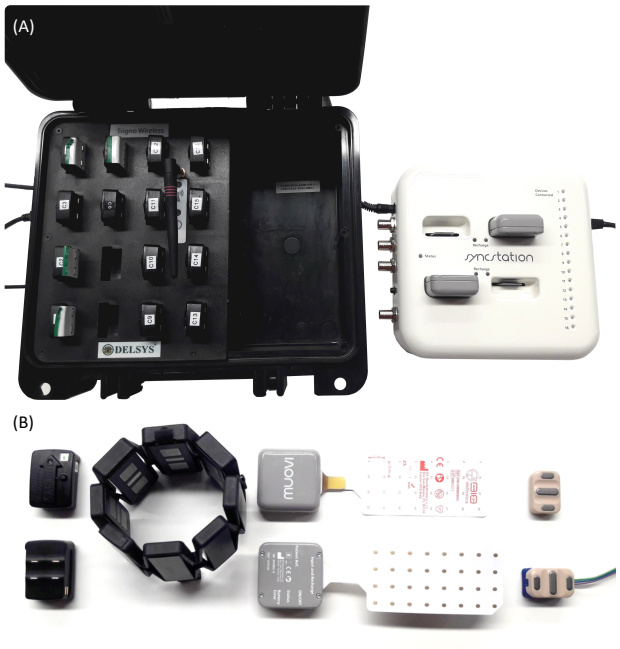

Figure 2.4: Electromyography sensors. (A) Acquisition box of Delsys (left) for the Trigno electrodes and of OTBioelettronica (right) for the MuoviPro electrodes. Both collect their electrode data via WiFi and transmit it to a computer via network cable and TCP. (B) From left to right: Delsys Trigno electrodes, Myoband from Thalmic Labs communicating directly via Bluetooth, HD-sEMG MuoviPro electrodes from OTBioelettronica, Myobock sensors from Ottobock.

studies [86, 87]. However, low reliability prevents better commercialization of the systems.

In 2013, the first pattern recognition system with up to 8 electrodes was made available by *Coapt*[1], allowing typically 3 to 6 different grasping patterns via a classification algorithm [88]. Similarly, *Ottobock* developed the *Myo Plus* system[2], and more recently *Esper Bionics* launched the *Esper Control*[3]. Despite being a remarkable step forward in the community, these systems are based on classification, which does not allow independent control: The speed of activated DoFs cannot be controlled independently if activated simultaneously. However, natural movements require independent and proportional control [34].

Research on SPC with sEMG is still ongoing, but the modality suffers from numerous drawbacks, and several factors can substantially affect the control, such as electrode shifts, motion artifacts, ambient noise, cross-talk among deep adjacent muscles, and muscular fatigue [26–29]. Thus, no commercially available solutions involving simultaneous and

[1] `http://www.coaptengineering.com/`
[2] `https://shop.ottobock.us/Prosthetics/Upper-Limb-Prosthetics/Myo-Plus/c/2901`
[3] `https://esperbionics.com/`

proportional control emerged. Consequently, alternative modalities are gaining a growing interest in the community.

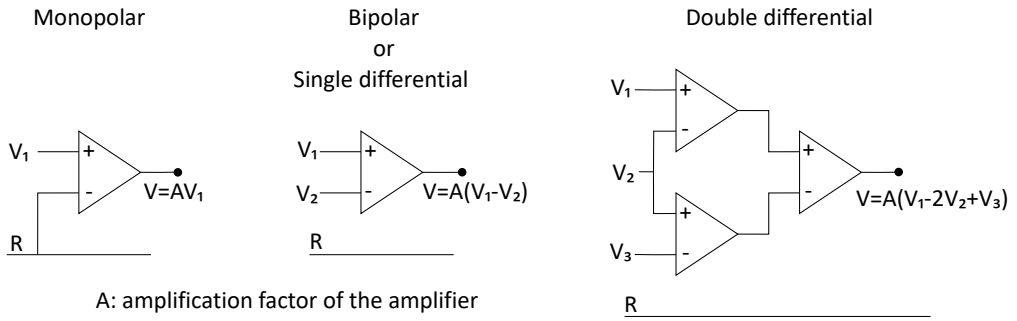

Figure 2.5: Electrode configurations for surface electromyography. For more details, refer to [16].

In recent years, other devices have emerged, allowing even more sEMG sensors to be placed on the forearm, leading to HD-sEMG with the *Quattrocento* and *MuoviPro* from *OTbioElettronica*[4] that are commercially available.

High-Density Surface Electromyography

High-density surface electromyography is based on the same principle as surface electromyography with a higher number of tiny surface electrodes, as shown in Fig. 2.4 with the *MuoviPro* electrode matrix. Even though the probes can be wireless, as in the *MuoviPro* from *OTBioElettronica*, their accompanying processing device is bulky and not easily portable for a prosthesis user. As a result, there are currently no end-user devices commercially available, and the primary use of such HD-sEMG devices is still for research purposes.

The substantial interest of HD-sEMG is that it allows, with some specific algorithms [89, 90], the decomposition of the signal into individual motor unit action potentials [91–93], as represented in Fig. 2.3. This motor unit decomposition is now also implemented online [94, 95] and has even been used for SPC of wrist and hand actions with significantly higher success rates than non-negative matrix factorization (NMF) or multiple linear regression (MLR) [96], with an nRMSE of ca. 11.4% for two simultaneously controlled DoFs.

2.2.2.2 Force Myography

Force myography (FMG) is a more recent technique that has benefited from a growing interest in the community in recent years. This technique consists in detecting, on the

[4] `https://otbioelettronica.it/en/`

surface of the skin, the pressure exerted by the muscles from the volumetric changes induced by their contraction (cf. Fig. 2.6). A simple solution to record FMG signals is to use pressure sensors such as force sensitive resistors (FSRs) based on Resistive Polymer Thick Film Sensors (RPTF). As well, other sensor technologies have been used for that purpose [97, 98], based e.g. on piezoelectric, pneumatic, capacitive, resistive fabric, or optical fiber-based sensors. Force myography was first introduced for forearm intention detection in [38, 99], showing that each hand action corresponds to a specific and repeatable pressure pattern. In [39], the authors used 32 FMG sensors in a prosthetic socket and showed that single-finger flexions were identifiable from the sensors. The technique was shown to be suitable for proportional control of the grip force in [40], with 14 FSRs.

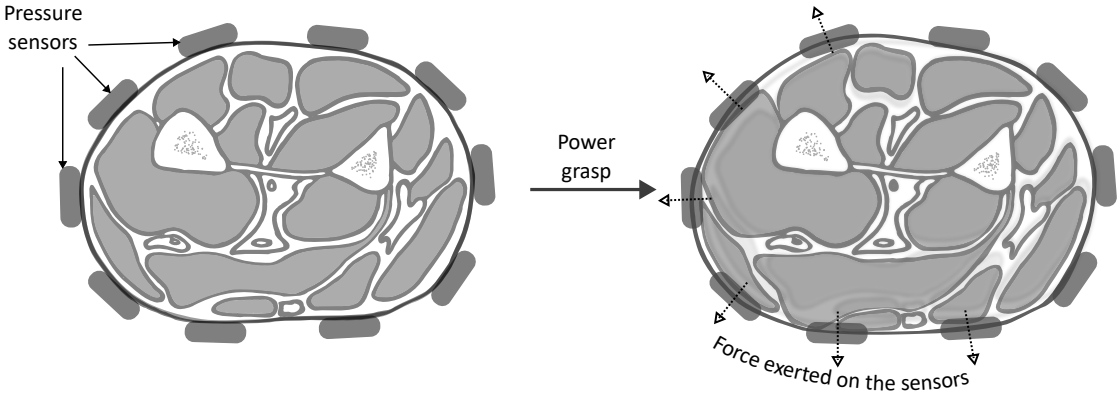

Figure 2.6: Illustration of the working principle of force myography on the cross-section of the forearm.

While sEMG and FMG are both surface sensing modalities, FMG might be able to detect better than sEMG the movements of deeper muscles, which are involved in pronation and supination for instance [100]. Indeed, deep muscle movements can be reflected at the surface with the resulting volumetric changes.

High-Density Force Myography

The electronics required for such a technique being very light and inexpensive, a high number of these sensors can be integrated into a bracelet more easily than with sEMG. As for sEMG, additional FMG sensors could mean better control of the prosthesis [42]. Furthermore, the increased density would enable considering the input data as an image rather than a collection of individual sensors that were previously handled as vectors, therefore opening up additional processing techniques for image analysis.

2.2.2.3 Kinematics and Inertial Measurements

An inertial measurement unit (IMU) is a module, sometimes a single integrated circuit, comprising a magnetometer, a gyroscope, and an accelerometer. Fusing each of these sensors' data gives a reliable estimation of the module's absolute orientation in space. While the use of a simple Kalman filter can suffice, some devices already offer an integrated solution with a fusion algorithm implemented in the firmware, such as the *BNO* series from *Bosch*[5].

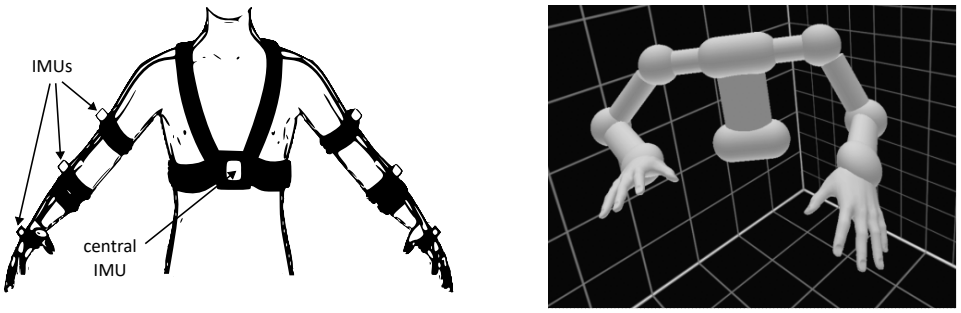

(A) **(B)**

Figure 2.7: Illustration of the working principle of an IMU-based tracking device. (A) Placement of IMUs on the body. (B) Virtual representation from the tracking device.

The idea behind an IMU-based body tracking device consists in placing an inertial sensor on each relevant segment limb to provide the body kinematics of the user (cf. Fig. 2.7). Whereas other kinematic tracking devices, such as the *VICON* system, are based on visual data and provide extremely precise positioning, an IMU-based one is still sufficiently precise for reliably tracking body movements, as shown in B.5 and has the advantage of not depending on any external source, being therefore entirely wearable.

The working principle of an IMU-based body tracking device consists in monitoring the absolute orientation of body segments in space and computing, from these measurements, the forward kinematics of the upper limbs. This can be automatically computed when using a game engine such as *Unity*, in which the position of a body segment is implicitly calculated relative to the parent's position, i.e. the body segment higher in the kinematic chain.

[5] `https://www.bosch-sensortec.com/products/smart-sensors/bno055/`

2.2.3 Deep Modalities

2.2.3.1 Electro-Impedance Tomography / Myography

Electro-Impedance Tomography (EIT), as its name indicates, relies on the impedance measured at the surface of the skin. This medical imaging technique was inspired by the same principle, named Electrical Resistivity Tomography, used in geophysics from the 1930s, with electrodes placed at the surface of the earth to locate resistivity anomalies.

With the medical imaging method, the conducting electrodes are placed on the skin's surface in a circular manner, as illustrated in Fig. 2.8. Electrical conductivity considerably varies depending on the type of tissue the current passes through. Based on this principle, a micro alternating current can be applied to one or more electrodes, and the resulting difference of potentials can be recorded from the remaining electrodes. This can be applied in different electrode configurations. In the simple configurations, the micro-current is applied to each electrode in turn until completing the circle of electrodes, each time measuring the difference of potentials between pairs of the remaining adjacent or opposing electrodes. These measurements are then used to reconstruct a tomographic image using algorithms such as backpropagation algorithms, as recovering the conductivity from the currents and potentials is a non-linear ill-posed problem.

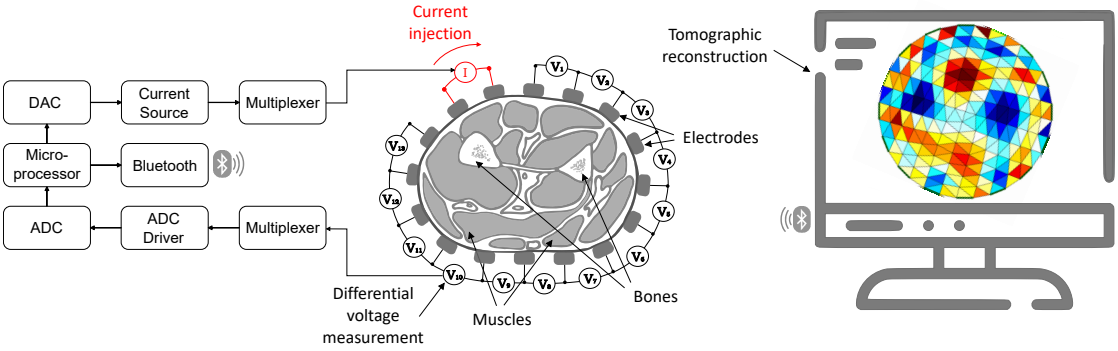

Figure 2.8: Illustration of the working principle of electro-impedance tomography on the cross-section of the forearm.

While the geophysics technique has been used since the 1930s, it was only much later that EIT was applied in the medical field. The first EIT image was produced in 1978 [101], although a medical EIT system was only presented by Barber and Brown in 1984 [102]. Since then, EIT has been proposed as a solution for brain activity imaging [103], to detect skin or breast cancer, or to assess cardiac function, pulmonary hypertension, and lung function [103]. However, it is only recently that the technology has gained interest for forearm intent detection with the advent of wearable EIT devices [50].

EIT signals can as well be used raw without the tomographic reconstruction generating images. While it has been referred to as raw EIT in A.3, it can also be called EIM for Electrical Impedance Myography [104].

Even though EIT is generally a non-invasive technique, it is worth mentioning that a research group investigated the use of implanted EIT. The approach demonstrated an improved spatial resolution, a higher signal-to-noise ratio, and an expanded frequency range. Implanted electrodes were also less sensitive to external noise and motion artifacts [105].

2.2.3.2 Sonomyography / Ultrasound

Ultrasound B-Mode and Hybrid-Mode

Medical ultrasound imaging, also called sonography or, in this case, sonomyography when targeting the muscles, uses sound waves as its name indicates. The technology appeared shortly after World War II, starting from the sonar, which has a similar principle [106]. The typical frequencies of the sound waves are around 2 MHz or higher. In order to avoid heating and cavitation effects, the power density is commonly less than one watt per square centimeter.

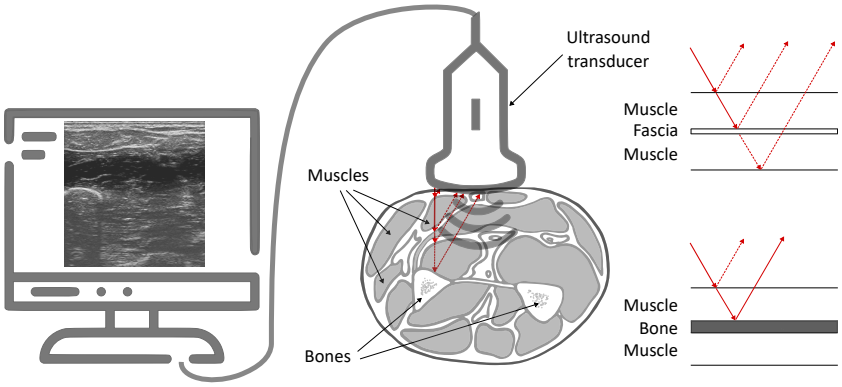

Figure 2.9: Illustration of the working principle of ultrasound on the cross-section of the forearm.

The principle of ultrasound is sound waves sent through the human tissues using a probe, as depicted in Fig. 2.9. A transducer comprises small piezo-electric elements, to which an alternating voltage signal is applied and will generate the vibration and sound of the element. Indeed, piezo-electric elements are composed of dipoles that can change the shape of the crystalline structure of the composing material when exposed to an electrostatic field. This is motor action, i.e. electrical energy is converted to mechanical energy. The pulses of ultrasound sent in the body are reflected on the tissues with different reflection properties and echoed back to the probe. Conversely, the received

sound echoes will be converted the other way around from mechanical energy to electrical energy. When the crystalline structure is exposed to mechanical stress, e.g. from sound waves, the crystal shows an electrostatic potential across the stress vector [106].

Ultrasound B-mode (B for brightness), also known as 2D mode or grey-scale imaging, presents a 2D image of the reflections. This is the principal mode used for ultrasound imaging. The depth (or y in the image) is determined by the return delay of the echoes to the transducer, while the direction of the beam determines the x position. Typically, in an ultrasound image, also called a sonogram, the brighter a zone is, the more intense and focused the echo is.

In addition, with phased-array, different angles can be obtained by adjusting the phases of each individual driving signal at each transmission, therefore swiping between angles [107]. This allows extended field-of-view sonomyograms [108].

With the advent of more portable ultrasound systems in recent years [109] and the demand for it rapidly increasing, ultrasound B-mode is further considered as a potential modality for myocontrol [110].

Ultrasound A-Mode

Ultrasound A-mode is typically the echoed signal of one transducer in one direction. It is often displayed as a 2D graph with the depth as x and the amplitude as y. However, it can also be considered as a vector, as within the prosthetic field. The bulkiness and power consumption of the traditional ultrasound machines have pushed the community to build new wearable devices comprising only a few single transducers (usually three to four) placed separately on a bracelet [111–113], using the A-mode signals for intent detection.

Some researchers use special techniques in order to reduce power usage. In [112], instead of the traditional pulse-echo approach, they use a frequency-modulated continuous wave imaging method. It allows using a linear chirp signal, also called linear frequency modulated waveform, in which the frequency increases or diminishes with time, which enables encoding the depth of the ultrasound reflections as different frequencies. With this technique, it is possible to construct a depth-resolved map of the reflections without the need to broadcast high-amplitude pulses.

2.2.4 Other Modalities

2.2.4.1 Near Infrared Spectroscopy / Photoplethysmography

Near Infrared Spectroscopy (NIRS) is often mentioned as a possible non-invasive method for myography [32, 114, 115]. Its principle consists in measuring the interaction of

infrared radiation, i.e. in the spectrum from 650nm to 1000nm [116] with the matter by absorption or reflection. It measures tissue oxygenation (hemodynamics) in the blood. Over the last 45 years, the technique has seen a growing interest in brain and muscle clinical applications [117].

In [45], NIRS was used for identifying 12 discrete gestures with 93.3% accuracy with all combinations of emitter/receiver. This modality is increasingly tested to identify gestures at the wrist level with high classification accuracy, such as in [118], in which "touchscreen" gestures, such as scroll or zoom, or in [119] with more standard gestures. Some studies yet show that the modality might suffer from a drift in the signals [120]. Still, the ability of NIRS to detect muscle oxygenation levels, and consequently muscle fatigue, has led many researchers to fuse the modality with sEMG [121, 122], showing an increase in classification accuracy, also for participants with amputation [123].

Photoplethysmography (PPG) uses light to measure blood volume changes generated by muscle movement in the microvascular bed of body tissues, which absorb different wavelengths [124]. PPG differs from NIRS by the type of LED used [125] and the features they measure.

Due to the high similarity of PPG with NIRS, they will be considered the same myography principle in this thesis.

2.2.4.2 Mechanomyography

Mechanomyography (MMG), as force myography, can be considered the mechanical counterpart of electromyography, which itself can be summarized as capturing the electrical manifestation of muscular movement. While FMG captures the low-frequency movement information, MMG captures muscle vibration in the high-frequency range. A muscle's vibrational characteristics can be captured using an accelerometer or a microphone [32, 126]. However, [127] has shown that an MMG signal could potentially be computed from a 10kHz-sampled FMG signal by applying a high-pass filter and a cut-off frequency of 2Hz.

2.2.4.3 Magnetomyography

Magnetomyography can be invasive or non-invasive, depending on the device and technique used [128].

The invasive technique of measuring muscle displacement with a myokinetic interface is worth mentioning here as an interesting method. The principle relies on implanted magnets within the different muscles and localizers placed at the surface of the forearm [129]. Additionally, such an interface could be used as a feedback device by remotely actuating the magnets [130].

While electromyography targets the electric field muscle activity, the non-invasive method of magnetomyography, instead of measuring muscle displacement as the previous method, records magnetic field muscle activity. This is performed by using a new cutting-edge technology, namely superconducting quantum interference devices (SQUID) sensors [131, 132], measuring very weak magnetic fields, in the order of pico-Tesla, from the skeletal muscles under controlled conditions. Albeit a promising technique that needs to be further tested, it is still bulky and costly for the moment.

2.3 Features

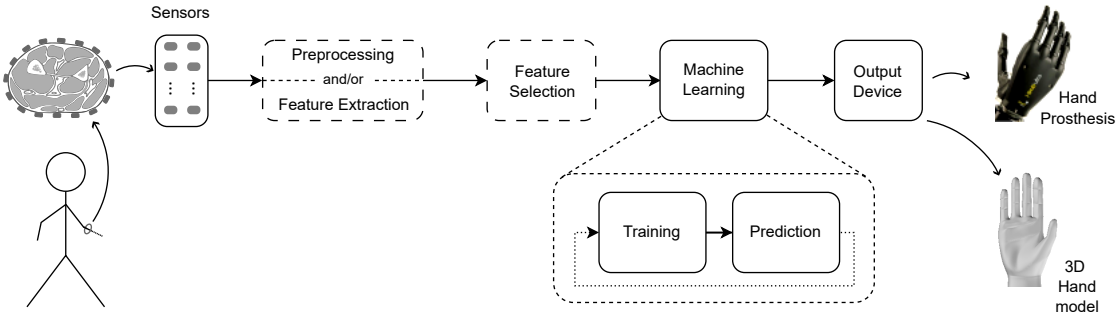

Figure 2.10: Illustration of a pipeline in the context of myocontrol.

In myocontrol, a typical pipeline consists in feeding features or raw data to a machine learning model, which will output a prediction after a training process, as depicted in Fig. 2.10.

Feature engineering is the process of using certain features, either extracted or selected, to improve the quality of the learned model, as opposed to feeding the learning algorithm with raw data.

2.3.1 Feature Selection

Feature selection consists in selecting the most relevant and significant features from a dataset. It becomes especially important when encountering high-dimensional data. The main point of feature selection is to reduce overfitting. It also helps to improve the model's performance and to reduce the training time.

As opposed to that, some features might be irrelevant or less significant for the interpretation needed. Including them in the model without using feature selection could have several adverse effects, including: an increase in the model's complexity, making it harder to interpret; an increased amount of time required for the model to be trained; a model with inaccurate or less reliable predictions.

There are three types of feature selection methods: Filter, Wrapper, and Embedded (cf. Fig. 2.11).

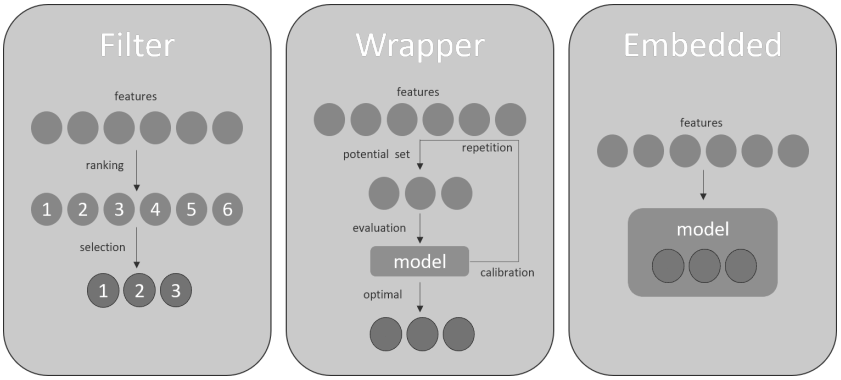

Figure 2.11: The different types of feature selection: Filter, Wrapper, and Embedded.

Filter: Filters do not test any model but rank the features according to their relevance to the problem and select the best ones. They are much faster than wrapper methods in terms of computation time and are also less prone to over-fitting. Examples of filter methods are: correlation, Chi-Square test, Analysis of Variance (ANOVA), or Information gain.

Wrapper: Wrappers evaluate a specific machine learning model sequentially, using each time a different potential subset of features and selecting the optimal one. Even though they have a high chance of success, this comes at the cost of computation time for datasets with many features, and they have a good chance of overfitting. Examples of Wrapper methods are: Forward selection, Backward elimination, or Stepwise selection.

Embedded: This group includes all the machine learning algorithms that have feature selection in their training stage by observing each iteration of the model training phase. These methods place themselves between the Filter and Wrapper methods in terms of time complexity. The embedded methods are often used to reduce overfitting by penalizing the too-large coefficients in a model. Typical examples of embedded methods are Lasso regression and Elastic net. In Lasso regression, the regularization shrinks the coefficients towards zero, penalizing the possibly overfitting complex models. It encourages coefficients to be set to zero, thus discarding some features. Ridge regression allows the coefficients to be very close to zero but never equal to zero. Therefore, it is arguable whether it can be named a feature selection method.

2.3.2 Feature Extraction

While feature selection is a well-defined process, feature extraction is a considerably broader topic, as there are no limits to the creation of features. Accordingly, it often

includes an extensive exploration that requires a considerable amount of time. Although the term "feature" may be used differently depending on the subject, in this work, features represent an addition of information (compared to the raw data) computed either on-board of each sensing modality or as a pre-processing step, such as filters. In this case, features could be considered according to their level: e.g. low-level for on-board features from analog filtering, mid-level for "simple" features with computed filtering, or high-level for more complex features that involve dimensionality reduction, typical in image processing, for instance.

Features extracted from streams of biological signals can be categorized in the time domain, frequency domain, and time-frequency domain. The time-domain features are usually extracted within a fixed-sized window that can overlap or not. Examples are mean, standard deviation, variance, median, signal magnitude, energy, or root mean square, among others. Features in the frequency domain can be e.g. Fast Fourier Transform (FFT), spectral energy, or discrete cosine transform [133]. In the case of images, e.g. with high-density devices such as HD-FMG, spatial features can be extracted by exploiting location information. Algorithms are often employed to detect and isolate desired portions or shapes (features) of an image.

2.4 Multimodality

Multimodality is present in every human being. It is necessary for any individual to combine different sensory modalities to interact with the environment, communicate, make rapid decisions, cross-validate, or strengthen a choice. For instance, a combination of smell, sight, taste, and touch can indicate whether something is edible. Therefore, it seems evident that in order to replicate the human body or understand its intent, it is necessary to call on a multimodality of sensors to analyze and obtain a more robust interpretation.

Multimodality is already used in the field of Biomedical imaging to understand brain functionality [134]. Researchers have tried to present different models to classify and represent sensor fusion [135], some more appropriate than others depending on the issue. This section introduces the ones that seem the most suitable to the topic presented in this thesis.

2.4.1 Fusion Types

Sensor fusion can be categorized by the type of sensor configuration. According to this criterion, Durrant-Whyte identifies three types (or processes, as named in [133]) of sensor fusion [136] (Fig. 2.12):

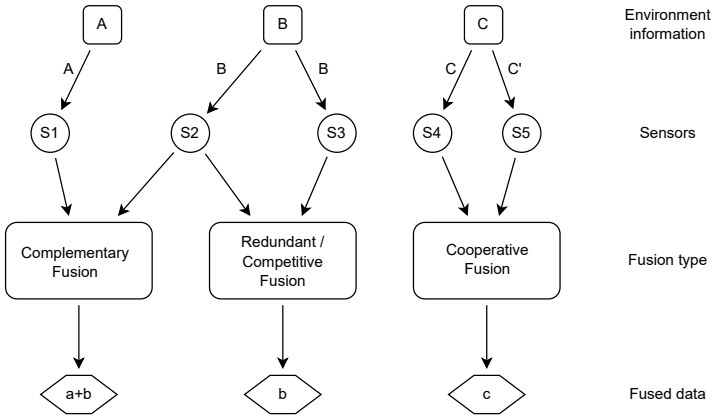

Figure 2.12: Durrant-Whyte's classification of fusion types with relation to data sources: complementary, competitive, and cooperative fusion.

Complementary: A sensor arrangement is said to be complementary if the sensors are not directly dependent on each other but can complement each other with independent information and provide a more comprehensive picture of the measured environment.

Competitive: A competitive sensor configuration would involve sensors that provide independent measurements of the same property of an object in the environment space.

Cooperative: In a cooperative configuration, data provided by two independent sensors are used to derive new information that cannot be acquired by the individual sensors. A good example is stereoscopic vision: by combining 2D images from slightly different viewpoints, a 3D image can be created.

2.4.2 Fusion Strategies

Among the various formalizations of fusion theory that exist [137], the conceptualization presented in [138] seems to be the most fitting one for the problem at hand and body sensor networks (BSN) [133]. The article presents a formal theory of information fusion relying on several subclasses: input-level fusion, layer-level fusion, and high-level fusion. While this thesis will briefly introduce the different types of fusion, the article in [133] additionally presents an interesting literature analysis of the parameters associated with each type in the activity-recognition domain.

Input-Level Fusion:

Input-level fusion (cf. Fig. 2.13), also called data-level, early, or low-level fusion, is the traditional method used in multimodal data analysis. This type of fusion combines several sources of raw data to produce new raw data expected to be more informative

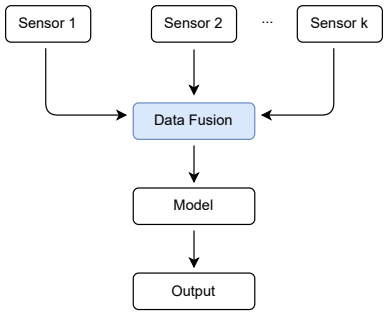

Figure 2.13: Early fusion or input-level fusion.

than the original sources.

One of the main disadvantages of input-level fusion is the possibly differing sampling rates of the different sensors. In that situation, it is desirable to use the same acquisition equipment for all of the sensors. The second disadvantage is that a large amount of data may be discarded in order to create a common ground for the fusion.

Layer-Level Fusion: Layer-level fusion, also called feature- or characteristic-level fusion, joint fusion, or intermediate fusion, consists, as its name implies, in fusing features or characteristics. The features can be, for instance, in the time domain or the frequency domain, as explained in Section 2.3.2. The features from each sensor node can be fused to create a new high-dimension feature vector (cf. Features S12 in Fig. 2.14). Typically, an optimal set of features can be selected using feature selection methods to obtain the most significant features. Therefore, one advantage of feature-level fusion is the detection of correlated features between the sensors and the creation of feature subsets optimizing the recognition accuracy.

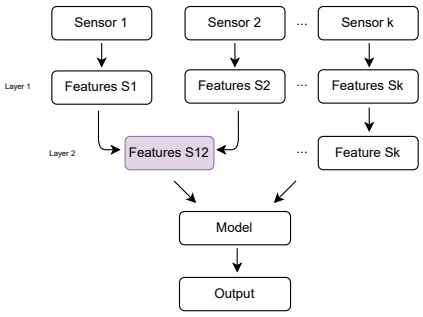

Figure 2.14: Intermediate fusion or layer-level fusion.

The Multiple Kernel Learning (MKL) method is an example of feature-level fusion. It is especially useful in the case of multimodal data. In particular, if each feature requires

a different similarity measure, each mode can have its own kernel, and the multimodal similarity is the weighted sum of each of the kernel functions, as described in more details in Section 3.2.6.

High-Level Fusion: High-level fusion, also called late fusion or decision-level fusion, consists in generating hypotheses or prediction outputs from models fed with extracted features to feed them to another data fusion model, such as majority voting or naive Bayesian approach [133], that would provide the final prediction, as shown in Fig. 2.15.

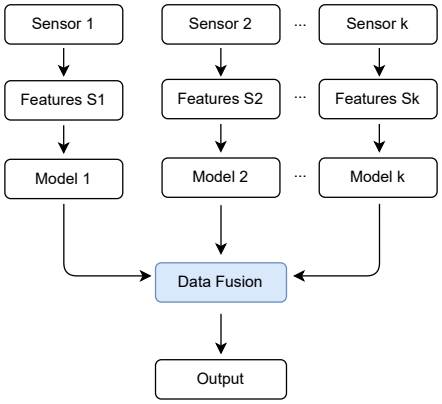

Figure 2.15: Late fusion or high-level fusion.

Multiple-Level Fusion: The fourth type of fusion, multiple-level fusion, uses data provided by different levels of abstraction when e.g. a measurement is combined with a feature to obtain a decision.

2.4.3 Examples for Myocontrol

Since research studies on myocontrol rarely make explicit use of sensor fusion theories, classifying each of them is a difficult task. As shown in [139], most fusion methods use simple concatenation of sensor data features, which could be classified as layer-level fusion. If they were to use raw data, which is uncommon, this could be classified as input-level fusion. The difficulty in labeling them relies on the ambiguity of the "feature" definition in such models. Indeed, while there are rarely any doubts about image-extracted features, filtering is another topic. For example, the typical Mean Average Value (MAV) feature, often associated with sEMG signals, is simply the output of an Average Rectified Value (ARV) filter, and the two terms are used interchangeably. Moreover, some sensors provide an already "featurized" or filtered output. For instance, the *Myobock* sensor from *Ottobock* directly outputs a rectified signal. Similarly, some IMUs perform embedded sensor fusion and provide a rotation vector directly.

Despite this, some exceptions do make use of sensor fusion theories and go further than simple concatenation. For example, in [140], both layer-level and high-level strategies were compared for multimodal fusion of PPG, FMG, and accelerometry. The layer-level algorithm consists in a multi-head attention mechanism fusion convolutional neural network (CNN-AF). In contrast, the high-level one consists in a multi-head decision fusion convolutional neural network (CNN-DF). The latter generally obtained the best performance for each sensor configuration.

In [141], the authors propose a multimodal grasp classifier that integrates sEMG, accelerometry and high-level visual feature representation of the object gazed at during the prehension. In their approach, each input sample consists of the concatenation of different sensor modalities, and the similarity between pairs of input samples is defined as a weighted sum of modality-specific kernel functions. The results show that the addition of gaze tracking marginally increases the classification accuracy.

Chapter 3

Methods

Il n'y a pas une méthode unique pour étudier les choses.

(Aristote)

Table of Contents

3.1 Sensor Modalities and Data Acquisition

This section describes the devices used or developed for multimodality acquisition, as well as the optimal way for collecting and comparing the different modalities.

3.1.1 Comparison of Sensor Modalities, Placement, and Data Acquisition

There are two options in terms of user study design. The between-subjects design consists in having different groups of participants for each condition, i.e. here every single modality. However, due to each individual having a diverse morphology, the comparison would be less efficient. In order to have statistical significance and due to the high number of sensor modalities possible, this method would require a very large amount of participants. The within-subjects design, in which all participants engage in every condition, is preferred to the between-subjects design, as it requires fewer subjects for stronger statistical significance. The following suggestions for sensor placements are based on the within-subjects design.

The ideal way to compare two modalities would be to place them at the exact same location on the forearm, i.e. in the same sensor housing, to ensure the measurement of the same phenomenon. Although novel co-located sensors have been built in recent years for some modalities, e.g. with sEMG and FMG [57, 142, 143], sEMG and EIT [144, 145], or sEMG and ultrasound A-mode [146], their integration is complex and time-consuming. Except for sEMG and IMUs within e.g. *Delsys Trigno* electrodes, there is currently no commercially available option for co-located sensors.

Another good alternative, albeit still time-consuming, is the development of a multi-modal acquisition device to have the same frame rate for a possible fusion of the modalities

collected. This was the chosen option for comparing FMG and sEMG in A.1. Integrating deep modalities into such a device, though not impossible, would require significantly more complex electronic circuits. Indeed, these modalities are not passive like FMG and sEMG, but active with the injection of current into the body in the case of EIT or sound-waves for ultrasound. In A.3, separate data acquisition devices for EIT and portable ultrasound were necessary, as the prototypes had been newly created by different research institutions.

In terms of placement of sensor modalities, a solution for comparison would be to place all modalities at once on the forearm of participants and perform an experiment. This solution was chosen in A.3 due to the high precision of the ultrasound modality and the fact that three modalities were tested. The placement order from the proximal to the distal position on the forearm is then important and will now be explained for each modality. In all the core publications of this thesis, the sensors of one modality are arranged evenly around the forearm, except for ultrasound, due to the nature of the probe and of the modality itself. It has been shown that exact location of sEMG electrodes is not necessary to extract distinct patterns [147–149], and the electrodes are commonly distributed uniformly around the forearm on the apex of the muscle bulge [150, 151], i.e. 2-3cm distal to the elbow crease, which is a similar position as within prostheses. In order to measure the muscular pressure generated at the surface of the forearm, the same location is preferable, at the apex of the muscle bulge [152]. Although EIT placement evaluations are still lacking for myocontrol, the modality has been shown to work both at the proximal (muscle bulge) [153] and distal (wrist) [50] position. However, the device developed in [154] has never been tested at the wrist level. Placement on the bulge of the forearm is thus preferred. For ultrasound, while the muscular distortion was shown to be significant between 30-50% of forearm length from the elbow [155], Mcintosh et al. found that the wrist area is the most efficient site for classifying discrete movements after evaluating various locations and orientations [156]. This location was further supported in [157], where an evaluation at the wrist showed a linear relation to finger position. The probe should be positioned on the ventral side of the forearm to avoid a large part of the pulses being reflected on the bones if it were located on the dorsal side. Therefore, in A.3, the modalities were placed in the following order from proximal to distal: first EIT, second FMG, and finally ultrasound.

While this solution was chosen in A.3 due to the high precision of the ultrasound modality, a different technique called mirrored training is possible. Based on the fact that, during mirrored bilateral contractions, the neuromuscular control information is similar in the two upper limbs [158, 159], several studies have used mirrored training for myocontrol [34, 148, 160]. As only two modalities were evaluated in A.1, this was the chosen solution to have the same location for each modality, FMG and sEMG, on the ipsilateral and contralateral sides.

Comparing all modalities at once, without any kind of integrated multimodal acquisition device, would be impossible, due to the limited space on the forearm for all modalities

and some of them potentially interfering with each other. Indeed, active and passive modalities should be carefully selected as, for instance, the current injected for EIT might influence the difference of potential measured by sEMG sensors. Hence, to simplify, a modality that would perform better than the gold standard sEMG could then be used as a reference for future comparisons.

3.1.2 Surface Electromyography

Surface electromyography, as Section 2.2.2.1 describes in more detail, measures the electrical activity in the muscles. As shown in Fig. 2.4, several systems exist for measuring this modality.

In the articles underlying this thesis, two types of sEMG sensors were used. The first one, in A.1, is the *MyoBock 13E200=50* sensor from *Ottobock*. Ten sensors were worn to gather the sEMG signals. They provide on-board amplification, rectification, and filtering. These sensors are standard in clinical applications, especially in prosthetic sockets. They were gathered by the data acquisition board developed in Section 3.1.3, providing data at a frequency of 100Hz, with a resolution of 12-bit unsigned.

The second type of sensor, used in A.4, is the Myo-armband from *Thalmic Labs*. Two bracelets were chosen over the data acquisition device with *Ottobock* sensors (cf. Fig. 3.1) from A.1, developed for this thesis, due to the fact that they are easy to don and doff and an IMU tracker can be easily placed on top of them. One bracelet has eight electrodes and runs at a frequency of 200Hz via Bluetooth with a resolution of 8-bit unsigned int. Both of these sensors should provide a double differential signal (cf. Fig. 2.5).

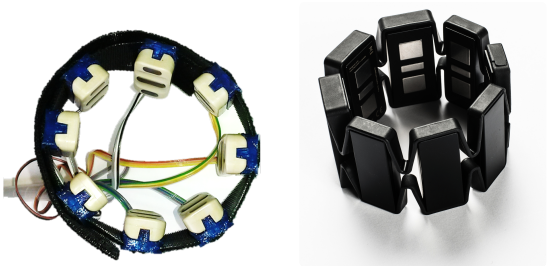

(A) **(B)**

Figure 3.1: Surface electromyography sensor bracelets used in the different core publications. (A) Sensor bracelet with *Myobock* sensors from *Ottobock* adapted for the custom-made data acquisition device of A.1. (B) Myo-armband from *Thalmic Labs* used in A.4.

3.1.3 Multimodal Sensor Acquisition Device: Force Myography and Electromyography

In order to compare force myography with surface electromyography in A.1, the ideal solution is to have the same data acquisition board and, therefore, the same sampling frequency for the two modalities. For this purpose, the device depicted in Fig. 3.2 was built. The device additionally provides a wearable setup adaptable for prosthesis use, as in [68].

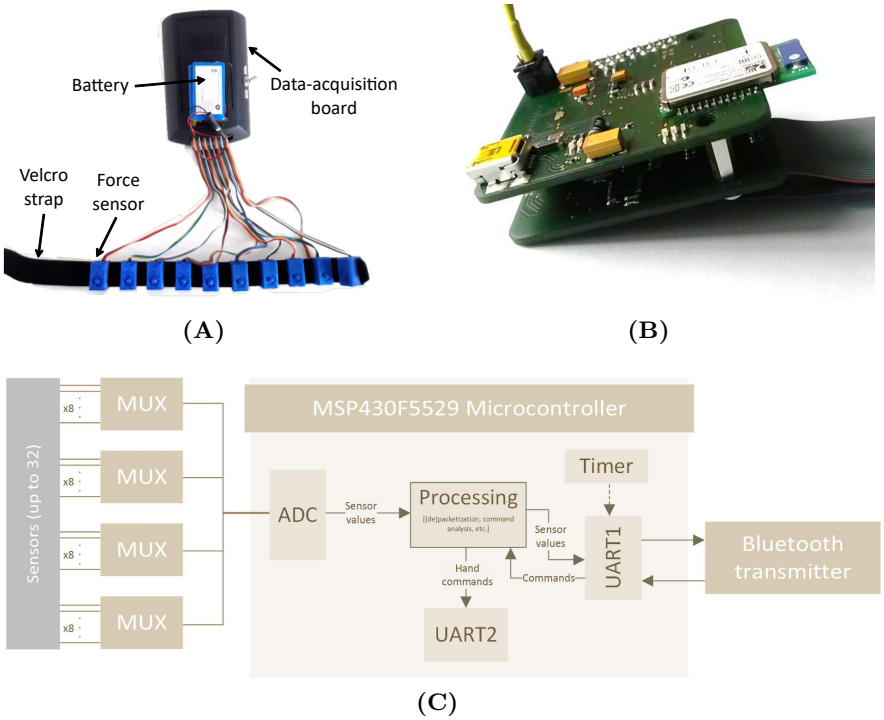

Figure 3.2: Multimodal device developed in A.1. (A) Custom-made data acquisition device for force myography. (B) Data acquisition board. (C) Functional block representation.

Data Acquisition Board Design

The data acquisition board consists of a *Texas Instrument MSP430F5529* microcontroller and an on-board Bluetooth chipset. It provides analog-to-digital conversion for both sEMG and FSR sensor signals. As the microcontroller supports only 15 AD-channels, analog multiplexers were added to provide AD-conversion for up to 32 sensors with a maximum sampling frequency of 192.5Hz. Since the sEMG sensors from *Ottobock* already provide a rectified and filtered signal with an evaluated bandwidth limited to 10Hz, the provided sampling rate is oversampling [161]. As it can be seen on Fig. 3.2C, two UARTs are fitted in the microcontroller, communicating respectively with the prosthesis (via

RS232 protocol) and the computing platform (via serial-over-Bluetooth), which can be either a computer or a smartphone.

Wearable Device Data Processing In order for the device to be usable at home by people with limb difference, the machine learning algorithm mentioned in 3.2.7 was implemented in an Android app, developed within the scope of this thesis, in which the user can collect data, train the model, update it, and control a prosthetic hand. The protocol was here developed for the *i-Limb* hand from *Össur* (formerly *Touch Bionics* before acquisition) but can be easily adapted for other prostheses. This device makes data collection in the home environment possible with its high modularity and flexibility.

Force Sensor Design The pressure sensors employed in this study also had to be designed and adapted to be functional when used jointly with the *Ottobock* sEMG sensors. Therefore, the FSR housings are created the same size as the *Ottobock* ones so that both type of sensors can be placed on one bracelet while still being in contact with the skin. The housing has been designed not only to be a retainer but also to transfer force between the muscle and the FSR's sensitive area with a conic shape pointing towards the sensor and held to the main part by a thin, flexible membrane (cf. Fig. 3.3). This flexibility of the housing was achieved by 3D-printing it with the *Ninjaflex* material of shoreness 85A.

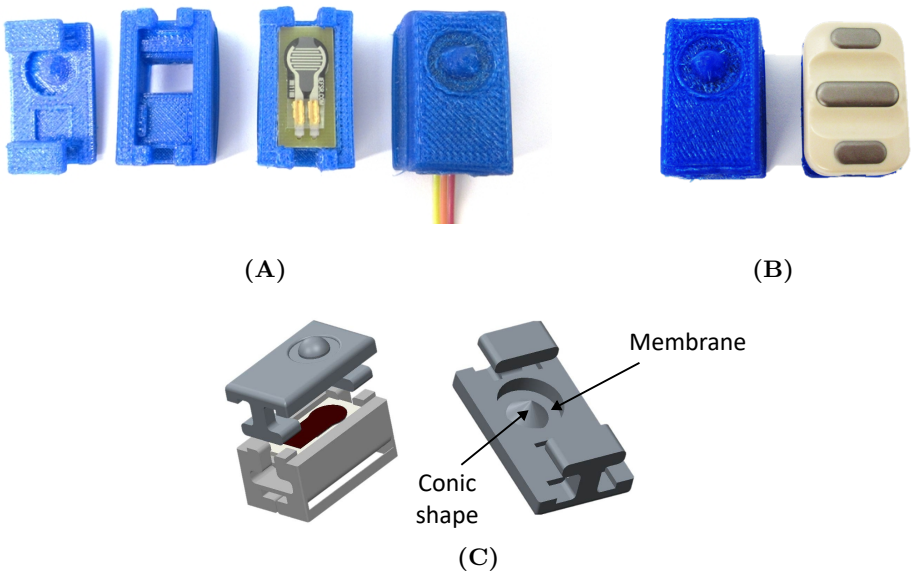

Figure 3.3: Pressure sensor design in A.1. (A) Decomposition of an FMG sensor with the FSR board and its 3D printed flexible housing. (B) Comparison of FMG and sEMG sensors. (C) Exploded view of the housing's CAD (Computer Aided Design) model.

3.1.4 High-Density Force Myography

The high-density force myography system used in A.2 was developed by the *University of Bielefeld (CI-TEC)* [162]. The Tactile Bracelet, as it is called, is typically worn on the muscle bulge around the forearm (cf. Fig. 3.4) and has a spatial resolution of 5mm. Up to 10 sensor modules, with 4x8 pressure cells each, can be placed around the forearm, depending on its circumference.

Each module is covered by a conductive elastomer foam and each pressure cell is composed of two M-shaped electrodes made of a golded Printed-Circuit-Board (PCB). A cell's resistance consists in the sum of the foam resistance and the two contact resistances between the foam and the electrodes. When the conductive foam is pressed, its resistance decreases as more contact points are made between the conductive particles. This principle enables the measurement of the pressure exerted on the modules.

The data of up to 320 tactile cells are sampled at 100Hz for each module, with a communication via Serial Peripheral Interface (SPI) protocol for every module. The readout electronics use a *Microchip PIC32MZ* microcontroller running at 80MHz. It was connected via a USB cable to a computer for performing the experiment described in Section 3.5.2 and powered via a medically certified power supply with a consumption of 12W.

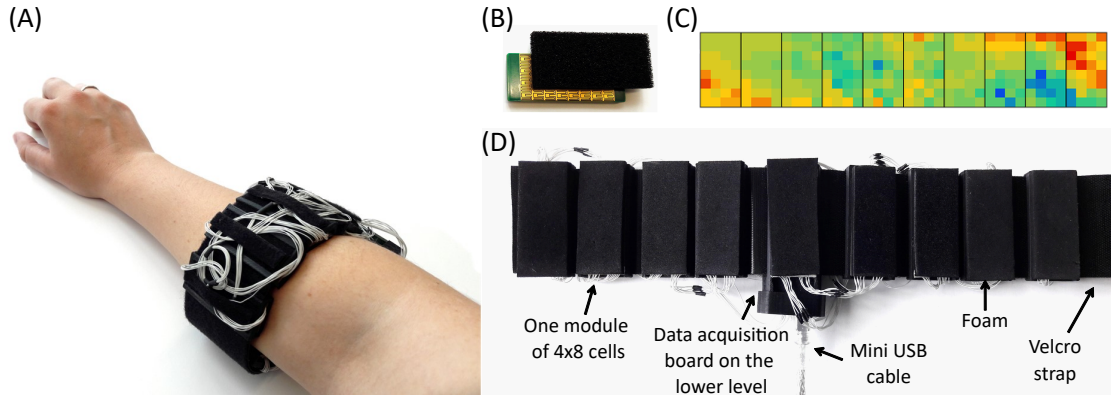

Figure 3.4: High-Density Force myography device used in A.2. (A) HD-FMG bracelet from Bielefeld University worn on the forearm. (B) One sensor board of the HD-FMG bracelet with its foam. (C) Map visualization of the HD-FMG data. (D) Description of the HD-FMG bracelet.

3.1.5 Ultrasound

The ultrasound system, called MoUsE (for Mobile Ultrasound Equipment), used for comparison in A.3, has been developed by the *IBMT Institute* of *Fraunhofer* [83]. It

uses 32 channels that both transmit and receive to control a phased array transducer (32 elements, 3MHz center frequency, 0.5mm pitch). It measures up to 21 plane wave angles per image with a variable depth (120mm in this case). The receiver has a bandwidth of 100 kHz–10 MHz and a sampling rate of up to 50MHz. The data is transmitted via USB3 to a *Surface* tablet computer from *Microsoft* (Intel M3-8100Y with integrated GPU and 8GB of internal RAM). The Beamforming reconstruction (cf. Fig. 3.5) is performed with a plane-wave compounding algorithm [163]. Considering the system frame rate and the achievable reconstruction speed, the bottleneck in terms of speed is actually the data transfer from the electronics to the tablet computer. The device has a power consumption of 12W and is powered by a medically certified power supply (12V DC), with a plan to develop a fully wearable version on Lithium-ion battery in the future [83].

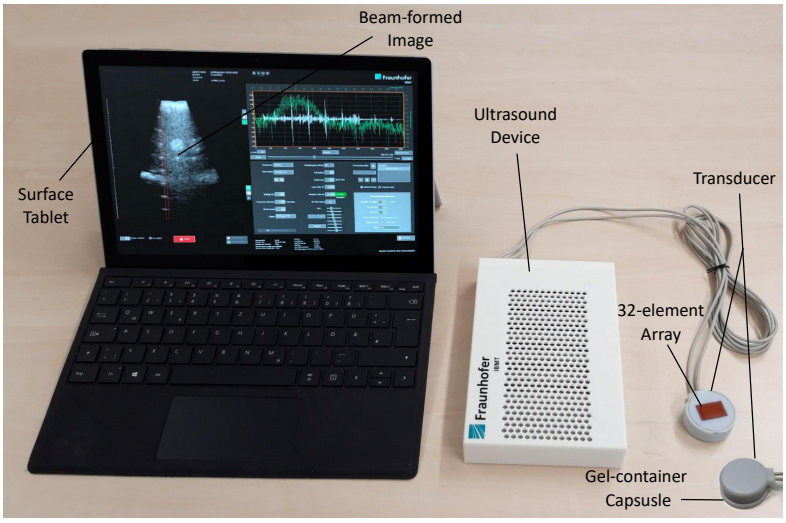

Figure 3.5: Ultrasound system MoUsE from the *IBMT Institute* of *Fraunhofer*.

3.1.6 Electro-Impedance Tomography

The Electro-Impedance Tomography device used to acquire the dataset in A.3 has been developed by the *University of Siegen* [154]. The modular system allows for different measurement patterns, data acquisition schemes, and excitation signals. Separate electrode contacts are employed for current injection and measurement (cf. Fig. 3.6). The excitation frequency is set at 50kHz (sinusoidal waveform with an RMS value of 5mA).

The bracelet comprises $N = 16$ electrodes and the adjacency pattern, also called the adjacent drive method [164], as explained in Section 2.2.3.1 and depicted in Fig. 2.8, is used for the data acquisition. The adjacent drive method consists in injecting a current in one pair of adjacent electrodes and recording the potential difference in the remaining adjacent pairs sequentially. The current is injected into all sequential pairs of electrodes

in turn until the completion of a full circle, therefore completing one measurement. Since it is not possible to measure the voltage accurately at the pair of electrodes injecting the current, these are excluded from the measurements. This method resulted in $N(N-3) = 208$ measurements per frame. For tomographic reconstruction, 256 values are processed, but the remaining $3 \times N = 48$ values are placeholders set to 0 to indicate where the current is presently being fed in. The system provides an overall frequency of ca. 2.7 frames per second.

For the tomographic reconstruction, we used the EIDORS library [165], an open-source library targeted specifically for EIT. The tomographic reconstruction of EIT data is explained in Section 3.3.2.3.

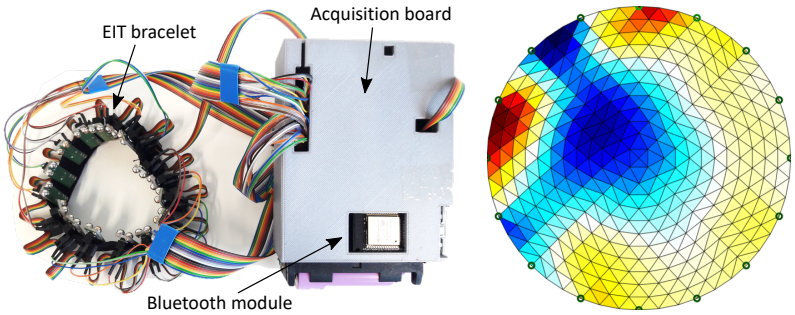

Figure 3.6: Electro-Impedance Tomography. (A) Custom-made EIT bracelet from the *University of Siegen*. (B) Example of a tomographic reconstruction from an EIT bracelet.

3.1.7 Kinematics Parameters and Inertial Measurements

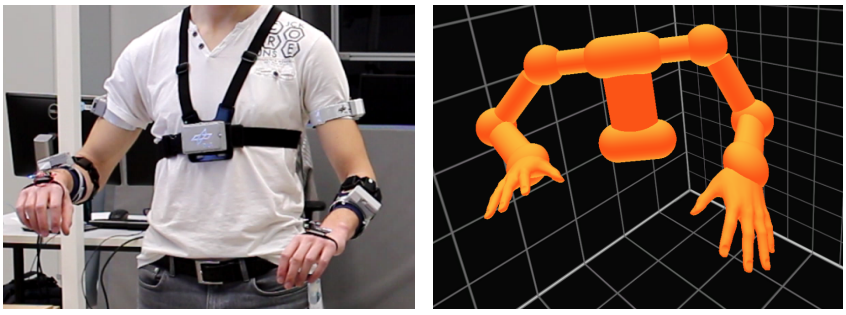

Figure 3.7: (A) The Bodyrig IMU-tracking device worn with a central IMU on the torso and additional IMUs on each limb segment. (B) 3D visualization with a virtual avatar controlled by the IMU-tracking device.

A wearable setup combining electromyography and kinematics was used in A.4. In order to determine the kinematics of the upper body, an IMU-based body tracking device, also called the Bodyrig, designed and developed specifically for this thesis, was employed (cf. Fig. 3.7). It measures, by using IMUs, the absolute orientation in space of a person's limbs and trunk. These orientations are then processed to calculate the forward kinematics of the upper body using a set of pre-defined link lengths.

The Bodyrig consists of three modules for each arm and one on the torso, as represented in Fig. 3.8. Each module is composed of a *Bosch BNO055* IMU connected via I^2C to a *Bluefruit Feather nRF52832* board from *Adafruit*, with BLE (Bluetooth Low Energy) capability. The central piece located on the torso gathers the data transmitted from the peripherals on the limbs and forwards it to a host computer via classic Bluetooth with Serial Port Profile (SPP), using an RN41 module from *Microchip Technology*.

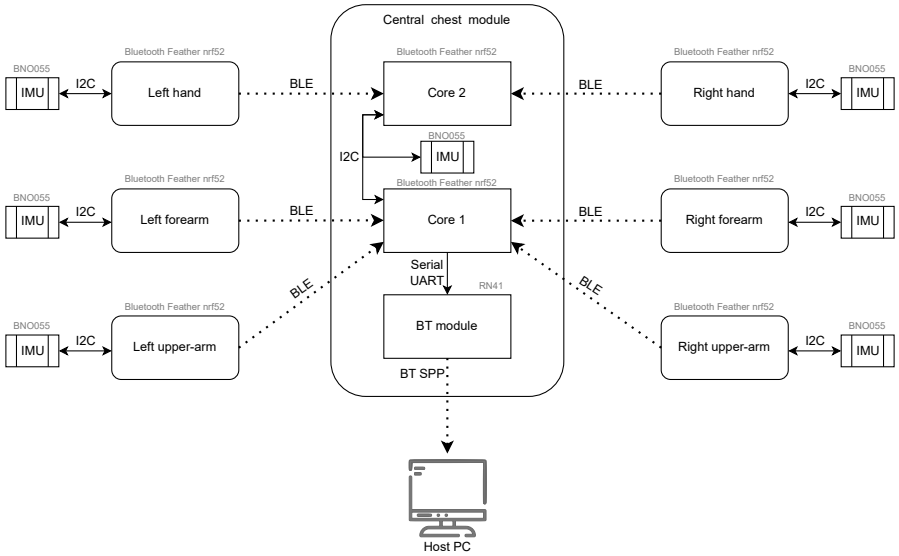

Figure 3.8: Block diagram of the hardware setup of the Bodyrig.

3.2 Machine Learning

The large majority of myocontrol studies involve classification [23, 139, 166]. Although some effort has been made to control more than one class at a time [167, 168], the speed of each DoF cannot be controlled independently when their respective classes are activated simultaneously [34]. Thus, despite the generally high levels of accuracy reported in offline studies, clinical classification-based approaches still remain with a sequential output [34], i.e. one DoF at a time, impeding intuitive and smooth movement control. Regression is the technique of choice in this thesis for assessing the various modalities, as it allows independent simultaneous and proportional control [34].

For the different modalities, it will be necessary to evaluate whether to use linear or non-linear regression. In fact, it is not obvious whether a linear or a non-linear approach is superior, depending on the kind of sensors being utilized and their density. Additionally, linear approaches are typically easier to understand and use, which is relevant for online myocontrol, where the user participates in the control loop. As this thesis will show, each of them has advantages and disadvantages.

The machine learning models employed in this thesis in order to associate data from biosensors to kinematic variables of the hand are based on the ridge regression algorithm [169]. Ridge regression generates a prediction matrix to control an output device, such as a virtual 3D model of a human hand or a hand prosthesis (cf. Fig. 2.10). This section explains how this prediction matrix is created.

3.2.1 Linear Regression

A linear regression algorithm estimates the parameters of a mapping vector $\mathbf{w}$ based on a set of input and output values. Supposing an output of only one DoF and given a training set of $m \in \mathbb{N}$ input-output pairs $(y_i, \mathbf{x}_i)$, with $y_i \in \mathbb{R}$, $\mathbf{x}_i \in \mathbb{R}^n$, n the number of features, and $i \in \{1, ..., m\}$, the linear regression equation is:

$$y_i = w_1 \, x_{i1} + ... + w_n \, x_{in} = \mathbf{x_i}^\mathsf{T} \, \mathbf{w} \; . \tag{3.1}$$

The vector of output values for all samples is then equal to:

$$\mathbf{y} = \boldsymbol{X}\mathbf{w} \; ,$$

with:

$\mathbf{y}$: m-dimensional vector, set of m samples of output values,
$\mathbf{w}$: n-dimensional vector, called parameter vector, or weight vector,
$\mathbf{x_i}$: n-dimensional vector,
$\boldsymbol{X}$: (m × n) matrix, called design matrix, $\boldsymbol{X} = \begin{bmatrix} \mathbf{x_1}^\mathsf{T} \\ \mathbf{x_2}^\mathsf{T} \\ \cdots \\ \mathbf{x_m}^\mathsf{T} \end{bmatrix}$.

For simplicity, a 1-DoF output was considered in this explanation. In the case of the experiments presented in the core publications of this thesis, the output of the machine learning model consists in several DoFs for controlling individual fingers and/or wrist movements. In such a case, it is the equivalent of training p 1-DoF regressors, with p being the number of DoFs to control.

3.2.2 Ridge Regression

Ridge regression is a commonly used regularization method for ill-posed problems. Specifically, ridge regression estimates the parameter $\mathbf{w}$ of a linear relationship (3.1) by

minimizing the loss function:

$$||\mathbf{y} - \boldsymbol{X}\mathbf{w}||^2 + ||\lambda\mathbf{w}||^2 \ ,$$

where $||.||$ is the Euclidian norm. Indeed, the classical approach to approximate the solution of over-determined systems of linear equations, such as

$$\mathbf{y} = \boldsymbol{X}\mathbf{w} \ ,$$

is called the method of least squares. This method consists in minimizing the sum of squared residuals

$$||\mathbf{y} - \boldsymbol{X}\mathbf{w}||^2 \ .$$

However, the $\boldsymbol{X}$ matrix can be ill-conditioned or not invertible, which can lead to a high number of solutions. In order to privilege a particular solution with interesting properties, a regularization term $\boldsymbol{\Gamma}$ is included:

$$||\mathbf{y} - \boldsymbol{X}\mathbf{w}||^2 + ||\boldsymbol{\Gamma}\mathbf{w}||^2 \ ,$$

where $\boldsymbol{\Gamma}$ is called Tikhonov matrix. It is often chosen as a multiple of the identity matrix: $\boldsymbol{\Gamma} = \lambda\boldsymbol{I}$. This is also known as L_2 regularization. The $\mathbf{w}$ that minimizes this sum is:

$$\mathbf{w} = arg\ \underset{\mathbf{w}}{min}\ ||\mathbf{y} - \boldsymbol{X}\mathbf{w}||^2 + ||\lambda\mathbf{w}||^2 \ .$$

The explicit solution is given by:

$$\mathbf{w} = (\boldsymbol{X}^\mathsf{T}\boldsymbol{X} + \lambda\boldsymbol{I})^{-1}\boldsymbol{X}^\mathsf{T}\mathbf{y} \ . \tag{3.2}$$

Training the model consists in finding the weight vector $\mathbf{w}$, by using a set of input-output samples, the output being the ground truth in that case. Once the weight vector is determined, it can be used to predict an output according to an input vector $\mathbf{x_i}$, following the Eq. (3.1).

3.2.3 Incremental Ridge Regression

One of the motivations for using the Ridge Regression is that it allows incremental learning: for each new sample, the model can be updated without storing former training samples, as the required information is contained in the model. Indeed, Eq. (3.2) can be rewritten:

$$\mathbf{w} = (\boldsymbol{X}^\mathsf{T}\boldsymbol{X} + \lambda\boldsymbol{I})^{-1}\boldsymbol{X}^\mathsf{T}\mathbf{y} = \boldsymbol{A}^{-1}\boldsymbol{\beta} \ , \tag{3.3}$$

with:

$\boldsymbol{A}$: (n × n) matrix $\boldsymbol{A} = \boldsymbol{X}^\mathsf{T}\boldsymbol{X} + \lambda\boldsymbol{I}$,
$\boldsymbol{\beta}$: n-dimensional vector $\boldsymbol{\beta} = \boldsymbol{X}^\mathsf{T}\mathbf{y}$.

Adding a new training sample $(\mathbf{x}_t, y_t)$ at time t corresponds to appending an extra row to both $\boldsymbol{X}$ and $\mathbf{y}$:

$$\boldsymbol{X}_t = \begin{bmatrix} \boldsymbol{X}_{t-1} \\ \mathbf{x}_t \end{bmatrix} \quad and \quad \mathbf{y_t} = \begin{bmatrix} \mathbf{y}_{t-1} \\ y_t \end{bmatrix} .$$

$\boldsymbol{X}_t$ may be replaced in the equation of matrix $\boldsymbol{A}$ to obtain:

$$\begin{aligned} \boldsymbol{A}_t &= \lambda\boldsymbol{I} + \boldsymbol{X}_t^\mathsf{T}\boldsymbol{X}_t \\ &= \lambda\boldsymbol{I} + \boldsymbol{X}_{t-1}^\mathsf{T}\boldsymbol{X}_{t-1} + \mathbf{x}_t\mathbf{x}_t^\mathsf{T} \\ &= \boldsymbol{A}_{t-1} + \mathbf{x}_t\mathbf{x}_t^\mathsf{T} . \end{aligned}$$

As shown in this equation, storing previous samples in memory is no longer necessary: incremental learning can be applied to reduce computational needs for future embedding.

Adding a new sample to the training consists in updating $\boldsymbol{A}$ and $\boldsymbol{\beta}$. Under this form, the Sherman-Morrison can be applied:

$$\boldsymbol{A}_t^{-1} = (\boldsymbol{A}_{t-1} + \mathbf{x}_t\mathbf{x}_t^\mathsf{T})^{-1} = \boldsymbol{A}_{t-1}^{-1} - \frac{\boldsymbol{A}_{t-1}^{-1}\mathbf{x}_t\mathbf{x}_t^\mathsf{T}\boldsymbol{A}_{t-1}^{-1}}{1 + \mathbf{x}_t^\mathsf{T}\boldsymbol{A}_{t-1}^{-1}\mathbf{x}_t}. \tag{3.4}$$

From this, the weight vector $\mathbf{w}$ of Eq. (3.3) can be recalculated with the additional update sample.

The initial training of this algorithm has a time complexity of $\mathcal{O}(mn^2)$, while the incremental update has a time complexity of $\mathcal{O}(n^2)$. The complexity for the prediction of one sample is $\mathcal{O}(n)$.

This algorithm has been used in the core publications A.2 and A.3.

3.2.4 Kernel Methods for Non-linear Regression

Like several other methods, Ridge regression learns the parameters based on the mutual similarity between couples of training samples in the input space. However, Ridge Regression is limited due to its linearity.

Non-linearity can be obtained by mapping the inputs in a feature space of interest and computing the similarity in that space. However, calculating the similarity between samples in an explicitly computed feature space can be computationally expensive, especially if the feature space is high-dimensional.

Alternatively, non-linearity can be achieved without explicitly mapping the inputs in a higher dimensional (possibly infinite) feature space by adopting specific similarity functions called kernel functions.

By definition, the effect of a kernel function is to compute the inner product between the images of the input samples into a kernel-induced feature space:

$$k(\mathbf{x_i}, \mathbf{x_j}) = \hat{\phi}(\mathbf{x_i})^\mathsf{T} \hat{\phi}(\mathbf{x_j}) \ ,$$

where $\hat{\phi} : \mathbb{R}^n \to \mathbb{R}^D$ is a mapping to the kernel-induced feature space and $\mathbf{x_i}$ and $\mathbf{x_j}$ are two samples.

The output of these kernel functions corresponds to the similarity between two samples in the kernel-induced feature space without having to map the samples in that space explicitly. This is known as the kernel trick [170].

The predicted function y for kernel ridge regression (KRR) [171] is obtained by the following formula:

$$y = \boldsymbol{y}(\boldsymbol{K} + \lambda' \boldsymbol{I})^{-1} \boldsymbol{k}(\boldsymbol{x}) \ , \tag{3.5}$$

where $\boldsymbol{y}$ is the m-dimensional vector of labels, $\boldsymbol{K}$ is the kernel matrix or Gram matrix, defined such that the i,j element is equal to $k(\mathbf{x_i}, \mathbf{x_j})$, where $\mathbf{x_i}, \mathbf{x_j}$ are samples of the training set. $\boldsymbol{k}(\boldsymbol{x})$ is defined such that the $\boldsymbol{k}(\boldsymbol{x}) = k(\boldsymbol{x_i}, \boldsymbol{x})$.

The initial training of kernel ridge regression has a time complexity of $\mathcal{O}(m^3)$. The complexity for the prediction of one sample is $\mathcal{O}(m)$.

This kernel trick is especially convenient if the desired feature space is high-dimensional. Specific kernels even allow implicit mapping in an infinite dimensional feature space. This is the case for the Gaussian kernel, also known as the Radial Basis Function Kernel, which is the most commonly used kernel.

3.2.5 Radial Basis Function Kernel

For two samples $\mathbf{x_i}$ and $\mathbf{x_j}$, the standard Radial Basis Function (RBF) kernel is defined as:

$$k_{RBF}(\mathbf{x_i}, \mathbf{x_j}) = exp(-\gamma ||\mathbf{x_i} - \mathbf{x_j}||^2) \quad for \quad \gamma > 0 \ . \tag{3.6}$$

If $\gamma = \sigma^{-2}$, the kernel is known as the Gaussian kernel of variance σ^2.

RBF kernels are known to perform very well on a large variety of problems as they are highly flexible. Their flexibility is partially due to their hyperparameter tuning, which allows adjustment between underfitting and overfitting.

3.2.6 Multimodal Kernel Integration

Among the different fusion methods described in Section 2.4.2, layer-level fusion, also known as mid-level integration, and more specifically the method of Multiple Kernel Learning or integration at the kernel level was chosen based on [141]. For multimodal data input vectors $(\mathbf{x}^1, ..., \mathbf{x}^L)$ with L modalities, the multimodal kernel is the weighted sum of the kernels for each modality. For two samples $\mathbf{x_i}$ and $\mathbf{x_j}$, the multimodal kernel is defined as:

$$k_{mmd}(\mathbf{x_i}, \mathbf{x_j}) = \sum_{p=1}^{L} w_p \, k_p(\mathbf{x_i}^p, \mathbf{x_j}^p) \; . \tag{3.7}$$

RBF kernels were used in A.3 to ensure that the outputs of the kernels of each modality are in the range $[0, 1]$. In A.3, three modalities were fused: FMG, EIT, and ultrasound. The multimodal kernel is a weighted sum of the modality-specific kernel functions:

$$\begin{aligned} k_{mmd}(\mathbf{x_i}, \mathbf{x_j}) = \; & w_{FMG} \, k_{RBF}^{FMG}(\mathbf{x_i}^{FMG}, \mathbf{x_j}^{FMG}) \\ & + w_{EIT} \, k_{RBF}^{EIT}(\mathbf{x_i}^{EIT}, \mathbf{x_j}^{EIT}) \\ & + w_{US} \, k_{RBF}^{US}(\mathbf{x_i}^{US}, \mathbf{x_j}^{US}) \; . \end{aligned} \tag{3.8}$$

The individual RBF kernels and the multimodal kernel require optimization of the regularization parameter λ, the RBF kernel hyperparameters γ_{RBF}, and the combination weights w_p, with $p \in \{1, ..., L\}$. The parameters were optimized with k-fold cross-validation on the repetitions. In the case of the experiment in A.3, the first two repetitions of the training set were used for the validation, one fold corresponding to one repetition.

By allowing its coefficients to be set to zero, thus discarding some features, ridge regression with RBF kernel can be considered as an embedded feature selection algorithm, as described in Section 2.3.1. It might therefore be an advantageous model for high-density modalities in order to avoid overfitting.

The multimodal algorithm with RBF kernels has been employed in Section 4.3.3 with the data of the core publication A.3, implemented with the help of the *Himalaya* python library [172].

3.2.7 Kernel Approximation with Random Fourier Features

Nevertheless, even though kernel methods highly increase the capacity of Ridge Regression, a side effect is that the computational cost for predictions and incremental updates is dependent on the number of training samples. This means that the time and memory consumption is increasing for each additional sample: Kernel Ridge Regression (KRR) is thus limited for real-time machine learning.

This constraint can be circumvented by approximating the kernel function with a finite-dimensional feature mapping. In their paper on Random Features for Large-Scale Kernel Machines [173], Rahimi and Recht have suggested using Random Fourier Features (RFF). The strategy consists in taking a finite number of random samples in the Fourier domain of shift-invariant kernel functions, such as the RBF kernel. The equation for the RFF can be given as [171, 174]:

$$\phi(\boldsymbol{X}) = \sqrt{2}\, cos(\boldsymbol{\Omega}^{\mathsf{T}} \boldsymbol{X} + \boldsymbol{B}) \;,$$

with:

$\boldsymbol{\Omega}$:	drawn from a Gaussian distribution, (m × D) matrix,
$\boldsymbol{B}$:	drawn from a uniform distribution from 0 to 2π, (D × n) matrix,
D:	number of Random Fourier Features.

3.2.8 Incremental Learning with Random Fourier Features

Then, the optimal D-dimensional weight vector $\widehat{\mathbf{w}}$ can be obtained with the following equation, replacing $\boldsymbol{X}$ by $\boldsymbol{\Phi} = \phi(\boldsymbol{X})$ in Eq. (3.2):

$$\widehat{\mathbf{w}} = (\boldsymbol{\Phi}^{\mathsf{T}} \boldsymbol{\Phi} + \lambda \boldsymbol{I})^{-1} \boldsymbol{\Phi}^{\mathsf{T}} \widehat{\mathbf{y}} \;, \tag{3.9}$$

with:

$\boldsymbol{\Phi}$:	$\boldsymbol{\Phi} = \phi(\boldsymbol{X})$, (D × n) matrix.

The formulation Eq. (3.9) is equivalent to Eq. (3.3), and the algorithm solution is the same, replacing $\boldsymbol{X}$ by $\boldsymbol{\Phi} = \phi(\boldsymbol{X})$.

The initial training of this algorithm has a time complexity of $\mathcal{O}(mD^2)$ while the incremental update has a time complexity of $\mathcal{O}(D^2)$. The complexity for the prediction of one sample is $\mathcal{O}(D)$.

This algorithm, called Ridge Regression with Random Fourier Features (RR-RFF), has been used in A.1 and A.4.

3.3 Features

3.3.1 Features for Low-Density Modalities

As mentioned in Section 2.3.2, for low-density modalities, features can be in the time domain or in the frequency domain. For sEMG specifically, several features have already been studied in the past decades: integrated EMG, mean absolute value, variance of EMG, root mean square, waveform length, zero crossing, and slope sign change are some

of these features [35, 175, 176].

The Mean Absolute Value (MAV), also called Averaged Rectified Value (ARV) filter, is one of the most used of the time-domain features. It consists in the mean of the rectified amplitude of the signal over a certain window length of N samples.

$$MAV = \frac{1}{N}\sum_{i=1}^{N} |\mathbf{x_i}| \, . \tag{3.10}$$

On the contrary to other more specific features that might be more adapted for classification, the MAV does not introduce non-linearity in the signal, which is a desired characteristic for testing combined actions, as evaluated in A.2.

For force myography, there are fewer features used in the literature as it is a relatively recent modality, and only a limited number of publications chose to extract features from FMG signals [97]. Although some researchers have evaluated more specific features for gesture classifications with FMG [177], the developed pipeline has only been tested for classifiers, not regressors. An extensive study on FMG feature extraction for regression is still necessary.

3.3.2 Features for High-Density Modalities

3.3.2.1 Region of Interest Gradient

In article A.2, a low-pass first-order Butterworth was implemented to filter the HD-FMG data with a cut-off frequency of 1Hz to attenuate the high-frequency noise, as already used in [5, 9].

Two feature selection methods were compared when fed to a RR algorithm. The first one had already been implemented successfully in previous online studies with the same HD-FMG bracelet [5, 9] and consisted of the data only processed by the Butterworth filter mentioned above. The data consisted of 288 filtered sensor data (9 boards of 32 sensors each).

The second feature selection approach was Gradient-based features extracted from Regions of Interest (ROIs) [178], also called Region of Interest Gradient (ROIG). The method was already exploited in ultrasound image processing for single-finger intent detection [48, 179, 180], including with regression models [48, 179]. Therefore, it was also one of the compared approaches in A.3, where different feature selection methods for sonomyography were evaluated.

An offline study investigating several feature extraction methods for HD-FMG compared the ROI gradient with other methods. The ROI gradients presented the highest

classification accuracy [181] over Harris corner extraction method [182] and the structural similarity index [183] on bicubic interpolated data.

From each ROI_i, with $i \in \{1, ..., 18\}$ in the case of the HD-FMG bracelet, three features were extracted $(\alpha_i, \beta_i, \gamma_i)$. They can be seen as a vector representing the second-moment axis of the ROI, i.e the line around which the ROI would have the lowest rotational moment when cut from a piece of rigid cardboard [184]. It can also be seen as the normal line to the planes that is optimal for all the observed ROI sensor values. The value distribution of the ROI can be approximated by a first-order regression plane:

$$\hat{G}(x, y) = \alpha_i(x - x_i) + \beta_i(y - y_i) + \gamma_i \ , \tag{3.11}$$

where $\hat{G}(x, y)$ corresponds to the point on the fitted plane at position (x, y), and (x_i, y_i) represents the point of interest in the upper left corner of the ROI_i [181].

The least squares fit the observed gray values $G(x, y)$ of the ROI and is obtained by α_i, β_i, and γ_i minimizing the sum of the squares of the distances between the points and the regression plane:

$$\varepsilon^2 = \sum_{(x,y) \in ROI_i} [\alpha_i(x - x_i) + \beta_i(y - y_i) + \gamma_i - G(x, y)]^2 \ . \tag{3.12}$$

As depicted in Fig. 3.9, for one ROI, α designates the mean image gradient along the x direction (row), β along the y (column), and γ is an offset corresponding to the mean gray value of the sensor values in the ROI after solving the equation.

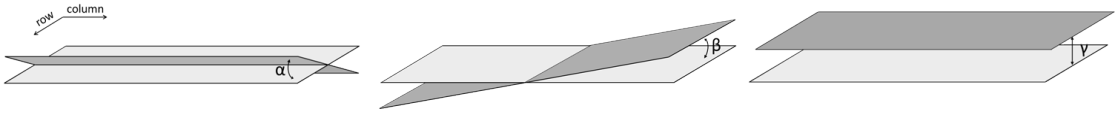

Figure 3.9: Visualization of the parameters alpha, beta, and gamma of a plane.

To calculate the parameters of a ROI, a ridge regression is performed:

$$\boldsymbol{w} = (\boldsymbol{A}^T\boldsymbol{A} + \lambda\boldsymbol{I})^{-1}\boldsymbol{A}^T\boldsymbol{r} \ , \tag{3.13}$$

$$\text{with } \boldsymbol{w} = \begin{bmatrix} \alpha_i \\ \beta_i \\ \gamma_i \end{bmatrix} , \ \boldsymbol{A} = \begin{bmatrix} 1 & x_1 & y_1 \\ 1 & x_2 & y_2 \\ \vdots & \vdots & \vdots \\ 1 & x_l & y_l \end{bmatrix} , \text{ and } \boldsymbol{r} = \begin{bmatrix} ROI_i(x_1, y_1) \\ \vdots \\ ROI_i(x_l, y_l) \end{bmatrix} .$$

The solution of the regression $\boldsymbol{w}$ corresponds to the parameters α_i, β_i, and γ_i, while $\boldsymbol{A}$ contains the coordinates within the ROI, and $\boldsymbol{r}$ the ROI's gray values in an $l \times l$ matrix, with l being the side length of the ROI square.

A schematic representation of the ROIs and associated gradients is illustrated in Fig. 3.10.

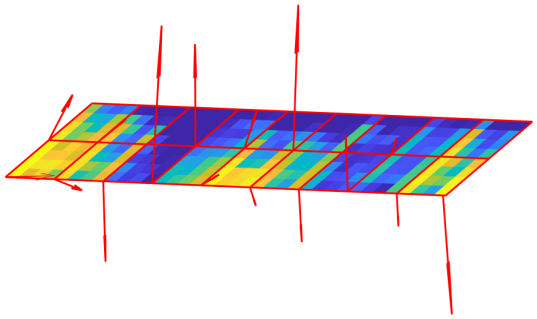

Figure 3.10: A schematic representation of ROIs and their gradient, obtained from HD-FMG data.

Considering a taxel as being one force sensor value, the ROIs for the HD-FMG data in A.2 were non-overlapping 4×4 taxel squares, as in [181], resulting therefore in two ROIs per board as represented in Fig. 3.10. As three features were extracted from each ROI, and each of the nine sensor boards had two ROIs, a 54-dimensional feature vector was fed to the machine learning model, which was also ridge regression in this case (RR-ROIG).

This feature has already been used successfully in [48] for ultrasound and was, therefore, one of the compared features for the portable ultrasound device in A.3. After preliminary tests, a square of 40px with a step size of 30px was chosen as ROI, resulting in 348 features. The method also inspired other researchers to adapt it for ultrasound A-mode [185].

3.3.2.2 Image Downsampling

In image processing, downsampling is a method that reduces the size of an image by selecting a subset of the original data. The subset is defined by choosing a parameter k, the step size, which specifies that every k^{th} row and column is to be extracted to create a new reduced image. Downsampling decreases the spatial resolution. While this might lead to information loss, this can be evaluated via Principal Component Analysis (PCA). Visually, it corresponds to zooming out of a picture. This technique was tested with different step sizes for ultrasound data against the ROI gradient in A.3.

3.3.2.3 Tomographic Reconstruction of EIT Data

The reconstruction of EIT data most often necessitates a differential imaging method [164] comparing newly collected images of the impedance change to a baseline condition,

for instance the rest position in the case of forearm myography.

In theory, producing images of absolute impedance should also be possible. However, this option is unfortunately too prone to errors due to the instrumentation or the difference between the object recorded and the model used for the reconstruction.

The measurements recorded from an EIT device can be transformed into tomographic images using similar methods to CT scans (X-ray Computed Tomography). While CT scans significantly evolved in the past years, going from Filtered Back Projection (1972-2008), through Iterative Reconstruction (2008-2018), to Deep-Learning Based Reconstruction since 2018, EIT reconstruction algorithms were initially based on a similar method to the backprojection algorithm used for CT. However, it was soon recognized that this model was inadequate due to the electric current propagating diffusely, therefore differently to x-rays photons. The backprojection algorithm, developed by Barber and Brown in 1984 for the original Sheffield EIT system [186] subsequently had several improvements and variations [187]. Since the late 1980s, the Gauss-Newton (GN) reconstruction approach has been widely used for EIT [188, 189]. It allows fast, real-time imaging by using sophisticated regularized models of the inverse problem, representing the solution as a linear reconstruction matrix.

In order to filter the noise, several priors have been implemented, such as the NOSER prior [189], a discrete Laplacian filter [190], or also a discrete high-pass Gaussian filter [191]. In article A.3, different priors have been tested to determine the best feature selection for EIT.

3.4 Evaluation Metrics

3.4.1 Quantitative Performance Metrics

The evaluation of different sensor modalities requires performance metrics in order to compare them consistently and for research reproducibility. Offline metrics are practical as they can be applied to almost any dataset properly labeled, while real-time evaluation is rarely practically feasible when comparing numerous methods with variable parameters. However, offline studies need to be confirmed by online evaluations, which remain closer to reality [192–195]. This could be explained by the fact that users can partially compensate for inaccuracies [196]. This section provides an overview of the offline and online metrics used in the underlying publications of this dissertation.

3.4.1.1 Metrics for Offline Myocontrol Evaluation

Stability over time: In order to have reliable intent detection for myocontrol, it is important to have a stable input signal over time, i.e. with a low standard deviation while the hand action is performed.

Separateness Index / Separability of the clusters: A reliable intent detection relies on a good separability of the signal patterns corresponding to the different hand/wrist actions to be predicted. Indeed, these should be different enough that the model does not confuse them. Of course, the more actions there are to control, the highest is the probability that some signal patterns are similar. Therefore, the number of actions to be trained and controlled is often a trade-off between functionality and stability.

Typically, higher separability of action clusters means better distinguishability by any pattern classification method and, therefore, implies higher stability of the related control [197]. In order to evaluate cluster separability, Fisher's Separateness Index [198] is evaluated for each pair of clusters (C_i, C_j). It is defined as the maximum value over w of $J(w)$, as described in equation 3.14.

$$J(w) = \frac{w^T \boldsymbol{S_B} w}{w^T \boldsymbol{S_W} w} \,, \tag{3.14}$$

with $\boldsymbol{S_B}$ the between-clusters scatter matrix as defined in Eq. (3.15), and $\boldsymbol{S_W}$ the within-clusters scatter matrix, provided by Eq. (3.16).

$$\boldsymbol{S_B} = (\mu_i - \mu_j)(\mu_i - \mu_j)^T, \tag{3.15}$$

where μ_i, μ_j are the means of clusters C_i, C_j, and with $(i, j) \in \{1, ..., p\}$ with p the number of trained actions.

$$\boldsymbol{S_W} = \sum_{n=i,j} \sum_{\boldsymbol{x} \in clust_n} (\boldsymbol{x} - \mu_n)(\boldsymbol{x} - \mu_n)^T, \tag{3.16}$$

where $\boldsymbol{x}$ represents the samples in each cluster. Each pairwise Fisher's index can be averaged across all participants of a study and collected in a matrix $\boldsymbol{S} = \{s_{ij}\}$.

Another measurement of cluster separation is called the Safety Index, implemented in [48] to evaluate the separateness on ultrasound data. The Safety Index is the ratio between the maximum standard deviation of cluster C_i (evaluated over all dimensions) and the Euclidean distance between cluster C_i and C_j,

$$s_{ij} = \frac{max(\sigma_i)}{||\mu_i - \mu_j||} \,, \tag{3.17}$$

where σ_i is the standard deviation and μ_i the mean of cluster C_i. The smaller the value s_{ij} is, the further the elements C_i are far from C_j, indicating a good separability between the two clusters.

PCA: The Principal Component Analysis (PCA) [199] is a method used for decomposing a multivariate dataset in a set of successive orthogonal components explaining a maximum amount of variance. It can be employed as a linear dimensionality-reduction method that can help to reduce the risk of overfitting in large datasets, but can also be used to visualize the main components of a dataset. For instance, selecting the first three

components can provide a 3D view of the data clusters, their separateness, and the path taken to reach an action. This method is limited as it does not provide the full signal variance but allows for a good visual estimation and a better comprehension of the signal.

nRMSE: The prediction accuracy, in the case of a regression algorithm, can be measured using the normalized Root Mean-Squared-Error (nRMSE) between the predicted and the stimulus values. Also called a scatter index, this is the primary offline error indicator method used to evaluate regression models.

$$RMSE(\mathbf{y}, \hat{\mathbf{y}}) = \sqrt{\sum_{i=0}^{n_{samples}-1} \frac{(y_i - \hat{y_i})^2}{n_{samples}}} \,, \tag{3.18}$$

with $\hat{y_i}$ the predicted value of sample i, and y_i its corresponding ground truth. The nRMSE is then obtained by the following equation:

$$nRMSE(\mathbf{y}, \hat{\mathbf{y}}) = \frac{RMSE(\mathbf{y}, \hat{\mathbf{y}})}{(y_{max} - y_{min})} \,, \tag{3.19}$$

3.4.1.2 Metrics for Online Assessment

As previously mentioned, online assessments are important for evaluating wearable devices and, in particular, for prosthetic control. While not always possible, it is crucial to be as close as possible to reality. One of the best scenario being the involvement of several target users (e.g. people with disabilities) wearing the device while performing activities of daily living (ADLs) in a user study. However, the more parameters are added, the more they can interfere with the variable being evaluated, e.g. the machine learning model. Therefore, more simple tests in specific conditions, e.g. a fixed arm position, are often necessary before proceeding with more sophisticated assessments involving ADLs. After an offline evaluation, an online target achievement control (TAC) test [200] is typically used to assess a new machine learning or feature selection method.

A TAC test consists in having the participant perform different pre-selected hand/wrist gestures by following e.g. a virtual 3D hand model on a computer screen while recording the data. Several repetitions of the actions are necessary for the machine learning model to be more accurate. The machine learning algorithm is then trained with the collected data, and the prediction of the model is used to control another virtual hand as depicted in Fig. 2.10. Target hand/wrist poses are pre-selected before the experiment and are shown on the screen with a 3D hand model next to the controlled one. The participant is then asked to reproduce the poses within a predefined amount of time, typically 15s in the experiments of this thesis, and to stay for 1.5s, as shown in Fig. 3.11. These time durations can vary slightly depending on the research group, but they are usually within the same range [200]. For the hand pose to be reproduced correctly, the absolute maximum of the prediction error is measured and compared to a threshold ε_{th} (typically

0.15, the maximum absolute value of each DoFs being 1):

$$max(|\mathbf{y} - \hat{\mathbf{y}}|) < \varepsilon_{th}$$

with ε_{th} the error threshold, $\mathbf{y}$ the prediction vector, and $\hat{\mathbf{y}}$ the target vector.

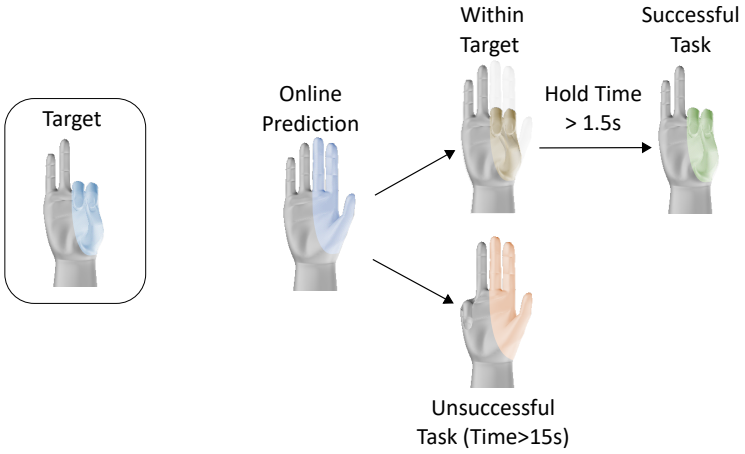

Figure 3.11: Illustration of a TAC test.

From this TAC test, several parameters are evaluated:

Time In the Task (TIT): The TIT is the cumulated time that the participant remained in the task, e.g. in the correct hand/wrist pose, as defined above with the threshold. This TIT is interesting for both the successful and unsuccessful tasks but needs to be separated for these two categories due to the 15s time limit to perform the task.

Task Completion Time (TCT): The TCT is the time necessary for the participant to complete the tasks, e.g. to stay in the target for 1.5s. This metric is, of course, only interesting for successful tasks as it is otherwise bounded at 15s for unsuccessful ones.

Success Rate (SR): The success rate is defined by the ratio of successful tasks to all tasks performed by the participant. The SR is usually first defined for each task over all repetitions for one participant. This SR can then be averaged for all participants for each task as well as over all tasks, depending for instance on the machine learning or feature selection algorithm evaluated.

Reachability: In some cases, a participant does not manage to reach a task at all during one repetition or several. Therefore, it is important to evaluate the reachability of a task when noticing a low success rate.

Number of Attempts: The number of attempts is not a metric of the TAC test, and the word "task" no longer refers to reproducing a 3D hand pose. It is rather used in a time-free experiment not limited by a number of repetitions and is defined as the number of attempts necessary for the participant to complete a task. It was used, for instance, in A.4 to evaluate the learning effect over the repetitions.

Traveled path and speed of motion: When time-free actions are performed, such as in a learning evaluation, possible metrics are the traveled path and speed of motion. If the hand speed over the repetitions of a task increases, this could imply better control of the device and possibly higher confidence. If an optimal path for a motion is available, the deviation by the traveled path and the cumulated distance can be evaluated.

3.4.2 Metrics for Device Evaluation

When evaluating a new sensor acquisition device or a new modality, several parameters are to be considered for possible use in myocontrol, either for teleoperation or prosthesis control.

Data Acquisition Speed: The data acquisition speed of a device is essential for myocontrol. The prediction of hand actions needs to be fluent for a better embodiment, and a delay can significantly impair the feeling of embodiment [201]. The rate of the sensors should therefore be high enough to match the bandwidth. Theoretically, a low sampling rate of 20-50Hz could be sufficient with muscular movements around 10Hz. Indeed, Mann et al. (1989) found that the bandwidth of the three DoFs of the wrist between 10-12Hz contains 75% of the signal [202], and slow finger movements would be between 8-10Hz [203]. Other studies have extended similar findings for the wrist, with significant coherence, around 6-12Hz, between acceleration and motor units [204], and between EMG and motor cortex via EEG signals [205]. A suggestion is that the motor control would be organized by a 10-Hz clock [206]. Moreover, pulses of acceleration every 100ms shown in [203] would suggest that even linear movements would have a 10-Hz discretization [207]. However, these discontinuities would be suppressed by low-pass filtering properties of the musculoskeletal dynamics [208].

Nevertheless, for some modalities, such as electromyography, a higher sampling frequency might be required, especially for some extracted features, since significant EMG activity is between 5 and 450Hz. However, this can be strongly influenced by several factors: for instance, intramuscular electrodes have a higher bandpass than surface ones because fat and skin act as low-pass filters; electrode material, shape, size, or prefilter circuitry should also be considered, among other criteria [209]. For instance, the *Myobock* electrodes from *Ottobock* have shown, from spectral analysis, to have their relevant bandwidth below 10-12Hz [148, 161]. Nonetheless, prediction results with the Mean Absolute Value (MAV), mainly used in this thesis, are only slightly influenced by lowering the sampling frequency compared to other measures [210, 211]. Moreover, given the substantial electronic hurdles that must be overcome to achieve frequencies of 1 to

2kHz for EMG data acquisition, lowering the sampling rate can be seen as a worthwhile trade-off to make HMIs more portable.

Wearability and Portability: In order for a human-machine interface to be as intuitive as possible, the wearability criterion is crucial and postulates portability. The portability of a device is the ability of a user to place the device on the body without it being too cumbersome and heavy. This device can, however, still be cabled to a computer. Complete wearability, on the other hand, requires the device to be wireless and to have embedded computation. A device has the best wearability when it is easy to don and doff, when the user is not aware of it and can quickly forget wearing it, when it can be worn under or above clothing without impairing movement, touch sensitivity, or requiring extra care, and when it does not require any external device. These criteria are all the more critical in the case of prostheses, as the sensors should be embedded within the socket. A further important criterion of wearability is the battery life of the device, which should ideally last at least for one day in the case of prostheses. Therefore, energy consumption plays an important role when invoking wearable devices. Thus, a particular attention should be given to the choice of processor and communication when conceptualizing such a wearable HMI, as these two factors are decisive regarding power consumption.

Additionally, people suffering from amputation have a different distribution of perspiration at the stump and within the current prosthetic sockets, the problem is amplified as they are very hermetic. Therefore, for the commercially available sockets, the sensors should be designed to limit sweat and heat [212]. This could change with smart prosthetic liners such as in [213, 214].

Spatial resolution: The spatial resolution of a modality is dependent on the amount of raw data it is able to provide with relation to the covered surface, as well as the sensor distribution and density on this surface. While the co-contraction method with two sEMG sensors is still the standard way to control prostheses, researchers have evaluated since the last decade the use of more of these sensors for a more intuitive control [215]. Some companies (e.g. *Coapt* and *Ottobock*) have started implementing it in the last years by using machine learning algorithms allowing multi-DoF control of upper-limb prostheses. Theoretically, the more electrodes there are until a certain limit depending on the modality [166], the better the classification accuracy is. As some modalities, such as ultrasound, allow a much higher spatial resolution than others, this comes with other issues in these cases, where the number of features is too high to be processed in an algorithm that could be embedded, e.g. the time complexity of simple algorithms such as ridge regression is too high. In these cases, feature selection is necessary, and overfitting needs to be particularly monitored.

3.4.3 User Evaluation Metrics

When evaluating a new sensor acquisition device, it is important to have user feedback in order to determine the possible improvement parameters. In these studies, three standard

tests have been used for this purpose: the System Usability Scale (SUS) [216], the NASA Task Load Index [217] and a modified version of the Microsoft Desirability Toolkit [218].

NASA Task Load Index (TLX) survey: The NASA Task Load Index [217] provides an overall workload score on six criteria: Mental, Physical and Temporal Demands, Own Performance, Effort, and Frustration. For each criterion, the answers are on a 21-point Likert scale, from 0-*very low* to 20-*very high* (Table 3.1).

NASA TLX Survey
How mentally demanding was the task?
How physically demanding was the task?
How hurried or rushed was the pace of the task?
How successful were you in accomplishing what you were asked to do?
How hard did you have to work to accomplish your level of performance?
How insecure, discouraged, irritated, stressed, and annoyed were you?

Table 3.1: List of questions of the NASA TLX survey.

After evaluating each criterion, the participant gives a weight of personal importance to each. The Raw TLX (RTLX) is a simplified version of the NASA TLX. While both assess the subjective workload during a task, the RTLX dismisses the individual subscale weighting to only report the "raw" values of the six workload criteria.

System Usability Scale (SUS) survey: The SUS [216] consists of ten statements (Table 3.2) to which users answer within a 5-point Likert scale (from *strongly disagree* to *strongly agree*).

SUS Survey
1. I felt comfortable with the device.
2. I found the device unnecessarily complex.
3. I thought the device was easy to use.
4. I think that I would need the support of a technical person to be able to use this device.
5. I found the various functions in this system were well integrated.
6. I thought there was too much inconsistency in this device.
7. I would imagine that most users would learn to use this device very quickly.
8. I found the device very cumbersome to use.
9. I felt very confident using the device.
10. I needed to learn a lot of things before I could get going with this device.

Table 3.2: List of statements of the SUS survey.

The scoring is such that answering the positive questions with *strongly agree* and the negative ones with *strongly disagree* produce a higher impact on the final score. This one is calculated, ranging from 0 (negative) to 100 (positive), by summing each item having a score contribution between 0 and 4. For statements 1, 3, 5, 7, and 9, the contribution is the scale position minus 1. For statements 2, 4, 6, 8, and 10, the score contribution is 5, minus the scale position. The final SUS score is then obtained by multiplying the sum of the contributions by 2.5. The meaning of this score can then be evaluated according to [219].

Microsoft Desirability Toolkit (MDT): The MDT survey [218] consists of several cards with adjectives that could apply to the evaluated system. The user should select five adjectives that most closely match their personal impression of the system (the original form of the study uses cards). In A.1, a list of 75 adjectives (most from the MDT questionnaire) was presented to the participants instead of the cards. The users were first asked to choose all adjectives that best described the device according to them. Then, they had to choose only the five most important words with a short explanation.

Likert Scale: A Likert scale is a unidimensional scale that researchers can use to evaluate participants' opinions, experiences, and feelings. It is one of the most common scale types for customized, specific questionnaires. For instance, in A.4, control scores and difficulty evaluations were included in the questionnaire. The participants were asked to score the control of the hand, of the body, the evaluated difficulty for the first repetition, and for the last, each on a separate Likert scale.

Improvement ratios: In order to evaluate the learning effect, improvement ratios can also be measured between repetitions. In A.4, improvement ratios were measured on the task completion time.

3.5 Protocols and Datasets

From opening a door to pouring a bottle of water, wrist movements are essential for flexible manipulation in activities of daily living [220]. Several studies highlight the importance of the wrist for prosthesis users [76], in particular for reducing compensatory movements [221], and wrist movements remain one of the fundamental features requested by the users for prosthesis improvement [23, 76].

Therefore, all of the studies presented in the core publications of this thesis involve wrist flexion, extension, pronation, and supination, in addition to the power grasp, as depicted in Fig. 3.12. Due to the high spatial resolution of ultrasound and its potentiality to better distinguish several actions, two additional gestures were added in A.3. With tasks inspired by ADLs and considering the arm position effect, only three actions were typically trained in A.4 when the body-tracking of the wrist was provided: namely rest, power grasp and the pointing gesture.

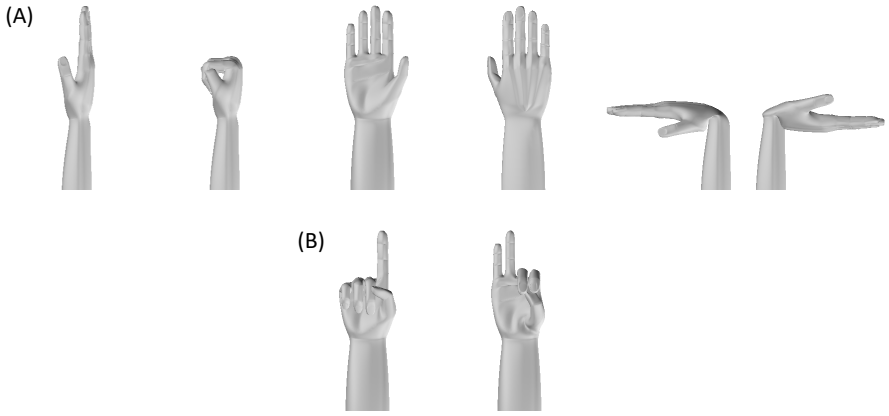

Figure 3.12: (A) Wrist and hand poses used in A.1, A.2, A.3, and to some extent in A.4. From left to right: rest, power, (wrist) supination, pronation, flexion, and extension. (B) Additional hand poses: point (A.3, A.4) and tridigital (A.3). Shown from a frontal point of view for a better visualization. The gesture tridigital is a type of pinch grasp consisting in pressing the tumb in between the extremities of the index and middle fingers.

3.5.1 Data Collection of Surface Modalities for Offline Evaluation

(A) **(B)**

Figure 3.13: (A) Overview of the system in A.1. A participant wears the mobile system with one FMG bracelet and one sEMG bracelet. The data acquisition device is placed on the upper-arm and transmits the data via Bluetooth to a smartphone for machine learning processing. (B) Bird-eye view of the experiment.

In A.1, the experiment involved force myography and electromyography recorded from the wireless data acquisition device developed in the framework of this thesis (cf. Section 3.1.3). The electromyography sensors from *Ottobock* were described in Section 3.1.2 and depicted in Fig. 3.3B. The recorded gestures were rest, power grasp, wrist flexion, extension, wrist pronation, and supination (cf. Fig. 3.12A). Additionally, wrist pronation and supination involve deep muscles [100], producing weaker and less distinguishable

signals for sEMG. The hypothesis was that FMG could better detect supination and pronation as the movements of the underlying muscles cause the surface muscles to create pressure that this modality can sense. The experiment involved ten participants without amputation (3 females, 7 males, 28±7 years old, one being left-handed). This article was an offline analysis; therefore, only a recording of the actions was performed. The sequence of gestures was repeated ten times by each participant. One bracelet with ten FMG sensors was placed on their right forearm, while another one with ten sEMG sensors was placed on the left. Due to the mobile nature of the acquisition device being tested, the gesture to perform was indicated on the smartphone located in front of the participant, and the experimenter was visually checking the correct performance of the movement.

3.5.2 Data Collection of Enhanced Surface Modalities for Online Evaluation

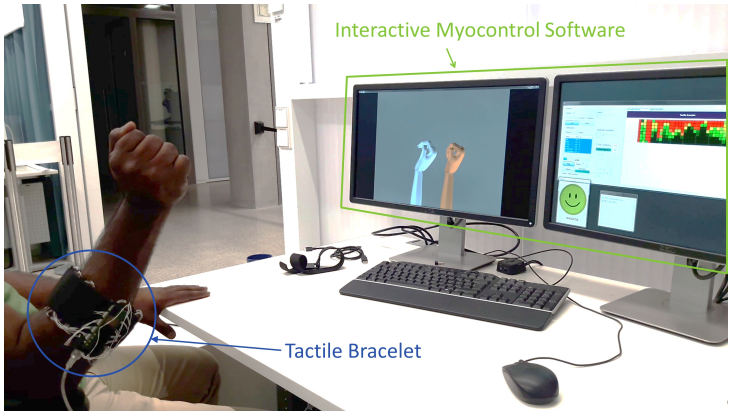

Figure 3.14: Bird-eye view of the experiment in A.2.

In A.2, high-density force myography, also called tactile myography, was evaluated from the tactile bracelet developed by the *University of Bielefeld (CITEC)* and described in Section 3.1.3. The trained actions were: rest, power grasp, wrist flexion, wrist extension, wrist supination, and wrist pronation (cf. Fig. 3.12(A)). The participants were tested with a TAC test with single actions and combined ones. The test was performed as described in Section 3.4.1.2. All possible combinations of actions were evaluated with a limitation of two combined actions. From an extensive literature analysis, the level of power grasp feasible while performing different wrist actions was assessed, and the targets of the TAC test were set accordingly, as specified in Table 3.3. As there is little to no research on two wrist motions combined, the target levels for this combination were set according to pre-tests.

Twelve participants (three females and nine males, 30.6 ± 6.6 years old) without amputation took part in the experiment, as well as one person with left-hand transradial

amputation (male, 35 years old). He was amputated in 2005 and used daily, since 2012, a *Variplus* prosthesis by *Ottobock* with standard two-electrode control and no rotation unit on the device. After an initial training phase of three repetitions and a familiarization phase, the participants had to perform three repetitions of, sequentially, two re-training and a task reaching phase (TAC test). The re-training of the machine learning model was necessary to prevent the drift of the prediction due to the foam of the tactile bracelet (cf. Fig. 3.4) creeping over time. A bird-eye view of the experiment is visible in Fig. 3.14.

#	Power grasp	Pronation	Supination	Extension	Flexion	comb. type
1	80% (**100%**)					
2		80% (**100%**)				
3			80% (**100%**)			single
4				80% (**100%**)		
5					80% (**100%**)	
6		56% (**70%**)			40% (**50%**)	
7		56% (**70%**)		40% (**50%**)		combined without power
8			56% (**70%**)		40% (**50%**)	
9			56% (**70%**)	40% (**50%**)		
10	70% (**87%**)	56% (**70%**)				
11	78% (**98%**)		56% (**70%**)			combined with power
12	78% (**97%**)			40% (**50%**)		
13	53% (**66%**)				40% (**50%**)	

Table 3.3: Single and combined actions performed during the experiment in A.2 with the different thresholds chosen for each action with an 80% factor. The values in the parentheses show the ones extracted from the literature or selected from a pre-round of experiments in the case where no power grasp is involved.

3.5.3 Data Collection of Surface and Deep Sensor Modalities for Offline Evaluation and Fusion

In A.3, three modalities were tested in an experiment: force myography, electro-impedance tomography, and ultrasound. FMG was chosen instead of the gold-standard sEMG because of the potential interference of EIT with sEMG, EIT injecting a micro-current to be able to measure its signals. Additionally, from the results of A.1, it was established that FMG had better separability and stability over time than sEMG. Due to the limited space available on the forearm, an FMG bracelet was used rather than an HD-FMG one. FMG was recorded with the data acquisition device developed within this thesis, mentioned in Section 3.1.3, and equipped with ten pressure sensors. The ultrasound device was the one from the *IBMT Institute* of *Fraunhofer*, described in more detail in Section 3.1.5, and the EIT data was recorded from the bracelet of the *University of Siegen*, detailed in Section 3.1.6. As Fig. 3.15 shows, the three devices: EIT, FMG, and ultrasound, were placed from proximal to distal on the forearm in this specific order. Half of the subjects wore the sensors on their left arm and the other half on their right arm. The sequence of actions consisted in rest, power, point, precision (tri-digital), wrist flexion, wrist extension, wrist supination, and wrist pronation (cf. Fig. 3.12(A) and (C))

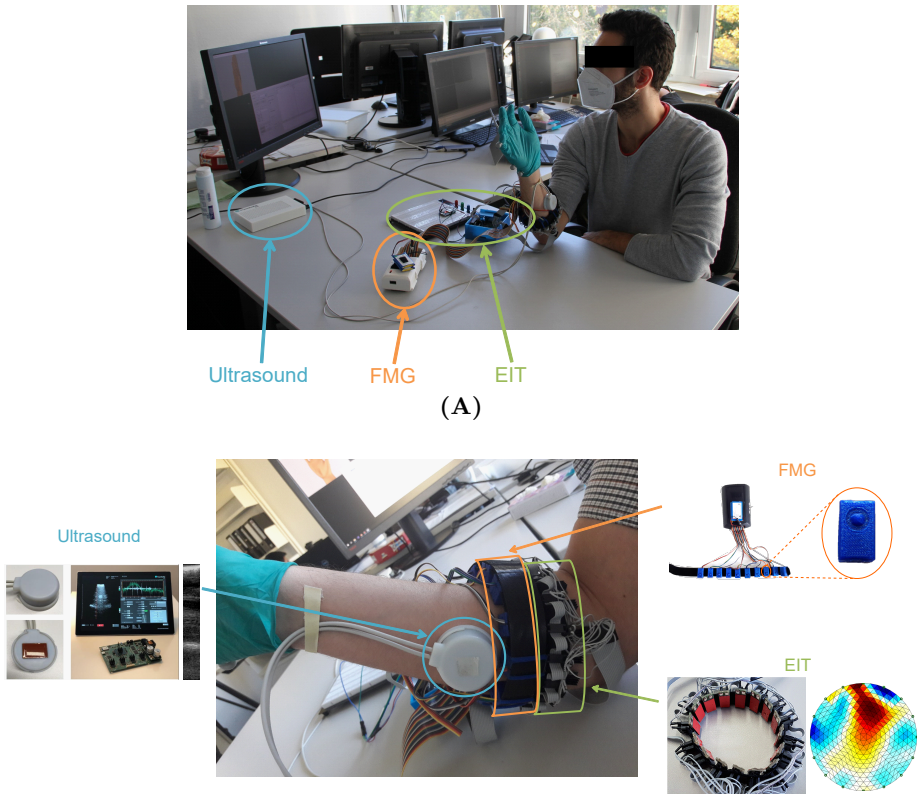

Figure 3.15: (A) Bird-eye view of the experiment in A.3. (B) Zoom on the different modalities.

in a randomized order. Three repetitions of the sequence of actions were recorded. More were not possible due to the lengthy process of saving ultrasound data. Ten people (2 females, 8 males, 32.5 ± 6.3 years old) took part in this experiment.

3.5.4 Application of Combined Modalities with Electromyography and Kinematics

In A.4, surface electromyography sensors and the Bodyrig, a complementary type of sensor providing kinematic tracking device based on IMU sensors, were both used in an application of combined modalities for teleoperating the bimanual humanoid robot TORO (which stands for TOrque-controlled humanoid RObot) developed at DLR [222]. For the kinematic tracking, the Bodyrig, an IMU-based tracking device developed for this thesis and described in Section 3.1.7 was used, while the sEMG data of the forearm were recorded with two Myo-armbands from *Thalmic Labs*, described in Section 3.1.2. Three hand poses were trained, namely rest, power, and point, as well as the wrist actions for the participants missing a limb (cf. Fig. 3.12 A and B). The Bodyrig data were processed to control the torso and arms of the humanoid robot, while the sEMG data was fed to a

(A) **(B)**

Figure 3.16: Bird-eye view of the experiment in A.4. (A) The double-sided amputee opening a bottle. (B) A non-disabled participant performing the task of pouring a bottle into a pot.

machine learning model, whose prediction controlled the robot's hands, and additionally the wrist(s) in the case of the participants with amputation. The tasks to perform by teleoperating the robot are described in Table 3.4.

These tasks were inspired by assessment protocols for prosthetics users, such as the Assessment of Capacity for Myoelectric Control (ACMC) [223] and the Chedoke Arm and Hand Activity Inventory (CAHAI) [224, 225], an upper-limb functional assessment for stroke recovery, already used in teleoperation studies [226, 227]. A bird-eye view of the experiment with some of the subjects performing the tasks is visible in Fig. 3.16.

Seven anatomically intact participants (all males, aged 28.4 $\pm$ 7.1 years) were involved in this experiment, as well as two persons with missing upper-limb(s) at the transradial level (cf. Section 2.1.1): one congenitally missing his right hand (D1) and the other one (D2) had undergone a double-amputation following a trauma. All participants performed a single experiment session, and one of the intact subjects repeated the session over five days. One session consisted in repeating each task, described in Table 3.4, four times. The subtasks had to be completed individually before starting a new repetition. Since the first repetition was considered a familiarization phase, the long-term participant only had to perform three repetitions for the remaining days of the experiment after the first session. As the learning effect was evaluated, there was no limitation in the number of attempts to perform a task. An attempt was considered finished if the participant could not regain a correct setting of the objects, without external help, to complete the task.

Task ID	Summary of the task	Detailed description of the task
1a	Take the lid off the pot and place it on the table.	Take the pot handle with the right hand. With the left hand, take the lid off the pot and place it on the table at place 2.
1b	Take an orange ball and put it in the pot.	With the left hand, take the foam ball from place 3 and place it in the pan. Take the pot's lid from place 2 and put it back on the pot in place 1.
2a	Unscrew the cap of the bottle	With the right hand, take the bottle from place 1, lift it, rotate it about 45nd with the left hand, and unscrew the cap.
2b	Pour the bottle's contents into the open pot.	With the left hand, take the pot handle. With the right hand, simulate pouring the contents of the bottle into the pot by rotating the wrist. (The bottle is filled with pebbles blocked at the opening with foam to avoid dangerous spreading in case of task failure.) Place the bottle back in place 1.
3	Type numbers on a fixed phone.	With the left hand, with a pointing index, type on the buttons 9, 1, 1. With the right hand, with a pointing index, press the loudspeaker key.

Table 3.4: Description of the Tasks in A.4.

Chapter 4

Summary of Publications and Additional Results

> Pour examiner la vérité, il est besoin, une fois dans sa vie, de mettre toutes choses en doute autant qu'il se peut.
>
> *(René Descartes)*

Table of Contents

4.1 Offline Evaluation of Surface Modalities

Primary Publication:
[1] M. Connan, E. R. Ramírez, B. Vodermayer, and C. Castellini, "Assessment of a wearable force- and electromyography device and comparison of the related signals for myocontrol," *Frontiers in Neurorobotics*, vol. 10, no. 17, pp. 1–13, nov 2016, doi: 10.3389/fnbot.2016.00017. A.1
Related Publications:
[11] B. W. Hallworth, A. W. Shehata, M. R. Dawson, F. Sperle, M. Connan, W. Friedl, B. Vodermayer, C. Castellini, J. S. Hebert, and P. M. Pilarski, "A transradial modular adaptable platform for evaluating prosthetic feedback and control strategies," in *MEC-Myoelectric Control Symposium*, pp. 1–4, 2020. B.5
[8] M. Sierotowicz, D. Brusamento, B. Schirrmeister, M. Connan, J. Bornmann, J. Gonzalez-Vargas, and C. Castellini, "Unobtrusive, natural support control of an adaptive industrial exoskeleton using force-myography," *Frontiers in Robotics and AI*, vol. 9, p. 223, sep 2022, doi: 10.3389/frobt.2022.919370. B.7

Surface electromyography is the gold standard for myoelectric control. This modality measures the difference of potential within the muscles, as explained more in detail in Section 2.2.2.1. Standard prostheses are equipped with two sEMG sensors placed respectively on the dorsal and ventral side of the forearm. The prosthesis user generates a trigger by co-contracting the opposite muscles, flexor and extensor, or by quickly contracting one muscle to switch between different hand gestures. Of course, this limits the number of possible hand movements and does not involve simultaneous control of several DoFs. For this reason, during the past decade, scientists have been studying more intuitive control by adding more sensors [215, 228]. With these data, two options are possible in terms of machine learning: either classification or regression. However, most classification approaches only control one action at a time, and the DoFs cannot be controlled independently at the same time [34]. Hence, classification does not allow to have independent proportional control. For a proportional control, regression is preferred, leading therefore to simultaneous and proportional control, which is the option chosen in this work.

Nonetheless, despite the advantage of additional sensors and SPC, no stable solution has yet been found in the community, and the level of abandonment of multi-fingered prostheses remains relatively high [22, 23, 25, 76]. The several drawbacks that sEMG suffers from, e.g. cross-talk among adjacent muscles, sweat, electrode shifts, ambient noise, motion artifacts, or muscular fatigue, among others [26–29], could indicate that the root of the problem is actually related to the sensors themselves. For that reason, researchers have been pushing for alternative sensors [30, 229]. One type of sensor in particular first caught the attention of the scientific community, namely force myography.

As detailed in Section 2.2.2.2, force myography relies on pressure sensors placed around the forearm, which measure the pressure exerted by the muscles on the surface of the forearm. As of 2016, some teams have started to evaluate its capacity for myocontrol [41, 230]. However, no study had compared the modality with the gold standard sEMG. This section and the underlying publication A.1 compare the two modalities and evaluate a new wireless data acquisition system acquiring both signal types developed in the context of this thesis.

4.1.1 Comparison of Electromyography and Force-Myography

As described in Section 3.1.3, a multimodality acquisition device was built in A.1 for the purpose of comparing sEMG and FMG, and fusing the two types of sensors. For the same purpose, a housing for the FSR sensor has also been specifically designed.

The protocol of the data collection is specified in Section 3.5.1. The article has shown that FMG provides better stability of the signal over time with a lower variance. This is due to the nature of the sEMG signal itself, presenting a peak at the beginning of the muscular activation because of muscular motor-unit recruitment [28, 231]. When verifying this on, e.g., wrist flexion for the first three repetitions of each participant, the standard deviation of the three sensors exhibiting the highest amplitude was significantly higher for sEMG than FMG (Student's paired t-test with $p < 0.01$).

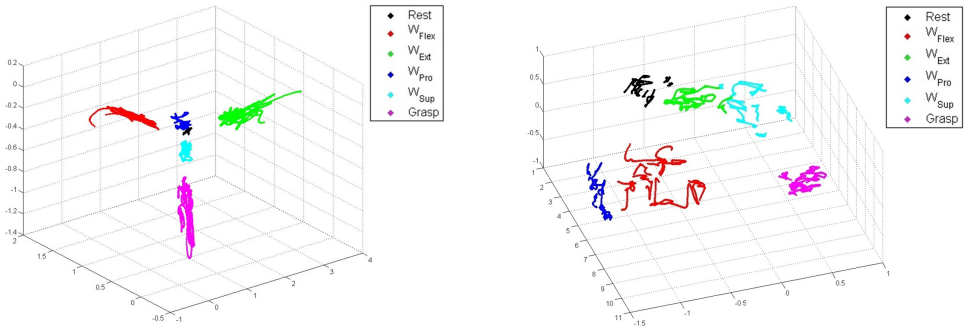

(A) **(B)**

Figure 4.1: 3D-reduced PCA visualization of the clusters of the different modalities in A.1, colored according to the different trained movements. (A) sEMG. (B) FMG.

In order to ensure that the actions do not interfere with each other, the separateness of the clusters for each modality is calculated as described in Section 3.4.1.1. The Fisher's index (cf. Fig. 4.2) shows a better separability of the clusters for FMG than sEMG with a statistical significance (Student's paired t-test, with $p < 0.001$), meaning that FMG generates better-separated patterns in the input space.

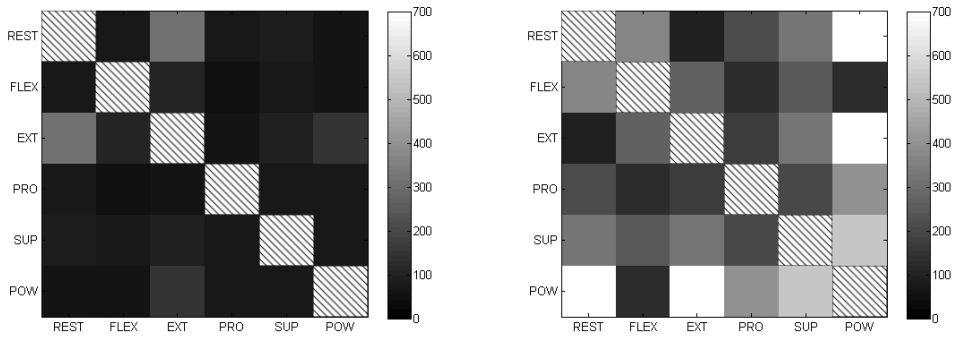

(A) **(B)**

Figure 4.2: Fisher's separateness index matrices for the different modalities in A.1 (*higher is better*). (A) sEMG. (B) FMG.

An RR-RFF algorithm (cf. Section 3.2) was trained on nine of the ten repetitions, respectively with the single modalities and with the combination of FMG and sEMG by stacking the two 10-dimensional vectors together. The nRMSE was calculated to evaluate the prediction accuracy of the algorithm by testing on the last repetition. No statistical difference was found between the modalities or the multimodality, according to a one-way ANOVA test.

4.1.2 Acceptance of the Device

In order to have user feedback regarding the acceptance of the built device, the participants filled out three different questionnaires at the end of the experiment to evaluate the device's usability, workload, and desirability (described more in detail in Section 3.4.3).

The system reached a SUS score of almost 85%, which is graded "Excellent" according to the score-grading scale [219]. Additionally, according to the RTLX test, the evaluated workload of the device was at 25%, which is relatively low. The adjective selection from the desirability study resulted in six most common adjectives in the final selection, namely, *Simple, Intuitive, Easy to use, Familiar, Reliable,* and *Stable.*

4.1.3 Summary

The study in A.1 showed an overall better stability of the signals and a better pattern separability in the input space for FMG compared to sEMG. The prediction accuracy in terms of nRMSE also proved to be significantly better with FMG than sEMG in this user study. According to the same measure, the fusion of the two concatenated modalities did not show any significant difference compared to the best performing method, i.e. FMG. However, this analysis was offline, and an online experiment would need to be performed

to confirm it.

Further research would also be required to compensate for the potential drawbacks of FMG. Indeed, a drift of the signal is possible depending on the sensor used, its design, and its placement. Artifacts generated by arm/forearm movements with accelerations inducing pressure on the force sensors can also negatively affect the signal. Artifacts can as well be caused by fat tissue accumulating in the elbow hollow when flexing the forearm, or induced by touching the socket, bumping into objects, laying the stump or the prosthesis on a table, or lifting heavy objects [41]. Although it can be arguable whether a mirrored acquisition is better than a same-arm acquisition, the difference between the two methods might only be minor if a uniform sensor placement is chosen instead of a target-muscle placement. A same-arm acquisition study actually showed the same results, as explained in 4.1.4.

In addition, the experiment and user evaluation confirmed the high degree of usability of the presented new device, a wearable, integrated multimodal system for myocontrol and intent detection combining sEMG and FMG. With the machine learning algorithm directly embedded into a smartphone, the autonomous mobility of the entire system was limited by the cell phone battery after about 11h. While this could be improved with, for instance, a wearable power bank, this duration was actually similar to the average recorded usage time of a prosthesis (11.1h) evaluated in [232]. By allowing use in the home environment, such a device could enhance studies by bringing them closer to the actual issues at stake.

4.1.4 Retrospective View with the State of the Art

Since the publication of A.1 in 2016, force myography has become more and more popular. This device specifically has been used in a total of 10 studies listed in Section 1.4.3 and some of them described below.

In [67], the authors use this system in an offline and single-subject online assessment of sEMG/FMG multimodality with several bracelet configurations and the same actions as in A.1. In this study, the hyperparameters were specifically optimized for each modality. The results show that sEMG alone performs worse with an nRMSE, using RR-RFF, at 0.091, while single FMG modality yields 0.053. Interestingly, mixing the two modalities either with the stacked method (same as in A.1) or the ensemble method did not result in better performance, with respectively 0.066 and 0.058. The online assessment on a single subject also indicates a significantly better performance of FMG over sEMG or multimodality, with 83.3% of SR and 4.33s of TCT.

This online comparison was further assessed in [70] with a larger subject pool, additionally evaluating three levels of contraction with the same gestures as the two previous studies. The results showed that FMG achieved a more robust myocontrol than sEMG,

including across activation levels. The stacked method for multimodality obtained similar results as FMG alone.

The device has also been adapted to fit the custom socket of one patient in [68]. Due to its wireless and wearable attributes, activities of daily living could be assessed with an actual socket over the term of one year, evaluating a standardized clinical procedure of training and assessment protocol involving co-adaptation. This shows that such a setup would allow more precise clinical studies with ADLs in the home environment.

In B.6, this same device is used for building a multimodal modular platform. This platform allows more realistic comparisons between persons with and without limb differences using a single setup instead of, respectively, a splint and a custom-made socket different for each amputation. The Modular-Adaptable Prosthetic Platform (MAPP) would allow a better evaluation of the drawbacks of FMG, in particular regarding the weight of an object influencing the FMG signals.

Apart from prosthetic control, a potential application for FMG is exoskeleton control. The study in B.7 proposed a machine learning-based control of an adaptive exoskeleton in real-time. The FMG device was able to successfully differentiate between no mass, 1kg, and 2kg and to provide adapted support by adjusting the length of the lever arm. FMG has the advantage over sEMG that it can be placed above the clothing, which is favorable in a factory setting.

The device has also been used in B.1 and B.2 as an acquisition instrument for sEMG, comparing it with HD-FMG. Indeed, one of the advantages of FMG is that it requires very little electronics compared to sEMG, and more sensors can therefore be integrated on the same surface. This quickly led to the development of HD-FMG devices and their evaluation, as described in the next section.

4.2 Online Evaluation of Enhanced Surface Modalities

Primary Publication:
[2] M. Connan, R. Kõiva, and C. Castellini, "Online natural myocontrol of combined hand and wrist actions using tactile myography and the biomechanics of grasping," *Frontiers in Neurorobotics*, vol. 14, no. 11, pp. 1–16, feb 2020, doi: 10.3389/fnbot.2020.00011. A.2
Related Publications:
[9] C. Nissler, M. Connan, M. Nowak, and C. Castellini, "Online tactile myography for simultaneous and proportional hand and wrist myocontrol," in *MEC2017 - Myoelectric Control Symposium*, 2017. B.1
[5] N. Jaquier, M. Connan, C. Castellini, and S. Calinon, "Combining electromyography and tactile myography to improve hand and wrist activity detection in prostheses," *Technologies*, vol. 5, no. 4, pp. 1–16, oct 2017, doi: 10.3390/technologies5040064. B.2

The previous evaluation in A.1 showed highly promising results for myocontrol with the FMG modality. The fact that the pressure sensors require a lower complexity of electronics compared to sEMG led to the fast development of HD-FMG bracelets for research purposes, such as the one developed by the *University of Bielefeld* [162], described in Section 3.1.4.

HD-FMG has already been used in [42], using 126 pressure sensors in a rigid housing around the forearm. The study also proved that it performed better than previous studies with sEMG sensors using a classifier. Although the comparison might seem unfair, some studies have shown that reducing the number of sEMG sensors to 6 or 8 does not significantly improve the classification/regression results [233, 234].

Increasing the number of sensors enables the creation of a pressure map of the forearm, measuring the movements of the underlying muscles, the displacement of the bones, and the soft tissue.

HD-FMG, also called tactile myography, has already been used in a study in B.1, testing SPC on the same actions as previously tested in A.1, namely rest, power, wrist flexion, extension, supination, and pronation by involving six persons without any limb difference and one with transradial amputation. HD-FMG outperformed sEMG by about 20% in the TAC test of this online study.

An essential point in SPC and for prosthesis users is to be able to control combined actions, especially wrist movements together with hand actions, e.g. power grasping and rotating the wrist simultaneously. While combined actions have been evaluated for sEMG, A.2 is the first study combining actions when using HD-FMG. However, the majority of earlier studies involve training the combined actions in addition to the single ones, which increases prediction instability because, as more actions are trained, the

harder it can be for the machine learning model to recognize so many different patterns. The number of sensors that HD-FMG provides could potentially allow ridge regression to achieve good results due to some linearity in the muscular contractions. The article A.2 poses the hypothesis that by training only on single actions, the algorithm could potentially reach combined actions without training on them.

Another important consideration in wearable Human Machine Interfaces is embedding algorithms on limited platforms, such as a smartphone or a microcontroller. Therefore feature selection needs to be thought of to reduce the time complexity. The article A.2, developed in this section, also evaluates the ROI Gradient feature selection algorithm for the HD-FMG modality in comparison with no feature selection.

4.2.1 The Biomechanics of Grasping for Combined Hand/Wrist Gestures

As the most interesting and practical combinations of actions to achieve are the wrist and power grasp, the same gestures as the previously described studies were evaluated. Before starting the experiment involving combined actions, it is necessary to evaluate the limits of the human body in order to avoid asking the participants for impossible movements. Indeed, as most people should have experienced without necessarily noticing, one example of it, named tenodesis, is the maximum voluntary contraction (MVC) of the power grasp decreasing while flexing the wrist (and increasing when extending it). Other limitations come into account, as explained more in detail in A.2. While some combinations of movements have not yet been studied in the literature, others have, especially those involving power grasping, as summarized in Table 4.1. The respective thresholds for the combined actions and the protocol of this experiment are specified in Section 3.5.2.

		Pronation			Neutral			Supination		
Literature	N[k]	Extension	Neutral	Flexion	Extension	Neutral	Flexion	Extension	Neutral	Flexion
Bhardwaj et al. (2011) [235] [a]	100				107%	100%	54%			
Parvatikar and Mukkannavar (2009) [236] [b]	50				91%	100%				
Mogk and Keir (2003) [237] [c]	10	95%	87%	50%	99%	100%	56%	98%	94%	61%
Fong and Ng (2001) [238]	30				102%	100%				
Claudon (1998) [239] [d]	15	93%	84%	62%	104%[e]	100%	73%	103%	101%	71%
De Smet et al. (1998) [240] [f]	40		92%			100%			101%	
Kattel et al. (1996) [241] [g]	15					100%	73%			
Richards et al. (1996) [242]	106		91%			100%			102%	
Zellers and Hallbeck (1995) [243]	20				98%	100%	84%			
Duque et al. (1995) [244][h]	20					100%	52%			
Marley and Wehrman (1992) [245] [i]	20		80%			100%			90%	
Terrell and Purswell (1976) [246] [j]	40	69%	88%	57%	77%	99%	70%	77%	100%	73%
MEAN		86%	**87%**	57%	**97%**	**100%**	**66%**	93%	**98%**	68%

The values in bold are used as a reference for the experiment's thresholds. [a]Force exerted while the wrist was immobilized at 30° flexion/extension. [b]Based on reported grip strength for shoulder at 0° of shoulder flexion and elbow at 90°. [c]Peak force was used to evaluate the maximum grip strength 100% of MVC. [d]Based on maximal voluntary flexion/extension. [e]Force exerted while the wrist was immobilized at 30° extension. [f]Non-immobilized wrist, full pronation/supination. [g]Based on the reported grip strength for shoulder at 0 elbow at 90° for all actions and when wrist flexion is involved, it is with 2/3 of maximum flexion. [h]Based on the reported percentage in full voluntary flexion. [i]Based on the reported percentage at 90° of elbow flexion. [j]Force exerted with the wrist at 50° of extension. [k]Number of participants in the study.

Table 4.1: Percentage of the maximal grip strength with combined wrist and forearm movements according to the literature A.2.

4.2.2 Target Achievement Control Test of Combined Actions with HD-FMG

In order to evaluate the HD-FMG modality, a TAC test was performed, as described in Section 3.4.1.2. The different actions were separated into three categories, namely "single actions", "combined actions with power grasp", and "combined actions without power grasp". The success rates of each of these three groups are described in Fig. 4.3 for both RR and RR-ROIG. For both feature selection methods, the average SR for "combined actions with power" is significantly lower than the one of the other two groups, by an average of 33% for RR and 22.8% for RR-ROIG. The "single actions" group reaches $70.0 \pm 21.2\%$ of SR, and "combined actions without power" $68.1 \pm 21.7\%$. Both groups are significantly different from "combined with power" with respectively $p = 0.0001$ for the first and $p = 0.0039$ for the second, after Holm-Bonferroni correction. The difference between the same groups is also significant with RR-ROIG, with respectively $p = 0.0007$ when comparing "combined actions with power" to "single actions" and $p = 0.0310$ to "combined actions without power". Both methods do not show any significant difference between the "single actions" and the "combined actions without power".

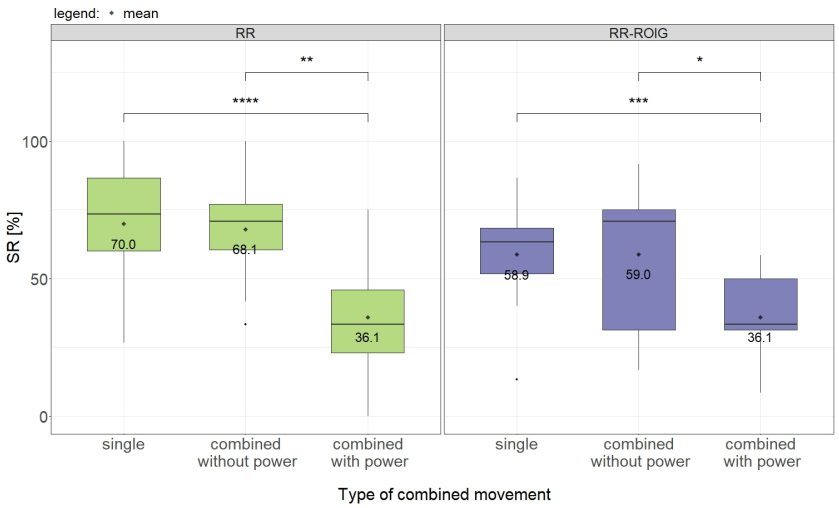

Figure 4.3: Boxplots and means of the success rates across all participants grouped according to the selected features and the type of combined movement in A.2. $*p \leq 0.05; **p \leq 0.01; ***p \leq 0.001; ****p \leq 0.0001$.

When analyzing the SRs action-wise, the combination of wrist extension with power grasp has a particularly low rate (16.7% for RR), before the supination with power (36.1%).

Regarding the feature selection algorithm, there is no statistical difference between the SRs of RR and of RR-ROIG (paired t-test, p=0.2123), respectively $59.0 \pm 17.6\%$ and $51.9 \pm 17.2\%$.

For the groups without the combined power grasp, the TCT was almost 2s faster than with the combined power grasp, confirming that actions combined with power were more challenging to reach. For all failed tasks, the TIT is relatively low compared to the goal of 1.5s, possibly meaning that the failed tasks were difficult to reach. The TIT for successful tasks is close to the target of 1.5s consecutively, implying that they would be achieved without wobbling around the goal.

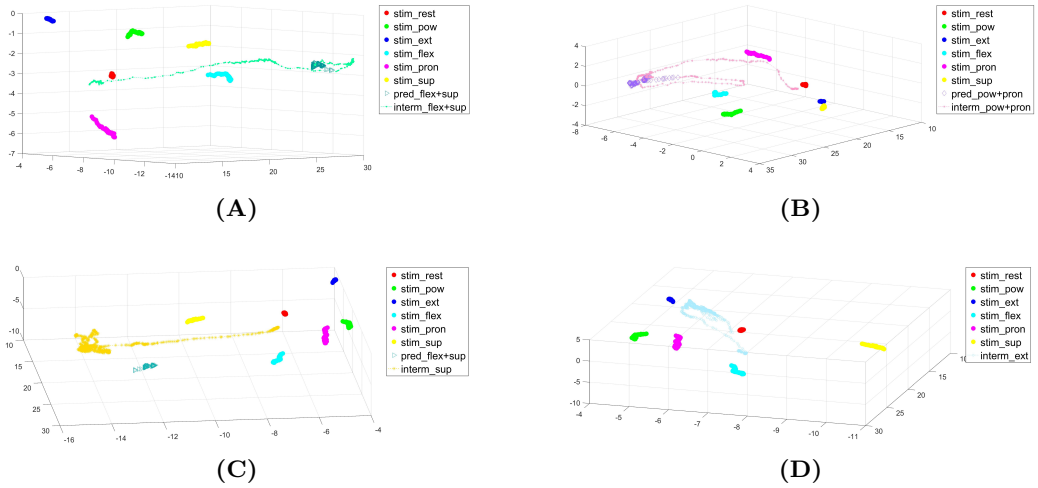

Figure 4.4: PCA of some failed or non-reachable actions performed by the amputee during the first repetition. Legend items starting with 'stim', 'pred', and 'interm' represent, respectively, the clusters of the trained actions, the samples when the participant is in the target, and the intermediate values while trying to reach the target in A.2. (A) PCA displaying failed flex.+sup. for RR. (B) PCA displaying failed pow.+pron. for RR-ROIG. (C) PCA displaying non-reachable supination action for RR. (D) PCA displaying non-reachable extension action for RR.

The amputated participant achieved $15.4 \pm 25.9\%$ of SR with RR and $20.5 \pm 21.7\%$ with RR-ROIG. This is relatively low compared to the participants without limb differences. When analyzing the possible reasons for these results more in detail, the reachability index shows that half or more of the action types were attainable at least once during the three repetitions. The PCAs plotted in Fig. 4.4 show some task-case where the participant seems like he could reach the target action (A and B) but could not stay for 1.5s within the target. When trying to reach the supinated target in Fig. 4.4C, the trajectory of the signals seems to pass by the targets, instead reaching a pattern somewhere between supination and flexion with supination. In Fig. 4.4D the participant tries to reach the extension target, and although the prediction signals seem to get closer, they never attains the target. This might be caused by worn-out muscles that are only occasionally used or be the result of some drift in the data.

4.2.3 Summary

The publication A.2 has shown for the first time that SPC of combined wrist and hand gestures is feasible with HD-FMG to some extent, without any need for prior training on the combined gestures. When adding a power grasp within the combination, the SR drops considerably. However, when considering single actions only, the performance is comparable to the previous literature B.1, and there is no significant difference with the combined actions without power grasp. Although the person with amputation had worse results than participants without amputation, further analysis showed that most of the actions were reachable, and some non-reachable ones might have been easier to achieve if targeting a lower level. The evaluation of previous literature regarding the biomechanics of grasping did not include amputee data due to the lack of studies on the subject. It might be interesting to record equivalent measurements via sEMG, despite the fact that generalization might be difficult depending on the surgery. Therefore, the thresholds chosen for the experiment might not reflect the difficulty or feasibility for amputees, who often have atrophied muscles at the stump level as they are not using them. This is a point to consider in future FMG/HD-FMG studies, although the muscles could potentially be trained to achieve a more distinguishable pressure mapping.

This study also evaluated a feature selection algorithm (ROIG) in comparison to direct data feed, and no significant difference was found between the two. This is a good indication that such an algorithm could help in future embedding on a wearable device. It might, however, still be useful in the future when more sensors come into play. The trade-off between the time complexity of the feature selection algorithm and the one of the entire data fed to the same regressor would need to be evaluated before actual embedding. This same HD-FMG bracelet was actually later on successfully tested when feeding the data to a micro-controller, in the master thesis of Shreyas Waichal [66]. It showed that the full data could be processed in real-time with RR and RR-RFF without requiring feature reduction, with some adjustments on the chosen number of RFF.

The experiment has shown that with a sufficient number of sensors of HD-FMG, simple ridge regression could provide combinations of actions by only training on single ones. This was further demonstrated for HD-sEMG in [234], with 192 as well as 16 monopolar sensors. The reason behind this is not entirely clear but could be explained by the sensor data reflecting some linearity in the muscles, which is also somewhat visible in Fig. 4.4 (A, B, and C), where the cluster for the combined actions is on a linear trajectory lying in between the clusters of the composing individual actions, as already shown in [247]. Therefore, by reducing the number of trained actions (not having to train on the combined ones), not only the training time is reduced but the complexity of the model as well, providing a more stable and reliable prediction.

4.2.4 Comparison of HD-FMG with sEMG and Offline Fusion of the Modalities

Related Publication:

[9] C. Nissler, M. Connan, M. Nowak, and C. Castellini, "Online tactile myography for simultaneous and proportional hand and wrist myocontrol," in *MEC2017 - Myoelectric Control Symposium*, 2017. B.1

[5] N. Jaquier, M. Connan, C. Castellini, and S. Calinon, "Combining electromyography and tactile myography to improve hand and wrist activity detection in prostheses," *Technologies*, vol. 5, no. 4, pp. 1–16, oct 2017, doi: 10.3390/technologies5040064. B.2

In B.1, sEMG and HD-FMG were compared in an online study using the device developed in A.1 for sEMG signal acquisition and the HD-FMG bracelet from the *University of Bielefeld* already mentioned in this chapter. RR-RFF was used for the 20 sEMG signals and RR for the 320 channels of the HD-FMG bracelet. It was shown that HD-FMG performed significantly better than sEMG in a study involving six participants and one user with transradial amputation.

Although RR has the considerable advantage of allowing combined actions as shown in A.2, non-linear algorithms should not be left aside as they often allow for better differentiability of the patterns. A non-linear algorithm for the same HD-FMG has been studied in B.2, namely Gaussian process regression (GPR). The hand/wrist actions performed in this experiment are slightly different from the previous studies by also involving single finger movements: wrist flexion, wrist extension, wrist supination, thumb flexion, index flexion, and little-finger flexion (cf. Fig. 3.12 A and B). The first experiment, an online TAC test with HD-FMG involving three repetitions of the six actions at three different activation levels, showed that GPR outperformed RR in terms of SR, TCT, TIT, and nRMSE. Although the SR is 20% lower than the one reported in B.1, this can be explained by the involvement of single-finger actions, which are more challenging to detect. The second experiment tested an offline multimodal fusion, mixing sEMG and HD-FMG. However, there was no significant difference between HD-FMG alone and the multimodality with sEMG. The offline study shows nevertheless that HD-FMG outperforms sEMG either with RR or GPR (with several distance measures).

4.3 Offline Evaluation and Fusion of Surface and Deep Modalities

Primary Publication:
[4] M. Connan, B. Yu, C. Gibas, R. Brück, E. A. Kirchner, and C. Castellini, "Deep and surface sensor modalities for myo-intent detection," in *Proceedings of MEC - Myoelectric Control Symposium*, 2022. A.3

The previous fusion experiments mentioned between FMG and sEMG in Section 4.1 and between HD-FMG and sEMG in Section 4.2 did not show any evident prediction improvement results from the multimodal fusion. One possible explanation for these results would be that all the previously fused modalities are *surface modalities*, i.e. they obtain their data from surface muscles. Indeed, even though FMG and HD-FMG can indirectly record some information about the deeper muscular activity, these techniques are still considered surface modalities.

In terms of deep modalities, ultrasound has already proved to achieve good results for myocontrol, even for single-finger control. An offline study showed an nRMSE of 1% or less for on-off training [48], which is the same training type as the experiment presented in this section (i.e. not taking into account the intermediate values when moving into the trained position). This was, however, by training on a tenth of the available data (5 repetitions per session), whereas in reality, the training would be performed on the first repetitions and the testing on the last ones. Training on on-off sessions and testing on unseen graded sessions (i.e. with intermediate values) showed an nRMSE of around 10%. The experiment in [49] demonstrated the control of individual fingers in order to play on a virtual piano, as shown in the video[1]. Single-transducer devices have also been implemented in recent years [111, 112], and the TAC test presented in [113] showed a 100% of success rate in combined wrist/grasp actions with 3 DoFs.

Another modality, able to get deep muscular activity, has gained interest in the community over the past years: electro-impedance tomography. The technique has already proved to be able to differentiate between hand movements offline, using support vector machine (SVM) [51] or other classification techniques [248, 249]. Some recent research studies also explore the integration of EIT and sEMG [145] or EIT, sEMG, and FMG [250] in one armband/sensor.

The use of deep modalities (Ultrasound and EIT) would theoretically improve intent detection of hand/wrist gestures, in particular, compared to FMG, as the latter is a surface modality that would theoretically be more impaired for detecting the wrist rotation movements, which rely on deeper muscles. Ultrasound is expected to perform better than the other modalities, and the goal is to develop a fusion algorithm of the

[1] `https://www.youtube.com/watch?v=1yoU1f_zwiY`

three modalities. Indeed, fusing data from deep muscles and surface muscles together could potentially improve myoelectric control. The study presented in A.3 provides a comparison and offline fusion of three modalities, namely FMG, EIT, and ultrasound, by involving ten subjects in performing wrist and grasp motions.

4.3.1 Comparison of the FMG, Ultrasound, and EIT Devices

FMG has already proven to be a portable solution (Section 3.1.3) with a maximum sampling frequency of 192.5Hz depending on the number of sensors, in this case 94.2Hz. Meanwhile, the ultrasound device's frequency depends on the parameters selected by the user, such as the depth of the signal. Additionally, the FMG bracelet was equipped with ten FSRs in this experiment due to the limited space on the forearm with the three modalities. As such, it had the lowest spatial resolution in this experiment.

The ultrasound device is on its way to becoming a portable solution [83]. The tablet computer used for processing could potentially be carried in a backpack. However, it still requires a power supply at the moment. Although some ultrasound solutions are already portable [112], they are A-mode versions, i.e. they only provide a few lines of the ultrasound image with three or four single transducers and are therefore more prone to noise or overfitting. The device's probe is considerably flatter than the standard transducers and is thus more fitting for potential integration in a prosthesis. Several steps would still need to be evaluated before reaching that goal. In particular, it needs to be taken into consideration that gel needs to be placed on the transducer to convey the acoustic energy from the transducer to the tissue without crossing through the air at any point. In this device, the gel is poured into a separate cap that can be screwed on the transducer (cf. Fig. 3.5). The frequency of the ultrasound device presented here depends on the depth of the image as well as the number of angles to swipe, parameters that can be tuned. However, for simplicity, the image of the native ultrasound software at angle 0 was streamed in this case to the experiment software and saved on the disk at a frequency of approximately 6Hz. Data could also be saved temporarily in the RAM for a faster frequency, but this would only be useful for offline processing and limits the experiment length and protocol. If no saving for experiment purposes is done, this could increase the frequency. The spatial resolution of the device depends on the parameters set. With images for every 21 angles, it is the highest-resolution device presented in this thesis so far. The limitation is on the processing time of this amount of data.

The EIT device provides a 256-dimension vector with 208 measurement values (the remaining ones being placeholders while the current is injected through these electrodes). A basic tomographic reconstruction provides a 32x32 image, of which only the central circle varies, resulting in 740 values. The spatial resolution is thereby higher than FMG but lower than ultrasound. The sampling frequency is the limitation of this device, with approximately 2.7Hz. For EIT to be considered in the future as a single modality for myocontrol, the frequency of the device needs to be improved by e.g. taking the measure-

ments in parallel instead of sequentially. Nonetheless, it might be used in conjunction with or as a complement to other modalities, which might as a result enhance them. The device is fully wearable and transmits its data via Bluetooth or WiFi. However, it needs to be taken into account that this modality is very sensitive to the movement of electrodes, sweat, or heat, which influence the measured impedance.

4.3.2 Feature Selection and Image Reconstruction

Some of these modalities have too many features for ridge regression to be able to process them in real-time, let alone more sophisticated algorithms. Additionally, some of the devices require image reconstruction via tomography and/or feature selection. The different methods to obtain the features, explained in more detail in Section 3.3, are compared via the nRMSE when using ridge regression since this algorithm, due to its linearity, can potentially allow the prediction of combined actions without training on them, as found out in A.2 for HD-FMG, therefore reducing the prediction complexity, making it more stable.

FMG, with only ten features, did not need any feature selection. Image reconstruction of the ultrasound data was already performed in the software provided with the device. However, images of size 1161x162 (188 082 features) cannot be processed in real-time and therefore need feature selection. Thus, the Region of Interest Gradient was employed, as it had been successfully used for ultrasound [48]. It was compared to a downsampling of the images with different steps (14, 20, 25, and 30). EIT data were tested, both raw and with different tomography reconstruction methods.

These different feature extraction and selection methods and modalities were evaluated by comparing the normalized root mean square error when using a ridge regression algorithm. The results showed that the ultrasound features performed better overall, whereas the EIT features performed worse. The comparison of the top feature extraction techniques for each modality for the different actions (cf. Fig. 4.5) revealed that the same modality did not always perform best for all actions, highlighting the possible need for multimodal algorithms.

Moreover, the FMG modality surprisingly performed better than the other ones for wrist pronation and supination, which are movements involving deeper muscles. This could be because surface muscles are also indirectly bulged when deeper muscles are activated, which can be reflected in the pressure map on the surface of the forearm. The lower results of the EIT system compared to the other modalities could be due to sweat-induced changes in skin bioimpedance over time. This drawback, as well as the low frequency, are limitations that need to be addressed before the device can be used online. However, the modality could serve as a complementary tool for other modalities.

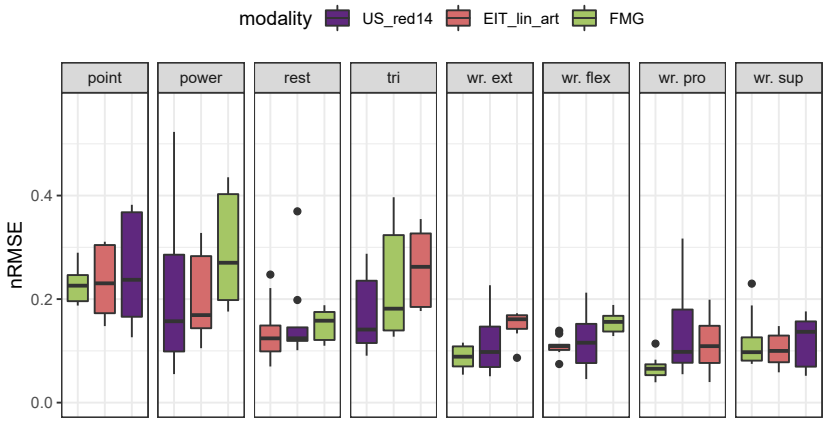

Figure 4.5: Best performing feature selection methods according to hand/wrist action.

4.3.3 Fusion of Surface and Deep Modalities

Data were collected according to the protocol described in Section 3.5.3. The best-performing feature selection methods of each modality were compared as single modalities to a multimodal model involving the same features.

A multimodal regression algorithm was developed with a radial basis function kernel for each modality as described in Section 3.2.6. The hyperparameters of the kernels were adjusted for each participant. Compared to individual modalities, the results show (cf. Fig. 4.6) that the multimodal algorithm performs overall better than the individual modalities, with a statistically significant difference with FMG and EIT.

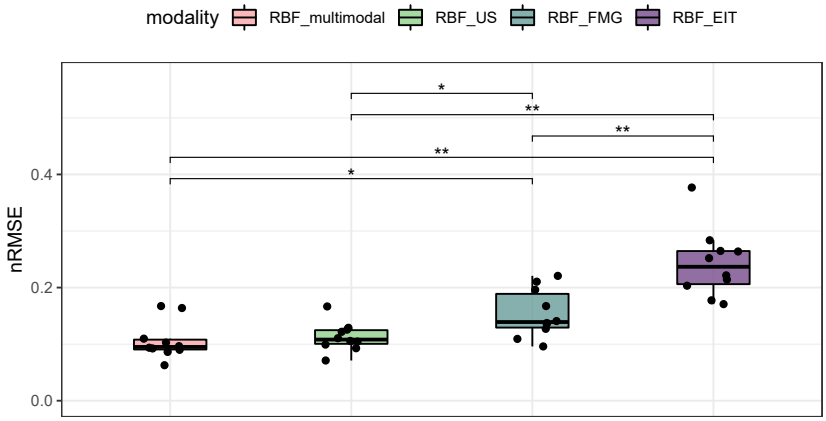

Figure 4.6: Multimodal algorithm with RBF kernels compared to individual feature selection methods.

4.3.4 Summary

In this experiment, several feature selection methods were evaluated for the different sensor types. Although none of them outperforms the others for each modality, the best-performing ones were selected and compared. The ultrasound approach was identified as one of the top-performing methods by the nRMSE and the cluster separateness index. Additionally, a multimodal algorithm based on RBF kernel was developed, and the fused approach obtained better performance results than every single modality with a significant difference with EIT, and FMG.

Additional feature exploration on the different modalities might reveal better-performing features with, for instance, the help of deep-learning algorithms. However, this might be at the cost of computation time. The lack of statistical significance between ultrasound and the fused model might be due to the low number of participants, and further evaluation might be needed. Future work also includes comparing pairs of fused modalities, which might expose a limitation of the fusion by one type of sensor, e.g. EIT. The fusion was now performed in the ideal case of RBF kernel with an infinite-dimensional feature space and hyperparameter optimization for each participant. Another interesting topic of investigation is the implementation of an approximated kernel for computation time reduction and incremental learning, in addition to online testing with the involvement of participants with hand amputation. Subject-wise hyperparameter optimization is often avoided in online studies due to the search for a population-wide model and the time constraint that such optimization comes with. This might be arguable in view of several studies that advocate in favor of user-specific models [71].

4.4 Application of Combined Modalities with Electromyography and Kinematics

Primary Publication:

[3] M. Connan, M. Sierotowicz, B. Henze, O. Porges, A. Albu-Schäffer, M. A. Roa, and C. Castellini, "Learning to teleoperate an upper-limb assistive humanoid robot for bimanual daily-living tasks," *Biomedical Physics & Engineering Express*, vol. 8, no. 1, pp. 1–17, dec 2021, doi: 10.1088/2057-1976/ac3881. A.4

Related Publications:

[12] M. Connan, M. Sierotowicz, B. Henze, O. Porges, A. Albu-Schäffer, M. A. Roa, and C. Castellini, "Learning teleoperation of an assistive humanoid platform by intact and upper-limb disabled users," in *Converging Clinical and Engineering Research on Neurorehabilitation IV. ICNR 2020. Biosystems & Biorobotics*, vol. 28, pp. 165–169, Springer. Springer International Publishing, oct 2020, doi: 10.1007/978-3-030-70316-5_27.

[10] O. Porges, M. Connan, B. Henze, A. Gigli, C. Castellini, and M. A. Roa, "A wearable, ultralight interface for bimanual teleoperation of a compliant, whole-body-controlled humanoid robot," in *Proceedings of ICRA-International Conference on Robotics and Automation*, vol. 35, no. 12, p. 2289, 2019. B.3

[7] M. Sierotowicz, M. Connan, and C. Castellini, "Human-in-the-loop assessment of an ultralight, low-cost body posture tracking device," *Sensors*, vol. 20, no. 3, p. 890, feb 2020, doi: 10.3390/s20030890. B.5

Multimodality does not necessarily require fusion algorithms: combining sensors can often be sufficient for some applications. The publication A.4 presents a new setup involving sEMG and IMU-based body tracking in order to teleoperate a humanoid robot. With the advent of robotic arms becoming increasingly available, an alternative started appearing for users with disabilities. Namely, to teleoperate such platforms for performing tasks they cannot achieve with their own body or for teleworking [251]. Such a platform in a home environment could also allow them to call a teleoperating center, where an operator could perform the task they do not manage to execute. For amputees, such a setup is a viable complement to their prosthesis. Indeed, as prostheses are constrained by several factors, such as size and weight, the integration of the required electronics and mechanics is limited. It is currently impossible to construct a prosthesis with 23 DoFs, as in the human hand. Robotic hands and arms, not limited by the prostheses constraints, would hence provide a higher level of functionality and additional DOFs for amputees. Furthermore, it would prevent potential artifacts at the sensor level that could be generated by carrying heavy loads, which alter the registered pattern.

An initial proof-of-concept trial was performed in the video of B.3, showing the humanoid robot teleoperated via sEMG and VR trackers to perform complex ADL tasks

such as opening a fridge, cooking, or giving a phone call. The experiment in A.4 confirms the teleoperation on a larger pool of subjects as well as on a longer term. It also presents a more portable setup using IMU-based tracking, which does not need additional hardware, conversely to Virtual Reality (VR) trackers that necessitate external VR base stations.

Such a setup additionally allows for a direct comparison between people with and without limb differences. With the potential exception of the device developed in B.6, amputees usually use their prosthesis sockets for experiment purposes, and non-disabled participants have been using bypass sockets so far. The setup presented here enables a more fair comparison of the two groups' performance. This study hypothesizes that people with disability would achieve similar performance compared to non-disabled participants after several repetitions of teleoperated tasks. Indeed, with the plasticity of the human brain [252], the more a person repeats a task, the more that person learns to perform it better. This "learning effect" is evaluated in this study on seven non-disabled participants, two with limb difference (D1 and D2), and one long-term participant, by using metrics such as TCTs, improvement ratios across repetitions/days, as well as user evaluation metrics, as described in Section 3.4.3. The protocol of this experiment and a description of the tasks are reported in Section 3.5.4.

4.4.1 Results of the Single-Session Participants

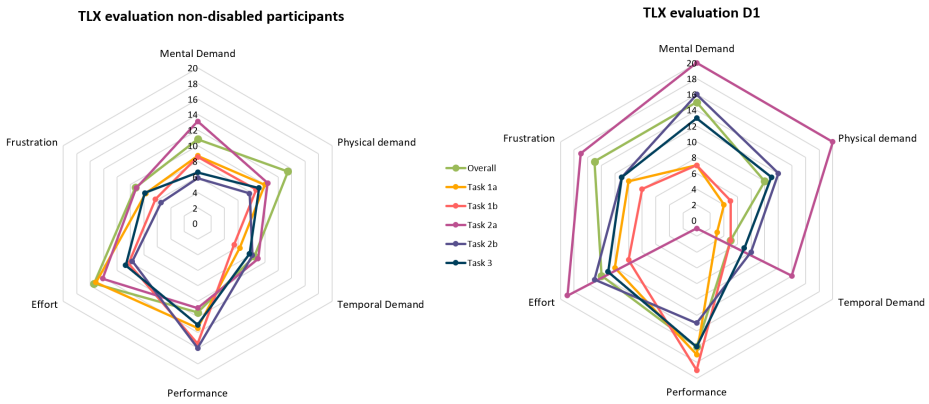

Figure 4.7: Results on successful attempts for the single-session participants in A.4. Spider plot of the average TLX evaluation for all non-disabled participants and for the disabled participant D1.

The results obtained from the subjective evaluation corroborate the TCTs. Both show, for instance, that Task 2a (opening a bottle), as described in Fig. 4.7, was the most challenging task to perform, with the worse scores in terms of performance, frustration, mental, physical, and temporal demand, and the second worse in terms of effort. D1's subjective evaluation has comparable ratings as all other participants, Task 2a being seemingly even more difficult for him. The TCTs of the participants with upper limb

differences were also in line with the ones of the other participants, including Task 2a for D1, despite his lower subjective ratings.

The participants additionally rated the control of the body pose and hands. Surprisingly, D1, who has an intact hand and a congenital difference at the transradial level, similarly rated the control of the right and left hands.

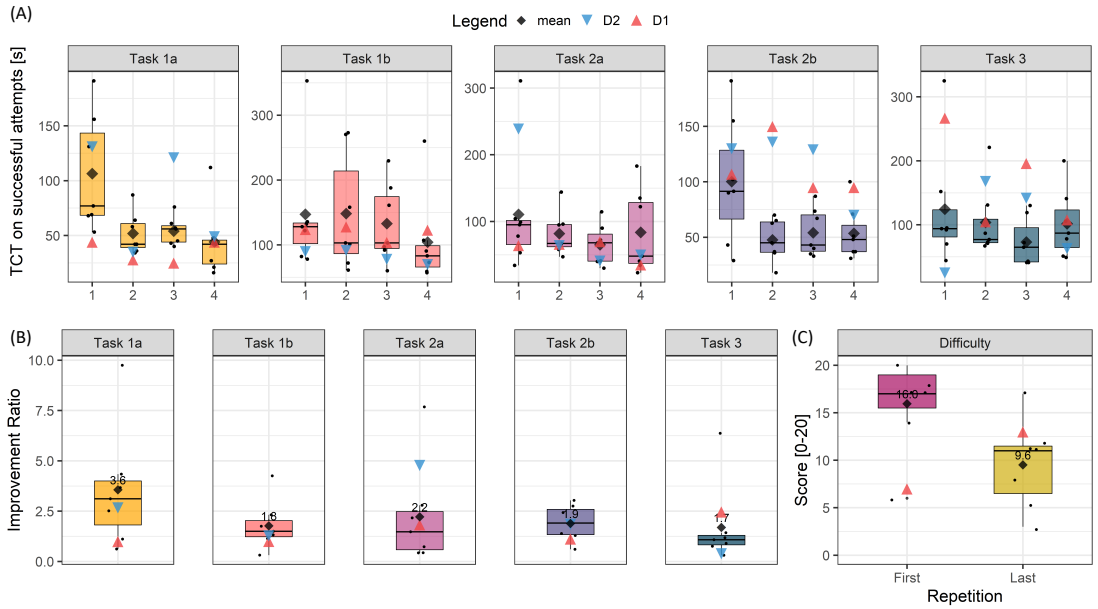

Figure 4.8: Results on successful attempts for the single-session participants in A.4. (A) Task-wise TCTs for each repetition on the successful attempts. (B) Task-wise improvement ratios on the TCTs of the successful attempts between the first and the last repetition. (the higher, the better). (C) Evaluated difficulty on the first and last repetitions (the lower, the better). D2 did not fill out the subjective assessment due to a time limitation.

A learning effect is visible across the four repetitions (cf. Fig. 4.8) and, considering all participants, a Linear Mixed-Effects Regression (LMER) analysis was performed with log(TCT), to normalize the data, as the dependent variable, the repetition and amputation condition as independent variables, and the participants and tasks as random effects to adapt to the different initial skill levels of each participant and the different difficulty of each task. The analysis showed a significant difference between the first repetition and all the other ones ($p = 0.040$ between 1 and 2, $p = 0.007$ between 1 and 3, and $p < 0.001$ between 1 and 4), and no significant difference from the amputation condition. On average, across all tasks, the non-disabled participants had an improvement ratio of 2.2 times. The subjective criteria evaluating the difficulty confirms that with a drop from 16.0 out of 20 for the first repetition to 9.6 for the last repetition. The improvement ra-

tios of the two participants with limb differences are also in line with the other participants.

The single-session participants show an increase in hand speed over the repetitions with a statistical significance between repetitions 1 and 3 ($p = 0.017$) and 1 and 4 ($p = 0.015$), after an LMER analysis with log(speed) as the dependent variable and the same independent variables and random effects as before. The participants with limb differences seem faster (0.071m/s) than the non-disabled ones (0.044m/s), although this might also be attributed to the slightly different wrist control due to the amputation.

4.4.2 Results of the Long-term Participant

A similar learning effect is visible across days for the long-term participant, who repeated the experiment over five days. All tasks show a decreasing trend over the days, except for the fifth day of Task 2b showing a slight increase, and Task 2a, which was judged the most complicated task, showing no clear trend.

The TLX test also confirms this trend with an overall self-evaluated performance rising from 8/20 on the 19/20 between the first and the last day, and an apparent learning curve for the overall evaluation (cf. Fig. 4.9). The participant, as for single-sessions, evaluated the perceived difficulty of the first and last repetitions each day: it also shows a decreasing trend until the last day with an equal level, indicating a learning effect by the stabilization of the difficulty. The overall improvement ratio between the first and last days was 2.5, with the main part of the learning happening between Days 1 and 2 with a ratio of 2.2. The long-term participant also increased speed over the sessions, reaching on the last day 0.053m/s.

4.4.3 Summary

This study validated the use of interactive myocontrol and this specific multimodal sensing setup to teleoperate a humanoid robot to perform highly complex bimanual tasks from activities of daily living. Learning curves were apparent in the result either across repetitions or across days, showing a decrease in completion times and an increase in speed. As hypothesized before the experiment, there was no significant difference from the amputation condition, and the results from participants who had a limb difference were consistent with those of participants who did not.

The learning effect is something not frequently analyzed in myocontrol studies (with some exceptions) due to the nature of the experiments themselves. The constraints of time and subject recruitment make them not ideally suitable for studying this learning effect. It is however something to take into consideration as the human brain is still more complex and capable than any machine learning algorithm: it can learn quickly and adjust to unsatisfactory control.

Figure 4.9: Results of the TLX test and improvement ratios of the long-term participant in A.4. (A) Evaluation of the different TLX criteria over the days for each task and overall in A.4. (B) Evaluation of the difficulty for the first and last repetitions over the session with a box plot gathering the results over all days. (the lower, the easier) (C) Evaluation of the quality of the body pose control and the hand pose control over the session with a box plot gathering the results over all days. (the lower, the better) (D) Task-wise improvement ratios on the TCTs of the successful attempts between the first and the last repetition. One data point represents the improvement ratio for one day. (the higher, the better) (E) Improvement ratios averaged over the tasks on the TCTs of the successful attempts between, respectively, Day 1 and Day 2 (RatioD12), Day 1 and Day 5 (RatioD15), and Day 2 and Day 5 (RatioD25). (the higher, the better).

4.5 Results Overview

The different publications underlying this dissertation can be summarized as follows:

(A.1) In order to compare different modalities (in this case, FMG and sEMG), a new wearable, low-cost, and power-efficient data acquisition device was developed and evaluated in a user study. A new flexible design of pressure sensor housing was proposed to transfer the muscle-exerted pressure to the force-sensitive resistor. The offline experiment compared the two modalities. The results show that FMG yields a more stable signal across time than sEMG when a gesture contraction is held. The two modalities, as well as the fused approach, show similar results without statistical significance when comparing the prediction of ridge regression with random Fourier features with the normalized root mean square error (nRMSE). This indicates that FMG is a viable alternative to sEMG although other fusion approaches should be tested to see if the sensors could have complementary data. Furthermore, the separateness index shows a significantly higher separability of FMG clusters over sEMG. This could therefore be a considerable advantage in future online performance evaluations.

(A.2) Due to the significantly less complicated electronics of FMG compared to sEMG, multiple sensors can be easily integrated into a single wearable bracelet, providing a much higher spatial resolution to HD-FMG. Such technology also seems to have a surprisingly advantageous ability that was demonstrated in a user study: by training on single actions only and using linear regression, combined 3-DoF hand/wrist actions can be performed. The study initially investigates the feasible limits of muscular activation during combined actions to propose a biomechanics approach for target definition in the context of target achievement control tests. From the experiment, combined wrist actions presented no significant difference from single actions. At the same time, a power grasp seemed to influence the control negatively. However, this might have been due to a saturation of the recorded pressure that could potentially be adapted by changing the pull-up resistors. Two different approaches were also evaluated during the TAC test showing no significant difference in the reduced version involving region of interest gradient feature extraction for the purpose of future embedding.

(A.3) While the fusion of surface modalities did not show any significant improvement in the previous studies and other literature, fusing deep and surface modalities might. Although deep modalities such as ultrasound perform already remarkably well, devices were previously bulky and not embeddable. However, with the advent of new portable devices, one might question whether the sensor still performs well for the different gestures and if there is room for improvement by adding other modalities. Force myography, ultrasound, and electro-impedance tomography were compared in an offline user study in which hand/wrist actions were recorded simultaneously. Several feature extraction and selection methods were evaluated to propose a new pipeline fusing the three modalities based on RBF-kernel regression with Multiple Kernel Learning, i.e. individual kernels

for each modality. Comparing the prediction in terms of nRMSE showed overall better results than the single modalities with a significant difference with EIT and FMG.

(A.4) An inertial-measurement-based body tracking device was developed and combined with two sEMG bracelets, one on each forearm, as a wearable human-machine interface to teleoperate a bimanual humanoid robot. The platform is proposed as an alternative to prostheses in complex tasks, allowing more functionality due to the embedding constraints of prostheses. It also offers a new assistive solution to people with disabilities, which can be additionally used as an option for them to remote work. Furthermore, it shows the ability of humans to adapt and learn to compensate for eventual weaknesses in the control, underlining the fact that co-adaptation is essential in HMIs.

Chapter 5

Discussion, Conclusion and Outlook

L'expérience est une lanterne attachée dans notre dos, qui n'éclaire que le chemin parcouru.

(Confucius)

Table of Contents

5.1 Discussion and Outlook

While some of the methods presented here offer advantages over the gold-standard sEMG, they all have their drawbacks. This section examines and compares the different modalities for myocontrol of the upper limb, highlighting their advantages and limitations. It also presents the possibilities for fusions of the different modalities, their path to future integration in a prosthesis, as well as the machine learning algorithms recommended for each purpose.

5.1.1 Suitability, Strengths, and Limitations of the Different Sensor Modalities for Wearable Myocontrol

Although this section presents limitations of different modalities for their usage in prostheses, the constraints are possibly less numerous for employing them as normal HMIs, depending on the use case. It also needs to be noted that HD-sEMG and Ultrasound A-mode were not examined in the publications of this dissertation and are mentioned here for the sake of completeness: the information on these modalities comes from the literature and personal experience in the case of HD-sEMG.

5.1.1.1 Surface Electromyography

Advantages The technique continues to have several benefits, which contributes to the fact that it is still the main sensor used in prostheses. It is self-contained and can be easily integrated into a prosthesis. The sensor solely reads body signals and does not require the injection of current or sound waves. Its sampling frequency is also more than sufficient for myocontrol. The rest state is easily identified by an almost null signal.

Drawbacks While sEMG control remains the gold standard of prosthesis control, despite its age, it has many drawbacks, and there is still a considerable gap between the control of a prosthesis and the human hand. For instance, it is sensitive to sweat, electrode shifts, ambient noise, motion artifacts, muscular fatigue, and cross-talk between adjacent muscles [26, 27, 29, 231]. When compared to FMG in A.1, it has less stability over time due to the nature of the two signals. It also has a worse separateness of pattern clusters than FMG. It requires extensive signal filtering and, thus, more circuitry than simpler techniques such as FMG. It additionally needs to be in contact with the skin in order to work.

5.1.1.2 Force Myography

Advantages The technology presents several advantages over sEMG. The experiment presented in A.1 showed that it has a better separability of the patterns than sEMG. It also has better stability over time with a plateau-shaped signal during the hand/wrist actions. This modality is one of the rare ones insensitive to sweat. Even though in the presented publications the sensor was inserted in a non-conductive housing, some other

unprotected sensors might still be sensitive to it (e.g. HD-FMG). It is also one of the only modalities that can be worn on clothes. Its price is very competitive compared to sEMG as it requires almost no electronics. Although low sampling rates may suffer from the aliasing effect, the required sampling rate of FMG is much lower than for sEMG, and a recent study suggests that a sampling rate of 60Hz or more should be sufficient [253]. Its spatial resolution can be easily higher than sEMG due to the simple electronics required. The online study presented in [70] showed a significantly better performance of FMG over sEMG when evaluating three contraction levels.

Drawbacks FMG, despite its high potential as an affordable new HMI, has numerous drawbacks that still need to be solved before a potential integration into a prosthesis. The signal is subject to drift, possibly due to the skin creeping over time, and the patterns might need an update when the skin has reached its maximum creeping point, which depends on each individual (e.g. elasticity of the skin, age, amount of water drunk during the day). The modality can be sensitive to arm movements, either with the acceleration creating pressure on the sensors or with fat tissue accumulation in the elbow hollow when flexing the forearm. It needs to be noted that the aforementioned disadvantages depend on the type of sensors used, and some of them might be surpassed with a different kind of FMG technology [97, 98]. However, two main disadvantages need to be considered. The first is the potential interference within the signal patterns when bumping into an object with the prosthesis/bracelet or when resting the arm on a table. The second main drawback for future prosthesis integration is the weight of lifted objects influencing the FSRs inside the socket. Having force sensors on the prosthesis as well as on the outside of the socket might help solve these issues.

5.1.1.3 High-Density Force Myography

Advantages As mentioned before, due to the simple electronics required for FMG, bracelets can have a high number of sensors, hence leading to HD-FMG. Such technology provides a precise pressure map, and as the article in A.2 demonstrated, its high density can provide combinations of movements without the need to train on them, which is a considerable advantage as it provides a more stable prediction by reducing the number of trained actions. The article in B.2 also showed that HD-FMG outperforms sEMG either when using RR or GPR algorithms in an offline assessment. Its sample frequency is more than sufficient for myocontrol, and its spatial resolution is considerably higher than sEMG and FMG, with, for instance, 320 sensors in the bracelet presented in this dissertation.

Drawbacks The conductive foam used in the HD-FMG bracelet of A.2 tended to creep over time, adding drift to the signals. It was also absorbing the sweat, thus changing its conductivity and making the technology sensitive to perspiration, which is highly undesired in a hermetic socket. Signal saturation can also happen depending on the foam

chosen and the amplification electronics. As well, the technology has the same drawbacks as its simpler version, FMG, regarding weights and external pressure.

5.1.1.4 High-Density Surface Electromyography

Advantages Researchers have demonstrated that above a certain number of electrodes, from 6 to 27, depending on the study [233, 234, 254, 255], adding more electrodes did not improve myocontrol. However, the emergence of HD-sEMG devices and their high spatial resolution has allowed some teams to go deeper into the process of electromyography by being able to decompose the signals into motor unit activations. This technique is becoming increasingly available and has a growing interest in the community. Similarly to HD-FMG, HD-sEMG can also be used to perform combined movements without training on them, as demonstrated in [234].

Drawbacks While wired devices such as the *Quattrocento* from *OTBioelettronica* work well, they are still bulky and unusable for wearable online myocontrol. Wireless HD-sEMG devices have started to emerge but are still in their early version and very sensitive to noise. Additionally, the wireless ones still need a base station to process the signals transmitted via Wifi, and such setups would be only usable in a home environment as of now. Furthermore, the electrode matrix patches needing an adhesive foam to be stuck on the skin and the conductive cream needing to be spread on the electrodes are still a lengthy process, extremely complicated on a daily basis out of lab conditions and with an impaired limb. Therefore, this setup would need to be revised for a possible prosthesis integration. The price of such a device is also, for the moment, only suitable for lab conditions, ranging from 17.000EUR for a wireless version of 128 channels to approximately 35.000EUR for a wired version of 384 channels. These setups are currently mostly intended for offline analysis.

5.1.1.5 Electro-Impedance Tomography

Advantages Electro-Impedance tomography is one of the rare modalities able to measure changes in deep muscles while still being a non-invasive technique and remaining inexpensive (as little as 50EUR for some devices [51]). Due to the different resistivity of tissues and bones, the placement of bones can be identified within a device. Therefore, by using this technology in combination with others, it can identify, e.g., the rotation of a bracelet of sEMG sensors, which can be useful if users get it on and off when myocontrol could be available across sessions.

Drawbacks The EIT device evaluated in A.3 unfortunately only had a frame rate of approximately 2.7Hz, which is insufficient for myocontrol when used as a single modality. However, modifying the electronics could potentially allow for 16Hz with the same number of electrodes, as indicated in [51]. The technology still suffers from several drawbacks and is severely impacted by movements of the electrodes, insufficient skin contact, or impedance transfer. Although tomography reconstruction algorithms partially filter

discrepancies in the signals, reconstructed images are still affected, and the reconstruction can also suffer from inaccuracies resulting from inter-individual anatomy. Additionally, as it injects micro-currents, it needs a custom-made device to be mixed with sEMG [145], since it would otherwise interfere with it.

5.1.1.6 Ultrasound B-mode

This section discusses the advantages and drawbacks of ultrasound devices able to provide beam-formed images and matrices of data.

Advantages Ultrasound is one of the most promising modalities, able to identify single finger movements [48]. It has the best offline performance compared to FMG and EIT, as shown in A.3 and Section 4.3. Its frame rate for one of the 21 angles is about 11Hz (depending on the chosen depth), which could be increased when reducing the number of angles. Online use would thus not be impaired by the frequency. However, the main bottleneck during experiments would be to save the data online, which would significantly drop the frequency due to the high spatial resolution of the device. The system presented in [83] and evaluated in A.3 is one of the first portable ultrasound devices providing extended-field-of-view images. The technology is cheaper than HD-sEMG, with an approximate price of 8000EUR. The probe is considerably flat compared to any other probe available on the market and is designed to avoid skin contact with the gel.

Drawbacks With a number of features in the order of hundreds of thousands, it is undoubtedly the modality offering the greatest insights into the forearm. However, no online algorithm can currently process this amount of data. Feature selection is therefore necessary, at the risk of losing some information. In addition, although researchers are working on a wireless version of the device, this one has yet to be made available. Ultrasound also requires gel to have a clear image: this is something considerably impractical for future prosthesis integration, but in the device used in this thesis [83], the probe was designed to be separated into two parts, in between which the gel could be filled (avoiding any air bubbles) before interlocking them back together. The flat probe could then be stuck to the skin via a custom double-sided adhesive tape.

5.1.1.7 Ultrasound A-mode

Although not evaluated in this dissertation, it is also important to consider the commonly called ultrasound A-mode, which consists of a few transducers, each collecting a line of data [111–113, 185]. Due to the limited number of individual transducers, the approach cannot provide precise imaging of the forearm or any beam-formed image.

Advantages While the device still provides considerably fewer features than Ultrasound B-mode, it can still control single-finger movements [111, 112] as well as wrist movements [113]. It also consumes substantially less power by sending a chirp signal (frequency-modulated waveform) encoding the depth of the reflections [112], as explained

in Section 2.2.3.2. For instance, the system presented in [185] has a power consumption of 6W, i.e. 6h of continuous data acquisition with a 3000mAh (12V, 127g) battery. Single transducers are much easier to integrate into a socket (as done in [256]) compared to other ultrasound probes. Its spatial resolution of a few thousand features requires less feature reduction than Ultrasound-B mode, whose high number of features might be unnecessary given that it cannot be processed online.

Drawbacks Limited to only three or four transducers, this technology is much more prone to error and over-fitting when moving accidentally [185]. Despite providing deep information, the modality cannot produce an image of the anatomical structure like B-mode can: only a predefined direction gathers muscular information on one line, whereas B-mode detects full muscle contraction [185]. As B-mode, it is sensitive to wrist rotation and requires gel for a high-quality signal [185].

5.1.1.8 Inertial Measurements

Although IMUs can be used in different ways, the publications in this thesis employed them as a body-tracking interface.

Advantages IMU-tracking, as presented in A.4, provides additional information, such as the arm position. While acceleration sensors were already fused to sEMG for improving classification accuracy [229], a complete setup enables precise positioning of the arm, which helps to assess occurring problems when performing ADLs at home. Such a device, combined with sEMG or potentially another modality, provides an HMI that could allow people with disabilities to remote work but also to have alternative platforms with more functionalities and DoFs than prostheses, as presented in A.4. The frequency of the approach is more than sufficient to track the movements in real-time.

Drawbacks Prosthesis users may find it more difficult to accept the setup, as it needs to be placed not only on the stump but on the upper arm and torso for precise tracking of the entire arm. Additionally, if a prosthesis user was equipped with an IMU-based body-tracking device, the IMU integrated into a standard prosthesis socket would only provide elbow flexion information and the upwards kinematic chain, not wrist rotation, as the socket is designed to be fitted around the elbow and rotational movement of the stump is limited. Electric cables in the ground can also influence the magnetic sensor of IMUs.

5.1.1.9 Summary

A recapitulation of the advantages and drawbacks of each modality is available in Table 5.1, and a comparison of the modalities according to different criteria can be found in Table 5.2.

Modality \ Criteria	Advantages	Drawbacks
sEMG	Already integrated into prostheses (gold standard); Long-term use; High-quality sensors can obtain signals from the muscles of people suffering from Spinal Muscular Atrophy; Rest state is easily identified with almost no signal	Sensitive to sweat; Sensitive to Muscular cross-talk; Sensitive to electrode shift; Sensitive to muscle fatigue; Requires to be placed on the skin; Price
HD-sEMG	Can be used for motor unit decomposition, also of single-fingers at wrist level [257]; Long-term use	Sensitive to sweat; Muscular cross-talk; Requires to be placed on the skin; Very sensitive to noise when wireless; Still needs a bulky base station for the use of wireless sensors; Usage of adhesive foam and conductive cream is unpractical for prosthesis use; Price
FMG	Insensitive to sweat; Robust to external electrical interference; Can be worn above clothes; Better stability and cluster separability than the gold-standard sEMG; Small size; High signal-to-noise ratio; Price	Potential creeping of the skin; Artifacts due to movement of the arm, or when bumping into something, or lifting an object; Extra care should be taken with the tightness of the device and winding forces, which can introduce discrepancies
HD-FMG	Robust to external electrical interference; Can be worn above clothes; Precise pressure map; Combined movements; Possibility of image processing techniques; Price	Creeping of the conductive foam material over the sensors; Conductive foam sensitive to sweat; Artifacts due to movement of the arm, or when bumping into something, or lifting an object; Bending influence for flexible sensor matrices
EIM / raw EIT	Get deep information; More complex hardware than sEMG [104]; Price	Sensitive to sweat and impedance of the skin; Requires to be placed on the skin; Very sensitive to sensor movement; More influenced by arm position than sEMG [104] ; Sends a microcurrent that can potentially interfere with other modalities; Low sampling rate
reconstructed EIT	Get deep information; Can identify the position of bones; Can be used at the wrist level with classification; More complex hardware than sEMG [104]; Price [50]	Sensitive to sweat and impedance of the skin; Requires to be placed on the skin; Very sensitive to sensor movement; More complex hardware than sEMG [104]; Price
US B-mode	Get deep information; Very high spatial resolution; Can predict single-finger movements [49]; No muscular cross-talk [112]; Can detect the full muscle contraction [185]; Less sensitive to probe shift than A-mode [185]	Needs gel for functioning well (in a contained capsule); Not yet powered on battery; Can be sensitive to wrist rotation depending on the probe [49]; Low sampling rate
US A-mode	Get deep information; High spatial resolution; Lower power than ultrasound B-mode; Can be more easily integrated into a prosthesis than B-mode; Immunity to moisture, sweat and electrical noises [111]; No muscular cross-talk [112]; Cheaper and more wearable than B-mode [185]	Needs gel for high-quality signal [185]; Sensitive to transducer movements with overfitting, and a slight shift of the transducer will significantly change the signals [185]; Cannot provide image of anatomical structure like ultrasound B-mode [185]; Only the muscle information on a predefined direction can be gathered, while B-mode can detect the full muscle contraction [185]; Sensitive to wrist rotation [185]
NIRS / PPG	Get deep information; No electronic interference; High spatial resolution; [258] Low cost; Robustness against bad skin coupling; Small size and thin sensor [45]	Sensitive to wrist rotation; Interference from powerful IR sources (e.g. sun) [45]; Response time of several dozen ms [259]; Sensitive to ambient light [258]; Sensitive to movement
MMG	Less sensitive to placement on the limb; Not sensitive to sweat or skin impedance; No pre-amplification; Price; Detects low-level activations [260]; Propagates through soft tissue [261]; In comparison to EMG, the frequency domain of MMG provides more pertinent data on the contractile characteristics and muscle fibre type composition [262]	Relatively low real-time accuracy [260]; Sensitivity to motion-induced artifacts [261, 263]; Sensitivity to ambient acoustic noise; Adjacent muscle cross-talk [258]; Lower information transfer rate; Lower separateness for classification of a high number of gestures [261]

Table 5.1: Advantages and drawbacks of the different modalities.

Modality \ Criteria	Sample rate	Spatial resolution	Suitability for combined gestures on RR	Separability of clusters	Sensitivity to sensor movements	Wireless	Wearability	Tested in the scope of this thesis
sEMG	++++	-	+	+	+++	yes	+++++	yes
HD-sEMG	+++	+	++	∗	+	yes[(1)]	-	yes
FMG	++++	.	.	++	++	yes	++++	yes
HD-FMG	++++	++	++	+++	++	yes	+++	yes
EIM / raw EIT	- - -	++	∗	-	- -	yes	+++	yes
reconstructed EIT	- - -	+++	∗	+++	-	yes	+++	yes
US B-mode	+	+++++	∗	++++	+	no[(2)]	++	yes
US A-mode	++	+++	∗	∗	-	yes	+++	no
NIRS / PPG	+	.	∗	∗	.	yes	++++	no
MMG	++++	.	∗	∗	-	yes	++++	no

∗ The information is not available and research studies need to be performed on that topic.
(1) HD-sEMG devices are now wireless to some extent, e.g. the *MuoviPro* from *OTbioelettronica*. While the sensor itself is wireless, it still requires an additional synchronization device that collects the data via WiFi (cf. Fig. 2.4), which constraints the user of the system to a limited range of motion.
(2) While no yet wireless, this is a work in progress [83].

Table 5.2: Comparison of the different non-invasive modalities.

5.1.2 Fusion of Modalities

The work in the scope of this thesis initiated several fusions of modalities that had previously never been tested. For instance, A.1 fused for the first time sEMG and FMG in a concatenated offline approach. The results yielded little difference with the best-performing modality, namely FMG. Later, these results were confirmed in an online experiment testing different concatenating fusion approaches [70]. HD-FMG was also fused in an offline experiment in B.2, with, as previously, ridge regression, but also with GPR. None of the two algorithms brought any significant impact by fusing the two modalities, and their performance did not differ much compared to the best-performing HD-FMG.

Making use of sensor fusion theories, a multimodal algorithm has been developed with the ultrasound, FMG, and EIT data of A.3 by using RBF kernels. The layer-level fusion algorithm yielded better results than all other modalities, obtaining a significant difference with FMG and EIT. The absence of significant difference with the best-performing ultrasound might yet be due to the limited pool of participants, and further experiments might be needed.

Several fusion approaches have been tested in the literature, as recapitulated in Table 5.4. Although very few of them involved regression [139], this section will evaluate if the performance of the fused method was better than the one of the individual modalities.

The literature review of [139] shows only a few approaches that seem to have statistically significantly better results with fusion than with the best-performing modality. The experiments presented below have been selected as presenting a statistically significant difference.

As presented in Section 2.4.3, the sensor fusion approach of [140], mixing PPG, MMG, and FMG, resulted in significantly better results than the individual modalities. Similarly, fusing sEMG, nIRS, and MMG for the evaluation of four gestures (power grasp, tip prehension, lateral prehension, and rest) resulted in better results than sEMG, or sEMG-nIRS, despite the fact that sEMG-MMG or MMG alone was not compared [264].

Additional fusion studies, not limited to hand/wrist gestures, can be found in [265, 266].

5.1.3 Pipelines

5.1.3.1 Machine Learning Algorithms

Several machine learning algorithms have been used in this dissertation: all based on regression. Indeed, regression is essential in order to have simultaneous and proportional control, as classification on its own does not allow independent proportional control of two DoFs at the same time [34].

Ridge regression allows not only incremental learning but also, due to its linearity, prediction of combined actions without training on them and by training only on the single actions, as shown in A.2 for HD-FMG and in [234] for HD-sEMG. This should be, therefore, the algorithm of choice to compare other algorithms to when using modalities with high spatial resolution. It was already shown in [34] that linear methods could achieve excellent results comparable to state-of-the-art non-linear algorithms when fed with the right features. In this case, it is also valid for the dimension of input space. An additional non-negligible argument in favor of linear algorithms is their significantly reduced computational demand and, consequently, training time complexity, making it very easy to implement on a low-power microcontroller and easing the process towards prosthesis integration.

However, non-linear algorithms should not be entirely disregarded. They have the advantage of better fitting the input data, enabling better cluster separability, and can be tuned as desired. For instance, with Kernel Regression, the kernel can be adapted to still allow for incremental learning, such as with Random Fourier Features (RR-RFF) implemented in A.1 and A.4, or to allow more sparsity in the data, therefore including dimensionality reduction in the process, like with the Radial Basis Function Kernel, implemented in A.3, which also has the advantage to produce a normalized output allowing it to be an algorithm of choice for multimodality. While the non-linearity of these algorithms sacrifices the possibility of train-less combined actions, they also generally yield better results, as demonstrated in B.2, where GPR outperformed RR, both offline

and online, at three different activation levels.

It needs to be noted that, despite the advantage of linear algorithms with high-dimensionality data discovered in A.2, the advent of overperforming modalities such as ultrasound [49] might change the game. Indeed, the recently-portable modality might provide a high number of distinguishable gestures that would not impede the machine learning algorithm. This remains however to be confirmed.

5.1.3.2 Features

Several features have been employed and compared in this dissertation. While the low-density modalities employed the MAV feature, the high-density modalities allowed the use of image processing techniques. For instance, the ROI gradient was used for HD-FMG and ultrasound, as well as image downsampling for the latter. For EIT, tomographic reconstruction with different priors was evaluated.

Feature extraction is an extensive field of research with limitless possibilities, and this thesis does not pretend to have explored every existing feature. However, as linear regression algorithms allow for train-less combined actions, as seen in A.2, feature choice should take this result into consideration when evaluating high-density modalities by possibly limiting the use of features introducing non-linearity.

5.1.4 Prosthesis Integration/Embedding

While some recent modalities appear to have interesting features, such as EIT identifying bone placement, or ultrasound able to predict single finger movements, there are still a few steps before their integration into a socket, as summarized in Table 5.3.

Force myography and HD-FMG need to solve the problem of unwanted signal artifacts created by external pressure or lifting an object with weight. While this could potentially be solved by adding more pressure sensors outside the socket and in the hand prosthesis, this also adds new issues as electronics within the prosthesis itself are greatly limited by space constraints. Another improvement to HD-FMG could be to replace its conductive foam with something not influenced by sweat and not creeping over time.

HD-sEMG devices are promising, especially their ability to perform motor unit decomposition. Some recent devices provide wireless sensors, such as the *MUOVI* from *OTbioelettronica*. However, they are more sensitive to noise due to their monopolar setup and the limited electronics on the sensors themselves. Additionally, for future prosthesis integration of HD-sEMG devices, the base station should be either avoided or be made wearable.

Modality \ Criteria	Roadmap before integration into prostheses	Steps before integration into prostheses
sEMG	+++++	None (gold standard)
HD-sEMG	++	Noise sensitivity of wireless devices needs to decrease; Less computationally intensive motor unit deconstruction techniques are needed; Adhesive foam and conductive cream usage might need to be adapted.
FMG	++	Solve the problem of the weight of a lifted object influencing the recognition patterns, and of external pressure-induced artifacts.
HD-FMG	++	Same steps as for FMG, and in addition solving the issue of sweat sensitivity of the foam.(1)
EIM / raw EIT	-	Improve frequency as presented in [51]; Study long-term effect of current injection on the body.
reconstructed EIT	-	Same as for raw EIT.
US B-mode	+	Needs to be wireless; Study long-term effect of soundwave injection on the body.
US A-mode	+++	Needs to solve the issue of overfitting and fix transducer to avoid any movement; Study long-term effect of soundwave injection on the body.

(1) This problem is specific to the HD-FMG device tested in this dissertation and other technologies not dependent on a conductive foam would not need to overcome this issue.

Table 5.3: Roadmap towards prosthesis integration.

Ultrasound imaging has been used for decades already, as the first B-mode scanner was made commercially available by *Meyerdirk & Wright* in 1963. It is generally considered safe imaging [267], although the long-term effects of wearing it all day long for prosthesis users should be evaluated more in detail, such as tissue heating [268]. While newly developed ultrasound research platforms are more and more portable [83, 111–113], with some being even wireless [112] or on the way to [83], there are still a few steps before potential prosthesis integration. For instance, the use of gel for a clear image is problematic inside a socket. Although encapsulated gel, as shown in [83], could be a solution, it is important to mention that liquid ultrasound gel might get dry during long-term use, while solid gel pads might be a solution to the issue [269]. Ultrasound with single transducers, commonly called ultrasound A-mode, is also concerned with the issue of over-fitting and involuntary movement of the transducer within the socket [185]. These are all problems to be solved for future prosthesis integration. Research on flexible piezoelectric sensors [270, 271] could be a step in that direction.

The EIT device tested would need to increase frequency before it can be considered as a potential modality on its own and not as a complement to another. However, this should be feasible as indicated in [51]. As for ultrasound, the long-term effect of micro-current injection should also be evaluated before integration. Additionally, the issue of electrode movement creating significant artifacts should be addressed in more detail.

All of the devices evaluated in this dissertation were research prototypes. Before a possible prosthesis integration, the biocompatibility of the materials in contact with the skin should be ensured. Moreover, the technology should go through a process to obtain medical certification and the risks inherent to the invasive modalities should be further analyzed in the long term.

In addition, the power consumption of the different modalities should be carefully planned. While the multimodal device for FMG and sEMG developed in A.1 was designed to be low-power, the issue is more challenging in the case of active modalities, such as EIT and ultrasound.

The robustness of the developed HMIs is another issue to take into account. Indeed, for an interface to be worn by a user all day, it should be particularly robust e.g. to sweat, external interference, or impacts.

An additional challenge in attempting to create wearable solutions is the implementation of machine learning algorithms into the microcontrollers of the sockets. A step in that direction was taken with A.1, in which the training and prediction were implemented on a smartphone, transmitting the commands via Bluetooth to the DAQ board's microcontroller communicating via RS232 to the prosthesis. A further integration step was taken by embedding machine learning algorithms on a microcontroller in [66]. While classifiers still need to be trained on a separate computer before being ported to the embedded hardware, the training of ridge regression with and without Random Fourier Features could already be implemented on a microcontroller, as in [66].

5.2 Applications, Limitations, and Outlook

5.2.1 Applications

The different modalities studied in this dissertation can be not only potentially applied to prosthesis control but also as new HMIs for teleoperation (cf. Fig. 5.1) in dangerous or inaccessible areas, for remote working for people with or without disabilities as presented in A.4, or for exoskeletons as shown in B.7, where the support could be adapted to the carried weight. It could also be applied to other medical devices, home automation or virtual/augmented reality. While datagloves are an option in some cases, the considerable benefit of such HMIs would be that they are unobtrusive and leave the hands free of any constraints.

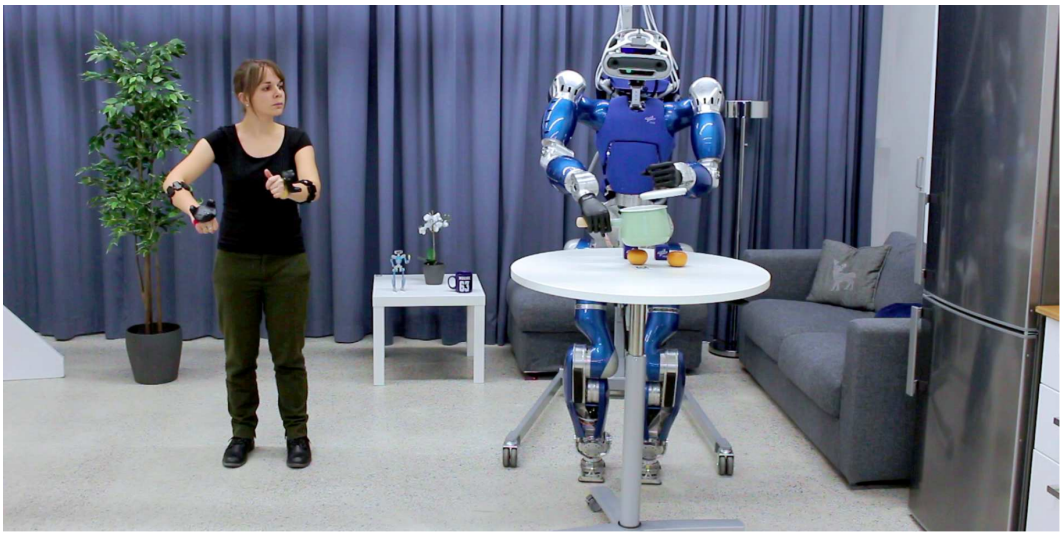

Figure 5.1: Bimanual teleoperation of the humanoid robot TORO using an ultralight and wearable input device, from B.3 and [17].

5.2.2 Open Research Questions and Directions

While the conducted research explored numerous innovative sensor modalities for simultaneous and proportional control, there are still a number of open challenges that need to be addressed.

Testing in Real-Life Conditions

Online Evaluations Several of the presented modalities and their fusion were evaluated exclusively offline as an initial exploration and comparison of the modalities. However, online assessments, which are still more accurate, must be performed to support the findings of offline investigations [192, 194]. While some of the presented modalities have also been assessed online for SPC, such as FMG in [67] or HD-FMG in A.2, others, such as EIT or fusions of modalities, remain to be evaluated online.

Limb Position Effect One of them concerns the limb position effect. In most studies, as in this research, the different sensor data are commonly acquired with the arm in a fixed position. This allows repeatable contraction patterns across trials but can lead to unrealistic performances. In reality, when moving the arm, the muscle configuration is modified, and the patterns associated with one hand gesture can significantly change as a result: this is called the limb position effect. This usually leads to an unstable grasp, and despite research ongoing in that direction, the most effective solution is still to train the model in every position [229]. While this issue has been identified for sEMG, it remains to be thoroughly investigated for the modalities presented here.

Functionality

Despite wrist movements being one of the main requirements of prosthesis users, independent finger actuation is still one of the high priorities in electric prostheses [76]. While this work mainly focuses on wrist and grasp actions, the emergence of deep wearable modalities raises the possibility of one day controlling each finger independently. This was already achieved successfully online with a conventional stationary ultrasound machine in [49], as well as with offline classification for HD-sEMG [272, 273], and should be examined with the recent wearable sensor technologies.

Improving the Sensors

Several sensor modalities have been presented in this thesis, each of which demonstrates pros and cons. The limitations are all the more important for prosthesis integration and its inherent constraints: several additional challenges must be overcome, some of which are listed in 5.3. While it might not be possible to overcome some limitations of the sensors, others need to be further investigated.

Skin-Sensor Coupling For instance, the wearability of HD-sEMG systems would be greatly improved by discarding the need for conductive cream to obtain good signal quality. This might be overcome with electronic skin [274] or textile electrodes, as with the very innovative ones presented in [275], in which a screen-printed textile electrode for HD-sEMG coated with a conductive polymer was developed as an electrode-skin interface. In the same way, the need for ultrasound gel limits the use of the modality, and solid gel pads [269] or flexible ultrasonic sensors [271] might be solutions to investigate. Smart tactile sensing systems are another direction of research to improve HD-FMG modalities [98]. The wearability of EIT could also potentially benefit from textile-based bioimpedance sensors [276].

Power Consumption Energy is yet another important topic, and while the hand prosthesis is the main power consumer in commercially available prostheses based on sEMG, this is another topic for ultrasound B-mode. Energy-harvesting technologies [274] and pressure-induced current-generating hydrogel [277] might be interesting avenues of research for that purpose.

Motor Unit Decomposition

Motor unit decomposition is a highly promising and interesting field of research. It consists, as explained in Section 2.2.2.1, in decomposing HD-sEMG signal into individual motor unit action potentials. Recently, real-time decomposition has also been made possible [94–96, 257], multiplying the possibilities of such a technique. These possibilities were further increased when a new non-invasive neural interface, able to provide spinal motor neuron activities at the wrist level, which is highly desirable for a wearable, was developed [257]. Online evaluation of this interface with a TAC test has shown high task completion rates even at the wrist level, with more than 93% on ten gestures involving individual and combined finger activation [257]. These ground-breaking findings offer a

crucial new perspective in neural interfacing for consumer electronics, medical devices, and generally for HMIs.

5.2.3 Outlook on Additional Open Challenges

Feedback Although sensors play an essential part in solving the remaining problems of myocontrol, other crucial topics have been hinted at in [29], such as feedback and enhancing robotic prostheses [76]. Some of them will be tackled in this section.

As shown in A.4, learning is an essential part of the process and can significantly improve control. The human brain can compensate for inaccurate predictions better than some algorithms. This is, for instance, the theory behind biofeedback presented in [278] in which the prediction of the machine learning, i.e. the input controlling the prosthesis, is provided to the user, who can adapt accordingly. Feedback from the end effectors is also essential for prosthesis control. Indeed, in the human arm, the sensory axons outnumber the motor axons by a ratio of at least 9:1 [279]. Such feedback can be provided to the user in a non-invasive manner, either with mechanical vibrators or electro-cutaneous stimulators [280]. The advantage of the latter is that there is no moving part and the stimulators maintain constant contact with the skin. They are simple to fabricate, do not require many electronic components, and are efficient in terms of power consumption [281]. The current and frequency can be adjusted to give different feelings, from slight touch to deep pressure [282].

There are numerous research prototypes that offer different types of feedback information, such as heat, hardness, pressure, or shear forces. In particular, the *Modular Prosthetic Limb* of *John Hopkins' Applied Physics Laboratory* includes fingertips that provide pressure, vibrations, shear, fine contact point, and temperature. Among the commercially available solutions, the sensorized *VariPlus Speed* and the *SensorHand Speed* by *Ottobock* are some examples of hook clamps. For multi-articulated hand prostheses with independent finger control, the only available prosthesis on the market currently is the *Ability Hand* from *Psyonic*, with force sensors in each finger and seven DoFs, including wrist rotation.

Prostheses Although multi-articulated hands are extremely important, it needs to be noted that prostheses are facing space problems due to their weight and size constraints. This is why adding individually-controlled flexion on each finger limits other movement possibilities, such as finger adduction/abduction. However, muscular synergies exist, and flexing one finger without flexing the others is something almost impossible to do naturally for the human hand (except for the thumb), contrary to what most current multi-articulated prostheses present today. This is the premise behind [283]: using only two motors to activate all fingers can free space for possibly other DoFs or sensors.

5.3 Conclusions

Modality	sEMG	FMG	HD-FMG	HD-sEMG	EIT	EIM	US-A	US-B	MMG	NIRS /PPG	IMU
sEMG	●	● c	●	.	c	c	c	.	◇ c	◇ c	●
FMG	● c	●	.	.	●	●	.	●	◇	.	◇
HD-FMG	●	.	●	.	.	.	.	.	.	.	.
HD-sEMG	.	.	.	●	.	.	.	.	.	.	◇
EIT	c	●	.	.	●	.	.	●	.	.	.
EIM	c	●	.	.	.	●	.	●	.	.	.
US-A	c	.	.	.	.	.	◇	.	.	.	.
US-B	.	●	.	.	●	●	.	●	.	.	.
MMG	◇ c	◇	.	.	.	.	.	.	◇	c	◇
NIRS / PPG	◇ c	.	.	.	.	.	.	.	c	◇	.
IMU	●	◇	.	◇	.	.	.	.	◇	.	●

The diagonal consists in the study of the modality on its own.
●: evaluated in the context of this thesis.
◇: evaluated in other studies.
c: evaluated in other studies with co-located sensors.

Table 5.4: Evaluations and fusions of the different modalities in this thesis and in the literature.

The main objective of this thesis can be summarized as identifying sensor modalities for myocontrol and presenting an approach to fuse them. In order to achieve this objective, three research questions were answered.

Research Question 1

What sensor modalities are viable alternatives or complements to surface electromyography?

Although no modalities were ruled out of potential complementarity, some modalities presented highly promising alternatives (or complements), in particular portable ultrasound B-mode, which has demonstrated the best results compared to FMG and EIT in A.3. The work presented in A.3 was the first experiment comparing FMG, EIT, and ultrasound. While EIT still has several challenges to overcome before being considered a viable modality, the results showed the high potential of ultrasound as an alternative and that FMG still performed remarkably well compared to ultrasound despite having a hundred times fewer features. FMG and, a fortiori, HD-FMG have also displayed better results compared to sEMG in A.1 and B.2, which makes them a desirable alternative for innovative HMIs.

For establishing these results, evaluation criteria have been previously defined, and different comparison platforms were proposed in this thesis. For instance, in A.1, a novel wearable multimodal device was developed and used in the comparison of FMG and sEMG. This device has been subsequently used in ten additional publications and raised

interest in the international community, generating joint projects. It also led to the publication of a patent involving exoskeleton control [13]. From this interface, another platform has also emerged in B.6, namely the Modular-Adaptable Prosthetic Platform, which consists in a multimodal socket that can be donned and doffed by either users or non-users of prostheses, and in which both FMG and sEMG sensors can be integrated. This allows a common device for the comparison of new methods without the influence of different sockets or orthoses for both groups of people.

Research Question 2

What pipelines are beneficial for the alternative modalities?

Regression algorithms were the chosen option in this dissertation as the only means to obtain independent simultaneous and proportional control. With combined hand/wrist actions being an essential part of daily living activities, integrating them into the machine learning model seems highly relevant. However, it usually requires training on each of the individual actions as well as on the combined ones, which can become cumbersome for the machine learning model and lead to prediction instability. In A.2, it was shown in an online experiment that, with HD-FMG, combined movements could be performed by training only on the single actions, i.e. without training on the combined movement, by using a linear regression algorithm. Not only this result reduces the prediction instability caused by numerous training actions, but it also reveals the potential of simple linear regression with high-density modalities. This encourages future studies to test for linear regression and to avoid non-linear features in the pipelines of such modalities. This result was then later on also demonstrated with HD-sEMG in [234] and would be a topic of future research for the ultrasound modality.

Additionally, a thorough study of the literature on combined grasp and wrist motions revealed a significant shortcoming in the state of the art: the biomechanics do not always allow for the maximum voluntary contraction of the power grasp when combined with wrist movements, which was not taken into account in experiment designs. This article, which is now used as a reference in several research studies, provides an understanding of challenges with combined gestures and has determined these limitations quantitatively for realistic targets in TAC tests.

As the objective of future integration in an embedded device should be kept in mind, this work also evaluated a feature extraction algorithm that reduces the overload that excessive data can bring in an integrated system. The method presented no significant difference with the complete set of features and is thus a viable option for future embedding. This topic was then investigated in more depth in [66].

In A.3, several features were proposed and compared for ultrasound, EIT, and FMG. Although feature extraction is a wide field of research and other features remain to be discovered for this specific purpose, image downsampling achieved the best results for ultrasound and the features from a tomographic reconstruction based on backpropagation with additional artificial data. For the low-density modality, FMG, the MAV was used, as for sEMG in the other core publications.

In summary, pipelines based on linear regression are recommended not only because they allow independent simultaneous and proportional control as regressors but mainly for their significant advantage in combined gestures. Based on that, features that do not introduce any non-linearity, such as the MAV for low-density modalities or image downsampling for ultrasound, are also recommended.

Research Question 3

Does a multimodal approach contribute to improving myocontrol?

The work presented in A.1 performed the first offline fusion of sEMG and FMG. The fused concatenated approach and the single FMG modality did not provide significantly different performance results, but this does not imply that the multimodal approach would not be beneficial in other scenarios or that a different fusion approach would not perform better. The same results were also confirmed in an online experiment in HD-FMG was additionally fused with sEMG in an offline experiment in Appendix B.2 in the stacked approach, using both ridge regression and a GPR algorithm without any significant difference between the performances of the fused model and HD-FMG alone.

While the state of the art of myocontrol rarely makes use of sensor fusion theories and models [139], this thesis presents an approach from the data of A.3 that does. The best-performing features of ultrasound, EIT, and FMG were selected according to an offline analysis for the implementation of a fusion algorithm, which is the first in the literature involving these three modalities and one of the few based on the theory of sensor fusion. The fused approach achieved better results than each individual modality, with especially a significant difference with EIT and FMG.

Although fusion algorithms based on the sensor fusion theory and regression have been relatively little used in the literature, this approach is still promising, and further research in that direction is needed.

Without specific fusion algorithms, multimodal myocontrol employing independent complementary sensor modalities was also successfully performed in A.4 to perform highly complex tasks in teleoperation. The multimodality allowed to share the controlled DoFs

and thus improved the myocontrol by relieving the machine learning model of additional burden.

In general, although the concatenated fusion approach brought little improvement in terms of performance for the combinations of sEMG with, separately, FMG and HD-FMG, the specific fusion algorithm developed in A.3 is still promising. Moreover, the power of multimodality might actually rely on the complementarity of each modality's drawbacks and advantages. For example, with the combined use of kinematic tracking and sEMG in A.4, the wearable teleoperation of a humanoid robot by a person missing both of his hands has been made possible by exploiting the strengths of each modality.

*

The field of human-machine interfaces represents a continuously evolving area of research, merging state-of-the-art knowledge from diverse disciplines such as neurology, material science, machine learning, assistive robotics, among others. The quest to develop the optimal interface is still ongoing and particularly driven by the objective of restoring mobility for people with disabilities. Throughout this journey, numerous innovative techniques have been developed and continue to emerge, with many already enhancing the quality of life for individuals worldwide.

***

Bibliography

[1] M. Connan, E. R. Ramírez, B. Vodermayer, and C. Castellini, "Assessment of a wearable force- and electromyography device and comparison of the related signals for myocontrol," *Frontiers in Neurorobotics*, vol. 10, no. 17, pp. 1–13, nov 2016, doi: 10.3389/fnbot.2016.00017.

[2] M. Connan, R. Kõiva, and C. Castellini, "Online natural myocontrol of combined hand and wrist actions using tactile myography and the biomechanics of grasping," *Frontiers in Neurorobotics*, vol. 14, no. 11, pp. 1–16, feb 2020, doi: 10.3389/fnbot.2020.00011.

[3] M. Connan, M. Sierotowicz, B. Henze, O. Porges, A. Albu-Schäffer, M. A. Roa, and C. Castellini, "Learning to teleoperate an upper-limb assistive humanoid robot for bimanual daily-living tasks," *Biomedical Physics & Engineering Express*, vol. 8, no. 1, pp. 1–17, dec 2021, doi: 10.1088/2057-1976/ac3881.

[4] M. Connan, B. Yu, C. Gibas, R. Brück, E. A. Kirchner, and C. Castellini, "Deep and surface sensor modalities for myo-intent detection," in *Proceedings of MEC - Myoelectric Control Symposium*, 2022.

[5] N. Jaquier, M. Connan, C. Castellini, and S. Calinon, "Combining electromyography and tactile myography to improve hand and wrist activity detection in prostheses," *Technologies*, vol. 5, no. 4, pp. 1–16, oct 2017, doi: 10.3390/technologies5040064.

[6] C. Nissler, M. Nowak, M. Connan, S. Büttner, J. Vogel, I. Kossyk, Z.-C. Márton, and C. Castellini, "VITA—An everyday virtual reality setup for prosthetics and upper-limb rehabilitation," *Journal of Neural Engineering*, vol. 16, no. 2, p. 026039, mar 2019, doi: 10.1088/1741-2552/aaf35f.

[7] M. Sierotowicz, M. Connan, and C. Castellini, "Human-in-the-loop assessment of an ultralight, low-cost body posture tracking device," *Sensors*, vol. 20, no. 3, p. 890, feb 2020, doi: 10.3390/s20030890.

[8] M. Sierotowicz, D. Brusamento, B. Schirrmeister, M. Connan, J. Bornmann, J. Gonzalez-Vargas, and C. Castellini, "Unobtrusive, natural support control of an adaptive industrial exoskeleton using force-myography," *Frontiers in Robotics and AI*, vol. 9, p. 223, sep 2022, doi: 10.3389/frobt.2022.919370.

[9] C. Nissler, M. Connan, M. Nowak, and C. Castellini, "Online tactile myography for simultaneous and proportional hand and wrist myocontrol," in *MEC2017 - Myoelectric Control Symposium*, 2017.

[10] O. Porges, M. Connan, B. Henze, A. Gigli, C. Castellini, and M. A. Roa, "A wearable, ultralight interface for bimanual teleoperation of a compliant, whole-body-controlled humanoid robot," in *Proceedings of ICRA-International Conference on Robotics and Automation*, vol. 35, no. 12, p. 2289, 2019.

[11] B. W. Hallworth, A. W. Shehata, M. R. Dawson, F. Sperle, M. Connan, W. Friedl, B. Vodermayer, C. Castellini, J. S. Hebert, and P. M. Pilarski, "A transradial modular adaptable platform for evaluating prosthetic feedback and control strategies," in *MEC-Myoelectric Control Symposium*, pp. 1–4, 2020.

[12] M. Connan, M. Sierotowicz, B. Henze, O. Porges, A. Albu-Schäffer, M. A. Roa, and C. Castellini, "Learning teleoperation of an assistive humanoid platform by intact and upper-limb disabled users," in *Converging Clinical and Engineering Research on Neurorehabilitation IV. ICNR 2020. Biosystems & Biorobotics*, vol. 28, pp. 165–169, Springer. Springer International Publishing, oct 2020, doi: 10.1007/978-3-030-70316-5_27.

[13] D. Brusamento, M. Connan, C. Castellini, B. Schirrmeister, J. Bornmann, and J. González-Vargas, "Verfahren zum Kontrollieren eines Exoskeletts, Exoskelett und Computerprogrammprodukt. DE Patent No 102021116202. Dec. 29, 2022," Patent.

[14] M. Zheng, M. S. Crouch, and M. S. Eggleston, "Surface electromyography as a natural Human–Machine Interface: A review," *IEEE Sensors Journal*, vol. 22, no. 10, pp. 9198–9214, may 2022, doi: 10.1109/JSEN.2022.3165988.

[15] C. J. De Luca, A. Adam, R. Wotiz, L. D. Gilmore, and S. H. Nawab, "Decomposition of surface EMG signals," *Journal of Neurophysiology*, vol. 96, no. 3, pp. 1646–1657, sep 2006, doi: 10.1152/jn.00009.2006.

[16] I. Campanini, A. Merlo, C. Disselhorst-Klug, L. Mesin, S. Muceli, and R. Merletti, "Fundamental concepts of bipolar and high-density surface EMG understanding and teaching for clinical, occupational, and sport applications: Origin, detection, and main errors," *Sensors*, vol. 22, no. 11, p. 4150, may 2022, doi: 10.3390/s22114150.

[17] B. Henze, "Whole-body control for multi-contact balancing of humanoid robots," Ph.D. dissertation, Springer, 2020.

[18] K. J. Zuo and J. L. Olson, "The evolution of functional hand replacement: From iron prostheses to hand transplantation," *Plastic Surgery*, vol. 21, no. 1, pp. 44–51, 2014, doi: 10.4172/plastic-surgery.1000852.

[19] R. Scott, "Myoelectric control of prostheses: A brief history," in *Proceedings of MEC - Myoelectric Control Symposium*. Myoelectric Symposium, 1992.

[20] P. A. Parker, K. Englehart, and B. Hudgins, "Myoelectric signal processing for control of powered limb prostheses," *Journal of electromyography and kinesiology*, vol. 16, no. 6, pp. 541—548, 2006.

[21] R. Reiter, "Eine neue elektrokunsthand," *Grenzgebiete der Medizin*, vol. 1, no. 4, pp. 133–135, Sep. 1948.

[22] E. Biddiss and T. Chau, "Upper-limb prosthetics: critical factors in device abandonment," *American Journal of Physical Medicine & Rehabilitation*, vol. 86, no. 12, pp. 977–987, dec 2007, doi: 10.1097/PHM.0b013e3181587f6c.

[23] B. Peerdeman, D. Boere, H. Witteveen, R. Huis in 't Veld, H. Hermens, S. Stramigioli, H. Rietman, P. Veltink, and S. Misra, "Myoelectric forearm prostheses: State of the art from a user-centered perspective," *Journal of Rehabilitation Research & Development*, vol. 48, no. 6, pp. 719–738, 2011, doi: 10.1682/JRRD.2010.08.0161.

[24] S. Salminger, H. Stino, L. H. Pichler, C. Gstoettner, A. Sturma, J. A. Mayer, M. Szivak, and O. C. Aszmann, "Current rates of prosthetic usage in upper-limb amputees – have innovations had an impact on device acceptance?" *Disability and Rehabilitation*, vol. 44, no. 14, pp. 3708–3713, dec 2020, doi: 10.1080/09638288.2020.1866684.

[25] L. C. Smail, C. Neal, C. Wilkins, and T. L. Packham, "Comfort and function remain key factors in upper limb prosthetic abandonment: findings of a scoping review," *Disability and Rehabilitation: Assistive Technology*, vol. 16, no. 8, pp. 821–830, mar 2020, doi: 10.1080/17483107.2020.1738567.

[26] M. Asghari Oskoei and H. Hu, "Myoelectric control systems-a survey," *Biomedical Signal Processing and Control*, vol. 2, no. 4, pp. 275–294, oct 2007, doi: 10.1016/j.bspc.2007.07.009.

[27] J. R. Cram and G. S. Kasman, *Cram's Introduction To Surface Electromyography*, 2nd ed. Jones and Bartlett Publishers, 2010, ch. The Basics, pp. 1–163.

[28] R. Merletti, M. Aventaggiato, A. Botter, A. Holobar, H. Marateb, and T. M. Vieira, "Advances in surface EMG: Recent progress in detection and processing techniques," *Critical Reviews in Biomedical Engineering*, vol. 38, no. 4, pp. 305–345, 2010, doi: 10.1615/critrevbiomedeng.v38.i4.20.

[29] C. Castellini, P. Artemiadis, M. Wininger, A. Ajoudani, M. Alimusaj, A. Bicchi, B. Caputo, W. Craelius, S. Dosen, K. Englehart, D. Farina, A. Gijsberts, S. Godfrey, L. Hargrove, M. Ison, T. Kuiken, M. Markovic, P. Pilarski, R. Rupp, and E. Scheme, "Proceedings of the first workshop on Peripheral Machine Interfaces: going beyond traditional surface electromyography," *Frontiers in Neurorobotics*, vol. 8, no. 22, pp. 1–17, aug 2014, doi: 10.3389/fnbot.2014.00022.

[30] N. Jiang, S. Dosen, K.-R. Müller, and D. Farina, "Myoelectric control of artificial limbs - is there a need to change focus?" *IEEE Signal Processing Magazine*, vol. 29, no. 5, pp. 148–152, sep 2012, doi: 10.1109/MSP.2012.2203480.

[31] A. Fougner, O. Stavdahl, P. J. Kyberd, Y. G. Losier, and P. A. Parker, "Control of upper limb prostheses: Terminology and proportional myoelectric control - a review," *IEEE Transactions on Neural Systems and Rehabilitation Engineering*, vol. 20, no. 5, pp. 663–677, 9 2012, doi: 10.1109/TNSRE.2012.2196711.

[32] Y. Fang, N. Hettiarachchi, D. Zhou, and H. Liu, "Multi-modal sensing techniques for interfacing hand prostheses: A review," *IEEE Sensors Journal*, vol. 15, no. 11, pp. 6065–6076, Nov 2015, doi: 10.1109/JSEN.2015.2450211.

[33] C. Chandrasekaran, "Computational principles and models of multisensory integration," *Current Opinion in Neurobiology*, vol. 43, pp. 25–34, apr 2017, doi: 10.1016/j.conb.2016.11.002.

[34] J. M. Hahne, F. Biebmann, N. Jiang, H. Rehbaum, D. Farina, F. C. Meinecke, K.-R. Muller, and L. C. Parra, "Linear and nonlinear regression techniques for simultaneous and proportional myoelectric control," *IEEE Transactions on Neural Systems and Rehabilitation Engineering*, vol. 22, no. 2, pp. 269–279, mar 2014, doi: 10.1109/tnsre.2014.2305520.

[35] M. Ison and P. Artemiadis, "The role of muscle synergies in myoelectric control: trends and challenges for simultaneous multifunction control," *Journal of Neural Engineering*, vol. 11, no. 5, p. 051001, sep 2014, doi: 10.1088/1741-2560/11/5/051001.

[36] N. Parajuli, N. Sreenivasan, P. Bifulco, M. Cesarelli, S. Savino, V. Niola, D. Esposito, T. J. Hamilton, G. R. Naik, U. Gunawardana *et al.*, "Real-time EMG based pattern recognition control for hand prostheses: A review on existing methods, challenges and future implementation," *Sensors*, vol. 19, no. 20, p. 4596, oct 2019, doi: 10.3390/s19204596.

[37] J. Lobo-Prat, P. N. Kooren, A. H. A. Stienen, J. L. Herder, B. F. J. M. Koopman, and P. H. Veltink, "Non-Invasive Control Interfaces for Intention Detection in Active Movement-Assistive Devices," *Journal of NeuroEngineering and Rehabilitation*, vol. 11, no. 1, p. 168, Dec. 2014, doi: 10.1186/1743-0003-11-168.

[38] W. Craelius, "The bionic man: Restoring mobility," *Science*, vol. 295, no. 5557, pp. 1018–1021, feb 2002, doi: 10.1126/science.295.5557.1018.

[39] S. L. Phillips and W. Craelius, "Residual kinetic imaging: A versatile interface for prosthetic control," *Robotica*, vol. 23, no. 3, pp. 277–282, may 2005, doi: 10.1017/S0263574704001298.

[40] M. Wininger, N. Kim, and W. Craelius, "Pressure signature of forearm as predictor of grip force," *Journal of Rehabilitation Research and Development*, vol. 45, no. 6, pp. 883–892, dec 2008, doi: 10.1682/jrrd.2007.11.0187.

[41] E. Cho, R. Chen, L.-K. Merhi, Z. Xiao, B. Pousett, and C. Menon, "Force myography to control robotic upper extremity prostheses: A feasibility study," *Frontiers in Bioengineering and Biotechnology*, vol. 4, no. March, pp. 1–12, 2016, doi: 10.3389/fbioe.2016.00018.

[42] A. Radmand, E. Scheme, and K. Englehart, "High-density force myography: A possible alternative for upper-limb prosthetic control," *Journal of Rehabilitation Research and Development*, vol. 53, no. 4, pp. 443–456, 2016, doi: 10.1682/JRRD.2015.03.0041.

[43] E. M. C. Hillman, J. C. Hebden, M. Schweiger, H. Dehghani, F. E. W. Schmidt, D. T. Delpy, and S. R. Arridge, "Time resolved optical tomography of the human forearm," *Physics in Medicine and Biology*, vol. 46, no. 4, pp. 1117–1130, mar 2001, doi: 10.1088/0031-9155/46/4/315.

[44] H. Zhao, F. Gao, Y. Tanikawa, K. Homma, and Y. Yamada, "NIR time domain diffuse optical tomographic experiments on human forearm," in *Optical Tomography and Spectroscopy of Tissue V*, B. Chance, R. R. Alfano, B. J. Tromberg, M. Tamura, and E. M. Sevick-Muraca, Eds., vol. 4955, no. July 2003, pp. 437–446. SPIE, jul 2003, doi: 10.1117/12.476557.

[45] J. McIntosh, A. Marzo, and M. Fraser, "Sensir: Detecting hand gestures with a wearable bracelet using infrared transmission and reflection," in *Proceedings of the 30th annual ACM symposium on user interface software and technology*, pp. 593–597. ACM, oct 2017, doi: 10.1145/3126594.3126604.

[46] D. T. Barry, J. A. Leonard, A. J. Gitter, and R. D. Ball, "Acoustic myography as a control signal for an externally powered prosthesis," *Archives of Physical Medicine and Rehabilitation*, vol. 67, no. 4, pp. 267–269, 1986, doi: 10.5555/uri:pii:0003999386903941.

[47] J. Silva, T. Chau, and A. Goldenberg, "MMG-based multisensor data fusion for prosthesis control," in *Engineering in Medicine and Biology Society, 2003. Proceedings of the 25th Annual International Conference of the IEEE*, vol. 3, pp. 2909–2912. IEEE, 2003, doi: 10.1109/IEMBS.2003.1280527.

[48] D. Sierra González and C. Castellini, "A realistic implementation of ultrasound imaging as a human-machine interface for upper-limb amputees," *Frontiers in Neurorobotics*, vol. 7, pp. 1–11, oct 2013, doi: 10.3389/fnbot.2013.00017.

[49] C. Castellini, K. Hertkorn, M. Sagardia, D. Sierra González, and M. Nowak, "A virtual piano-playing environment for rehabilitation based upon ultrasound imaging," in *Proceedings of BioRob - IEEE International Conference on Biomedical Robotics and Biomechatronics*, pp. 548–554. IEEE, aug 2014, doi: 10.1109/BIOROB.2014.6913835.

[50] Y. Zhang and C. Harrison, "Tomo: Wearable, low-cost electrical impedance tomography for hand gesture recognition," in *Proceedings of the 28th Annual ACM Symposium on User Interface Software & Technology*, pp. 167–173. ACM, nov 2015, doi: 10.1145/2807442.2807480.

[51] Y. Zhang, R. Xiao, and C. Harrison, "Advancing hand gesture recognition with high resolution electrical impedance tomography," in *Proceedings of the 29th Annual Symposium on User Interface Software and Technology*, pp. 843–850. ACM, oct 2016, doi: 10.1145/2984511.2984574.

[52] M. Georgi, C. Amma, and T. Schultz, "Recognizing Hand and Finger Gestures with IMU based Motion and EMG based Muscle Activity Sensing," *Proceedings of the International Conference on Bio-inspired Systems and Signal Processing*, pp. 99–108, 2015, doi: 10.5220/0005276900990108.

[53] J. G. Colli-Alfaro, A. Ibrahim, and A. L. Trejos, "Design of user-independent hand gesture recognition using multilayer perceptron networks and sensor fusion techniques," in *2019 IEEE 16th International Conference on Rehabilitation Robotics (ICORR)*. IEEE, jun 2019, doi: 10.1109/icorr.2019.8779533.

[54] Y. Xue, Z. .Ju, K. Xiang, J. Chen, and H. Liu, "Multimodal human hand motion sensing and analysis—a review," *IEEE Transactions on Cognitive and Developmental Systems*, vol. 11, no. 2, pp. 162–175, jun 2019, doi: 10.1109/TCDS.2018.2800167.

[55] I. Herrera-Luna, E. J. Rechy-Ramirez, H. V. Rios-Figueroa, and A. Marin-Hernandez, "Sensor fusion used in applications for hand rehabilitation: A systematic review," *IEEE Sensors Journal*, vol. 19, no. 10, pp. 3581–3592, may 2019, doi: 10.1109/jsen.2019.2897083.

[56] X. Jiang, L.-K. Merhi, Z. G. Xiao, and C. Menon, "Exploration of force myography and surface electromyography in hand gesture classification," *Medical Engineering & Physics*, vol. 41, pp. 63–73, mar 2017, doi: 10.1016/j.medengphy.2017.01.015.

[57] A. Ke, J. Huang, L. Chen, Z. Gao, and J. He, "An ultra-sensitive modular hybrid EMG–FMG sensor with floating electrodes," *Sensors*, vol. 20, no. 17, p. 4775, aug 2020, doi: 10.3390/s20174775.

[58] C. Ahmadizadeh, L.-K. Merhi, B. Pousett, S. Sangha, and C. Menon, "Toward intuitive prosthetic control: Solving common issues using force myography, surface electromyography, and pattern recognition in a pilot case study," *IEEE Robotics & Automation Magazine*, vol. 24, no. 4, pp. 102–111, dec 2017, doi: 10.1109/mra.2017.2747899.

[59] I. Kyranou, A. Krasoulis, M. S. Erden, K. Nazarpour, and S. Vijayakumar, "Real-Time classification of multi-modal sensory data for prosthetic hand control," *Proceedings of the IEEE RAS and EMBS International Conference on Biomedical Robotics and Biomechatronics*, pp. 536–541, jun 2016, doi: 10.1109/BIOROB.2016.7523681.

[60] A. Krasoulis, I. Kyranou, M. S. Erden, K. Nazarpour, and S. Vijayakumar, "Improved prosthetic hand control with concurrent use of myoelectric and inertial measurements," *Journal of NeuroEngineering and Rehabilitation*, vol. 14, no. 1, jul 2017, doi: 10.1186/s12984-017-0284-4.

[61] J. Zeng, Y. Zhou, Y. Yang, J. Wang, and H. Liu, "Feature fusion of sEMG and ultrasound signals in hand gesture recognition," in *International Conference on Systems, Man, and Cybernetics (SMC)*, pp. 3911–3916. Toronto, Canada: IEEE, oct 2020, doi: 10.1109/SMC42975.2020.9282818.

[62] X. Yang, J. Yan, and H. Liu, "Comparative analysis of wearable a-mode ultrasound and sEMG for muscle-computer interface," *IEEE Transactions on Biomedical Engineering*, vol. 67, no. 9, pp. 2434–2442, sep 2020, doi: 10.1109/tbme.2019.2962499.

[63] X. Zhang, X. Chen, Y. Li, V. Lantz, K. Wang, and J. Yang, "A framework for hand gesture recognition based on accelerometer and EMG sensors," *IEEE Transactions on Systems, Man, and Cybernetics Part A:Systems and Humans*, vol. 41, no. 6, pp. 1064–1076, nov 2011, doi: 10.1109/TSMCA.2011.2116004.

[64] Z. Ju and H. Liu, "Human hand motion analysis with multisensory information," *IEEE/ASME Transactions on Mechatronics*, vol. 19, no. 2, pp. 456–466, apr 2014, doi: 10.1109/tmech.2013.2240312.

[65] Y. Xue, Z. Ju, K. Xiang, J. Chen, and H. Liu, "Multiple sensors based hand motion recognition using adaptive directed acyclic graph," *Applied Sciences*, vol. 7, no. 4, p. 358, apr 2017, doi: 10.3390/app7040358.

[66] S. V. Waichal, "Comparison of solutions for efficient implementation of sensor based hand prosthesis control on a microcontroller using regression based machine learning and neural networks," Master's thesis, Technical University of Munich, 2020.

[67] M. Nowak, T. Eiband, and C. Castellini, "Multi-modal myocontrol: Testing combined force-and electromyography," in *2017 International Conference on Rehabilitation Robotics (ICORR)*, pp. 1364–1368. IEEE, jul 2017, doi: 10.1109/icorr.2017.8009438.

[68] M. Nowak, R. M. Bongers, C. K. van der Sluis, and C. Castellini, "Introducing a novel training and assessment protocol for pattern matching in myocontrol: case-study of a trans-radial amputee," in *Proceedings of the Myoelectric Control Symposium (MEC)*, 2017, doi: 10.13140/RG.2.2.28846.61768.

[69] R. Meattini, M. Nowak, C. Melchiorri, and C. Castellini, "Automated instability detection for interactive myocontrol of prosthetic hands," *Frontiers in Neurorobotics*, vol. 13, p. 68, aug 2019, doi: 10.3389/fnbot.2019.00068.

[70] M. Nowak, T. Eiband, E. R. Ramírez, and C. Castellini, "Action interference in simultaneous and proportional myocontrol: Comparing force- and electromyography," *Journal of Neural Engineering*, vol. 17, no. 2, p. 026011, mar 2020, doi: 10.1088/1741-2552/ab7b1e.

[71] M. Nowak, R. M. Bongers, C. K. van der Sluis, A. Albu-Schäffer, and C. Castellini, "Simultaneous assessment and training of an upper-limb amputee using incremental machine-learning-based myocontrol: A single-case experimental design," dec 2022, doi: 10.21203/rs.3.rs-2357029/v1.

[72] M. Sierotowicz, N. Lotti, R. Rupp, L. Masia, and C. Castellini, "A comprehensive framework for the modelling of cartesian force output in human limbs," in *2022 International Conference on Rehabilitation Robotics (ICORR)*, pp. 1–6. IEEE, jul 2022, doi: 10.1109/ICORR55369.2022.9896547.

[73] C. L. McDonald, S. Westcott-McCoy, M. R. Weaver, J. Haagsma, and D. Kartin, "Global prevalence of traumatic non-fatal limb amputation," *Prosthetics and orthotics international*, vol. 45, no. 2, pp. 105–114, dec 2020, doi: 10.1177/0309364620972258.

[74] C. Behrend, W. Reizner, J. A. Marchessault, and W. C. Hammert, "Update on advances in upper extremity prosthetics," *The Journal of Hand Surgery*, vol. 36, no. 10, pp. 1711–1717, oct 2011, doi: 10.1016/j.jhsa.2011.07.024.

[75] K. Ziegler-Graham, E. J. MacKenzie, P. L. Ephraim, T. G. Travison, and R. Brookmeyer, "Estimating the prevalence of limb loss in the united states: 2005 to 2050," *Archives of Physical Medicine and Rehabilitation*, vol. 89, no. 3, pp. 422–429, mar 2008, doi: 10.1016/j.apmr.2007.11.005.

[76] F. Cordella, A. L. Ciancio, R. Sacchetti, A. Davalli, A. G. Cutti, E. Guglielmelli, and L. Zollo, "Literature review on needs of upper limb prosthesis users," *Frontiers in Neuroscience*, vol. 10, pp. 1–14, may 2016, doi: 10.3389/fnins.2016.00209.

[77] A. L. Muilenburg and M. A. LeBlanc, "Body-powered upper-limb components," in *Comprehensive Management of the Upper-Limb Amputee*. Springer New York, 1989, pp. 28–38.

[78] J. S. Day, "The clinical performance of UHMWPE in elbow replacements," in *UHMWPE Biomaterials Handbook*, third edition ed., S. M. Kurtz, Ed. Oxford: Elsevier, 2016, pp. 179–196. ISBN 978-0-323-35401-1

[79] S. J. Sebastin, M. E. Puhaindran, A. Y. T. Lim, I. J. Lim, and W. H. Bee, "The prevalence of absence of the palmaris longus – a study in a chinese population and a review of the literature," *Journal of Hand Surgery*, vol. 30, no. 5, pp. 525–527, oct 2005, doi: 10.1016/j.jhsb.2005.05.003.

[80] S. J. Sebastin, A. Y. T. Lim, W. H. Bee, T. C. M. Wong, and B. V. Methil, "Does the absence of the palmaris longus affect grip and pinch strength?" *Journal of Hand Surgery*, vol. 30, no. 4, pp. 406–408, aug 2005, doi: 10.1016/j.jhsb.2005.03.011.

[81] A. Cetin, M. Genc, S. Sevil, and Y. K. Coban, "Prevalence of the palmaris longus muscle and its relationship with grip and pinch strength: A study in a turkish pediatric population," *HAND*, vol. 8, no. 2, pp. 215–220, apr 2013, doi: 10.1007/s11552-013-9509-6.

[82] A. Asghar, R. K. Jha, A. Patra, B. Chaudhary, and B. Singh, "The prevalence and distribution of the variants of Gantzer's muscle: a meta-analysis of cadaveric studies," *Anatomy Cell Biology*, vol. 55, no. 1, pp. 3–13, mar 2022, doi: 10.5115/acb.21.141.

[83] M. Fournelle, T. Grün, D. Speicher, S. Weber, M. Yilmaz, D. Schoeb, A. Miernik, G. Reis, S. Tretbar, and H. Hewener, "Portable ultrasound research system for use in automated bladder monitoring with machine-learning-based segmentation," *Sensors*, vol. 21, no. 19, p. 6481, sep 2021, doi: 10.3390/s21196481.

[84] S. Pizzolato, L. Tagliapietra, M. Cognolato, M. Reggiani, H. Müller, and M. Atzori, "Comparison of six electromyography acquisition setups on hand movement classification tasks," *PLoS ONE*, vol. 12, no. 10, pp. 1–17, oct 2017, doi: 10.1371/journal.pone.0186132.

[85] P. Visconti, F. Gaetani, G. A. Zappatore, and P. Primiceri, "Technical features and functionalities of myo armband: An overview on related literature and advanced applications of myoelectric armbands mainly focused on arm prostheses," *International Journal on Smart Sensing and Intelligent Systems*, vol. 11, no. 1, pp. 1–25, jan 2018, doi: 10.21307/ijssis-2018-005.

[86] F. C. P. Sebelius, B. N. Rosén, and G. N. Lundborg, "Refined myoelectric control in below-elbow amputees using artificial neural networks and a data glove," *Journal of Hand Surgery*, vol. 30A, no. 4, pp. 780–789, July 2005, doi: 10.1016/j.jhsa.2005.01.002.

[87] C. Cipriani, C. Antfolk, M. Controzzi, G. Lundborg, B. Rosen, M. C. Carrozza, and F. Sebelius, "Online myoelectric control of a dexterous hand prosthesis by transradial amputees," *IEEE Transactions on Neural Systems and Rehabilitation Engineering*, vol. 19, no. 3, pp. 260–270, June 2011, doi: 10.1109/TNSRE.2011.2108667.

[88] M. Atzori and H. Müller, "Control capabilities of myoelectric robotic prostheses by hand amputees: A scientific research and market overview," *Frontiers in systems neuroscience*, vol. 9, p. 162, nov 2015, doi: 10.3389/fnsys.2015.00162.

[89] F. Negro, S. Muceli, A. M. Castronovo, A. Holobar, and D. Farina, "Multi-channel intramuscular and surface EMG decomposition by convolutive blind source separation," *Journal of Neural Engineering*, vol. 13, no. 2, p. 026027, feb 2016, doi: 10.1088/1741-2560/13/2/026027.

[90] T. Kapelner, I. Vujaklija, N. Jiang, F. Negro, O. C. Aszmann, J. Principe, and D. Farina, "Predicting wrist kinematics from motor unit discharge timings for the control of active prostheses," *Journal of NeuroEngineering and Rehabilitation*, vol. 16, no. 1, pp. 1–11, apr 2019, doi: 10.1186/s12984-019-0516-x.

[91] V. T. Ramaekers, C. Disselhorst-Klug, J. Schneider, J. Silny, J. Forst, R. Forst, F. Kotlarek, and G. Rau, "Clinical application of a noninvasive multi-electrode array EMG for the recording of single motor unit activity," *Neuropediatrics*, vol. 24, no. 03, pp. 134–138, jun 1993, doi: 10.1055/s-2008-1071530.

[92] D. Farina, F. Negro, M. Gazzoni, and R. M. Enoka, "Detecting the unique representation of motor-unit action potentials in the surface electromyogram," *Journal of Neurophysiology*, vol. 100, no. 3, pp. 1223–1233, sep 2008, doi: 10.1152/jn.90219.2008.

[93] T. Kapelner, M. Sartori, F. Negro, and D. Farina, "Neuro-musculoskeletal mapping for man-machine interfacing," *Scientific reports*, vol. 10, no. 1, pp. 1–10, apr 2020, doi: 10.1038/s41598-020-62773-7.

[94] C. Chen, S. Ma, X. Sheng, D. Farina, and X. Zhu, "Adaptive real-time identification of motor unit discharges from non-stationary high-density surface electromyographic signals," *IEEE Transactions on Biomedical Engineering*, vol. 67, no. 12, pp. 3501–3509, dec 2020, doi: 10.1109/tbme.2020.2989311.

[95] Y. Zheng, G. Xu, Y. Li, and W. Qiang, "Improved online decomposition of non-stationary electromyogram via signal enhancement using a neuron resonance model: a simulation study," *Journal of Neural Engineering*, vol. 19, no. 2, p. 026030, apr 2022, doi: 10.1088/1741-2552/ac5f1b.

[96] C. Chen, Y. Yu, X. Sheng, D. Farina, and X. Zhu, "Simultaneous and proportional control of wrist and hand movements by decoding motor unit discharges in real time," *Journal of Neural Engineering*, vol. 18, no. 5, p. 056010, apr 2021, doi: 10.1088/1741-2552/abf186.

[97] Z. G. Xiao and C. Menon, "A review of force myography research and development," *Sensors*, vol. 19, no. 20, p. 4557, oct 2019, doi: 10.3390/s19204557.

[98] L. Zou, C. Ge, Z. J. Wang, E. Cretu, and X. Li, "Novel tactile sensor technology and smart tactile sensing systems: A review," *Sensors*, vol. 17, no. 11, p. 2653, 2017, doi: 10.3390/s17112653.

[99] D. J. Curcie, J. A. Flint, and W. Craelius, "Biomimetic finger control by filtering of distributed forelimb pressures," *IEEE Transactions on Neural Systems and Rehabilitation Engineering*, vol. 9, no. 1, pp. 69–75, 2001.

[100] E. V. Biryukova and V. Z. Yourovskaya, *A Model of Human Hand Dynamics*. Boston, MA: Springer US, 1994, pp. 107–122. ISBN 978-1-4757-9107-5

[101] R. P. Henderson and J. G. Webster, "An impedance camera for spatially specific measurements of the thorax," *IEEE Transactions on Biomedical Engineering*, vol. BME-25, no. 3, pp. 250–254, may 1978, doi: 10.1109/tbme.1978.326329.

[102] D. C. Barber and B. H. Brown, "Applied potential tomography," *Journal of Physics E: Scientific Instruments*, vol. 17, no. 9, pp. 723–733, 1984, doi: 10.1088/0022-3735.

[103] D. S. Holder, "Electrical impedance tomography (EIT) of brain function," *Brain Topography*, vol. 5, no. 2, pp. 87–93, 1992, doi: 10.1007/bf01129035.

[104] J. M. Hahne, M. Markovic, L. A. Pardo, R. Kusche, M. Ryschka, and A. F. Schilling, "On the utility of bioimpedance in the context of myoelectric control," *IEEE Sensors Journal*, vol. 21, no. 17, pp. 19 505–19 515, sep 2021, doi: 10.1109/jsen.2021.3090949.

[105] M. Faulkner, S. Hannan, K. Aristovich, J. Avery, and D. Holder, "Feasibility of imaging evoked activity throughout the rat brain using electrical impedance tomography," *Neuroimage*, vol. 178, pp. 1–10, sep 2018, doi: 10.1016/j.neuroimage.2018.05.022.

[106] M. A. Haidekker, *Medical Imaging Technology*. Springer New York, 2013.

[107] L. Demi, "Practical guide to ultrasound beam forming: Beam pattern and image reconstruction analysis," *Applied Sciences*, vol. 8, no. 9, p. 1544, 2018, doi: 10.3390/app8091544.

[108] P. L. Cooperberg, J. J. Barberie, T. Wong, and C. Fix, "Extended field-of-view ultrasound," in *Seminars in Ultrasound, CT and MRI*, vol. 22, no. 1, pp. 65–77, Elsevier. Elsevier BV, feb 2001, doi: 10.1016/s0887-2171(01)90019-8.

[109] A. Srivastav, K. Bhogi, S. Mandal, and M. Sharad, "An adaptive low-complexity abnormality detection scheme for wearable ultrasonography," *IEEE Transactions on Circuits and Systems II: Express Briefs*, vol. 66, no. 8, pp. 1466–1470, aug 2019, doi: 10.1109/TCSII.2018.2881612.

[110] V. Nazari and Y.-P. Zheng, "Controlling upper limb prostheses using sonomyography (SMG): A review," *Sensors*, vol. 23, no. 4, p. 1885, feb 2023, doi: 10.3390/s23041885.

[111] N. Hettiarachchi, Z. Ju, and H. Liu, "A new wearable ultrasound muscle activity sensing system for dexterous prosthetic control," in *2015 IEEE International Conference on Systems, Man, and Cybernetics*, pp. 1415–1420. IEEE, oct 2015, doi: 10.1109/smc.2015.251.

[112] S. Acuña, S. Engdahl, A. Bashatah, P. Otto, R. Kaliki, and S. Sikdar, "A wearable sonomyography system for prosthesis control," in *Proceedings of MEC - Myoelectric Control Symposium*, 2022.

[113] X. Yang, Z. Chen, N. Hettiarachchi, J. Yan, and H. Liu, "A wearable ultrasound system for sensing muscular morphological deformations," *IEEE Transactions on Systems, Man, and Cybernetics: Systems*, vol. 51, no. 6, pp. 3370–3379, jun 2019, doi: 10.1109/tsmc.2019.2924984.

[114] T. Bianchi, D. Zambarbieri, G. Beltrami, and G. Verni, "NIRS monitoring of muscle contraction to control a prosthetic device," in *Biomedical Sensors, Fibers, and Optical Delivery Systems*, F. Baldini, N. I. Croitoru, M. Frenz, I. Lundstroem, M. Miyagi, R. Pratesi, and O. S. Wolfbeis, Eds., vol. 3570, pp. 157–163, SPIE. SPIE, jan 1999, doi: 10.1117/12.336926.

[115] H. Wang, S. Zuo, M. Cerezo-Sánchez, N. Ghahremani Arekhloo, K. Nazarpour, and H. Heidari, "Wearable super-resolution muscle-machine interfacing," *Frontiers in Neuroscience*, vol. 16, nov 2022, doi: 10.3389/fnins.2022.1020546.

[116] M. Ferrari and V. Quaresima, "A brief review on the history of human functional near-infrared spectroscopy (fNIRS) development and fields of application," *NeuroImage*, vol. 63, no. 2, pp. 921–935, nov 2012, doi: 10.1016/j.neuroimage.2012.03.049.

[117] M. Ferrari, "Progress of near-infrared spectroscopy and topography for brain and muscle clinical applications," *Journal of Biomedical Optics*, vol. 12, no. 6, p. 062104, nov 2007, doi: 10.1117/1.2804899.

[118] S. Cofer, T. N. Chen, J. J. Yang, and S. Follmer, "Detecting touch and grasp gestures using a wrist-worn optical and inertial sensing network," *Robotics and Automation Letters*, vol. 7, no. 4, pp. 10 842–10 849, oct 2022, doi: 10.1109/lra.2022.3191173.

[119] A. Maereg, Y. Lou, E. Secco, and R. King, "Hand gesture recognition based on near-infrared sensing wristband," in *Proceedings of the 15th International Joint Conference on Computer Vision, Imaging and Computer Graphics Theory and Applications*. SCITEPRESS - Science and Technology Publications, 2020, doi: 10.5220/0008909401100117.

[120] M. Sikora and S. Paszkiel, "Muscle activity measurement using visible light and infrared," *IFAC-PapersOnLine*, vol. 52, no. 27, pp. 329–334, 2019, doi: 10.1016/j.ifacol.2019.12.682.

[121] S. Herrmann and K. Buchenrieder, "Fusion of myoelectric and near-infrared signals for prostheses control," in *Proceedings of the 4th International Convention on Rehabilitation Engineering & Assistive Technology*, ser. iCREATe '10, no. 54, pp. 1–4. Singapore Therapeutic, Assistive & Rehabilitative Technologies (START) Centre, Jul. 2010.

[122] W. Guo, P. Yao, X. Sheng, H. Liu, and X. Zhu, "A wireless wearable sEMG and NIRS acquisition system for an enhanced human-computer interface," in *2014 IEEE International Conference on Systems, Man, and Cybernetics October 5-8, San Diego, CA, USA*, pp. 2192–2197. IEEE, 2014, doi: 10.1109/smc.2014.6974249.

[123] W. Guo, X. Sheng, H. Liu, and X. Zhu, "Toward an enhanced human-machine interface for upper-limb prosthesis control with combined EMG and NIRS signals," *IEEE Transactions on Human-Machine Systems*, vol. 47, no. 4, pp. 564–575, 2017, doi: 10.1109/THMS.2016.2641389.

[124] J. Allen, "Photoplethysmography and its application in clinical physiological measurement," *Physiological Measurement*, vol. 28, no. 3, pp. 1–39, feb 2007, doi: 10.1088/0967-3334/28/3/r01.

[125] S. Grushko, T. Spurnỳ, and M. Černỳ, "Control methods for transradial prostheses based on remnant muscle activity and its relationship with proprioceptive feedback," *Sensors*, vol. 20, no. 17, p. 4883, aug 2020, doi: 10.3390/s20174883.

[126] M. A. Islam, K. Sundaraj, R. B. Ahmad, N. U. Ahamed, and M. A. Ali, "Mechanomyography sensor development, related signal processing, and applications: a systematic review," *IEEE Sensors Journal*, vol. 13, no. 7, pp. 2499–2516, jul 2013, doi: 10.1109/jsen.2013.2255982.

[127] D. Esposito, E. Andreozzi, A. Fratini, G. D. Gargiulo, S. Savino, V. Niola, and P. Bifulco, "A piezoresistive sensor to measure muscle contraction and mechanomyography," *Sensors*, vol. 18, no. 8, p. 2553, 2018, doi: 10.3390/s18082553.

[128] S. P. Mendez, M. Gherardini, G. V. d. P. Santos, D. M. Muñoz, H. V. H. Ayala, and C. Cipriani, "Data-driven real-time magnetic tracking applied to myokinetic interfaces," *IEEE Transactions on Biomedical Circuits and Systems*, vol. 16, no. 2, pp. 266–274, apr 2022, doi: 10.1109/TBCAS.2022.3161133.

[129] S. Tarantino, F. Clemente, D. Barone, M. Controzzi, and C. Cipriani, "The myokinetic control interface: tracking implanted magnets as a means for prosthetic control," *Scientific reports*, vol. 7, no. 1, pp. 1–11, dec 2017, doi: 10.1038/s41598-017-17464-1.

[130] J. Montero, Z. Thumser, F. Masiero, D. Beckler, F. Clemente, P. Marasco, and C. Cipriani, "The myokinetic stimulation interface: activation of proprioceptive neural responses with remotely actuated magnets implanted in rodent forelimb muscle," *Journal of Neural Engineering*, vol. 19, no. 2, p. 026048, apr 2022, doi: 10.1088/1741-2552/ac6537.

[131] D. Murzin, D. J. Mapps, K. Levada, V. Belyaev, A. Omelyanchik, L. Panina, and V. Rodionova, "Ultrasensitive magnetic field sensors for biomedical applications," *Sensors*, vol. 20, no. 6, p. 1569, mar 2020, doi: 10.3390/s20061569.

[132] S. Zuo, J. Schmalz, M.-Ö. Özden, M. Gerken, J. Su, F. Niekiel, F. Lofink, K. Nazarpour, and H. Heidari, "Ultrasensitive magnetoelectric sensing system for pico-tesla magnetomyography," *IEEE Transactions on Biomedical Circuits and Systems*, vol. 14, no. 5, pp. 971–984, oct 2020, doi: 10.1109/TBCAS.2020.2998290.

[133] R. Gravina, P. Alinia, H. Ghasemzadeh, and G. Fortino, "Multi-sensor fusion in body sensor networks: State-of-the-art and research challenges," *Information Fusion*, vol. 35, pp. 68–80, may 2017, doi: 10.1016/j.inffus.2016.09.005.

[134] D. Lahat, T. Adali, and C. Jutten, "Multimodal data fusion: An overview of methods, challenges, and prospects," *Proceedings of the IEEE*, vol. 103, no. 9, pp. 1449–1477, 2015, doi: 10.1109/jproc.2015.2460697.

[135] W. Elmenreich, "An introduction to sensor fusion," *Vienna University of Technology, Austria*, vol. 502, pp. 1–28, 2002.

[136] H. F. Durrant-Whyte, *Sensor Models and Multisensor Integration.* New York, NY: Springer New York, 1990, pp. 73–89. ISBN 978-1-4613-8997-2

[137] F. Castanedo, "A review of data fusion techniques," *The Scientific World Journal*, vol. 2013, pp. 1–19, 2013, doi: 10.1155/2013/704504.

[138] M. M. Kokar, J. A. Tomasik, and J. Weyman, "Formalizing classes of information fusion systems," *Information Fusion*, vol. 5, no. 3, pp. 189–202, sep 2004, doi: 10.1016/j.inffus.2003.11.001.

[139] H. Zhou and G. Alici, "Non-invasive human-machine interface (HMI) systems with hybrid on-body sensors for controlling upper-limb prosthesis: A review," *IEEE Sensors Journal*, vol. 22, no. 11, pp. 10 292–10 307, jun 2022, doi: 10.1109/jsen.2022.3169492.

[140] H. Wang, P. Kang, Q. Gao, S. Jiang, and P. B. Shull, "A novel PPG-FMG-ACC wristband for hand gesture recognition," *IEEE Journal of Biomedical and Health Informatics*, vol. 26, no. 10, pp. 5097–5108, oct 2022, doi: 10.1109/jbhi.2022.3194017.

[141] A. Gigli, V. Gregori, M. Cognolato, M. Atzori, and A. Gijsberts, "Visual cues to improve myoelectric control of upper limb prostheses," in *2018 7th IEEE International Conference on Biomedical Robotics and Biomechatronics (Biorob)*, pp. 783–788. IEEE, aug 2018, doi: 10.1109/biorob.2018.8487923.

[142] J. Sanford, R. Patterson, and D. O. Popa, "Concurrent surface electromyography and force myography classification during times of prosthetic socket shift and user fatigue," *Journal of Rehabilitation and Assistive Technologies Engineering*, vol. 4, p. 205566831770873, jan 2017, doi: 10.1177/2055668317708731.

[143] S. Jiang, Q. Gao, H. Liu, and P. B. Shull, "A novel, co-located EMG-FMG-sensing wearable armband for hand gesture recognition," *Sensors and Actuators A: Physical*, vol. 301, p. 111738, jan 2020, doi: 10.1016/j.sna.2019.111738.

[144] R. Kusche and M. Ryschka, "Combining bioimpedance and EMG measurements for reliable muscle contraction detection," vol. 19, pp. 11 687–11 696, 2019, doi: 10.1109/jsen.2019.2936171.

[145] C. Ngo, C. Munoz, M. Lueken, A. Hülkenberg, C. Bollheimer, A. Briko, A. Kobelev, S. Shchukin, and S. Leonhardt, "A wearable, multi-frequency device to measure muscle activity combining simultaneous electromyography and electrical impedance myography," *Sensors*, vol. 22, no. 5, p. 1941, mar 2022, doi: 10.3390/s22051941.

[146] W. Xia, Y. Zhou, X. Yang, K. He, and H. Liu, "Toward portable hybrid surface electromyography/a-mode ultrasound sensing for human–machine interface," vol. 19, pp. 5219–5228, 2019, doi: 10.1109/jsen.2019.2903532.

[147] T. Tsuji, H. Ichinobe, K. Ito, and M. Nagamachi, "Discrimination of forearm motions from EMG signals by error back propagation typed neural network using entropy," *Transactions of the Society of Instrument and Control Engineers*, vol. 29, no. 10, pp. 1213–1220, 1993, doi: 10.9746/sicetr1965.29.1213.

[148] C. Castellini, E. Gruppioni, A. Davalli, and G. Sandini, "Fine detection of grasp force and posture by amputees via surface electromyography," *Journal of Physiology (Paris)*, vol. 103, no. 3-5, pp. 255–262, may 2009, doi: 10.1016/j.jphysparis.2009.08.008.

[149] F. V. Tenore, A. Ramos, A. Fahmy, S. Acharya, R. Etienne-Cummings, and N. V. Thakor, "Decoding of individuated finger movements using surface electromyography," *IEEE Transactions on Biomedical Engineering*, vol. 56, no. 5, pp. 1427–1434, may 2009, doi: 10.1109/tbme.2008.2005485.

[150] G. Li, A. E. Schultz, and T. A. Kuiken, "Quantifying pattern recognition-based myoelectric control of multifunctional transradial prostheses," *IEEE Transactions on Neural Systems and Rehabilitation Engineering*, vol. 18, no. 2, pp. 185–192, apr 2010, doi: 10.1109/TNSRE.2009.2039619.

[151] M. Atzori, A. Gijsberts, S. Heynen, A.-G. Mittaz-Hager, O. Deriaz, P. van der Smagt, C. Castellini, B. Caputo, and H. Müller, "Building the {NINAPRO} database: a resource for the biorobotics community," in *Proceedings of {BioRob} - IEEE International Conference on Biomedical Robotics and Biomechatronics*, pp. 1258–1265, 2012, doi: 10.1109/BioRob.2012.6290287.

[152] M. Sakr and C. Menon, "Study on the force myography sensors placement for robust hand force estimation," in *2017 IEEE International Conference on Systems, Man, and Cybernetics (SMC)*. IEEE, oct 2017, doi: 10.1109/smc.2017.8122807.

[153] X. Liu, E. Zheng, and Q. Wang, "Real-time wrist motion decoding with high framerate electrical impedance tomography (EIT)," *IEEE Transactions on Neural Systems and Rehabilitation Engineering*, pp. 1–1, 2022, doi: 10.1109/tnsre.2022.3228018.

[154] C. Gibas, A. Grünewald, S. Büchner, and R. Brück, "An EIT system for mobile medical diagnostics," in *Medical Imaging 2018: Biomedical Applications in Molecular, Structural, and Functional Imaging*, vol. 10578, p. 105782E. International Society for Optics and Photonics, 2018.

[155] N. Akhlaghi, C. A. Baker, M. Lahlou, H. Zafar, K. G. Murthy, H. S. Rangwala, J. Kosecka, W. M. Joiner, J. J. Pancrazio, and S. Sikdar, "Real-time classification of hand motions using ultrasound imaging of forearm muscles," *IEEE Transactions on Biomedical Engineering*, vol. 63, no. 8, pp. 1687–1698, aug 2016, doi: 10.1109/TBME.2015.2498124.

[156] J. Mcintosh, A. Marzo, M. Fraser, and C. Phillips, "EchoFlex: Hand Gesture Recognition using Ultrasound Imaging," in *Proceedings of the 2017 CHI Conference on Human Factors in Computing Systems*, pp. 1923–1934. ACM, may 2017, doi: 10.1145/3025453.3025807.

[157] C. Castellini and G. Passig, "Ultrasound image features of the wrist are linearly related to finger positions," *IEEE International Conference on Intelligent Robots and Systems*, pp. 2108–2114, 2011, doi: 10.1109/IROS.2011.6048503.

[158] S. Oda, "Motor control for bilateral muscular contractions in humans," *The Japanese Journal of Physiology*, vol. 47, no. 6, pp. 487–498, 1997, doi: 10.2170/jjphysiol.47.487.

[159] M. Post, H. van Duinen, A. Steens, R. Renken, B. Kuipers, N. Maurits, and I. Zijdewind, "Reduced cortical activity during maximal bilateral contractions of the index finger," *NeuroImage*, vol. 35, no. 1, pp. 16–27, mar 2007, doi: 10.1016/j.neuroimage.2006.11.050.

[160] J. L. G. Nielsen, S. Holmgaard, N. Jiang, K. B. Englehart, D. Farina, and P. A. Parker, "Simultaneous and proportional force estimation for multifunction myoelectric prostheses using mirrored bilateral training," *IEEE Transactions on Biomedical Engineering*, vol. 58, no. 3, pp. 681–688, march 2011, doi: 10.1109/TBME.2010.2068298.

[161] C. Castellini and P. Van Der Smagt, "Surface EMG in advanced hand prosthetics," *Biological Cybernetics*, vol. 100, no. 1, pp. 35–47, nov 2009, doi: 10.1007/s00422-008-0278-1.

[162] R. Koiva, E. Riedenklau, C. Viegas, and C. Castellini, "Shape conformable high spatial resolution tactile bracelet for detecting hand and wrist activity," 2015.

[163] G. Montaldo, M. Tanter, J. Bercoff, N. Benech, and M. Fink, "Coherent plane-wave compounding for very high frame rate ultrasonography and transient elastography," *IEEE Transactions on Ultrasonics, Ferroelectrics and Frequency Control*, vol. 56, no. 3, pp. 489–506, mar 2009, doi: 10.1109/tuffc.2009.1067.

[164] A. Adler and D. Holder, *Electrical impedance tomography: methods, history and applications*, ser. Series in Medical Physics and Biomedical Engineering. CRC Press, nov 2021. ISBN 9781420034462

[165] A. Adler and W. R. Lionheart, "Uses and abuses of eidors: an extensible software base for EIT," *Physiological measurement*, vol. 27, no. 5, p. S25, 2006.

[166] E. Scheme and K. Englehart, "Electromyogram pattern recognition for control of powered upper-limb prostheses: state of the art and challenges for clinical use," *Journal of Rehabilitation Research & Development*, vol. 48, no. 6, pp. 643–659, 2011, doi: 10.1682/jrrd.2010.09.0177.

[167] Y. Geng, D. Tao, L. Chen, and G. Li, "Recognition of combined arm motions using support vector machine," in *Informatics in Control, Automation and Robotics*. Springer Berlin Heidelberg, 2011, pp. 807–814.

[168] A. J. Young, L. H. Smith, E. J. Rouse, and L. J. Hargrove, "Classification of simultaneous movements using surface EMG pattern recognition," *IEEE Transactions on Biomedical Engineering*, vol. 60, no. 5, pp. 1250–1258, 2013.

[169] A. E. Hoerl and R. W. Kennard, "Ridge regression: Biased estimation for nonorthogonal problems," *Technometrics*, vol. 12, no. 1, pp. 55–67, 1970, doi: 10.1080/00401706.2000.10485983.

[170] R. Rifkin, G. Yeo, T. Poggio *et al.*, "Regularized least-squares classification," *Nato Science Series Sub Series III Computer and Systems Sciences*, vol. 190, pp. 131–154, 2003.

[171] A. Gijsberts, "Incremental learning for robotics with constant update complexity (ph. d. thesis)," Ph.D. dissertation, University of Genoa, 2011.

[172] T. D. la Tour, M. Eickenberg, and J. L. Gallant, "Feature-space selection with banded ridge regression," *bioRxiv*, may 2022, doi: 10.1101/2022.05.05.490831.

[173] A. Rahimi and B. Recht, "Random features for large-scale kernel machines," in *Advances in Neural Information Processing Systems 20*, J. Platt, D. Koller, Y. Singer, and S. Roweis, Eds., vol. 20, no. 1, pp. 1177–1184. Curran Associates, Inc., 2008.

[174] A. Gijsberts, R. Bohra, D. Sierra González, A. Werner, M. Nowak, B. Caputo, M. A. Roa, and C. Castellini, "Stable myoelectric control of a hand prosthesis using non-linear incremental learning," *Frontiers in Neurorobotics*, vol. 8, no. FEB, pp. 1–15, 2014, doi: 10.3389/fnbot.2014.00008.

[175] A. Phinyomark, S. Hirunviriya, A. Nuidod, P. Phukpattaranont, and C. Limsakul, "Evaluation of EMG feature extraction for movement control of upper limb prostheses based on class separation index," in *IFMBE Proceedings*, pp. 750–754. Springer Berlin Heidelberg, 2011, doi: 10.1007/978-3-642-21729-6_183.

[176] A. Phinyomark, P. Phukpattaranont, and C. Limsakul, "Feature reduction and selection for EMG signal classification," *Expert Systems with Applications*, vol. 39, no. 8, pp. 7420–7431, 2012, doi: https://doi.org/10.1016/j.eswa.2012.01.102.

[177] M. Asfour, C. Menon, and X. Jiang, "A machine learning processing pipeline for reliable hand gesture classification of FMG signals with stochastic variance," *Sensors*, vol. 21, no. 4, p. 1504, feb 2021, doi: 10.3390/s21041504.

[178] R. Haralick and L. Shapiro, "Computer and robot vision, vol. 1, addison-welsey," *Reading, Mass, USA*, 1992.

[179] C. Castellini, G. Passig, and E. Zarka, "Using ultrasound images of the forearm to predict finger positions," *IEEE Transactions on Neural Systems and Rehabilitation Engineering*, vol. 20, no. 6, pp. 788–797, nov 2012, doi: 10.1109/TNSRE.2012.2207916.

[180] V. Ortenzi, S. Tarantino, C. Castellini, and C. Cipriani, "Ultrasound imaging for hand prosthesis control: a comparative study of features and classification methods," in *Proceedings of ICORR - International Conference on Rehabilitation Robotics*, vol. 2015-Septe, pp. 1–6. IEEE, aug 2015, doi: 10.1109/ICORR.2015.7281166.

[181] C. Castellini, R. Kõiva, C. Pasluosta, C. Viegas, and B. M. Eskofier, "Tactile myography: An off-line assessment of able-bodied subjects and one upper-limb amputee," *Technologies*, vol. 6, no. 2, p. 38, mar 2018, doi: 10.3390/technologies6020038.

[182] C. Harris, M. Stephens *et al.*, "A combined corner and edge detector," in *Alvey vision conference*, vol. 15, no. 50, pp. 10–5244, Citeseer. Alvey Vision Club, 1988, doi: 10.5244/c.2.23.

[183] A. Boschmann and M. Platzner, "A computer vision-based approach to high density EMG pattern recognition using structural similarity," in *Myoelectric Controls/Powered Prosthetics Symposium (MEC): Fredericton, NB, Canada*, 2014.

[184] J. C. Russ, *The image processing handbook*. CRC Press, Inc., 1998.

[185] X. Yang, X. Sun, D. Zhou, Y. Li, and H. Liu, "Towards wearable A-mode ultrasound sensing for real-time finger motion recognition," *IEEE Transactions on Neural Systems and Rehabilitation Engineering*, vol. 26, no. 6, pp. 1199–1208, jun 2018, doi: 10.1109/tnsre.2018.2829913.

[186] B. H. Brown and A. D. Seagar, "The sheffield data collection system," *Clinical Physics and Physiological Measurement*, vol. 8, no. 4A, pp. 91–97, nov 1987, doi: 10.1088/0143-0815/8/4a/012.

[187] W. R. Lionheart, "EIT reconstruction algorithms: pitfalls, challenges and recent developments," *Physiological measurement*, vol. 25, no. 1, pp. 125–142, feb 2004, doi: 10.1088/0967-3334/25/1/021.

[188] T. J. Yorkey, J. G. Webster, and W. J. Tompkins, "Comparing reconstruction algorithms for electrical impedance tomography," *IEEE Transactions on Biomedical Engineering*, vol. BME-34, no. 11, pp. 843–852, 1987, doi: 10.1109/tbme.1987.326032.

[189] M. Cheney, D. Isaacson, J. C. Newell, S. Simske, and J. Goble, "NOSER: An algorithm for solving the inverse conductivity problem," *International Journal of Imaging Systems and Technology*, vol. 2, no. 2, pp. 66–75, 1990, doi: 10.1002/ima.1850020203.

[190] M. Vauhkonen, D. Vadász, P. A. Karjalainen, E. Somersalo, and J. P. Kaipio, "Tikhonov regularization and prior information in electrical impedance tomography," *IEEE Transactions on Medical Imaging*, vol. 17, no. 2, pp. 285–293, apr 1998, doi: 10.1109/42.700740.

[191] A. Adler and R. Guardo, "Electrical impedance tomography: regularized imaging and contrast detection," *IEEE Transactions on Medical Imaging*, vol. 15, no. 2, pp. 170–179, apr 1996, doi: 10.1109/42.491418.

[192] B. Lock, K. Englehart, and B. Hudgins, "Real-time myoelectric control in a virtual environment to relate usability vs. accuracy," in *Proceedings of MEC - Myoelectric Control Symposium*, 2005.

[193] N. Jiang, I. Vujaklija, H. Rehbaum, B. Graimann, and D. Farina, "Is accurate mapping of EMG signals on kinematics needed for precise online myoelectric control?" *IEEE Transactions on Neural Systems and Rehabilitation Engineering*, vol. 22, no. 3, pp. 549–558, may 2013, doi: 10.1109/TNSRE.2013.2287383.

[194] M. Ortiz-Catalan, F. Rouhani, R. Brånemark, and B. Håkansson, "Offline accuracy: a potentially misleading metric in myoelectric pattern recognition for prosthetic control," in *2015 37th Annual International Conference of the IEEE Engineering in Medicine and Biology Society (EMBC)*, pp. 1140–1143. IEEE, aug 2015, doi: 10.1109/embc.2015.7318567.

[195] A. Gigli, A. Gijsberts, and C. Castellini, "The merits of dynamic data acquisition for realistic myocontrol," *Frontiers in Bioengineering and Biotechnology*, vol. 8, p. 361, apr 2020, doi: 10.3389/fbioe.2020.00361.

[196] J. M. Hahne, M. Markovic, and D. Farina, "User adaptation in myoelectric man-machine interfaces," *Scientific reports*, vol. 7, no. 1, pp. 1–10, jun 2017, doi: 10.1038/s41598-017-04255-x.

[197] N. E. Bunderson and T. A. Kuiken, "Quantification of feature space changes with experience during electromyogram pattern recognition control," *IEEE Transactions on Neural Systems and Rehabilitation Engineering*, vol. 20, no. 3, pp. 239–246, may 2012, doi: 10.1109/TNSRE.2011.2182525.

[198] R. A. Fisher, "The use of multiple measurements in taxonomic problems," *Annals of Eugenics*, vol. 7, no. 2, pp. 179–188, sep 1936, doi: 10.1111/j.1469-1809.1936.tb02137.x.

[199] M. Ringnér, "What is principal component analysis?" *Nature Biotechnology*, vol. 26, no. 3, pp. 303–304, mar 2008, doi: 10.1038/nbt0308-303.

[200] A. M. Simon, L. J. Hargrove, B. A. Lock, and T. A. Kuiken, "Target Achievement Control test: Evaluating real-time myoelectric pattern-recognition control of multifunctional upper-limb prostheses," *The Journal of Rehabilitation Research and Development*, vol. 48, no. 6, p. 619, 2011, doi: 10.1682/jrrd.2010.08.0149.

[201] J. Fröhner, G. Salvietti, P. Beckerle, and D. Prattichizzo, "Can wearable haptic devices foster the embodiment of virtual limbs?" *IEEE Transactions on Haptics*, vol. 12, no. 3, pp. 339–349, jul 2018, doi: 10.1109/toh.2018.2889497.

[202] K. A. Mann, F. W. Wernere, and A. K. Palmer, "Frequency spectrum analysis of wrist motion for activities of daily living," *Journal of Orthopaedic research*, vol. 7, no. 2, pp. 304–306, mar 1989, doi: 10.1002/jor.1100070219.

[203] A. Vallbo and J. Wessberg, "Organization of motor output in slow finger movements in man." *The Journal of Physiology*, vol. 469, no. 1, pp. 673–691, sep 1993, doi: 10.1113/jphysiol.1993.sp019837.

[204] N. Kakuda, M. Nagaoka, and J. Wessberg, "Common modulation of motor unit pairs during slow wrist movement in man," *The Journal of Physiology*, vol. 520, pp. 929–940, 1999, doi: 10.1111/j.1469-7793.1999.00929.x..

[205] B. A. Conway, C. Reid, and D. M. Halliday, "Low frequency cortico-muscular coherence during voluntary rapid movements of the wrist joint," *Brain Topography*, vol. 16, no. 4, pp. 221–224, 2004, doi: 10.1023/B:BRAT.0000032855.99865.31.

[206] R. R. Llinás, *I of the vortex: From neurons to self*. MIT press, 2002. ISBN 0262122330

[207] J. Lisman, "The challenge of understanding the brain: Where we stand in 2015," *Neuron*, vol. 86, no. 4, pp. 864–882, may 2015, doi: 10.1016/j.neuron.2015.03.032.

[208] L. H. Salmond, A. D. Davidson, and S. K. Charles, "Proximal-distal differences in movement smoothness reflect differences in biomechanics," *Journal of neurophysiology*, vol. 117, no. 3, pp. 1239–1257, 2017, doi: 10.1152/jn.00712.2015.

[209] R. Merletti and P. Di Torino, "Standards for reporting EMG data," *J Electromyogr Kinesiol*, vol. 9, no. 1, pp. 3–4, 1999.

[210] A. Phinyomark, R. N. Khushaba, and E. Scheme, "Feature extraction and selection for myoelectric control based on wearable EMG sensors," *Sensors*, vol. 18, no. 5, p. 1615, may 2018, doi: 10.3390/s18051615.

[211] H. Chen, Y. Zhang, Z. Zhang, Y. Fang, H. Liu, and C. Yao, "Exploring the relation between EMG sampling frequency and hand motion recognition accuracy," in *2017 IEEE International Conference on Systems, Man, and Cybernetics (SMC)*, pp. 1139–1144. IEEE, oct 2017, doi: 10.1109/smc.2017.8122765.

[212] G. Klute, G. Rowe, A. Mamishev, and W. Ledoux, "The thermal conductivity of prosthetic sockets and liners," *Prosthetics and orthotics international*, vol. 31, no. 3, pp. 292–299, sep 2007, doi: 10.1080/03093640601042554.

[213] B. Oldfrey, A. Tchorzewska, R. Jackson, M. Croysdale, R. Loureiro, C. Holloway, and M. Miodownik, "Additive manufacturing techniques for smart prosthetic liners," *Medical Engineering & Physics*, vol. 87, pp. 45–55, jan 2021, doi: 10.1016/j.medengphy.2020.11.006.

[214] C. M. Webber and B. L. Davis, "Design of a novel prosthetic socket: Assessment of the thermal performance," *Journal of biomechanics*, vol. 48, no. 7, pp. 1294–1299, 2015, doi: 10.1016/j.jbiomech.2015.02.048.

[215] P. Beckerle, C. Castellini, and B. Lenggenhager, "Robotic interfaces for cognitive psychology and embodiment research: a research roadmap," *Wiley Interdisciplinary Reviews: Cognitive Science*, vol. 10, no. 2, p. e1486, nov 2018, doi: 10.1002/wcs.1486.

[216] J. Brooke, *Usability Evaluation in Industry*. Taylor & Francis, 1996, ch. SUS: A "qu, pp. 189–194.

[217] NASA, *NASA Task Load Index (TLX) v 1.0 Paper and Pencil Package*, Human Performance Research Group, NASA Ames Research Center, Moffett Field, California, 1986.

[218] J. Benedek and T. Miner, "Measuring desirability: New methods for evaluating desirability in a usability lab setting," *Proceedings of Usability Professionals Association*, vol. 2003, no. 8-12, p. 57, 2002.

[219] A. Bangor, P. Kortum, and J. Miller, "Determining what individual SUS scores mean: Adding an adjective rating scale," *Journal of usability studies*, vol. 4, no. 3, pp. 114–123, 2009.

[220] A. Vega-Gonzalez, B. J. Bain, P. M. Dall, and M. H. Granat, "Continuous monitoring of upper-limb activity in a free-living environment: a validation study," *Medical & Biological Engineering & Computing*, vol. 45, no. 10, pp. 947–956, jul 2007, doi: 10.1007/s11517-007-0233-7.

[221] F. Montagnani, M. Controzzi, and C. Cipriani, "Is it finger or wrist dexterity that is missing in current hand prostheses?" *IEEE Transactions on Neural Systems and Rehabilitation Engineering*, vol. 23, no. 4, pp. 600–609, jul 2015, doi: 10.1109/tnsre.2015.2398112.

[222] C. Ott, M. A. Roa, F. Schmidt, W. Friedl, J. Englsberger, R. Burger, A. Werner, A. Dietrich, D. Leidner, B. Henze, O. Eiberger, A. Beyer, B. Bäuml, C. Borst, and A. Albu-Schäffer, "Mechanisms and design of dlr humanoid robots," *Humanoid Robotics: A Reference; Goswami, A., Vadakkepat, P., Eds*, pp. 1–26, 2016, doi: 10.1007/978-94-007-7194-9_132-1.

[223] L. M. Hermansson, A. G. Fisher, B. Bernspång, and A.-C. Eliasson, "Assessment of capacity for myoelectric control: a new rasch-built measure of prosthetic hand control," *Journal of rehabilitation medicine*, vol. 37, no. 3, pp. 166–71, 2005.

[224] C. Schuster, S. Hahn, and T. Ettlin, "Objectively-assessed outcome measures: a translation and cross-cultural adaptation procedure applied to the chedoke mcmaster arm and hand activity inventory (cahai)," *BMC medical research methodology*, vol. 10, no. 1, pp. 1–9, 2010.

[225] S. Barreca, C. Gowland, P. Stratford, M. Huijbregts, J. Griffiths, W. Torresin, M. Dunkley, P. Miller, and L. Masters, "Development of the chedoke arm and hand activity inventory: theoretical constructs, item generation, and selection," *Topics in stroke rehabilitation*, vol. 11, no. 4, pp. 31–42, 2004.

[226] L. V. Herlant, R. M. Holladay, and S. S. Srinivasa, "Assistive teleoperation of robot arms via automatic time-optimal mode switching," in *11th ACM/IEEE International Conference on Human-Robot Interaction (HRI)*, pp. 35–42. IEEE, 2016, doi: 10.1109/hri.2016.7451731.

[227] R. Pocius, N. Zamani, H. Culbertson, and S. Nikolaidis, "Communicating robot goals via haptic feedback in manipulation tasks," in *Companion of the 2020 ACM/IEEE International Conference on Human-Robot Interaction*, pp. 591–593, 2020.

[228] F. Tenore, A. Ramos, A. Fahmy, S. Acharya, R. Etienne-Cummings, and N. V. Thakor, "Towards the control of individual fingers of a prosthetic hand using surface EMG signals," in *Annual International Conference of the IEEE Engineering in Medicine and Biology Society (EMBS).*, pp. 6146–6149. IEEE, aug 2007, doi: 10.1109/iembs.2007.4353752.

[229] A. Fougner, E. Scheme, A. D. C. Chan, K. Englehart, Ø. Stavdahl, and O. Stavdahl, "Resolving the limb position effect in myoelectric pattern recognition," *IEEE Transactions on Neural Systems and Rehabilitation Engineering*, vol. 19, no. 6, pp. 644–651, dec 2011, doi: 10.1109/TNSRE.2011.2163529.

[230] V. Ravindra and C. Castellini, "A comparative analysis of three non-invasive human-machine interfaces for the disabled," *Frontiers in Neurorobotics*, vol. 8, no. 24, pp. 1–10, oct 2014, doi: 10.3389/fnbot.2014.00024.

[231] R. Merletti, A. Botter, C. Cescon, M. A. Minetto, and T. M. M. Vieira, "Advances in surface EMG: Recent progress in clinical research applications," *Critical Reviews in Biomedical Engineering*, vol. 38, no. 4, pp. 347–379, 2010, doi: 10.1615/CritRevBiomedEng.v38.i4.20.

[232] P. M. Stevens, B. Motawar, K. Buchanan, and S. H. Frey, "Impact of unilateral transradial prosthesis in upper limb utilization relative to able-bodied controls:

insights from wireless accelerometer data," in *Proceedings of MEC - Myoelectric Control Symposium*, 2022.

[233] S. Muceli, N. Jiang, and D. Farina, "Extracting signals robust to electrode number and shift for online simultaneous and proportional myoelectric control by factorization algorithms," *IEEE Transactions on Neural Systems and Rehabilitation Engineering*, vol. 22, no. 3, pp. 623–633, may 2014, doi: 10.1109/TNSRE.2013.2282898.

[234] M. Nowak, I. Vujaklija, A. Sturma, C. Castellini, and D. Farina, "Simultaneous and proportional real-time myocontrol of up to three degrees of freedom of the wrist and hand," *IEEE Transactions on Biomedical Engineering*, pp. 1–12, 2022, doi: 10.1109/TBME.2022.3194104.

[235] P. Bhardwaj, S. S. Nayak, A. M. Kiswar, and S. R. Sabapathy, "Effect of static wrist position on grip strength," *Indian Journal of Plastic Surgery: Official Publication of the Association of Plastic Surgeons of India*, vol. 44, no. 1, p. 55, jan 2011, doi: 10.1055/s-0039-1699481.

[236] V. Parvatikar, P. Mukkannavar *et al.*, "Comparative study of grip strength in different positions of shoulder and elbow with wrist in neutral and extension positions," *Journal of Exercise Science and Physiotherapy*, vol. 5, no. 2, pp. 67–75, 2009.

[237] J. P. M. Mogk and P. J. Keir, "The effects of posture on forearm muscle loading during gripping." *Ergonomics*, vol. 46, no. 9, pp. 956–975, jul 2003, doi: 10.1080/0014013031000107595.

[238] P. W. Fong and G. Y. Ng, "Effect of wrist positioning on the repeatability and strength of power grip," *American Journal of Occupational Therapy*, vol. 55, no. 2, pp. 212–216, 2001, doi: 10.5014/ajot.55.2.212.

[239] L. Claudon, "Evaluation of grip force using electromyograms in isometric isotonic conditions," *International Journal of Occupational Safety and Ergonomics*, vol. 4, no. 2, pp. 169–184, jan 1998, doi: 10.1080/10803548.1998.11076388.

[240] L. De Smet, B. Tirez, and K. Stappaerts, "Effect of forearm rotation on grip strength," pp. 360–362, 1998.

[241] B. P. Kattel, T. K. Fredericks, J. E. Fernandez, and D. C. Lee, "The effect of upper-extremity posture on maximum grip strength," *International Journal of Industrial Ergonomics*, vol. 18, no. 5-6, pp. 423–429, 1996, doi: 10.1016/0169-8141(95)00105-0.

[242] L. G. Richards, B. Olson, and P. Palmiter-Thomas, "How Forearm Position Affects Grip Strength," *American Journal of Occupational Therapy*, vol. 50, no. 2, pp. 133–138, 1996, doi: 10.5014/ajot.50.2.133.

[243] K. K. Zellers and M. S. Hallbeck, "The effects of gender, wrist and forearm position on maximum isometric power grasp force, wrist force, and their interactions," *Proceedings of the Human Factors and Ergonomics Society Annual Meeting*, vol. 39, no. 10, pp. 543–547, 1995.

[244] J. Duque, D. Masset, and J. Malchaire, "Evaluation of handgrip force from EMG measurements," *Applied Ergonomics*, vol. 26, no. 1, pp. 61–66, 1995, doi: 10.1016/0003-6870(94)00003-H.

[245] R. J. Marley and R. R. Wehrman, "Grip Strength as a Function of Forearm Rotation and Elbow Posture," *Human Factors and Ergonomics Society Annual Meeting*, vol. 36, no. 10, pp. 791–795, 1992, doi: 10.1177/154193129203601033.

[246] R. Terrell and J. L. Purswell, "The influence of forearm and wrist orientation on static grip strength as a design criterion for hand tools," vol. 20, no. 1, pp. 28–32, 1976, doi: 10.1177/154193127602000115.

[247] M. Nowak, "Simultaneous and proportional control of hand prostheses with multiple degrees of freedom: A new method of improving the training process," Master's thesis, Technical University of Munich, Germany, 2014.

[248] B. B. Atitallah, Z. Hu, D. Bouchaala, M. A. Hussain, A. Ismail, N. Derbel, and O. Kanoun, "Hand sign recognition system based on EIT imaging and robust CNN classification," *IEEE Sensors Journal*, vol. 22, no. 2, pp. 1729–1737, jan 2021, doi: 10.1109/jsen.2021.3130982.

[249] D. P. Leins, C. Gibas, R. Brück, and R. Haschke, "Toward more robust hand gesture recognition on EIT data," *Frontiers in Neurorobotics*, vol. 15, p. 110, aug 2021, doi: 10.3389/fnbot.2021.659311.

[250] A. Briko, V. Kapravchuk, A. Kobelev, A. Hammoud, S. Leonhardt, C. Ngo, Y. Gulyaev, and S. Shchukin, "A way of bionic control based on EI, EMG, and FMG signals," *Sensors*, vol. 22, no. 1, p. 152, dec 2021, doi: 10.3390/s22010152.

[251] K. Takeuchi, Y. Yamazaki, and K. Yoshifuji, "Avatar work: Telework for disabled people unable to go outside by using avatar robots," in *Companion of the 2020 ACM/IEEE International Conference on Human-Robot Interaction*, pp. 53–60. ACM, mar 2020, doi: 10.1145/3371382.3380737.

[252] C. S. Green and D. Bavelier, "Exercising your brain: a review of human brain plasticity and training-induced learning." *Psychology and Aging*, vol. 23, no. 4, pp. 692–701, 2008, doi: 10.1037/a0014345.

[253] Z. G. Xiao and C. Menon, "An investigation on the sampling frequency of the upper-limb force myographic signals," *Sensors*, vol. 19, no. 11, p. 2432, may 2019, doi: 10.3390/s19112432.

[254] M. Rojas-Martínez, M. Mañanas, J. Alonso, and R. Merletti, "Identification of isometric contractions based on high density EMG maps," *Journal of Electromyography and Kinesiology*, vol. 23, no. 1, pp. 33–42, feb 2013, doi: 10.1016/j.jelekin.2012.06.009.

[255] C. Amma, T. Krings, J. Böer, and T. Schultz, "Advancing muscle-computer interfaces with high-density electromyography," in *Proceedings of the 33rd Annual ACM Conference on Human Factors in Computing Systems*, pp. 929–938. ACM, apr 2015, doi: 10.1145/2702123.2702501.

[256] S. Engdahl, S. Acuña, A. Bashatah, A. Dhawan, E. King, B. Mukherjee, R. Holley, B. Monroe, G. Lévay, R. Kaliki, and S. Sikdar, "Assessing the feasibility of using sonomyography for upper limb prosthesis control," in *Proceedings of MEC - Myoelectric Control Symposium*, 2022.

[257] I. Mendez Guerra, D. Y. Barsakcioglu, I. Vujaklija, D. Z. Wetmore, and D. Farina, "Far-field electric potentials provide access to the output from the spinal cord from wrist-mounted sensors," *Journal of Neural Engineering*, vol. 19, no. 2, p. 026031, apr 2022, doi: 10.1088/1741-2552/ac5f1a.

[258] A. Marinelli, N. Boccardo, F. Tessari, D. D. Domenico, G. Caserta, M. Canepa, G. Gini, G. Barresi, M. Laffranchi, L. D. Michieli, and M. Semprini, "Active upper limb prostheses: a review on current state and upcoming breakthroughs," *Progress in Biomedical Engineering*, vol. 5, no. 1, p. 012001, jan 2023, doi: 10.1088/2516-1091/acac57.

[259] M. Paleari, R. Luciani, and P. Ariano, "Towards NIRS-based hand movement recognition," in *2017 International Conference on Rehabilitation Robotics (ICORR)*. IEEE, jul 2017, doi: 10.1109/icorr.2017.8009461.

[260] S. Wilson and R. Vaidyanathan, "Upper-limb prosthetic control using wearable multichannel mechanomyography," in *2017 International Conference on Rehabilitation Robotics (ICORR)*. IEEE, jul 2017, doi: 10.1109/icorr.2017.8009427.

[261] M. Gardner, C. S. M. Castillo, S. Wilson, D. Farina, E. Burdet, B. C. Khoo, S. F. Atashzar, and R. Vaidyanathan, "A multimodal intention detection sensor suite for shared autonomy of upper-limb robotic prostheses," *Sensors*, vol. 20, no. 21, p. 6097, oct 2020, doi: 10.3390/s20216097.

[262] T. W. Beck, T. J. Housh, G. O. Johnson, J. T. Cramer, J. P. Weir, J. W. Coburn, and M. H. Malek, "Does the frequency content of the surface mechanomyographic signal reflect motor unit firing rates? a brief review," *Journal of Electromyography and Kinesiology*, vol. 17, no. 1, pp. 1–13, feb 2007, doi: 10.1016/j.jelekin.2005.12.002.

[263] S. Wilson, H. Eberle, Y. Hayashi, S. O. H. Madgwick, A. McGregor, X. Jing, and R. Vaidyanathan, "Formulation of a new gradient descent marg orientation

algorithm: Case study on robot teleoperation," *Mechanical Systems and Signal Processing*, vol. 130, pp. 183–200, sep 2019, doi: 10.1016/j.ymssp.2019.04.064.

[264] X. Sheng, X. Ding, W. Guo, L. Hua, M. Wang, and X. Zhu, "Toward an integrated multi-modal sEMG/MMG/NIRS sensing system for human–machine interface robust to muscular fatigue," *IEEE Sensors Journal*, vol. 21, no. 3, pp. 3702–3712, feb 2021, doi: 10.1109/jsen.2020.3023742.

[265] A. Dwivedi, H. Groll, and P. Beckerle, "A systematic review of sensor fusion methods using peripheral bio-signals for human intention decoding," *Sensors*, vol. 22, no. 17, p. 6319, aug 2022, doi: 10.3390/s22176319.

[266] D. Novak and R. Riener, "A survey of sensor fusion methods in wearable robotics," *Robotics and Autonomous Systems*, vol. 73, pp. 155–170, nov 2015, doi: 10.1016/j.robot.2014.08.012.

[267] C. Merritt, "Ultrasound safety: what are the issues?" *Radiology*, vol. 173, no. 2, pp. 304–306, nov 1989, doi: 10.1148/radiology.173.2.2678243.

[268] J. H. Rigby, R. M. Taggart, K. L. Stratton, G. K. Lewis Jr, and D. O. Draper, "Intramuscular heating characteristics of multihour low-intensity therapeutic ultrasound," *Journal of Athletic Training*, vol. 50, no. 11, pp. 1158–1164, nov 2015, doi: 10.4085/1062-6050-50.11.03.

[269] B. Klucinec, "The effectiveness of the aquaflex gel pad in the transmission of acoustic energy," *Journal of Athletic Training*, vol. 31, no. 4, p. 313, 1996.

[270] M. C. Sanchez, S. Zuo, A. Moldovan, S. Cochran, K. Nazarpour, and H. Heidari, "Flexible piezoelectric sensors for miniaturized sonomyography," in *2021 43rd Annual International Conference of the IEEE Engineering in Medicine & Biology Society (EMBC)*, pp. 7373–7376. IEEE, nov 2021, doi: 10.1109/embc46164.2021.9630342.

[271] I. AlMohimeed and Y. Ono, "Ultrasound measurement of skeletal muscle contractile parameters using flexible and wearable single-element ultrasonic sensor," *Sensors*, vol. 20, no. 13, p. 3616, jun 2020, doi: 10.3390/s20133616.

[272] C. Dai and X. Hu, "Extracting and classifying spatial muscle activation patterns in forearm flexor muscles using high-density electromyogram recordings," *International Journal of Neural Systems*, vol. 29, no. 01, p. 1850025, jan 2019, doi: 10.1142/s0129065718500259.

[273] ——, "Finger joint angle estimation based on motoneuron discharge activities," *IEEE Journal of Biomedical and Health Informatics*, vol. 24, no. 3, pp. 760–767, mar 2020, doi: 10.1109/jbhi.2019.2926307.

[274] Y.-G. Park, S. Lee, and J.-U. Park, "Recent progress in wireless sensors for wearable electronics," *Sensors*, vol. 19, no. 20, p. 4353, oct 2019, doi: 10.3390/s19204353.

[275] L. P. Murciego, A. Komolafe, N. Peřinka, H. Nunes-Matos, K. Junker, A. G. Díez, S. Lanceros-Méndez, R. Torah, E. G. Spaich, and S. Dosen, "A novel screen-printed textile interface for high-density electromyography recording," *Sensors*, vol. 23, no. 3, p. 1113, jan 2023, doi: 10.3390/s23031113.

[276] M. Jose, M. Lemmens, S. Bormans, R. Thoelen, and W. Deferme, "Fully printed, stretchable and wearable bioimpedance sensor on textiles for tomography," *Flexible and Printed Electronics*, vol. 6, no. 1, p. 015010, feb 2021, doi: 10.1088/2058-8585/abe51b.

[277] Y. Dobashi, D. Yao, Y. Petel, T. N. Nguyen, M. S. Sarwar, Y. Thabet, C. L. W. Ng, E. S. Glitz, G. T. M. Nguyen, C. Plesse, F. Vidal, C. A. Michal, and J. D. W. Madden, "Piezoionic mechanoreceptors: Force-induced current generation in hydrogels," *Science*, vol. 376, no. 6592, pp. 502–507, apr 2022, doi: 10.1126/science.aaw1974.

[278] S. Dosen, M. Markovic, K. Somer, B. Graimann, and D. Farina, "EMG biofeedback for online predictive control of grasping force in a myoelectric prosthesis," *Journal of NeuroEngineering and Rehabilitation*, vol. 12, no. 1, pp. 1–13, jun 2015, doi: 10.1186/s12984-015-0047-z.

[279] B. Gesslbauer, L. A. Hruby, A. D. Roche, D. Farina, R. Blumer, and O. C. Aszmann, "Axonal components of nerves innervating the human arm," *Annals of neurology*, vol. 82, no. 3, pp. 396–408, sep 2017, doi: 10.1002/ana.25018.

[280] J. W. Sensinger and S. Dosen, "A review of sensory feedback in upper-limb prostheses from the perspective of human motor control," *Frontiers in Neuroscience*, vol. 14, p. 345, jun 2020, doi: 10.3389/fnins.2020.00345.

[281] A. Y. Szeto and F. A. Saunders, "Electrocutaneous stimulation for sensory communication in rehabilitation engineering," *IEEE Transactions on Biomedical Engineering*, vol. BME-29, no. 4, pp. 300–308, apr 1982, doi: 10.1109/tbme.1982.324948.

[282] T. Tashiro and A. Higashiyama, "The perceptual properties of electrocutaneous stimulation: Sensory quality, subjective intensity, and intensity-duration relation," *Perception & Psychophysics*, vol. 30, no. 6, pp. 579–586, nov 1981, doi: 10.3758/bf03202013.

[283] C. Della Santina, C. Piazza, G. Grioli, M. G. Catalano, and A. Bicchi, "Toward dexterous manipulation with augmented adaptive synergies: The pisa/IIT SoftHand 2," *IEEE Transactions on Robotics*, vol. 34, no. 5, pp. 1141–1156, oct 2018, doi: 10.1109/tro.2018.2830407.

nani gigantum humeris insidentes

(Bernard de Chartres)

Appendix A

Core Publications

Table of Contents

A.1 "Assessment of a Wearable Force- and Electromyography Device and Comparison of the Related Signals for Myocontrol"

Authors Mathilde Connan, Eduardo Ruiz Ramírez, Bernhard Vodermayer and Claudio Castellini

Journal Frontiers in Neurorobotics

Year 2016

Number of pages 13

Review Peer-reviewed

Abstract In the frame of assistive robotics, multi-finger prosthetic hand/wrists have recently appeared, offering an increasing level of dexterity; however, in practice their control is limited to a few hand grips and still unreliable, with the effect that pattern recognition has not yet appeared in the clinical environment. According to the scientific community, one of the keys to improve the situation is multi-modal sensing, i.e., using diverse sensor modalities to interpret the subject's intent and improve the reliability and safety of the control system in daily life activities. In this work, we first describe and test a novel wireless, wearable force- and electromyography device; through an experiment conducted on ten intact subjects, we then compare the obtained signals both qualitatively and quantitatively, highlighting their advantages and disadvantages. Our results indicate that force-myography yields signals which are more stable across time during whenever a pattern is held, than those obtained by electromyography. We speculate that fusion of the two modalities might be advantageous to improve the reliability of myocontrol in the near future.

Author contributions System Design; Software Design; Test setup and conduction of user surveys; Drafting of the Manuscript; Critical Revision; Final Approval.

Citation M. Connan, E. R. Ramírez, B. Vodermayer, and C. Castellini, "Assessment of a wearable force- and electromyography device and comparison of the related signals for myocontrol," *Frontiers in Neurorobotics*, vol. 10, no. 17, pp. 1–13, nov 2016, doi: 10.3389/fnbot.2016.00017

frontiers in Neurorobotics

ORIGINAL RESEARCH
published: 17 November 2016
doi: 10.3389/fnbot.2016.00017

Assessment of a Wearable Force- and Electromyography Device and Comparison of the Related Signals for Myocontrol

Mathilde Connan, Eduardo Ruiz Ramírez, Bernhard Vodermayer and Claudio Castellini*

Cognitive Robotics, Institute of Robotics and Mechatronics, German Aerospace Center (DLR), Wessling, Germany

In the frame of assistive robotics, multi-finger prosthetic hand/wrists have recently appeared, offering an increasing level of dexterity; however, in practice their control is limited to a few hand grips and still unreliable, with the effect that pattern recognition has not yet appeared in the clinical environment. According to the scientific community, one of the keys to improve the situation is multi-modal sensing, i.e., using diverse sensor modalities to interpret the subject's intent and improve the reliability and safety of the control system in daily life activities. In this work, we first describe and test a novel wireless, wearable force- and electromyography device; through an experiment conducted on ten intact subjects, we then compare the obtained signals both qualitatively and quantitatively, highlighting their advantages and disadvantages. Our results indicate that force-myography yields signals which are more stable across time during whenever a pattern is held, than those obtained by electromyography. We speculate that fusion of the two modalities might be advantageous to improve the reliability of myocontrol in the near future.

Keywords: surface electromyography, force myography, multi-modal intent detection, machine learning, human-machine interfaces, rehabilitation robotics

OPEN ACCESS

Edited by:
Ricardo Chavarriaga, École Polytechnique Fédérale de Lausanne (EPFL), Switzerland

Reviewed by:
Sebastian Amsuess, Otto Bock, Germany
Francesco Clemente, Scuola Superiore Sant'Anna, Italy

****Correspondence:***
Bernhard Vodermayer
bernhard.vodermayer@dlr.de

Received: *18 July 2016*
Accepted: *21 October 2016*
Published: *17 November 2016*

Citation:
Connan M, Ruiz Ramírez E, Vodermayer B and Castellini C (2016) Assessment of a Wearable Force- and Electromyography Device and Comparison of the Related Signals for Myocontrol. Front. Neurorobot. 10:17. doi: 10.3389/fnbot.2016.00017

1. INTRODUCTION

The human hand is a prodigious natural tool, comprising 27 bones and 33 muscles, resulting in a total of 22 degrees of freedom (DOFs) (Biryukova and Yourovskaya, 1994); its sensorial equipment enables us to drive, browse through the pages of a book, hold and manipulate delicate objects as well as heavy tools. Due to this complexity, artificially reproducing its functions is still a challenge for the roboticians. Nevertheless, a mechatronic tool getting close to the human hand is highly desirable in the context, e.g., of dexterous hand prosthetics. Despite the fact that multi-fingered hand prostheses have appeared on the market during the last decade, their level of abandonment remains relatively high (Biddiss and Chau, 2007; Peerdeman et al., 2011). Touch Bionics' *i-LIMB*, Otto Bock's *Michelangelo*, Vincent Systems' *Vincent Evolution 2* and RSL Steeper's *Bebionic3* are among these examples: with as many as six DOFs, they still are a limited replacement of the hand of an amputee, not mirroring the capabilities of a real human hand. A prosthetic wrist adds at least one DOF to the device and further improves its potential dexterity, but empowering amputees to control such artifacts (myocontrol) is still an open issue.

The academic state-of-the-art of myocontrol relates to the possibility of proportionally and independently controlling each DOF of the prosthesis according to the patient's intent (Sebelius et al., 2005; Cipriani et al., 2011a); however, low stability and accuracy prevent a successful commercialization of such an approach. Myocontrol is still limited to a few DOFs (Arjunan and Kumar, 2010; Yang et al., 2014), and surface electromyography (sEMG) signals are deemed to be no longer enough (Jiang et al., 2012a). Researchers have tried to address this issue by increasing the number of sensors (Tenore et al., 2007), although it is known that four to six channels are acceptable for pattern detection (Young et al., 2012), and/or to find their optimal placement given the characteristics of the stump (Castellini and van der Smagt, 2009; Fang et al., 2015); several pattern recognition algorithms have been studied, such as artificial neural networks (Baspinar et al., 2013), linear discriminant analysis (Khushaba et al., 2009) and non-linear incremental learning (Gijsberts et al., 2014). However, one of the major drawbacks of sEMG signals is their variable nature: sweat, electrode shifts, motion artifacts, ambient noise, cross-talk among deep adjacent muscles and muscular fatigue can crucially affect them (Oskoei and Hu, 2007; Cram and Kasman, 2010; Merletti et al., 2011a; Castellini et al., 2014). In general, any change in the muscle configuration during and after the training of the machine learning algorithm (e.g., the position of the limb and the body and the weights to be lifted during grasping and carrying) must be taken into account (Scheme et al., 2010; Cipriani et al., 2011b). As a result, simultaneous and proportional (s/p) control of each DOF is slow and laborious. Therefore, the application of other types of sensors and sensor combinations is an active field of research (Fougner et al., 2011; Jiang et al., 2012a).

Among non-invasive approaches other than sEMG, electroencephalography (EEG), mechanomyography (MMG), ultrasound imaging also known as sonomyography (SMG), force myography (FMG), functional magnetic resonance imaging and more are considerable options (Lobo-Prat et al., 2014; Ravindra and Castellini, 2014; Fang et al., 2015). Such Human Machine Interfaces (HMIs) have been implemented in distinct studies. However, the research community is recently pushing the development of multi-modal sensing techniques in the field of upper-limb rehabilitation (Fang et al., 2015). For instance, experiments have shown that accelerometer sensor signals can improve the classification accuracy of EMG electrodes (Fougner et al., 2011), as well as a multimodal technique with EMG and Near Infrared Spectroscopy (NIS) (Herrmann and Buchenrieder, 2010), or a combination of EEG and electroneurography (ENG) (Rossini and Rossini, 2010). In brief, a full comparison of the advantages and disadvantages of each type of signal, as well as the possibilities offered by their fusion, is still lacking.

In this study we focus on the joint usage of sEMG and FMG sensors. Surface EMG Merletti et al. (2011b) detects Motor Unit Activation Potentials, that is, electrical fields generated by motor units during muscle contraction, whereas FMG (Phillips and Craelius, 2005; Wininger et al., 2008) detects the pressure exerted by the muscles toward the surface of the skin by volumetric changes induced during muscle activity. Due to the very different nature of the signals gathered by these two techniques, it seems reasonable that they could be proficiently fused in order to better detect a subject's intent. A simple and low-cost option to record FMG signals is represented by force-sensing resistors (FSRs), whose resistance changes according to the pressure applied to them. This is also our option of choice. These sensors are cheap and very compact. Castellini and Ravindra (2014) already proved their effectiveness, and established that finger forces can be predicted with the same accuracy than sEMG sensors (Ravindra and Castellini, 2014). Cho et al. (2016) tested their force sensing system on four amputees and demonstrated that it is possible to classify six primary grips using only FMG with an accuracy of above 70% in the residuum. We describe a novel, modular approach for joint FMG/sEMG intent detection: thanks to a newly developed, fully mobile and wireless acquisition system, we simultaneously gathered FMG and sEMG signals during an experiment in which ten intact subjects performed a repetitive sequence of wrist and hand movements. The collected data was used to assess the desirable characteristics of each modality, while self-assessment questionnaires were used to check that the device was acceptable for the subjects. In the end, we claim that a fusion of the two approaches is potentially better than using them independently for dexterous myocontrol.

2. MATERIALS AND METHODS

In order to assess the combined data acquisition of sEMG and FMG for myocontrol, we have built a prototype fully wearable, wireless multi-modal myocontrol system. To study its performance, its usability, and the characteristics of the obtained signals, we have involved ten intact human subjects in an experiment with the device as its core. **Figure 1** (left panel) shows the system as worn by a subject: the device is composed of three modules: a set of mixed sEMG/FMG sensors (in this case, arranged on two Velcro bracelets), a Bluetooth analog-to-digital conversion board gathering and transmitting the signals, and a smartphone receiving the data via Bluetooth and able to perform myocontrol via a machine learning algorithm. The board was based upon the work of Brunelli et al. (2015), whereas the learning algorithm is Incremental Ridge Regression with Random Fourier Features (see below for more details), already been evaluated (in a non-wearable control system) by Gijsberts et al. (2014) and Strazzulla et al. (2016). Although not extensively used in this specific experiment, the machine learning algorithm can produce control signals in real time and transmit them to the sensor board, which serves as a relay routing them to a hand prosthetic device connected to it. A block diagram of the whole system is presented in **Figure 1** (right panel).

2.1. Experimental Setup

2.1.1. Sensors

Ten Ottobock *MyoBock 13E200 = 50* sensors were used to gather the sEMG signals. They provide on-board amplification, rectification and filtering. Sensors of this kind are a standard in clinical applications, especially in prosthetic sockets.

FMG signals were registered by ten *FSR 400 Short* force-sensing resistors by Interlink Electronics. Made of a robust polymer thick film, each FSR has a 5.6 mm-diameter sensitive

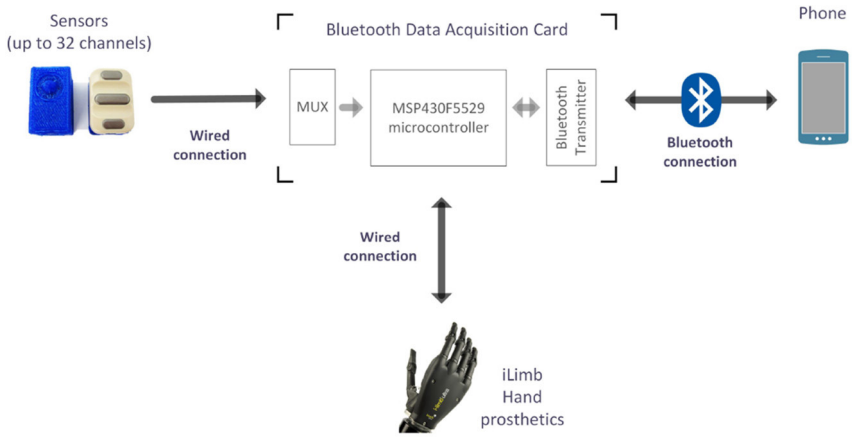

FIGURE 1 | (Left) Overview of the experimental setup. The subject is wearing the mobile system with a wired connection to two sensor bracelets, one endowed with FMG sensors, the other one with sEMG sensors. The Bluetooth data acquisition board is located in a box placed on the right upper-arm. **(Right)** Block diagram of the system; an i-LIMB prosthetic hand by Touch Bionics (not used in this experiment) can be directly controlled by the device.

area: when a force is applied to its surface, the electrical resistance of the FSR decreases correspondingly. These sensors are cheap (5€ apiece), but despite the specified remarkably large sensitivity range (0.2N–40N), they have non-negligible hysteresis at high forces, no guarantee of repeatability and a non-linear transfer function. Nonetheless, Castellini and Ravindra (2014) have shown that for small forces (0N–15N) their behavior is largely comparable and their transfer function is almost linear. In our setup, a small printed circuit board with a voltage amplifier (see **Figure 2**) provides the amplification of the FMG signals. The output of the sensor circuit is $V_{out} = \frac{R_2 V_{CC}}{R_1+R_2} - \frac{R_1 R_4 V_{CC}}{R_1+R_2} \times \frac{1}{R_{FSR}}$, yielding a lowest admissible resistance of $R_{FSR} = \frac{R_1 R_4}{R_2} = 6k\Omega$, which corresponds to a theoretical maximum force observed on the FSR's surface of $3.33\,N$ (InterlinkElectronics, 2014).

In order to provide maximum flexibility in arranging the sensors on the subject's body, specifically on the forearm or stump, uniform 3D-printed housings have been designed for both kinds of sensors. The housings are made of flexible thermoplastic polyurethane and provide adherence to the subject's skin as they are tightened to the arm by a Velcro strap. Each housing provides braces to allow sliding on the strap, so that its position can be individually adjusted and maintained, regardless of the type of sensor (see **Figure 3**). The FSR sensor housing not only serves as a retainer for the sensor and the amplifier, but furthermore comprises a structured geometric body that is divided into two parts: approximately one half is shaped like a cone and pointing toward the FSR sensor's sensitive area, the other half, shaped like a hemisphere, is pointing toward the skin. This geometric shape has been specifically designed to concentrate the force exerted by the muscles on the FSR sensor's sensitive area. The bearing of this structure is realized by a surrounding, thin and flexible membrane with a thickness of 0.5 mm and a total area of 47.5 mm^2 (small diameter 6.3 mm, large diameter 10 mm), linking it to the housing. Even if the elastic and damping properties of the membrane have not been subject to further investigation so far, it is assumed that the membrane may increase the signal stability, i.e., it could hypothetically add a mechanical filtering to the bio-signal. This solution offers the capability to create any combination of FMG and sEMG electrodes. In order to gather signals from the complete circumference of the forearm, the sensors are placed evenly spaced around the forearm/stump. This arrangement, also called *low-density surface electrode layout* or *uniform electrode positioning* (Fang et al., 2015), has already been proven effective for robotic hand prosthesis control in a number of previous publications (Castellini and van der Smagt, 2009, 2013).

The typical voltage output of the FSR/amplifier/housing complex has further been characterized. The measurements have been performed with a Zwick Roell *ZMART.PRO* compression test device providing fixture of the sensor setup as well as controlled exertion of force with an accuracy of 100 mN. The corresponding output voltage of the device has been measured with a FLUKE 289 Multimeter with an accuracy of 1 mV. The relationship between voltage output and applied force, in a range from 0 to 5.2 N, is linear with a residual average error of about 7% (see **Table 1**). It is worth noting that, during the experiment (see below), no FSR ever reached the saturation point, meaning that the FMG signals have all been correctly captured. This matches to a large extent the results obtained in Castellini and Ravindra (2014) and Ravindra and Castellini (2014) for a similar device.

2.1.2. Analog-Digital Conversion and Data Transfer

A Bluetooth ADC board (**Figure 4**), consisting of a Texas Instrument *MSP430F5529* microcontroller and an on-board Bluetooth chipset, provides analog-to-digital conversion (ADC) of the signals of both the sEMG and FSR sensors, and their wireless transmission. As the microcontroller natively supports only 15 AD-channels, AD-conversion of up to 32 sensors is realized via analog multiplexing, providing a maximum sampling rate of 192.5 Hz for each channel. Since the sEMG sensors already provide rectified and filtered signals with an evaluable

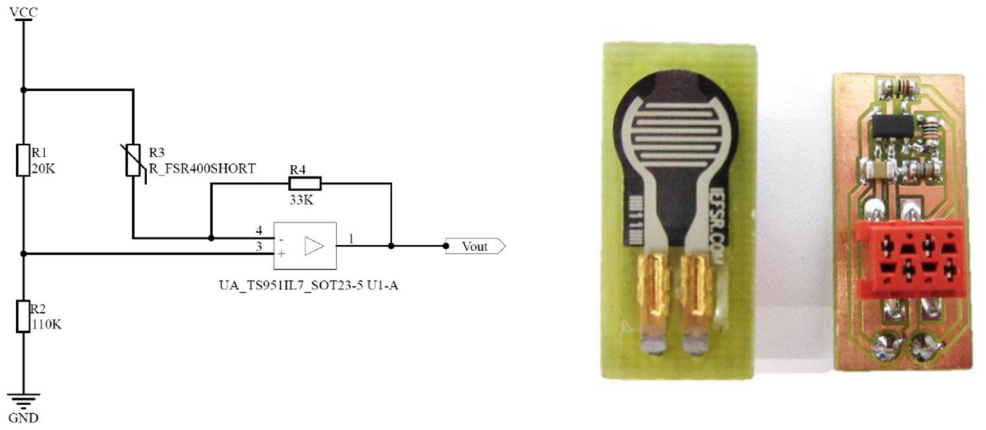

FIGURE 2 | (Left) The amplification circuit for the FSR. **(Right)** The FSR sensor's PCB.

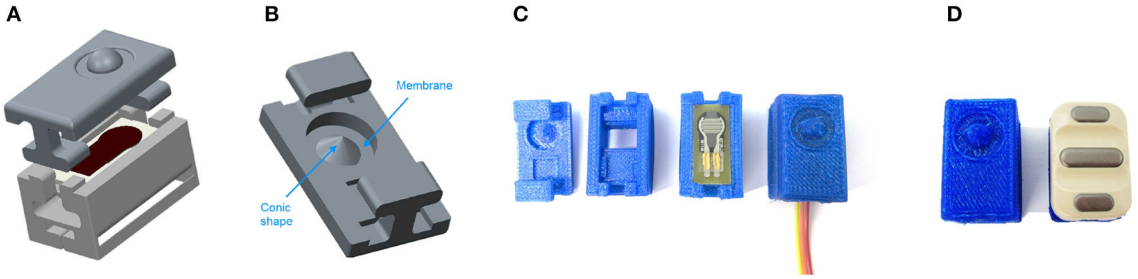

FIGURE 3 | (A) Exploded view of the 3D-model of the FSR housing. **(B)** 3D-model of the top part of the FSR housing, where the membrane and the conic shape are identified. **(C)** Assembly process of the housing and the FSR sensor. **(D)** Comparison between the final FSR sensor and the EMG sensor.

TABLE 1 | Characterization table for one FSR, including the FSR sensor, the amplifier board and the housing.

Applied force [N]	0.0	0.4	0.8	1.2	1.6	2.0	2.4	2.8	3.2	3.6	4.0	4.4	4.8	5.2
Output voltage	0.00	0.16	1.02	1.37	1.66	1.98	2.31	2.51	2.73	3.10	3.27	3.49	3.72	3.85

The standard deviation with respect to a linear fit is 6.9%. The provided values have been inverted by the zero-value offset voltage (4.2874V).

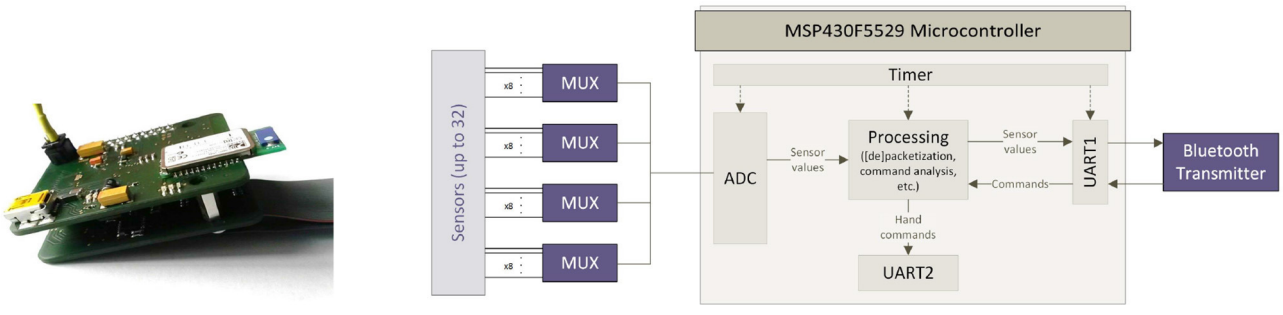

FIGURE 4 | The bluetooth analog-to-digital conversion board and its functional block representation.

bandwidth limited to 10 Hz, the provided sampling frequency is an overshoot (see e.g., Castellini and van der Smagt, 2009). The same argument obviously holds for the FMG signals (Ravindra and Castellini, 2014).

The board employs two UARTs, communicating in turn with the smartphone (via a serial-over-Bluetooth connection) and the prosthesis (in our case, via a simplified RS232 protocol). Hence, the board can also relay control commands to a hand

prosthesis. The final cost of the system is estimated to be below 150€.

2.1.3. Myocontrol Host

The wearable myocontrol system is completed by a standard commercial smartphone (Huawei *Honor 6* with a commercial value of about 300€), on which the data processing is performed. This device is equipped with a quad-core Cortex-A15 processor running at 1.7 GHz, 2 GB of RAM and a 3100 mAh Li-Po battery, claimed to keep the smartphone running for 2 full days at moderate usage. Its operating system is Android 4.4 KitKat. The smartphone weighs 132 g and easily fits in a pocket (7 × 0.8 × 14 cm) with its 5-inch display. A C# application similar to the one used in Strazzulla et al. (2016) was implemented, optimized and ported to the smartphone. The application enforces the following functionalities: (a) receiving and storing the data from the ADC board's serial-over-BT port; (b) displaying a visual stimulus, both on the smartphone screen and using the prosthesis; (c) building a prediction model for the control commands; and (d) sending them off to the prosthetic hand at a 10 Hz frequency, through the ADC board's serial-over-BT port. The machine learning method of choice was—coherent with our own previous work—Incremental Ridge Regression with Random Fourier Features (Gijsberts et al., 2014). As speculated in previous work and now proven, this method provides real-time capable non-linear multivariate regression while saving a lot of computational resources to the point that the maximum usage of the smartphone's CPU showed to be at 14%. Moreover, with the program running and the cell phone display activated and fully lighted, the battery endurance is at approximately 6 h, whereas an endurance of 11 h can be achieved with the display being switched off. For receiving the sample data and sending control commands to the prosthetic hand, the cell phone's internal Bluetooth peripheral has to be activated all the time.

2.2. Experiment Description

2.2.1. Subjects

Ten intact subjects, nine of which were right-handed (subject No. 9 being the left-handed one), joined the experiment (3 females and 7 males, 28 ± 7 years old, weighing 72.4 ± 9.91 kg, 177.8 ± 12.14 cm tall). Each subject received a thorough description of the experiment, both in oral and written form. Informed written consent was obtained from all participants. Experiments with sEMG and FMG were approved by the Ethical Committee of the DLR.

2.2.2. Experimental Protocol

The experiment consisted of performing ten times the following sequence of wrist and hand movements: (1) wrist flexion, (2) wrist extension, (3) wrist pronation, (4) wrist supination and (5) power grasp. To enforce the opening of the hand the relaxed stance was used, in order to mimic a more natural form of myocontrol. Each movement was visually stimulated on the screen of the smartphone (the name of the required motion would appear on the screen), while the experimenter was visually checking that the movement was actually being enforced, to ensure a correct execution. Each stimulation was administered as follows: the visual stimulus would appear for 2 s to allow the subject reach the full movement, then for 6 s data were captured representing the maximal activation for that particular movement ("activation phase": only this phase was considered in the offline analysis), then the stimulus would disappear for 2 s to allow the subject return to the resting position. The sequence was administered in the same order to all subjects. The choice of this set of movements was motivated by the well-known importance of controlling at least the wrist pronation/supination (see e.g., Jiang et al., 2012b) together with grasping; for instance, pronation and supination of the wrist are operated by deep muscles (Biryukova and Yourovskaya, 1994), meaning that they are usually hard to detect using sEMG. It is worth mentioning that, to the best of our knowledge, there is so far no commercially available 2-active-DOFs prosthetic wrist, but a few prototypes are being studied [see e.g., the device embedded in the DEKA arm, https://www.youtube.com/watch?v=KCUwoxuAdYQ, and the prototype by Ottobock which appears for instance in Amsuess et al. (2016)].

For this specific experiment, the sensors were separated in two different bracelets, the first one with ten sEMG sensors on the left forearm and the second one with ten FSR sensors on the right forearm. The bracelets were located approximately 10 cm below the subject's elbows. This further choice, rather than that of placing twenty sensors on one single forearm, was motivated by the relatively small space available on the forearm of some of the subjects, which would have potentially limited the adhesion of each sensor to the subjects' skin. (A similar problem was reported of, e.g., in Castellini and Ravindra, 2014). Of course, this diminishes the comparability of the results from the two sets of sensors, but myocontrol literature has already presented cases in which, for instance, training of a machine-learning-based method has been performed bilaterally, i.e., gathering data and training from the intact forearm and predicting using data from the impaired limb (Castellini et al., 2009; Nielsen et al., 2011). In both these works, no difference was reported in performance whether the forearm to be used was the dominant or non-dominant one.

During the whole experiment, the subjects sat in a relaxed position with their forearms over their thighs and the hands in a lateral position (with the palms looking toward each other); they were advised to perform each movement bilaterally (**Figure 5**). The recorded data kept trace of the FSR and sEMG signals as well as of a numerical identifier univocally representing the stimulated movement. This index was used as the ground truth during the supposed maximal activation of the muscles—an instance of *on-off goal-directed stimuli* as already used in, e.g., Sierra González and Castellini (2013).

2.2.3. Data Processing

The signals recorded during the experiment were stored to the smartphone's internal memory, then analyzed off-line. Low-pass filtering was applied to both signals (3rd order low-pass digital Butterworth filter with a cutoff frequency of 1 Hz) in order to remove high-frequency disturbances. This is a standard procedure in the field (see e.g., Atzori et al., 2014). For the data

FIGURE 5 | A bird's-eye view of the experiment.

processing and the subsequent statistical analysis, the following approaches have been chosen:

1) *Stability over time:* To investigate which type of signal has the most stability over time, the standard deviation of each signal was calculated and Student's paired-sample t-test was applied.
2) *Separability of clusters:* Stability of the signals during activation should somehow be reflected in the separability of patterns in the input space, resulting in, e.g., a better classification accuracy when a classification method is employed. Typically (see e.g., Bunderson and Kuiken, 2012), higher separability of clusters means better distinguishability by any pattern classification method and therefore higher stability of the related control. To check whether this was the case, for each subject in the experiment and each pair of clusters (C_i, C_j) we evaluated Fisher's Separateness Index (Fisher, 1936), defined as the maximum value over w of $J(w)$, where $J(w) = \frac{w^T S_B w}{w^T S_W w}$. Here S_B is the between-clusters scatter matrix, while S_W is the within-clusters scatter matrix. S_B is given by $S_B = (\mu_i - \mu_j)(\mu_i - \mu_j)^T$ where μ_i, μ_j are the means of clusters C_i, C_j, while $S_W = \sum_{n=i,j} \sum_{x \in clust_n} (x - \mu_n)(x - \mu_n)^T$, where x are the samples in each cluster. Each pairwise Fisher's index was averaged across all subjects and collected in a matrix $S = \{s_{ij}\}$.
3) *sEMG/FMG regression for myocontrol:* A comparative regression accuracy analysis was performed, in order to assess whether sEMG, FMG or their juxtaposition would be significantly better in the framework of wrist/hand prostheses control. The learning algorithm of choice was Incremental Ridge Regression with Random Fourier Features, already successfully used multiple times, e.g., in Gijsberts et al. (2014) and Ravindra and Castellini (2014). Ridge Regression builds a linear model $f(x) = w^T x$, where x denotes the sensor values, w is a weighting vector and $f(x)$ is the predicted output; Random Fourier Features further employ a non-linear mapping from the input space to a higher-, finite-dimensional feature space, where the linear regression is more likely to succeed. (For more details about this algorithm applied for hand prosthesis control, see Gijsberts et al. (2014)). Ten-fold "leave-one-repetition-out" cross-validation was applied by training each machine on nine of the ten repetitions and testing on the remaining one. The input space was chosen to be either the FMG values, the sEMG values, or their combination, meaning that the FMG and sEMG samples were simply stacked in a 20-dimensional vector and used with the same learning method. The prediction accuracy was measured using the normalized Root Mean-Squared-Error (nRMSE) between the predicted values and the stimulus values. A one-way ANOVA test was performed to investigate whether there was a statistically significant difference in between the three inputs.

2.2.4. Satisfaction Surveys

Additionally, at the end of the experiment, three surveys were administered to each subject, in order to complete the envisaged system assessment with respect to its usability: the System Usability Scale (SUS) (Brooke, 1996), the NASA Task Load Index (NASA, 1986) and a reworking of the Microsoft Desirability Toolkit by Travis (2008). The SUS consists of ten questions (**Table 2**) with answers represented on a 5 point Likert scale (1 - *strongly disagree* to 5 - *strongly agree*). The scoring in this survey is such that the answers to the *strongly agree* positive questions and to the *strongly disagree* negative questions generate a higher impact over the final score. The NASA Task Load Index provides an overall workload score on six subscales: Mental, Physical and Temporal Demands; Own Performance, Effort and Frustration. For each subscale, the answer could be in a range of 21 points, reaching from *very low* to *very high* (**Table 2**).

Lastly, Travis's survey consists in a series of "reaction cards" with adjectives that could be applied to the system to be tested; the user is asked to select the five cards that most closely match their personal reactions to the system. For the experiment, we used a list of 75 adjectives instead of the cards (most of them based on Travis's questionnaire), then the subject was asked to choose all adjectives he or she felt more related with the device. After that, in a more precise selection, the user had to choose only the 5 most important words and try to give a simple reason about his or her decision.

3. EXPERIMENTAL RESULTS

3.1. Stability Over Time

Figure 6 shows typical FMG and sEMG signals obtained while a subject was performing two repetitions of the five instructed movements (plus the resting state). Due to the carefully chosen amplification/filtering stages of the sensors themselves, the amplitude of the signals obtained from both FMG and sEMG sensors are comparable, and each single produced movement appears as a distinct pattern, well separated in time from the next one as well as from the 2-s intervals allowed for resting and for preparing the next movement. Such behavior is clear, e.g., during the wrist-flexion movement enforced from 60 to 70 s in the Figure (second red bar just above the x-axis).

Visual inspection seems to indicate that FMG signals are more stable over time *while the subjects are holding the position* than sEMG signals: this is apparent by looking at the "plateaus" created

TABLE 2 | The statements found in the SUS and NASA TLX surveys.

SUS SURVEY
I felt comfortable with the device.
I found the device unnecessarily complex.
I thought the device was easy to use.
I think that I would need the support of a technical person to be able to use this device.
I found the various functions in this system were well integrated.
I thought there was too much inconsistency in this device.
I would imagine that most users would learn to use this device very quickly.
I found the device very cumbersome to use.
I felt very confident using the device.
I needed to learn a lot of things before I could get going with this device.
NASA TLX SURVEY
How mentally demanding was the task?
How physically demanding was the task?
How hurried or rushed was the pace of the task?
How successful were you in accomplishing what you were asked to do?
How hard did you have to work to accomplish your level of performance?
How insecure, discouraged, irritated, stressed, and annoyed were you?

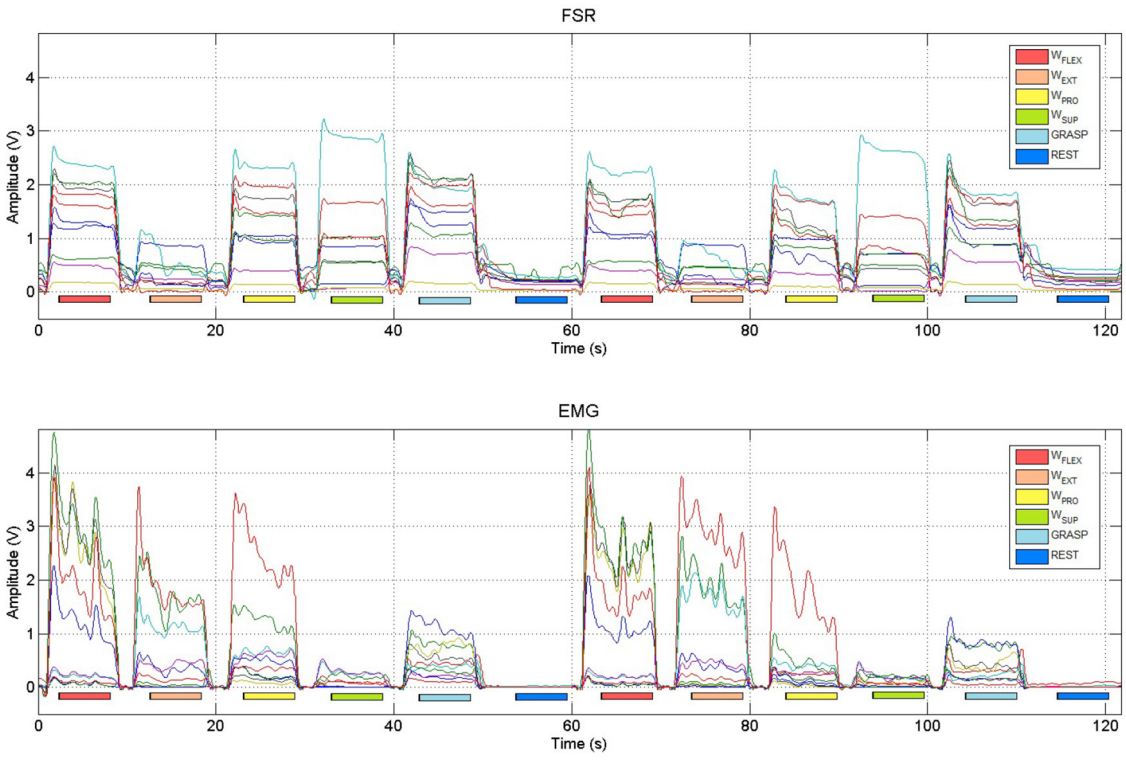

FIGURE 6 | Typical FSR and sEMG signals obtained from two repetitions of the instructed hand and wrist movements (wrist flexion, wrist extension, wrist pronation, wrist supination, power grasp and rest). Colored bars denote the activation phases, during which data were collected to represent the maximal activation of the stimulated movement.

by the FSRs while each movement was enforced; as opposed to that, sEMG signals exhibit the typical oscillating down-ramp pattern due to muscular motor-unit recruitment (Merletti et al., 2011a,b). To verify that this is the case in general, we evaluated the standard deviation of the FMG and sEMG signals obtained by each subject while performing the first three repetitions of the wrist flexion movement considering the signals during the activation phases only. (Only the three sensors for each set

that exhibited the highest amplitude were taken into account.) Considering **Table 3**, sEMG signals actually exhibit a significantly higher standard deviation when compared to FMG signals (mean values 0.0087 and 0.0025 in turn, Student's paired-sample t-test $p < 0.01$).

3.2. Separability of Clusters

Figure 7 shows typical FMG and sEMG data reduced to three dimensions via Principal Component Analysis (PCA) and colored according to each movement for the cluster separability analysis carried out for both input spaces. In the figure, sEMG clusters appear more stretched than FMG clusters, a behavior very likely due to the above-mentioned oscillations while a movement is being held.

Figure 8 shows the matrices for sEMG and FMG, while **Table 4** lists the means of Fisher's Indexes for each subject (the diagonal-zero values are not considered to evaluate the mean values). The Fisher's Index of FMG is higher (therefore better) than that of sEMG (mean values 368.82 and 94.1) with high statistical significance (Student's paired-sample t-test $p < 0.001$).

3.3. sEMG/FMG Regression for Mycontrol

Table 5 shows the prediction accuracy obtained by each subject on one movement repetition (the nRMSE value showed is a mean of all the nRMSE obtained by the cross-validation). **Figure 9** shows the nRMSE values for all subjects. While the nRMSE values range from 0.13 to 0.21, in line with previous literature (Ravindra

TABLE 3 | Standard deviation of FMG and sEMG sensor signals obtained by each subject during the first three repetitions of the wrist flexion movement.

Subject #	1	2	3	4	5	6	7	8	9	10	Mean
FMG	0.0018	0.0026	0.0006	0.0030	0.0033	0.0042	0.0018	0.0016	0.0028	0.0031	0.0025
sEMG	0.0202	0.0111	0.0019	0.0038	0.0144	0.0082	0.0037	0.0065	0.0082	0.0091	0.0087

Considering the three sensors that exhibited the highest signal amplitude.

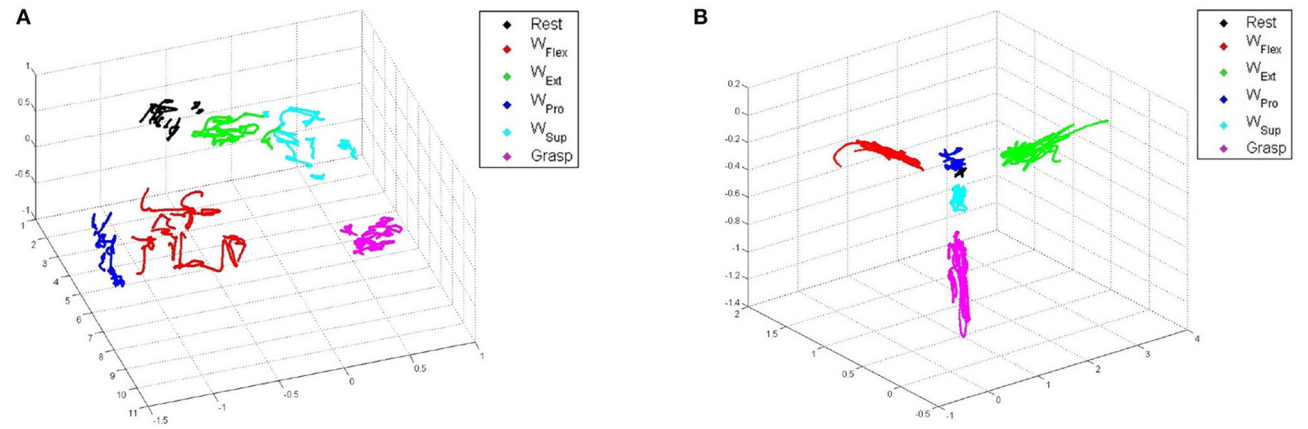

FIGURE 7 | 3D-reduced PCA projections of typical data for each type of sensor, colored according to the stimulated movements. (A) FMG. **(B)** sEMG.

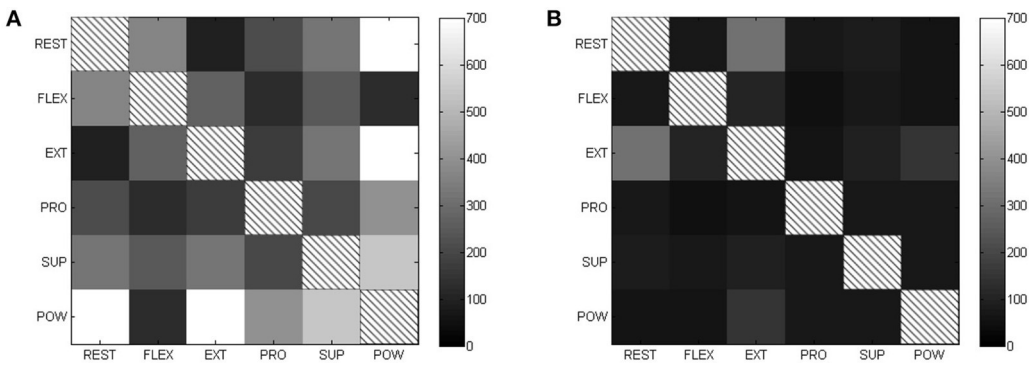

FIGURE 8 | Fisher's Index matrices for each type of sensor (higher is better). (A) FSR Fisher's index. **(B)** EMG Fisher's index.

TABLE 4 | Mean Fisher's Index values for each subject and type of sensors.

Subject #	1	2	3	4	5	6	7	8	9	10	Mean
Fisher's Index, FMG	291.08 ± 227.9	616.47 ± 893.5	340.22 ± 259.7	108.11 ± 50	157.50 ± 72.8	391.26 ± 527.2	432.3 ± 342.2	513.18 ± 453.9	455.85 ± 532.4	382.21 ± 722.2	368.82 ± 154.2
Fisher's Index, sEMG	87 ± 74.3	69.46 ± 45.2	71.24 ± 23.6	38.03 ± 16.9	208.34 ± 279.3	67.78 ± 23.3	66.12 ± 46.2	25.69 ± 11.3	239.38 ± 387.1	67.93 ± 39.1	94.1 ± 71

TABLE 5 | Prediction accuracy (nRMSE) obtained by Incremental Ridge Regression with Random Fourier Features when trained on FMG, sEMG and combined values.

Subject #	1	2	3	4	5	6	7	8	9	10
FMG	0.17 ± 0.016	0.1687 ± 0.0173	0.1495 ± 0.007	0.1636 ± 0.011	0.1762 ± 0.0087	0.173 ± 0.0184	0.1728 ± 0.0121	0.1893 ± 0.0352	0.1548 ± 0.0133	0.1803 ± 0.0222
sEMG	0.1494 ± 0.0138	0.1573 ± 0.0175	0.1458 ± 0.0123	0.2056 ± 0.047	0.1673 ± 0.0098	0.1857 ± 0.0126	0.1736 ± 0.0193	0.2037 ± 0.0343	0.1346 ± 0.0061	0.1801 ± 0.045
Comb.	0.1649 ± 0.0137	0.1608 ± 0.0199	0.1385 ± 0.0083	0.1595 ± 0.0161	0.1636 ± 0.0066	0.1658 ± 0.0139	0.1736 ± 0.0139	0.2054 ± 0.0267	0.1367 ± 0.0048	0.1526 ± 0.013

and Castellini, 2014), no statistically significant difference in accuracy is apparent (one-way ANOVA $p > 0.05$).

3.4. User Satisfaction

For the SUS, the total result of each subject and the mean score are presented in **Table 6**. Notice that the higher the score, the more usable the user judged the device. In this survey, the statements that had the worst scores were "I think that I would need the support of a technical person to be able to use this device" and "I felt very confident using the device."

For the NASA TLX, the total result for each subscale of each subject and overall workload are shown in **Table 7**. Here the highest the score, the more workload the user had, when using the device. A plot with average percentages of the workload by subscale is visible in **Figure 10**.

The first two surveys applied comprised suitable results with a usability score of almost 85% and an overall workload of 25%.

Finally, for the desirability survey proposed by Travis, two kinds of results were obtained, the first one using all the words chosen by the user in the first selection, and the second one considering only the 5 final selections. In order to have a different visualization, two word clouds have been created (**Figure 11**), where the bigger and darker the font is, the more often the word was selected.

Considering only the most common adjectives in the final selection, the device can be considered *Simple*, *Intuitive*, *Easy to use*, *Familiar*, *Reliable* and *Stable*. An important thing to mention about this last survey is that even though the instructions and the questions were oriented toward the device, some answers referred to the experiment performance. For instance, the adjective *familiar* was chosen in some cases because the subject had already performed other experiments with EMG sensors before taking part in this specific experiment.

To highlight the results of the user satisfaction surveys, a radial chart (**Figure 12**) was built, which separates the results in different categories (Low Workload Demand, Stability, Task Accomplishment, Interface, Easy to Use, Comfort and Setup) and represents the main features appreciated by the user. The figure for Low Workload Demand has been inverted on the scale to achieve better comparability with the other figures (i.e., Workload Demand is positively rated if being low). All of these categories can furthermore be separated in two kinds of classes: usability related features (Interface, Easy to Use, Comfort and Setup) and performance related features (Workload Demand, Stability and Task Accomplishment).

4. DISCUSSION

This work had two main aims: to assess whether a wearable combined sEMG/FMG device would be accepted by human subjects using it, and to determine whether significant qualitative and quantitative differences could be observed between sEMG and FMG signals obtained during a simple experiment aimed at myocontrol.

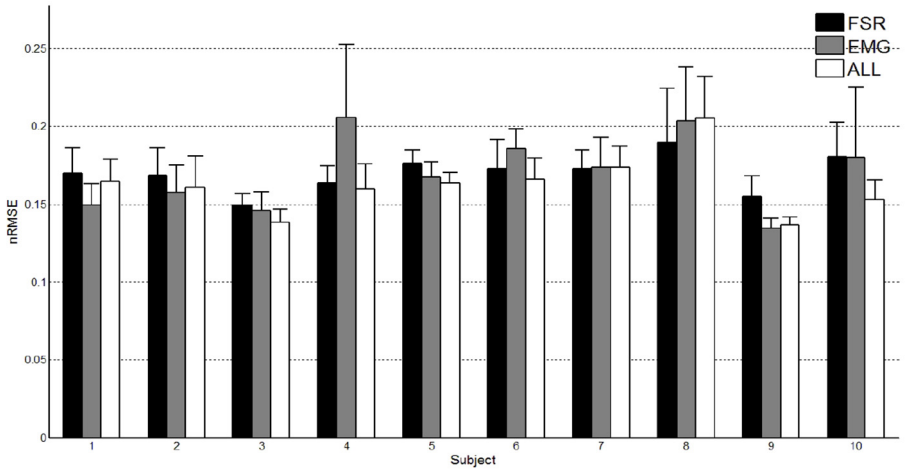

FIGURE 9 | Prediction accuracy obtained by FMG, sEMG and their combination.

TABLE 6 | Subject's system usability total scores.

ID	1	2	3	4	5	6	7	8	9	10	Mean
SUS	85	90	100	77.5	92.5	67.5	75	85	100	75	84.75

TABLE 7 | NASA TLX workload percentages.

ID	1	2	3	4	5	6	7	8	9	10	Mean
Mental demand	66.66	19.04	9.52	14.28	23.8	28.57	9.52	14.28	4.76	9.52	20
Physical demand	33.33	23.8	14.28	14.28	23.8	23.8	9.52	14.28	4.76	76.19	23.8
Temporal demand	71.42	61.9	52.38	14.28	52.38	57.14	14.28	61.9	4.76	33.33	42.38
Performance	28.57	28.57	19.04	14.28	14.28	19.04	52.38	14.28	4.76	38.09	23.33
Effort	52.38	19.04	23.8	9.52	52.38	19.04	52.38	14.28	4.76	38.09	28.57
Frustration	19.04	14.28	4.76	19.04	23.8	9.52	9.52	9.52	4.76	14.28	12.85
Overall WL	45.2381	27.77	20.63	14.28	31.74	26.19	24.6	21.42	4.76	34.92	25.15

(Subject #9 actually gave a uniform scoring.)

4.1. Acceptance of the Device

Consider Section 3.4, in particular **Figure 12**. The results clearly show that the device, together with its user interface, posed no problems to the subjects using it, and even had some appeal. Even though the subjects involved in the experiment are not part of the potential user population (i.e., amputated subjects controlling a self-powered prosthesis), their opinions and impressions about the device are helpful for future improvements and corrections. The subjects uniformly reported that the device felt reliable and stable; that the setup was easy to use, simple and comfortable, with a low frustration rate; that the user interface was friendly, intuitive and well structured; and that the data acquisition still required a considerable amount of time (this aspect having the highest workload demand).

The keywords obtained in Travis's survey, the workloads obtained in the NASA TLX survey, and the successful performance reflected in the SUS test, already give hints about the usage risk of a possible future medical device. Of course, this cannot replace a thorough risk analysis and a widespread usability study. Furthermore, it must be remarked that the positive results obtained in the surveys could have been influenced by the subjects' behaviors themselves, as explained by Travis. All in all, it is worthwhile to stress that no online experiment was performed in this study, therefore, from the user survey results, we can provide no conclusive results about either the performance of this device in general, or the usefulness of a combined sEMG/FMG approach in myocontrol.

4.2. Comparison of sEMG and FMG

In previous literature (Yungher et al., 2011; Ravindra and Castellini, 2014) it has been shown that FMG shows higher *overall* stability over time than sEMG, meaning that, e.g., the variance of its signals is lower than that of sEMG, while human subjects are engaged in repetitive, fatiguing tasks. This is probably due to the lower influence that muscle fatigue has on FMG signals, due to its nature. Now, from the qualitative/quantitative comparison

of sEMG and FMG carried out in Sections 3.1 and 3.2, two statistically significant differences between the two approaches emerge, namely (a) that FMG signals are more stable over time *during single movements too*, and (b) that they generate better separated patterns in the input space. Most likely, (b) is a consequence of (a); we speculate that this difference might arise from the very nature of the sEMG signals, which exhibit noise due to the recruitment of motor units while keeping an isometric hand/wrist posture. Of course, FMG would not be affected by this problem. All things considered, it seems reasonable to claim that FMG signals are more stable than sEMG ones.

About pattern separateness: if a classification approach were to be used to enforce myocontrol using such signals, better pattern separability would definitely represent a further advantage of FMG with respect to sEMG; in the case of simultaneous and proportional control, however, it is not clear whether this is an advantage or not. This kind of control requires some way to understand not only what pattern the subject desires, but also how much force/torque is involved; distant and smaller clusters for the maximal activations might contain less information about this specific feature. In our case, the regression method used in Section 3.3 is trained on maximal and minimal activation signals only, whereas it predicts the intermediate activation values by non-linear interpolation. We are in no position at this time, to claim that FMG or sEMG is better in this case (and this is reflected in the non-stastically-significant accuracy results obtained by such method, see **Table 5** again).

On a more qualitative side, we note that FMG, at least enforced using this cheap approach (that is, Force-Sensing Resistors), presents the drawback of being affected by hysteresis. Although the return to the resting state is apparent, this induces the FMG signals even to rise during the resting states, but not to come back exactly to zero or the previously measured resting states after a movement is performed. As opposed to this, sEMG signals remain almost at zero even when the user is not in the same initial position; this seems reasonable, since the resting phase involves no muscle activation. This problem can be countered by employing a smarter technique to gather FMG signals, for instance the capacitive approach, or (high-density) tactile sensing. Also, a fully-fledged, online FMG approach will need to take into account the inevitable artifacts generated by the

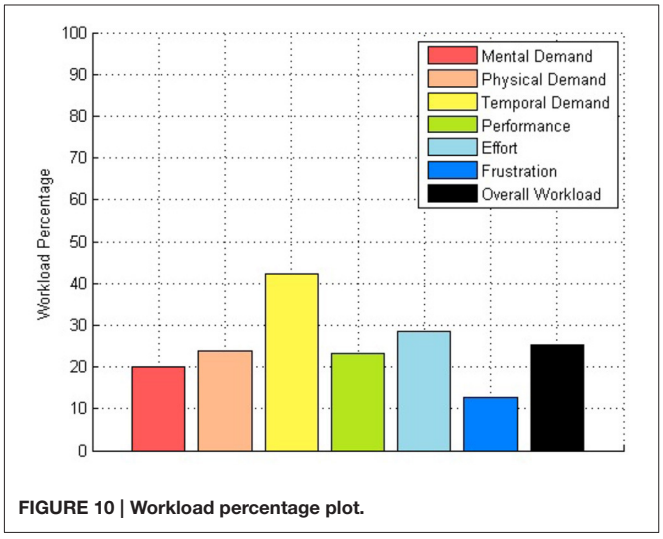

FIGURE 10 | Workload percentage plot.

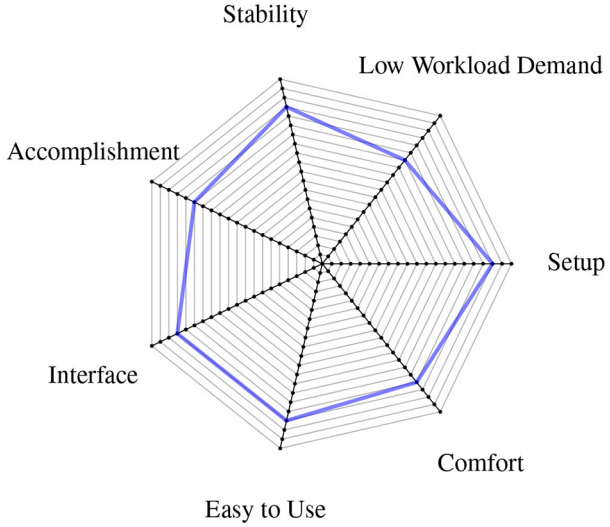

FIGURE 12 | Radial chart showing the user satisfaction surveys' results summarized in different device features.

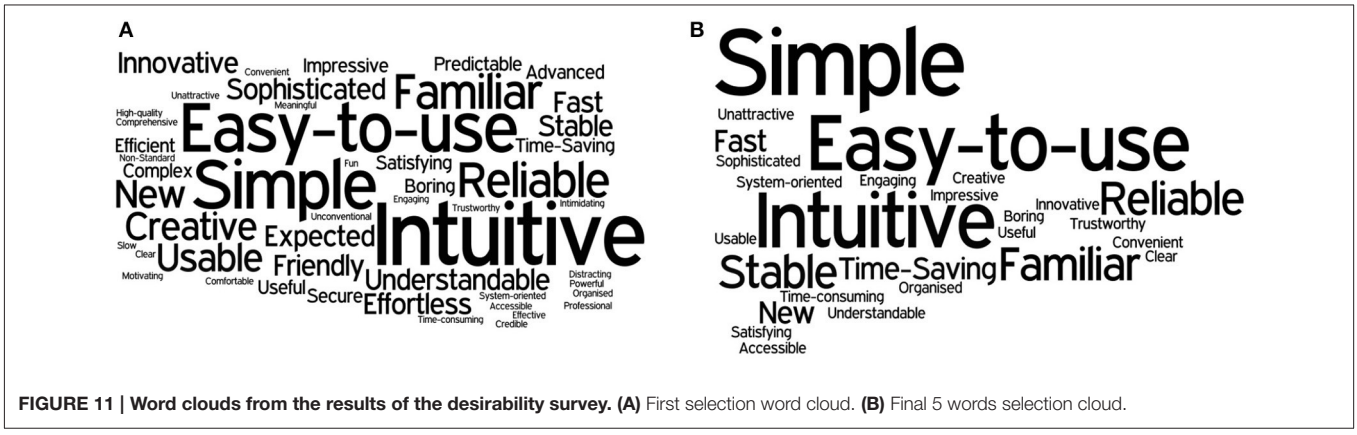

FIGURE 11 | Word clouds from the results of the desirability survey. (A) First selection word cloud. **(B)** Final 5 words selection cloud.

arm/forearm movement (i.e., accelerations inducing pressure on the sensors) and those induced by touching the socket, bumping into objects, laying the stump on a table, etc.

What we can conclude, we believe beyond any reasonable doubt, is that sEMG and FMG can be miniaturized and employed in such a framework, and that they carry different kinds of information, leading to different behaviors and signal features. We speculate that a structured sensor-fusion approach (that is, deeper than simply stacking the signals as we have done in this work) might lead to a better exploitation of each modality's characteristics.

One last remark is in order about the cost of each approach. Apparently, FMG is up to two orders of magnitude cheaper than sEMG, but this is mainly due at this stage to (a) it being enforced through Force-Sensing Resistors, which might not live up to the expectations as previously remarked; and (b) the necessity, in the very end, to produce a *medically certified* FMG approach and device, which might dramatically raise its costs. Again, we believe that an *integrated* approach is the way ahead to improve myocontrol using this still novel technique alongside sEMG. To this aim, the assessment of the wearable sEMG/FMG device we carried out is promising, as it shows that at least the required electronic machinery can be embedded in an effective, light and acceptable device.

4.3. Conclusions and Future Work

In this article, we have described a wearable, integrated sEMG/FMG system, targeting myocontrol and human intent detection. The experiment we conducted endorses the system's high degree of usability, indicating that it has the potential to become an integrated medical product. Still, the autonomous mobility of about 11 h is restricted by the cell phone battery, thus recharging strategies during the patient's daily use or the deployment of a secondary device could be a solution for now. In near future, the development of a highly integrated, low energy system, where the phone serves only for teaching and displaying information, seems to be advisable. Additionally, we explored the application of FMG as a potential complement to sEMG and provided evidence that the two techniques can be integrated, but that a smart sensor fusion approach might be required to obtain the best results. Results from user satisfaction surveys presented in the paper give strong indication for the setup to be on the right track. In the near future, more experiments are planned to check the feasibility of mixed sEMG/FMG for online myocontrol, possibly down to the level of individual finger movements, and immersed in daily-life activities.

AUTHOR CONTRIBUTIONS

System Design BV, MC, CC; Software Design MC, BV; Test setup and conduction of user Surveys ER, MC, CC; Analysis and Interpretation of data ER, CC; Drafting of manuscript MC, ER, BV; Internal Revision BV, CC; Critical Revision BV, CC, MC, ER; Final Approval MC, ER, BV, CC; Agreement on accountability by MC, ER, BC, CC.

ACKNOWLEDGMENTS

The authors thank Mr. Miguel Neves of the DLR for designing and building the housings of the sensors. This work was partially supported by the DFG project "TACT_HAND: Improving control of prosthetic hands using tactile sensors and realistic machine learning" (Sachbeihilfe CA1389/1-1).

REFERENCES

Amsuess, S., Vujaklija, I., Goebel, P., Roche, A. D., Graimann, B., Aszmann, O. C., et al. (2016). Context-dependent upper limb prosthesis control for natural and robust use. *IEEE Trans. Neural Syst. Rehabil. Eng.* 24, 744–753. doi: 10.1109/TNSRE.2015.2454240

Arjunan, S. P., and Kumar, D. K. (2010). Decoding subtle forearm flexions using fractal features of surface electromyogram from single and multiple sensors. *J. Neuroeng. Rehabil.* 7:53. doi: 10.1186/1743-0003-7-53

Atzori, M., Gijsberts, A., Castellini, C., Caputo, B., Mittaz Hager, A.-G., Elsig, S., et al. (2014). Electromyography data for non-invasive naturally-controlled robotic hand prostheses. *Sci. Data* 1:140053. doi: 10.1038/sdata.2014.53

Baspinar, U., Varol, H. S., and Senyurek, V. Y. (2013). Performance comparison of artificial neural network and Gaussian mixture model in classifying hand motions by using sEMG signals. *Biocybern. Biomed. Eng.* 33, 33–45. doi: 10.1016/S0208-5216(13)70054-8

Biddiss, E., and Chau, T. (2007). Upper-limb prosthetics: critical factors in device abandonment. *Am. J. Phys. Med. Rehabil.* 86, 977–987. doi: 10.1097/PHM.0b013e3181587f6c

Brooke, J. (1996). "SUS: A "quick and dirty" usability scale," in *Usability Evaluation in Industry*, eds P. W. Jordan, B. Thomas, B. A. Weerdmeester, and A. L. McClelland (London: Taylor & Francis), 189–194.

Brunelli, D., Tadesse, A. M., Vodermayer, B., Nowak, M., and Castellini, C. (2015). "Low-cost wearable multichannel surface EMG acquisition for prosthetic hand control," in *2015 6th International Workshop on Advances in Sensors and Interfaces (IWASI)* (Gallipoli: IEEE), 94–99. doi: 10.1109/IWASI.2015.7184964

Bunderson, N. E., and Kuiken, T. A. (2012). Quantification of feature space changes with experience during electromyogram pattern recognition control. *IEEE Trans. Neural Syst. Rehabil. Eng.* 20, 239–246. doi: 10.1109/TNSRE.2011.2182525

Castellini, C., Artemiadis, P., Wininger, M., Ajoudani, A., Alimusaj, M., Bicchi, A., et al. (2014). Proceedings of the first workshop on peripheral machine interfaces: going beyond traditional surface electromyography. *Front. Neurorobot.* 8:22. doi: 10.3389/fnbot.2014.00022

Castellini, C., Gruppioni, E., Davalli, A., and Sandini, G. (2009). Fine detection of grasp force and posture by amputees via surface electromyography. *J. Physiol. (Paris)* 103, 255–262. doi: 10.1016/j.jphysparis.2009.08.008

Castellini, C., and Ravindra, V. (2014). "A wearable low-cost device based upon force-sensing resistors to detect single-finger forces," in *5th IEEE RAS/EMBS International Conference on Biomedical Robotics and Biomechatronics* (São Paulo: IEEE), 199–203. doi: 10.1109/BIOROB.2014.6913776

Castellini, C., and van der Smagt, P. (2009). Surface EMG in advanced hand prosthetics. *Biol. Cybern.* 100, 35–47. doi: 10.1007/s00422-008-0278-1

Castellini, C., and van der Smagt, P. (2013). Evidence of muscle synergies during human grasping. *Biol. Cybern.* 107, 233–245. doi: 10.1007/s00422-013-0548-4

Cho, E., Chen, R., Merhi, L.-K., Xiao, Z., Pousett, B., and Menon, C. (2016). Force myography to control robotic upper extremity prostheses: a feasibility study. *Front. Bioeng. Biotechnol.* 4:18. doi: 10.3389/fbioe.2016.00018

Cipriani, C., Antfolk, C., Controzzi, M., Lundborg, G., Rosen, B., Carrozza, M., et al. (2011a). Online myoelectric control of a dexterous hand prosthesis by

transradial amputees. *IEEE Trans. Neural Syst. Rehabil. Eng.* 19, 260–270. doi: 10.1109/TNSRE.2011.2108667

Cipriani, C., Sassu, R., Controzzi, M., Kanitz, G., and Carrozza, M. C. (2011b). "Preliminary study on the influence of inertia and weight of the prosthesis on the EMG pattern recognition robustness," in *Proceedings of the 2011 MyoElectric Controls/Powered Prosthetics Symposium* (Fredericton, NB).

Cram, J., and Kasman, G. (2010). "The basics of surface electromyography," in *Cram's Introduction To Surface Electromyography*, 2nd Edn., ed E. Criswell (Sudbury, MA: Jones and Bartlett Publishers), 1–163.

Fang, Y., Hettiarachchi, N., Zhou, D., and Liu, H. (2015). Multi-modal sensing techniques for interfacing hand prostheses: a review. *IEEE Sens. J.* 15, 6065–6076. doi: 10.1109/JSEN.2015.2450211

Fisher, R. A. (1936). The use of multiple measurements in taxonomic problems. *Ann. Eugen.* 7, 179–188. doi: 10.1111/j.1469-1809.1936.tb02137.x

Fougner, A., Scheme, E., Chan, A. D. C., Englehart, K., and Stavdahl, O. (2011). Resolving the limb position effect in myoelectric pattern recognition. *IEEE Trans. Neural Syst. Rehabil. Eng.* 19, 644–651. doi: 10.1109/TNSRE.2011.2163529

Gijsberts, A., Bohra, R., Sierra González, D., Werner, A., Nowak, M., Caputo, B., et al. (2014). Stable myoelectric control of a hand prosthesis using non-linear incremental learning. *Front. Neurorobot.* 8:8. doi: 10.3389/fnbot.2014.00008

Biryukova, E. V., and Yourovskaya, V. Z. (1994). "A model of human hand dynamics," in *Advances in the Biomechanics of the Hand and Wrist.* Vol. 256, eds F. Schuind, K. N. An, W. P. Cooney III, and M. Garcia-Elias (Springer), 107–122.

Herrmann, S., and Buchenrieder, K. (2010). "Fusion of myoelectric and near-infrared signals for prostheses control," in *Proceedings of the 4th International Convention on Rehabilitation Engineering & Assistive Technology, (Singapore Therapeutic, Assistive and Rehabilitative Technologies (START) Centre), iCREATe '10* (Shanghai), 54:1–54:4.

Interlink Electronics (2014). *FSR Integration Guide*. Available online at: http://www.interlinkelectronics.com/FSR400short.php [Online]. (Accessed February 15, 2016).

Jiang, N., Dosen, S., Müller, K.-R., and Farina, D. (2012a). Myoelectric control of artificial limbs - is there a need to change focus? *IEEE Signal Process. Magazine* 29, 148–152.

Jiang, N., Vest-Nielsen, J., Muceli, S., and Farina, D. (2012b). EMG-based simultaneous and proportional estimation of wrist/hand kinematics in uni-lateral trans-radial amputees. *J. Neuroeng. Rehabil.* 9:42. doi: 10.1186/1743-0003-9-42

Khushaba, R. N., Al-Jumaily, A., and Al-Ani, A. (2009). Evolutionary fuzzy discriminant analysis feature projection technique in myoelectric control. *Patt. Recogn. Lett.* 30, 699–707. doi: 10.1016/j.patrec.2009.02.004

Lobo-Prat, J., Kooren, P. N., Stienen, A. H., Herder, J. L., Koopman, B. F., and Veltink, P. H. (2014). Non-invasive control interfaces for intention detection in active movement-assistive devices. *J. Neuroeng. Rehabil.* 11:168. doi: 10.1186/1743-0003-11-168

Merletti, R., Aventaggiato, M., Botter, A., Holobar, A., Marateb, H., and Vieira, T. (2011a). Advances in surface EMG: recent progress in detection and processing techniques. *Crit. Rev. Biomed. Eng.* 38, 305–345. doi: 10.1615/CritRevBiomedEng.v38.i4.10

Merletti, R., Botter, A., Cescon, C., Minetto, M., and Vieira, T. (2011b). Advances in surface EMG: recent progress in clinical research applications. *Crit. Rev. Biomed. Eng.* 38, 347–379. doi: 10.1615/CritRevBiomedEng.v38.i4.20

NASA (1986). *NASA TASK LOAD INDEX (TLX) v 1.0 Paper and Pencil Package*. Moffett Field, CA: Human Performance Research Group, NASA Ames Research Center.

Nielsen, J. L., Holmgaard, S., Jiang, N., Englehart, K. B., Farina, D., and Parker, P. A. (2011). Simultaneous and proportional force estimation for multifunction myoelectric prostheses using mirrored bilateral training. *IEEE Trans. Biomed. Eng.* 58, 681–688. doi: 10.1109/TBME.2010.2068298

Oskoei, M. A., and Hu, H. (2007). Myoelectric control systems—a survey. *Biomed. Signal Proc. Control* 2, 275–294. doi: 10.1016/j.bspc.2007.07.009

Peerdeman, B., Boere, D., Witteveen, H., in't Veld, R. H., Hermens, H., Stramigioli, S., et al. (2011). Myoelectric forearm prostheses: state of the art from a user-centered perspective. *J. Rehabil. Res. Dev.* 48, 719–738. doi: 10.1682/JRRD.2010.08.0161

Phillips, S. L., and Craelius, W. (2005). Residual kinetic imaging: a versatile interface for prosthetic control. *Robotica* 23, 277–282. doi: 10.1017/S0263574704001298

Ravindra, V., and Castellini, C. (2014). A comparative analysis of three non-invasive human-machine interfaces for the disabled. *Front. Neurorobot.* 8:24. doi: 10.3389/fnbot.2014.00024

Rossini, L., and Rossini, P. M. (2010). "Combining ENG and EEG integrated analysis for better sensitivity and specificity of neuroprosthesis operations," in *2010 Annual International Conference of the IEEE Engineering in Medicine and Biology* (Buenos Aires: IEEE), 134–137. doi: 10.1109/IEMBS.2010.5627402

Scheme, E., Fougner, A., Stavdahl, Ø., Chan, A. D. C., and Englehart, K. (2010). "Examining the adverse effects of limb position on pattern recognition based myoelectric control," in *2010 Annual International Conference of the IEEE Engineering in Medicine and Biology* (Buenos Aires: IEEE), 6337–6340. doi: 10.1109/IEMBS.2010.5627638

Sebelius, F. C. P., Rosén, B. N., and Lundborg, G. N. (2005). Refined myoelectric control in below-elbow amputees using artificial neural networks and a data glove. *J. Hand Surg.* 30A, 780–789. doi: 10.1016/j.jhsa.2005.01.002

Sierra González, D., and Castellini, C. (2013). A realistic implementation of ultrasound imaging as a human-machine interface for upper-limb amputees. *Front. Neurorobot.* 7:17. doi: 10.3389/fnbot.2013.00017

Strazzulla, I., Nowak, M., Controzzi, M., Cipriani, C., and Castellini, C. (2016). Online bimanual manipulation using surface electromyography and incremental learning. *IEEE Trans. Neural Syst. Rehabil. Eng.* doi: 10.1109/TNSRE.2016.2554884. [Epub ahead of print].

Tenore, F., Ramos, A., Fahmy, A., Acharya, S., Etienne-Cummings, R., and Thakor, N. V. (2007). "Towards the control of individual fingers of a prosthetic hand using surface EMG signals," in *Proceedings of the 29th Annual International Conference of the IEEE EMBS* (Lyon), 6146–6149.

Travis, D. (2008). *Measuring Satisfaction: Beyond the Usability Questionnaire*. Available online at: http://www.userfocus.co.uk/articles/satisfaction.html [Online]. (Accessed June 10, 2016).

Wininger, M., Kim, N. H., and Craelius, W. (2008). Pressure signature of forearm as predictor of grip force. *J. Rehabil. Res. Dev.* 45, 883–892. doi: 10.1682/JRRD.2007.11.0187

Yang, D., Jiang, L., Huang, Q., Liu, R., and Liu, H. (2014). Experimental study of an EMG-controlled 5-dof anthropomorphic prosthetic hand for motion restoration. *J. Intell. Robot. Syst.* 76, 427–441. doi: 10.1007/s10846-014-0037-6

Young, A. J., Hargrove, L. J., and Kuiken, T. A. (2012). Improving myoelectric pattern recognition robustness to electrode shift by changing interelectrode distance and electrode configuration. *IEEE Trans. Biomed. Eng.* 59, 645–652. doi: 10.1109/TBME.2011.2177662

Yungher, D., Wininger, M., Baar, W., Craelius, W., and Threlkeld, A. (2011). Surface muscle pressure as a means of active and passive behavior of muscles during gait. *Med. Eng. Phys.* 33, 464–471. doi: 10.1016/j.medengphy.2010.11.012

Conflict of Interest Statement: The authors declare that the research was conducted in the absence of any commercial or financial relationships that could be construed as a potential conflict of interest.

A.2 "Online Natural Myocontrol of Combined Hand and Wrist Actions Using Tactile Myography and the Biomechanics of Grasping"

Authors Mathilde Connan, Risto Kõiva and Claudio Castellini

Journal Frontiers in Neurorobotics

Year 2020

Number of pages 16

Review Peer-reviewed

Abstract *Objective:* Despite numerous recent advances in the field of rehabilitation robotics, simultaneous, and proportional control of hand and/or wrist prostheses is still unsolved. In this work we concentrate on myocontrol of combined actions, for instance power grasping while rotating the wrist, by only using training data gathered from single actions. This is highly desirable since gathering data for all possible combined actions would be unfeasibly long and demanding for the amputee. *Approach:* We first investigated physiologically feasible limits for muscle activation during combined actions. Using these limits we involved 12 intact participants and one amputee in a Target Achievement Control test, showing that tactile myography, i.e., high-density force myography, solves the problem of combined actions to a remarkable extent using simple linear regression. Since real-time usage of many sensors can be computationally demanding, we compare this approach with another one using a reduced feature set. These reduced features are obtained using a fast, spatial first-order approximation of the sensor values. *Main results:* By using the training data of single actions only, i.e., power grasp or wrist movements, subjects achieved an average success rate of 70.0% in the target achievement test using ridge regression. When combining wrist actions, e.g., pronating and flexing the wrist simultaneously, similar results were obtained with an average of 68.1%. If a power grasp is added to the pool of actions, combined actions are much more difficult to achieve (36.1%). *Significance:* To the best of our knowledge, for the first time, the effectiveness of tactile myography on single and combined actions is evaluated in a target achievement test. The present study includes 3 DoFs control instead of the two generally used in the literature. Additionally, we define a set of physiologically plausible muscle activation limits valid for most experiments of this kind.

Author contributions Conceptualization; Methodology; Validation; Data Interpretation; Software design; Formal Analysis; Investigation; Writing original draft; Review and editing; Visualization.

Video https://www.frontiersin.org/articles/10.3389/fnbot.2020.00011/full#supplementary-material

Citation M. Connan, R. Kõiva, and C. Castellini, "Online natural myocontrol of combined hand and wrist actions using tactile myography and the biomechanics of grasping," *Frontiers in Neurorobotics*, vol. 14, no. 11, pp. 1–16, feb 2020, doi: 10.3389/fnbot.2020.00011

frontiers in Neurorobotics

ORIGINAL RESEARCH
published: 27 February 2020
doi: 10.3389/fnbot.2020.00011

Online Natural Myocontrol of Combined Hand and Wrist Actions Using Tactile Myography and the Biomechanics of Grasping

Mathilde Connan[1]*, *Risto Kõiva*[2] and *Claudio Castellini*[1]

[1] German Aerospace Center (DLR), Institute of Robotics and Mechatronics, Wessling, Germany, [2] Research Institute Cognitive Interaction Technology, Bielefeld University, Bielefeld, Germany

Objective: Despite numerous recent advances in the field of rehabilitation robotics, simultaneous, and proportional control of hand and/or wrist prostheses is still unsolved. In this work we concentrate on myocontrol of combined actions, for instance power grasping while rotating the wrist, by only using training data gathered from single actions. This is highly desirable since gathering data for all possible combined actions would be unfeasibly long and demanding for the amputee.

Approach: We first investigated physiologically feasible limits for muscle activation during combined actions. Using these limits we involved 12 intact participants and one amputee in a Target Achievement Control test, showing that tactile myography, i.e., high-density force myography, solves the problem of combined actions to a remarkable extent using simple linear regression. Since real-time usage of many sensors can be computationally demanding, we compare this approach with another one using a reduced feature set. These reduced features are obtained using a fast, spatial first-order approximation of the sensor values.

Main results: By using the training data of single actions only, i.e., power grasp or wrist movements, subjects achieved an average success rate of 70.0% in the target achievement test using ridge regression. When combining wrist actions, e.g., pronating and flexing the wrist simultaneously, similar results were obtained with an average of 68.1%. If a power grasp is added to the pool of actions, combined actions are much more difficult to achieve (36.1%).

Significance: To the best of our knowledge, for the first time, the effectiveness of tactile myography on single and combined actions is evaluated in a target achievement test. The present study includes 3 DoFs control instead of the two generally used in the literature. Additionally, we define a set of physiologically plausible muscle activation limits valid for most experiments of this kind.

Keywords: myocontrol, tactile myography, prosthetics, combined actions, grip strength, high-density force myography (HD-FMG), biomechanics of grasping

OPEN ACCESS

Edited by:
Ganesh R. Naik,
Western Sydney University, Australia

Reviewed by:
Wellington Pinheiro dos Santos,
Federal University of Pernambuco, Brazil
Strahinja Dosen,
University Medical Center Göttingen, Germany
Fernando Vidal-Verd,
University of Mlaga, Spain
Angelo Davalli,
Istituto Nazionale per l'Assicurazione Contro gli Infortuni sul Lavoro (INAIL), Italy

***Correspondence:**
Mathilde Connan
mathilde.connan@dlr.de

Received: *24 May 2019*
Accepted: *30 January 2020*
Published: *27 February 2020*

Citation:
Connan M, Kõiva R and Castellini C (2020) Online Natural Myocontrol of Combined Hand and Wrist Actions Using Tactile Myography and the Biomechanics of Grasping. Front. Neurorobot. 14:11. doi: 10.3389/fnbot.2020.00011

1. INTRODUCTION

The umbrella term *myocontrol* denotes, in contemporary assistive robotics, the control of a mechatronic device exerted by a human subject using coordinated muscle contractions. Informally, it is about *reliably* turning patterns of biological signals into "actions," usually to be executed by a prosthetic device, such as e.g., a "power grasp" or the "flexion of the wrist." In this framework, *reliably* means that the prosthesis should be able to execute what the amputee desires, exactly when he/she desires it, and in a transparent (natural) way. To this aim, the keywords *natural control* (Castellini et al., 2014; Ortiz-Catalan and Branemark, 2014) and *simultaneous and proportional control* (Jiang et al., 2009; Muceli et al., 2014) have appeared in literature, denoting continuous, real-time, and graded control over many degrees of freedom (DoF) of the prosthesis—potentially, all of them. This idea is particularly well illustrated in Fougner et al. (2012) (consider **Figure 2** in the paper), which dates back to 2012.

There are multiple reasons why decades of academic research have yet hardly turned into commercial solutions (two remarkable exceptions are the *Complete Control* system by CoApt Engineering[1] and *Myo Plus* by Ottobock[2]), the most prominent among which is, probably, the lack of reliability of said form of control. At the time of writing this article, seven years have gone by since the appearance of Jiang et al. (2012), a paper in which the community of myocontrol was incited, among other things, to find novel sensing techniques for intent detection. The traditional biosignals used in myocontrol, surface electromyography (sEMG), are deemed to be insufficient, and the research community is underway of finding alternatives. At present, no widely accepted and exhaustively tested alternative exists. We argue that a prominent option could likely be *tactile/force myography*. Since Craelius et al.'s experiments in the early 2000s (Curcie et al., 2001; Craelius, 2002) it has been clear that each pattern of muscle activation corresponding to a desired action also corresponds to a specific, repeatable pattern of external forearm pressure produced by the volumetric variation of the underlying muscles. Such a deformation could be detected by force/pressure sensors and associated to the action, thereby used as an alternative or parallel technique to surface electromyography. Examples of comparisons and mixtures of the two techniques can already be found in literature (Fang et al., 2015; Cho et al., 2016; Connan et al., 2016; Castellini et al., 2018). This approach, involving several independent force sensors has been called, among other ways, *force myography* or FMG.

In this work, we try to advance the state of the art in the usage of a closely related technique for myocontrol, namely *tactile myography* (TMG). The term TMG is used for high-density FMG: a technique in which many force/pressure sensors are put in contact with the subject's limbs. TMG has already been proved at least in Radmand et al. (2016) and Jaquier et al. (2017) and it has been shown to offer an unprecedented detail about the muscle patterns under examination. However, in these different works, combined motions were not tested. On another note, TMG can also be embedded in a socket-like structure or in a shape-conformable bracelet for ease of use and the bare application of linear regression on its values yields good results in intent detection.

Specifically, we hereby show that TMG and linear regression can be used proficiently in an online goal-reaching task, and that it suffices to gather data from the subject for single actions only (i.e., a list primary actions that we define in Subsection 3.4) to also be able to predict combined actions (e.g., flexing and pronating the wrist at the same time). Firstly, we carry out a study of existing literature about *muscle activation limits* in complex actions, and propose a set of physiologically feasible maximal activations, apt for any future experiment involving combined actions. Indeed the physiology of the hand and wrist as well as forearm limits the possibilities of mobilizing multiple muscles at the same time. For instance, each forearm or wrist action has an influence on the level of power grasp's strength one is able to produce.

Furthermore, we engage 12 subjects and one amputee in an instance of the Target Achievement Control (TAC) test (Simon et al., 2011) with control over 3 DoF[3]. Our experimental results show that, when using linear regression and TMG, combined actions can be predicted by gathering data about single movements only. However, power grasping seems to have a remarkable negative influence on the test. The high resolution of TMG is probably the reason why linear regression suffices. Actually, in other cases in which no high-resolution approach could be used, researchers needed to resort to artificial combinations of existing data clusters (Nowak and Castellini, 2015, 2016; Nowak et al., 2016), especially when dealing with more than 2 DOFs. In these works we have already proposed to "dope" the dataset of a myocontrol system with synthetic data obtained by linearly combining pre-existing sEMG patterns, in order to be able to predict combined activations of complex actions without the need to gather data directly related to them. In this study, too, we compare using bare linear regression on the sensor values with a set of features reducing the dimensions of the input space to one sixth. This idea could help whenever limited computational power is available, e.g., in a future implementation running on an embedded battery-powered prosthesis controller.

Related Work

Previous research proposed control over combined actions with electromyography. In particular, Jiang et al. (2009) did an offline

Abbreviations: APL, Abductor Pollicis Longus; CPU, Central Processing Unit; DoF, Degree of Freedom; ECRB, Extensor Carpi Radialis Brevis; ECRL, Extensor Carpi Radialis Longus; ECU, Extensor Carpi Ulnaris; ED, Extensor Digitorum; EDM, Extensor Digiti Minimi; EPL, Extensor Pollicis Longus; FCU, Flexor Carpi Ulnaris; FCR, Flexor Carpi Radialis; FDP, Flexor Digitorum Profundus; FDS, Flexor Digitorum Superficialis; FMG, Force Myography; FPL, Flexor Pollicis Longus; HD-FMG, High-Density Force Myography; MVC, Maximum Voluntary Contraction; ROI, Region Of Interest; ROIG, Region Of Interest Gradient; ROM, Range of Motion; RR, Ridge Regression; RR-ROIG, Ridge Regression with Region Of Interest Gradient; sEMG, Surface Electromyography; SD, Standard Deviation; SR, Success Rate; TAC, Target Achievement Control; TCT, Time to Complete Task; TIT, Time in Task; TMG, Tactile Myography

[1]http://www.coaptengineering.com/

[2]https://www.youtube.com/watch?v=B8Z_2tMUeiw

[3]With a slight abuse of language, we will consider a power grasp as one single DoF along this article.

analysis of EMG data collected with restriction of the wrist and proposes a linear model (non-negative matrix factorization - NMF) built on neural muscle synergies: single-DoF wrist activations are extracted by a linear decomposition of the sEMG signals.

Several studies also used this idea of a linear decomposition of the sEMG signals. For example, Nagata and Magatani (2011) presents a preliminary offline experiment where the high-density electromyography (HD-EMG) data of only two subjects performing combined motions is collected and activations are separated by a Canonical Discriminant Analysis to construct basic motions. Furthermore, in Yatsenko et al. (2007), a PCA-based (Principal Component Analysis) technique built on sEMG energies is used offline to separate combined hand and wrist motions. Despite the limited number of subjects (2 intact subjects and 1 amputee), they present preliminary results of the same combined motions presented in our experiment, i.e., wrist flexion/extension, wrist pronation/supination, and power grasp.

In Kent and Engeberg (2011), control of the combined 2 DoFs power grasp and wrist flexion/extension is possible thanks to a biomimetic controller taking into consideration the muscular structure of the forearm. Amsuss et al. (2014) tested the same NMF algorithm with muscle synergy-inspired decomposition as in Jiang et al. (2009), combined with a Linear Discriminant Analysis, in a free test of 1h in which 2 amputees tried rotation of the wrist combined with wrist flexion/extension while manipulating objects and performing a clothes pin test. The subjects were equipped with a socket containing 8 EMG Ottobock electrodes. Unfortunately, training the NMF algorithm with the same 3 DoFs, as in our study, resulted in very unreliable results. Using only 8 EMG electrodes and simple linear regression, Hahne et al. (2018) tested the control of combined wrist rotation and grasping on 5 amputees in a series of activities of daily living. In this paper, they used a control scheme based on non-intuitive mapping. It consists in a training phase based on motor skill learning and brain plasticity, i.e., the subject is involved in a longer signal-inspection phase where the experimenter searches for the best-looking signals and uses the associated movements to train the algorithm: for example, a radial/ulnar deviation can be mapped to a power grasp. The cognitive load of such a training is thus higher than in the case of a direct mapping like in our case. Additionally, it limits the number of DoFs that can be controlled simultaneously.

HD-EMG was also investigated for combined motions in several articles. For example, Ison et al. (2016) applied motor skill learning, a.k.a. non-intuitive mapping, and HD-EMG in an online experiment to control a 7-DoF robotic arm. In their experiment, it was possible for the subjects to switch in between 2 modes of each 4 DoFs (with a common DoF between the 2 modes being the power grasp); meaning simultaneous control could be established over 4 DoFs. Finally, Muceli et al. (2014) realized a similar online experiment as the one presented in our research and showed that, using reduced HD-EMG, with 2 DoF fed to the NMF machine learning, the subjects could control combined actions.

2. LIMITATION OF THE POWER GRASP STRENGTH WITH RELATION TO THE HAND AND WRIST BIOMECHANICS

Although the functional Range of Motion (ROM) of the hand and wrist joints has been studied in several papers (Palmer et al., 1985; Hume et al., 1990; Ryu et al., 1991), while combining hand and wrist movements, limitations come into place. Indeed, wrist and hand movements are due to combinations of muscle synergies (Mussa-Ivaldi et al., 1994; D'Avella et al., 2003); changing the forearm position can potentially change the length of the extrinsic muscles of the hand, which determine most of the grip strength. The combinations of joints' ROM can thus be altered (Brand and Hollister, 1999). This point needed to be taken into account in order to provide realistic and feasible targets for hand/wrist positions to our subjects. For this reason, in the following section we study the limits of the hand and wrist's joint motions.

Several studies have shown that forearm and wrist positions have an influence on power grasp (Terrell and Purswell, 1976; Richards et al., 1996; Claudon, 1998; De Smet et al., 1998; Mogk and Keir, 2003) or other types of grasps (Dempsey and Ayoub, 1996). The shoulder position also has its influence (Halpern and Fernandez, 1996; Kattel et al., 1996). Both the physiological cross-sectional area (PCSA) and the length-tension relationship of a muscle have their influence on determining to which extent they contribute to one action (Zellers and Hallbeck, 1995; Brand and Hollister, 1999). In order to produce maximal contraction, each muscle has its optimal length, any elongation or shortening of the muscles dedicated to the finger and thumb flexion could have an influence on the power grasp strength (Brand and Hollister, 1999). Changing the configuration of the arm (at the shoulder, elbow, or wrist joints) physically affects the spatial relationship between the extrinsic muscles of the hand and wrist.

Wrist flexion/extension and power grasp: Studies have shown that the maximum voluntary contraction (MVC) of the hand decreases with wrist flexion and increases with wrist extension (Claudon, 1998; Fong and Ng, 2001; Bhardwaj et al., 2011), sometimes to a higher level than the one in neutral position (despite some studies showing the contrary Terrell and Purswell, 1976; Mogk and Keir, 2003, probably due to the angle of wrist extension). This phenomenon is actually an orthopedic observation known under the name of *tenodesis*. This can be a result of the long flexor and extensor muscles of the fingers passing through the wrist, finger and elbow joints: they work in synergy to stabilize the intermediate wrist joints and to activate the distal joints, such as the ones of the fingers (Richards et al., 1996). This synergy between the finger flexors and extensors allows, once the wrist joint is stabilized, an optimal flexion of the finger joints, i.e., a maximal power grasp strength (Austin, 2005). Moreover, a wrist extension brought by the ECU, ECRL and ECRB[4] muscles generate a passive tension in the extrinsic finger tendons (FDS and FDP), which are stretched over the extended wrist. When considering this and the previously mentioned

[4]All muscle's abbreviations are the standard ones and are explained in the abbreviation section.

TABLE 1 | Percentage of the maximal grip strength with combined wrist and forearm movements to estimate the thresholds for actions combined with a power grasp.

Study	N^k	Pronation			Neutral			Supination		
		Extension (%)	Neutral (%)	Flexion (%)	Extension (%)	Neutral (%)	Flexion (%)	Extension (%)	Neutral (%)	Flexion (%)
Bhardwaj et al. (2011)[a]	100				107	100	54			
Parvatikar and Mukkannavar (2009)[b]	50				91	100				
Mogk and Keir (2003)[c]	10	95	87	50	99	100	56	98	94	61
Fong and Ng (2001)	30				102	100				
Claudon (1998)[e]	15	93	84	62	104[d]	100	73	103	101	71
De Smet et al. (1998)[f]	40		92			100			101	
Kattel et al. (1996)[g]	15					100	73			
Richards et al. (1996)	106		91			100			102	
Zellers and Hallbeck (1995)	20				98	100	84			
Duque et al. (1995)[h]	20					100	52			
Marley and Wehrman (1992)[i]	20		80			100			90	
Terrell and Purswell (1976)[j]	40	69	88	57	77	99	70	77	100	73
MEAN		86	**87**	57	**97**	**100**	**66**	93	**98**	68

[a]*Force exerted while the wrist was immobilized at 30° flexion/extension.*
[b]*Based on reported grip strength for shoulder at 0° of shoulder flexion and elbow at 90°.*
[c]*Peak force was used to evaluate maximum grip strength 100% of MVC.*
[d]*Force exerted while the wrist was immobilized at 30° extension.*
[e]*Based on maximal voluntary flexion/extension.*
[f]*Non-immobilized wrist, full pronation/supination.*
[g]*Based on reported grip strength for shoulder at 0°, elbow at 90° for all actions and when wrist flexion is involved, it is with 2/3 of maximum flexion.*
[h]*Based on reported percentage in full voluntary flexion.*
[i]*Based on reported percentage at 90° of elbow flexion.*
[j]*Force exerted with the wrist at 50° of extension.*
[k]*Number of participants to the study.*
The values in bold are the ones used as references for choosing the experiment's thresholds (cf. ***Table 2****).*

synergy to stabilize the wrist, one could conclude that the reciprocal relationship between the wrist muscles and the finger flexors is the reason for an optimal power grasp in a slightly extended and stable wrist position. On the contrary, during a wrist flexion, the tendons of the FDS and FDP release, while the tendons of the ED, EDM and EPL distend: this passive tension on the finger extensors allows the fingers to stretch. This has been confirmed in an electromyographic study by Claudon in which he shows that the activity of the ED is lower than that of the FDS during maximal extension of the wrist; he also observed the opposite result in maximal flexion (Claudon, 1998).

Wrist flexion and thumb: Additionally, as for the extrinsic muscles of the fingers, the wrist position also influences the thumb: during wrist flexion, the flexion at the interphalangeal joint of the thumb (due to the FPL) is significantly reduced (Austin, 2005); hence the power grasp is furthermore hindered.

Wrist supination/pronation and power grasp: Several researchers have also studied the influence of forearm rotation (pronation/supination) in relation to the grasp strength (Terrell and Purswell, 1976; Marley and Wehrman, 1992; Richards et al., 1996; Claudon, 1998; De Smet et al., 1998; Mogk and Keir, 2003). It has to be noted that though often referred as a DoF of the wrist joint in the robotic field, the forearm/wrist rotation is biomechanically an elbow DoF. Most of the studies show that a forearm pronation decreases the grip strength while a supination tends to increase it (Terrell and Purswell, 1976; Richards et al., 1996; Claudon, 1998; De Smet et al., 1998). It is supposed that the decreased strength in supination shown in two studies (Marley and Wehrman, 1992; Mogk and Keir, 2003) can be due to the method used or due to the angle of supination and pronation. One explanation to the increased strength during supination could be that in this position, the long flexors of the fingers (ED, FDP, FDS) are able to contract maximally. Indeed, to move the wrist from a supinated to a pronated position, the radius rotates over the ulna and the extrinsic flexor muscles of the fingers are wrapped around the radius during the rotation (Richards et al., 1996). This could result in a change of the length of these muscles, hence affecting their optimum length-tension relationship and reducing the strength of the power grasp.

A summary of the different studies analysing grip strength according to forearm and wrist motions can be found in **Table 1**. Not being used in our study, ulnar and radial deviations (Terrell and Purswell, 1976) were purposefully left out for the sake of readability of the table.

3. MATERIALS AND METHODS

3.1. Experimental Setup

3.1.1. Tactile Bracelet

For the experiment presented in this work, we used an improved version of our previously developed tactile bracelet (Kõiva et al., 2015) [cf. **Figure 1**]. The tactile bracelet, worn typically around

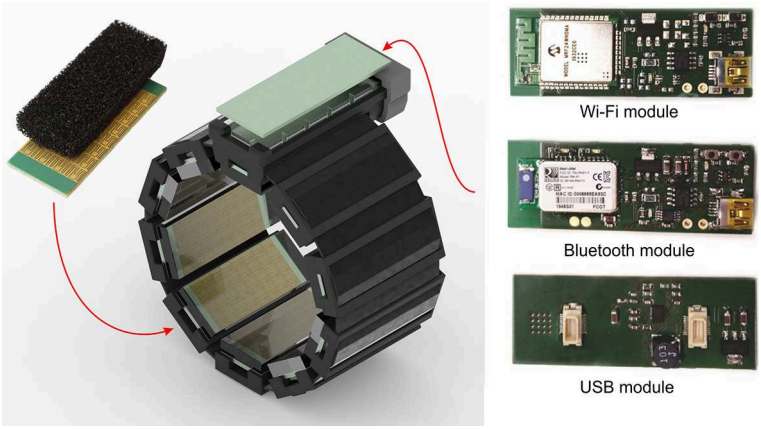

FIGURE 1 | The second generation tactile bracelet: **(left)** the bracelet and a single sensor module in the upper left; **(right)** three communication modules — USB, Bluetooth and Wi-Fi. The wireless modules include the circuitry for battery charging, powered through a dedicated USB connection.

the forearm, measures the bulges of the muscles with a spatial resolution of 5 mm. Depending on the thickness of the arm, up to ten sensor modules, with 4 × 8 tactile cells each, can be used. The modular design and the attachment around the arm using hook-and-loop band allow the bracelet to conform on various arm sizes and shapes, the latter especially important in case of residual limbs. The data from up to 320 tactile cells is sampled at 100 Hz.

The improved second generation tactile bracelet has more robust sensors and improved readout electronics. The conductive elastomer foam located as the outmost surface of the sensors and the material touching the human skin, was changed to 3 mm thick PANA Foamtec GmbH PE-K45EVAELS, a closed-cell cross-linked polyethylene foam with EVA content. The more dense foam made the tactile bracelet significantly more robust and less tear-prone when accidental shear forces are exerted during handling, e.g., while donning and doffing it. **Figure 2** shows the sensor characteristic using the new elastomer foam.

As is apparent from **Figure 2**, the taxel response is not linear. This helps to exploit the sensors' dynamic range as much as possible. We intentionally decided not to linearise the response in order to save computational effort, and not alter the signal-to-noise ratio. See, e.g., Castellini et al. (2018) for more thorough description of the device and its pros and cons.

The readout electronics was completely redesigned to make use of a newer microcontroller model and freshly rewritten software stack. The second generation tactile bracelet readout electronics uses a Microchip PIC32MZ microcontroller, running at 200 MHz. The software was rewritten to make use of FreeRTOS real-time-operating-system, resulting in a greatly simplified firmware code while still maintaining precise timing required to read out the high number of AD7490 ADCs connected to high-impedance tactile cells. The bracelet can now optionally be used in battery-powered wireless mode, the captured signal being transmitted over Bluetooth or Wi-Fi. For the experiment in this paper though, the wired USB connectivity was used. A described

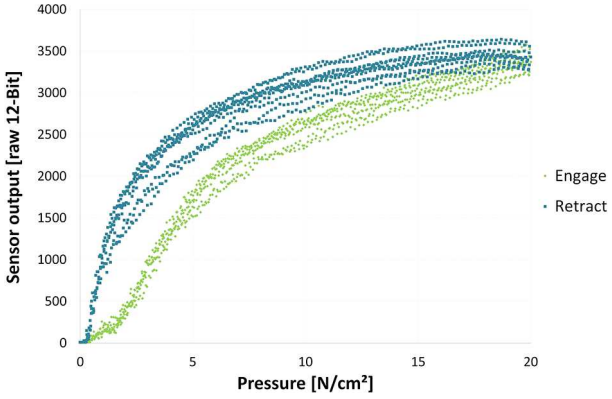

FIGURE 2 | Sensor characteristics measured over 10 trials from no contact to 20 N/cm^2 and back to no contact using the new 3 mm thick PANA Foamtec GmbH PE-K45EVAELS. The green samples are collected while pressure onto the sensor was increased whereas the blue ones are sampled during the retraction phase.

picture of the tactile bracelet and a visual representation of the data can be found in **Figure 3**.

3.2. Data Processing and Intent Detection

3.2.1. Machine Learning Algorithm

The algorithm of choice was ridge regression (Hoerl and Kennard, 1970), already used successfully several times with the tactile bracelet, in e.g., Nissler et al. (2017). The ridge regression algorithm estimates the parameters of a mapping matrix $\mathbf{W} \in \mathbb{R}^{D\times d}$, with D the number of input sensors or features and d the number of output activations. We call it "activation" because it stems from the voluntary activation of a set of muscles, which we somehow recorded (i.e. wrist flexion and extension are two different activations). This mapping matrix $\mathbf{W}$ is based on a set of m training pairs of input-output values, $\mathbf{X} \in \mathbb{R}^{m\times D}$ and $\mathbf{Y} \in \mathbb{R}^{m\times d}$, and the regularization coefficient λ, uniformly set

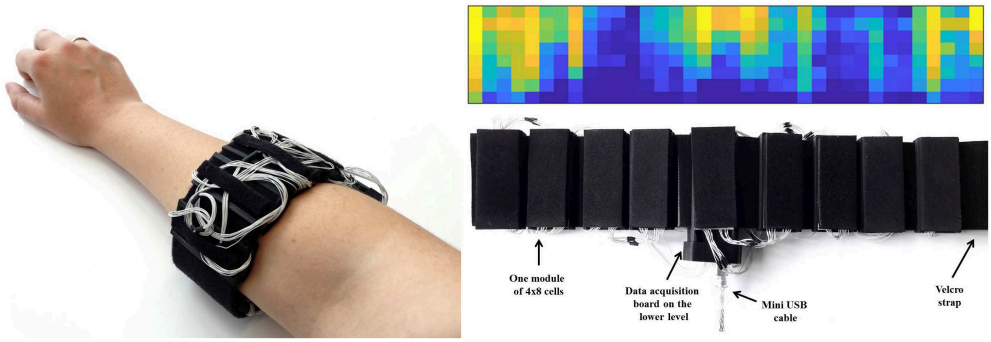

FIGURE 3 | Picture of the tactile bracelet, consisting of 9 boards of 32 cells each (8 vertical and 4 horizontal), and visual representation of the data.

at the standard value of 1 in this case (also previously chosen in Nissler et al., 2017). We obtain the mapping matrix with the following equation:

$$\mathbf{W} = (\mathbf{X}^T\mathbf{X} + \lambda\mathbf{I})^{-1}\mathbf{X}^T\mathbf{Y} \quad (1)$$

The output vector $\hat{\mathbf{y}} \in \mathbb{R}^d$, resulting from the input vector $\hat{\mathbf{x}} \in \mathbb{R}^D$, is then equal to:

$$\hat{\mathbf{y}} = \mathbf{W}^T\hat{\mathbf{x}} \quad (2)$$

The position of the virtual hand was then controlled thanks to this output vector, having one value between 0 and 1 for each activation.

3.2.2. Feature Selection

Captured tactile data was filtered by a low-pass first-order Butterworth filter with a cut-off frequency of 1 Hz to attenuate the high-frequency noise, which was previously tested in an initial round of experiment and showed not to impair the speed. In this study, two feature selection methods were used in order to determine the prediction.

The first one had already been used successfully in previous online studies with the first generation tactile bracelet (Jaquier et al., 2017; Nissler et al., 2017) and consists of the unprocessed data (except the Butterworth filter mentioned above) directly fed to a simple ridge regression (RR) algorithm. More precisely, the data consists of 288 filtered sensor data (9 boards of the 32 sensors each).

The second feature selection method, Gradient-based features extracted from Regions of Interest (ROIs) (Haralick and Shapiro, 1992), has already been used in ultrasound image processing and more specifically to identify finger movements (Castellini et al., 2012; Sierra González and Castellini, 2013; Ortenzi et al., 2015), also together with regression-based algorithms (Castellini et al., 2012; Sierra González and Castellini, 2013). More recently, this method has been further tested in an offline study investigating different methods of feature extraction for the Tactile Bracelet: the ROI gradients gave the highest classification accuracy (Castellini et al., 2018) over Harris corner extraction (Harris et al., 1988) and the structural similarity index (Boschmann and Platzner, 2014) on bicubic interpolated data. Unlike the round-shaped overlapping ROIs used in Sierra González and Castellini (2013) for ultrasound image processing and due to the low resolution of the tactile bracelet compared to ultrasound, a simpler strategy was adopted here after several pre-tests, delimiting each ROI as a non-overlapping 4×4 taxel square (Castellini et al., 2018) (a taxel being the value of one sensor), resulting in two ROIs per board (cf. **Figure 5**). Three features $(\alpha_i, \beta_i, \gamma_i)$ were extracted from each ROI_i, with $i \in [\![1, 18]\!]$. These features can also be considered as a vector that represents the second moment axis of the ROI area, i.e., the line around which the ROI would have the lowest moment of rotation if it were cut from a rigid and uniform cardboard (Russ, 1999) or the normal line to the planes that best fits all the observed taxels of the ROI. The value distribution of the ROI is approximated by a first order regression plane:

$$\hat{G}(x, y) = \alpha_i(x - x_i) + \beta_i(y - y_i) + \gamma_i. \quad (3)$$

where $\hat{G}(x, y)$ is the point on the fitted plane at the position (x, y), and (x_i, y_i) the interest point defined in the upper left corner of the ROI_i (Castellini et al., 2018).

The least squares fit to the observed gray values $G(x, y)$ of the ROI and is obtained from α_i, β_i, and γ_i that minimize the sum of the squares of the distances between our points and the plane:

$$\varepsilon^2 = \sum_{(x,y)\in ROI_i} [\alpha_i(x - x_i) + \beta_i(y - y_i) + \gamma_i - G(x, y)]^2. \quad (4)$$

Represented in **Figure 4** for one ROI only, α denotes the mean image gradient along the x direction (row), β along the y (column) and γ is an offset (mean gray value of the taxels in the ROI after resolution of the equation).

The computation of the parameters for one ROI is performed with ridge regression:

$$\boldsymbol{w} = (A^TA + \lambda I)^{-1}A^T\boldsymbol{r}, \quad (5)$$

$$\text{with } \boldsymbol{w} = \begin{bmatrix} \alpha_i \\ \beta_i \\ \gamma_i \end{bmatrix}, A = \begin{bmatrix} 1 & x_1 & y_1 \\ 1 & x_2 & y_2 \\ \vdots & \vdots & \vdots \\ 1 & x_l & y_l \end{bmatrix}, \text{and } \boldsymbol{r} = \begin{bmatrix} ROI_i(x_1, y_1) \\ \vdots \\ ROI_i(x_l, y_l) \end{bmatrix}.$$

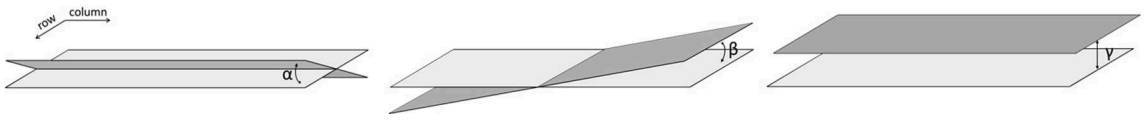

FIGURE 4 | Visualization of the parameters alpha, beta, and gamma of a plane.

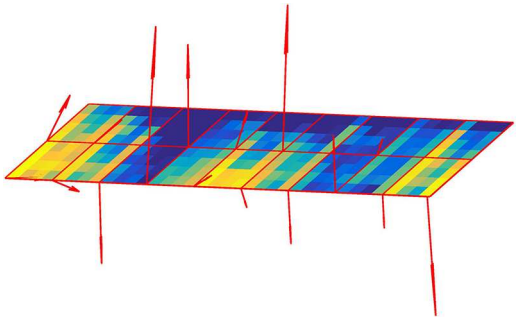

FIGURE 5 | A schematic representation of ROIs and their gradient, obtained from real data.

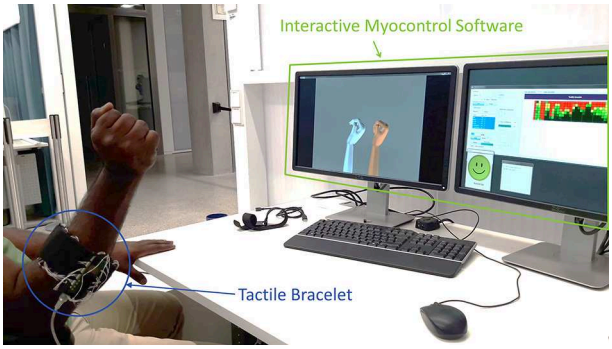

FIGURE 6 | A bird's-eye view of the experiment.

Solution of the linear regression, $\boldsymbol{w}$ contains the parameters α_i, β_i, and γ_i, while A contains the coordinates of the ROI and $\boldsymbol{r}$ contains the gray values of the ROI in an $l \times l$ matrix, with l being the side length of the square ROI.

A representation of the ROIs and the gradients can be seen in **Figure 5**. Since we had 2 ROIs on each of the 9 sensor boards and that three features were extracted from each ROI, a 54-dimensional feature vector was fed to the RR algorithm, namely RR-ROIG in this article.

3.3. Participants

Twelve able-bodied right-handed volunteers participated in the experiment (30.6 $\pm$ 6.6 years old, three females and nine males). One left-hand amputee (male, 35 years old) also took part in the experiment. He was trans-radially amputated in 2005 and uses daily, since 2012, a Variplus prosthesis by Ottobock with standard two-electrode control and no rotation unit on the device.

The experimental procedure was thoroughly explained to the participants in both oral and written form before the experiment and each of the participants was given a written informed consent form. The experiment was performed according to the WMA Declaration of Helsinki and was preliminarily approved by the Work Ethical Committee of DLR.

3.4. Experimental Protocol

Each subject would sit comfortably, their back against the backrest of the chair and their elbow placed near the furthest edge of the armrest relative to them (cf. **Figure 6**). The hand with which the participants would perform the experiment would be alternatively switched between subjects. The tactile bracelet was placed at the lower arm location with the greatest muscle bulge, i.e., near the proximal end of the forearm, as shown in **Figure 6**. In order to avoid any undesired change in the signals due to tissue accumulation between the tactile bracelet and the inner side of the elbow, the subjects were told to keep their forearm at an angle of 90° with their upper arm. The default/resting hand position was a flat hand with the palm facing the side of the body.

The experiment consisted of a training session on a set of single activations of the hand and wrist actions (*rest, power, flexion, extension, pronation, supination*) and of tasks to reproduce single and combined actions that are detailed in **Table 2**. The above mentioned set of actions (except "rest") are labeled as "single actions": subjects train on them and these actions should be reproduced individually during the task reaching test. Additionally, we define any combination of single actions as combined actions. Each action to be reproduced had a specific level to make it realistically possible in terms of muscle coordination and to prevent muscle overload (cf. Section 2).

In order to set the different levels and limitations of the power grasp for the visual stimulus, an average over all studies (over the methods) of **Table 1** was calculated.

Since to the best of our knowledge there are no studies on the limitation of forearm and wrist DoFs without the power grasp (i.e., pronation/supination and flexion/extension), we defined these specific threshold limitations according to an initial round of trials. The amputee performed the experiment with the same target thresholds as the able-bodied subjects.

We added an alleviating factor of 80% to these extreme limits of the hand and wrist movements in order to make the experiment more comfortable for the participants and to leave a safety margin to impossible target positions.

On the computer screen, positioned in front of the participants, two realistic 3D hand models were displayed: one acted as the visual stimulus, which pose the subject had to match with his/her own hand (or with a virtual hand

TABLE 2 | Single- and multi-action combinations performed during the experiment with the different thresholds chosen for each action with an 80% factor.

#	Power grasp	Pronation	Supination	Extension	Flexion	Comb. type
1	80% (**100%**)					
2		80% (**100%**)				
3			80% (**100%**)			Single
4				80% (**100%**)		
5					80% (**100%**)	
6		56% (**70%**)			40% (**50%**)	
7		56% (**70%**)		40% (**50%**)		Combined without power
8			56% (**70%**)		40% (**50%**)	
9			56% (**70%**)	40% (**50%**)		
10	70% (**87%**)	56% (**70%**)				
11	78% (**98%**)		56% (**70%**)			Combined with power
12	78% (**97%**)			40% (**50%**)		
13	53% (**66%**)				40% (**50%**)	

The values in bold represent the ones extracted from the literature or chosen from a pre-round of testing in the case where no power grasp was involved.

prosthesis in case of the amputee) and the second one showed the predicted intended movement, calculated by the machine learning algorithm working on the captured tactile bracelet data. The experiment started with a training phase, in which the recording would take around 2 min: each participant was asked to perform three repetitions of the stimulated single actions defined previously. The data collected during this phase was used to train the learning machines (RR and RR-ROIG as explained in Subsection 3.2), which in the later stage of the experiment would drive the second hand model. Then, in order to counter the learning effect and to adapt to the system, each participant was asked to perform a familiarization phase, consisting of six tasks to reproduce. Additionally, pressure-based data are prone to drifting: a problem that was already identified in Castellini et al. (2018). This is supposedly due to the elasticity of the skin and the memory effect of the foam (cf. Subsection 3.1.1). To avoid this issue, 2 repetitions of training were inserted after the familiarization phase and in between each repetition of task-reaching phases.

A task-reaching phase is a TAC test consisting of 26 tasks (13 tasks for each tested machine learning algorithm) in a randomized order while still maintaining an alternation between RR and RR-ROIG, every other subject starting with RR. These tasks can be single actions, or a simultaneous combination of actions with a certain percentage of the full activation defined in **Table 2**. The desired task was demonstrated by the visual stimulus and the subject had 15s to match it with the second virtual hand, driven by his muscle stimulus. To succeed in the task, the participant had to keep the controlled virtual hand in the same position as the visual stimulus for 1.5 s. Matching was defined as remaining within 20% of each target activation value. For the amputee this error threshold was set to 25% and the starting machine learning was RR. The task-reaching phase was repeated 3 times with 2 repetitions of training in between each of them in order to counter the drift induced by the bracelet. **Figure 7** shows the experimental procedure.

To evaluate the performance of the participants for each action and the different machine learning algorithms, we assessed

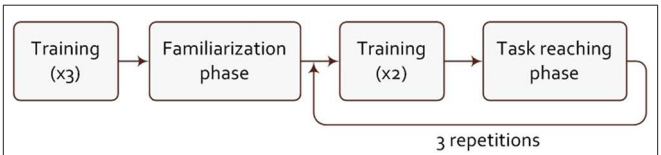

FIGURE 7 | Diagram of the experimental procedure.

the success rate over all 39 tasks (SR - Success Rate), the time that the subject took to accomplish the task (TCT - Time to Complete Task) and the cumulative time in the target (TIT - Time in Target). A video of the TAC test showing the experiment with an amputee and one able-bodied participant can be found in the **Supplementary Material**.

3.5. Statistical Analysis

For the statistical analysis we used the libraries provided by the programming language R. We first performed a Friedman test to see the influence of the repetitions on the SRs, which could eventually indicate a learning effect. Its result ($p = 0.3927$) showed that there was no statistical difference between the three repetitions of the TAC test. We can suppose that the familiarization phase was efficient and we will therefore aggregate the data of the 3 repetitions for the rest of the analysis. To evaluate the difference of SRs between the two feature selection methods, we tested the normality of the aggregated dataset with both Shapiro–Wilk and Jarque–Bera normality tests which both concluded that the distribution of the data is not significantly different from normal distribution. Therefore, we performed a paired t-test on the two feature selection methods. Then, after an initial round of analysis between "single actions" and "combined actions," we realized that the power grasp was creating the difference between the two groups. For this reason, we decided to carry out the analysis with the Holm-Bonferroni adjustment method for these three subgroups: "single actions," "combined actions without the power grasp," and "combined actions including the power grasp." We tested the normality of the aggregated datasets before each pairwise statistical test with both Shapiro–Wilk and Jarque–Bera normality tests. Both tests resulted in not rejecting the normality hypothesis. To assess the difference between the three previously mentioned subgroups, we used the multiple pairwise t-test with Holm-Bonferroni adjustment method as well as Cohen's d effect size. Regarding the time-related performance measures, no inferential statistical test was performed due to the fact that the condition of completeness of the dataset was not observed: the TCT can only be considered for successful tasks since a time limit of 15 s was fixed and, for the same reason, we decided to separate the analysis of the TIT between successful and failed tasks. Therefore, we kept this part of the statistical analysis on a descriptive level.

4. EXPERIMENTAL RESULTS

This section provides the results of the experiment described in the previous section. First, a detailed analysis on the results of

the 12 able-bodied participants will be presented. In particular, in Subsection 4.1, we compare the two machine learning methods, and present the difference between the single and the combined actions and the success rate action by action. In Subsection 4.2, we analyse the results of the TCT and TIT relative to the learning algorithm and the type of combined movement. Then, we analyse the results of the amputated subject in Subsection 4.3.

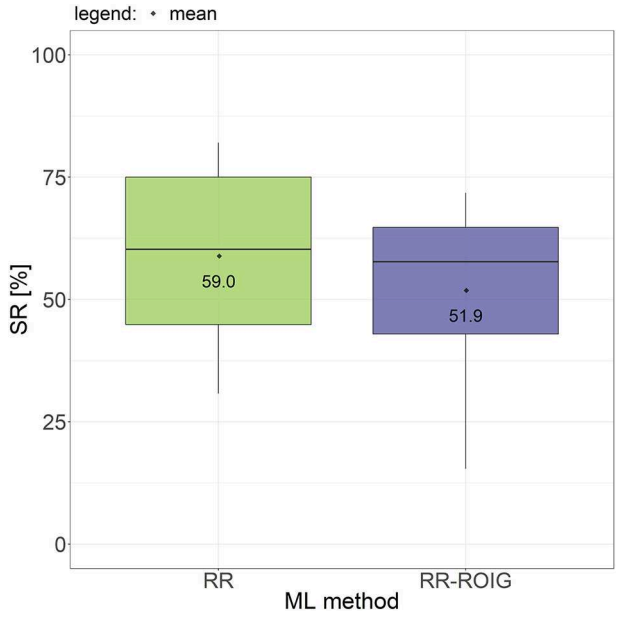

FIGURE 8 | Boxplots and means of the success rates for all tasks across all participants grouped according to the machine learning method used.

4.1. Success Rate

Figure 8 shows the difference of the success rates according to the machine learning method tested across all subjects. No statistically significant difference can be observed (paired t-test $p = 0.2123$), although the average performance of RR was around 8% better than that of RR-ROIG (59.0 ± 17.6% vs. 51.9 ± 17.2%).

When comparing the success rate action-wise, we can subdivide it in three groups: "single actions," "combined actions without the power grasp," and "combined actions including the power grasp" (as detailed in **Table 2**). The SR of RR and RR-ROIG in each of these three groups is described in **Figure 9**. The difference within each group is also not statistically significant between the two algorithms: $p = 0.17$ for "single actions," $p = 0.48$ for "combined actions without the power grasp" and $p = 0.86$ for "combined actions including the power grasp."

As we can take from **Figure 9**, the average SR of the "combined actions including the power grasp" — for RR 36.1 ± 21.7% — is much lower, by more than 30%, than the average SRs of the two other groups — for RR 68.1 ± 20.4% for "combined actions without the power grasp" and 70 ± 21.2% for "single actions." This difference is also present for the RR-ROIG algorithm with 22.8% between the SR of "combined actions without the power grasp" and the SR of the two other groups. In order to assess the significance of this difference, a multiple paired sample *t*-test with Holm-Bonferroni adjustment method was performed.

For RR, the difference between "combined actions including the power grasp" is highly significant when compared with "single actions" ($p = 0.0001$, $d = 1.5802$) as well as when compared with "combined actions without the power grasp" ($p = 0.0039$, $d = 1.5178$) after the Holm–Bonferroni correction. For RR-ROIG, the difference between "combined actions including the power grasp" is significant ($p = 0.0007$, $d = 1.3362$) when compared with "single actions," and also significant when

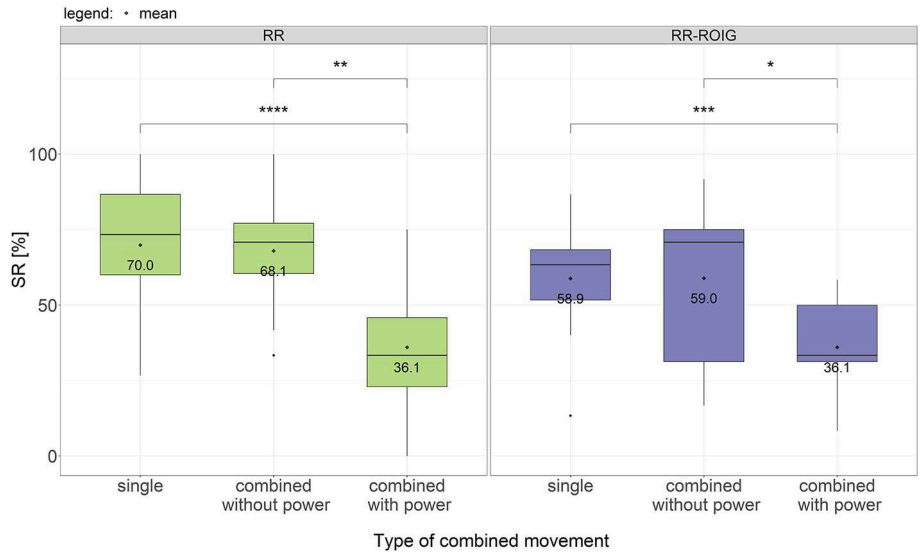

FIGURE 9 | Boxplots and means of the success rates across all participants grouped according to the machine learning method and the type of combined movement used. *$p \leq 0.05$; **$p \leq 0.01$; ***$p \leq 0.001$; ****$p \leq 0.0001$.

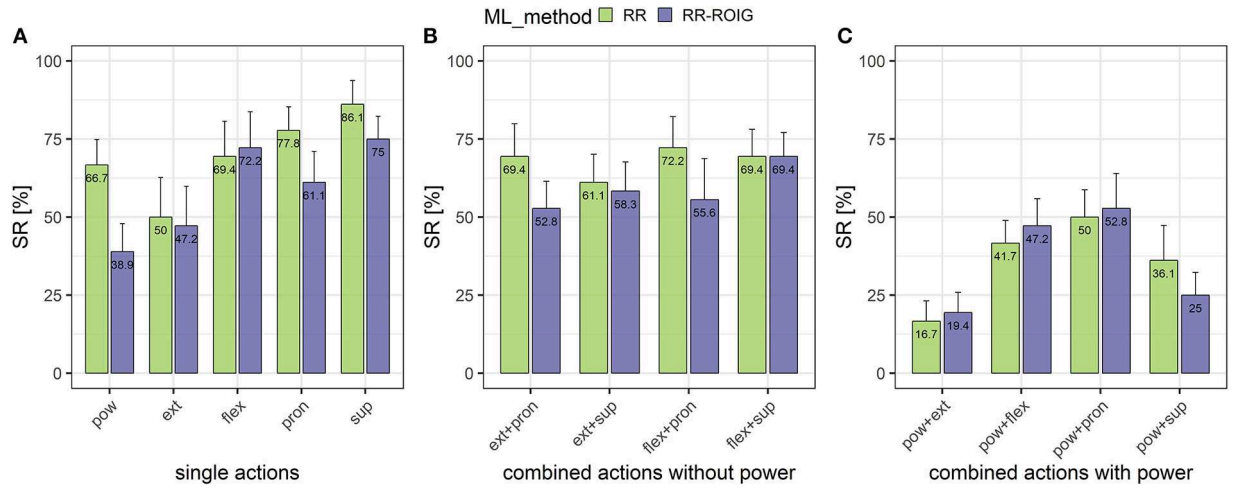

FIGURE 10 | Means and standard errors of the success rates per actions separated into 3 groups: single actions **(A)**, combined actions without the power grasp **(B)** and combined actions including the power grasp **(C)**.

compared with "combined actions without the power grasp" ($p = 0.0310$, $d = 1.0764$) after the Holm–Bonferroni correction. For both methods, there is no significant difference between "single actions" and "combined actions without the power grasp."

Figure 10 describes the SR action-wise among all participants. The "combined actions including the power grasp" are seemingly lower than the "single actions" and the "combined actions without the power grasp." In particular, power grasp combined with wrist extension and power grasp combined with supination seemed to be the most difficult tasks to achieve.

4.2. Time-Related Metrics

Other than the success rate, the Time to Complete the Task (TCT) and the total cumulative Time In the Target (TIT) were also measured.

TCT for successful tasks: We can see in **Figure 11** that the TCT for "single actions" and "combined actions without the power grasp" was almost 2 s faster than the TCT for "combined actions including the power grasp," which would indicate that actions combined with a power grasp were harder to reach.

TIT for failed tasks: For the combined actions in general, irrespective if the power grasp was included or not, the TIT was higher with RR than with RR-ROIG. On the contrary for single actions, the TIT seems higher with RR-ROIG. For all failed tasks the TIT is relatively low compared to the fixed goal of 1.5 s.

TIT for successful tasks: The cumulative TIT for successful tasks is relatively close to the targeted time of consecutive 1.5 s: this means that when a task could be completed, it would usually be achieved without wobbling around the goal and it would not depend on the type of action it is (combined or not).

4.3. Results Obtained by the Amputated Subject

The amputee achieved 20.5 ± 21.7% of success rate over all tasks with RR-ROIG and 15.4 ± 25.9% with RR. We here introduce a new performance index of reachability to verify if the task was reached by being in the target for one sample) at least once during the TAC test. The SR is however still measured the same way as previously described in the Experimental Procedure section, the subject having to keep the target during 1.5 s within the time of 15 s. As shown in **Table 3**, half or more of the types of action were attainable at least once during the three repetitions for each of the three combination groups. However, the success rates were on average 17.9 ± 23.5%. By calculating the time to complete the successful tasks, **Table 3** shows that it took on average 5.1 ± 4.3*s* for "single actions," 7.6 ± 4.1*s* for "combined actions without the power grasp," and 9.0 ± 5.0*s* for "combined actions including the power grasp."

When comparing the same data grouped according to the repetition of the task-reaching phase in **Table 4**, we can see that in the first repetition the participant achieved relatively high reachability with an average of 38.5 ± 49.6% and a success rate of 46.2 ± 51.9% for the RR-ROIG algorithm. The two remaining repetitions did not seem to increase the SR nor the reachability of the tasks with respectively 15.4 ± 36.8% and 26.9 ± 45.2% for repetitions 2 and 3.

Moreover, it has to be noted that for the second repetition of task-reaching phases, the control of the 3D-hand model was blocked after approximately half of the tasks and that the extension and power were problematic during the third repetition. This might be due to a drift in the signals or a sliding of the tactile bracelet on the stump that has a conical shape to which the tactile bracelet is not adapted.

Additionally, some trajectories of reached-but-failed tasks and of non-reachable tasks are depicted in **Figure 12** with PCA (Principal Component Analysis) for a 3D visualization with a percentage of variance of 88.41% for RR and of 84.82% for RR-ROIG. It can be seen in **Figure 12** that the amputated subject went from the rest position (red) to a target position that seems to be a somehow linear combination of supination (yellow) and flexion (cyan). The subject then reached the target but did not

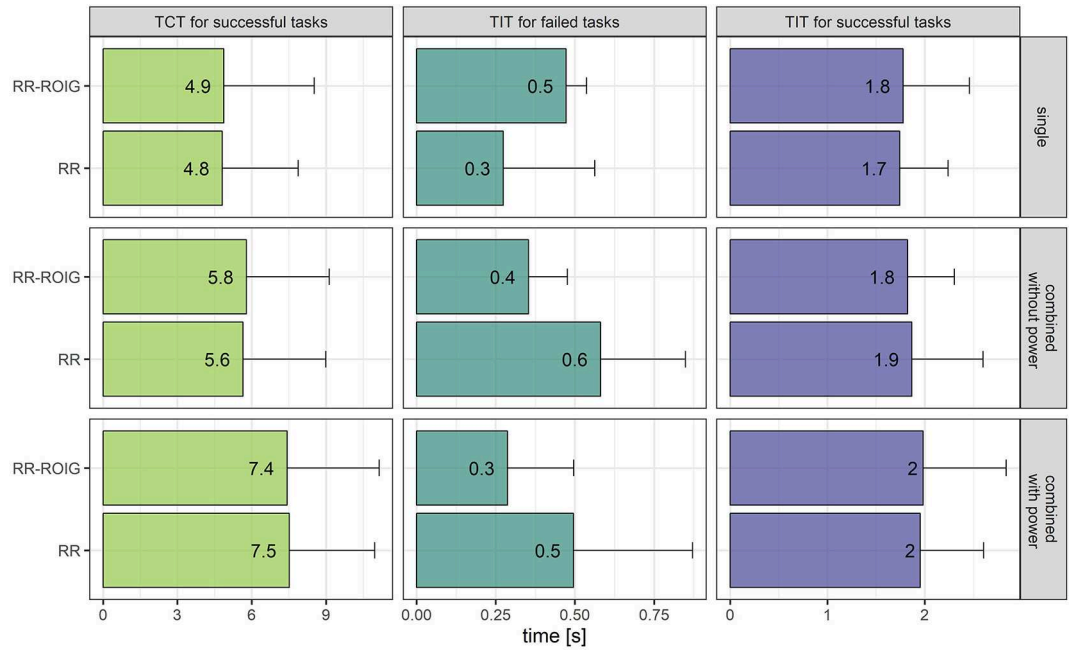

FIGURE 11 | Means and standard deviations of the TCT for successful tasks, TIT for failed tasks, TIT for successful tasks according to the machine learning method and the type of combined movement.

TABLE 3 | Means and standard deviations of the reachability of the tasks, the success rate, the time in task and the time to complete the successful tasks for the amputee according to the type of combined movement.

Type of combined movement	ML method	Reachable (%)		SR (%)		TIT (s) [successful tasks only]		TCT (s) [successful tasks only]	
Single	RR	60.0 (54.8)	50.0 (53.5)	13.3 (18.3)	13.3 (17.2)	2.1 (0.8)	1.8 (0.6)	7.0 (6.2)	5.1 (4.3)
	RR-ROIG	40.0 (54.8)		13.3 (18.3)		1.5 (0.0)		3.2 (1.6)	
Combined without power	RR	25.0 (50.0)	62.5 (51.8)	16.7 (33.3)	25.0 (29.5)	3.1 (0.2)	2.3 (0.8)	9.6 (3.2)	7.6 (4.1)
	RR-ROIG	100.0 (0.0)		33.3 (27.2)		1.8 (0.6)		6.6 (4.5)	
Combined with power	RR	25.0 (50.0)	50.0 (52.7)	16.7 (33.3)	16.7 (52.2)	1.9 (0.5)	1.7 (0.3)	7.3 (7.8)	9.0 (5.0)
	RR-ROIG	75.0 (50.0)		16.7 (19.2)		1.5 (0.0)		10.6 (1.7)	
All actions	RR	38.5 (50.6)	53.8 (50.8)	15.4 (25.9)	17.9 (23.5)	2.4 (0.8)	2.0 (0.7)	8.0 (1.8)	7.3 (4.3)
	RR-ROIG	69.2 (48.0)		20.5 (21.7)		1.7 (0.4)		6.8 (4.2)	

TABLE 4 | Means and standard deviations of the reachability of the tasks, the success rate, the time in task and the time to complete the successful tasks for the amputated subject according to the three repetitions of the task-reaching phase.

Repetition	ML method	Reachable (%)		SR (%)		TIT (s) [successful tasks only]		TCT (s) [successful tasks only]	
Rep. 1	RR	23.1 (43.9)	38.5 (49.6)	15.4 (37.6)	30.8 (47.1)	3.0 (0.5)	2.0 (0.7)	10.1 (3.8)	6.9 (4.4)
	RR-ROIG	53.8 (51.9)		46.2 (51.9)		1.7 (0.5)		5.9 (4.3)	
Rep. 2	RR	7.7 (27.7)	15.4 (36.8)	7.7 (27.7)	7.7 (27.2)	1.5 (NA)	1.5 (0.0)	1.8 (NA)	4.3 (3.6)
	RR-ROIG	23.1 (43.9)		7.7 (27.7)		1.5 (NA)		6.9 (NA)	
Rep. 3	RR	30.8 (48.0)	26.9 (45.2)	23.1 (43.9)	15.4 (36.8)	2.2 (0.8)	2.1 (0.7)	8.6 (5.2)	9.4 (4.5)
	RR-ROIG	23.1 (43.9)		7.7 (27.7)		1.5 (NA)		11.9 (NA)	

successfully maintain the virtual hand in the position for the required amount of time of 1.5 s. Subjects were advised at the beginning of the experiment that it can be easier to first execute one of the actions of the combination and then the other one to move toward the target; however, they could choose which strategy to actually use. This proposed strategy can be very well

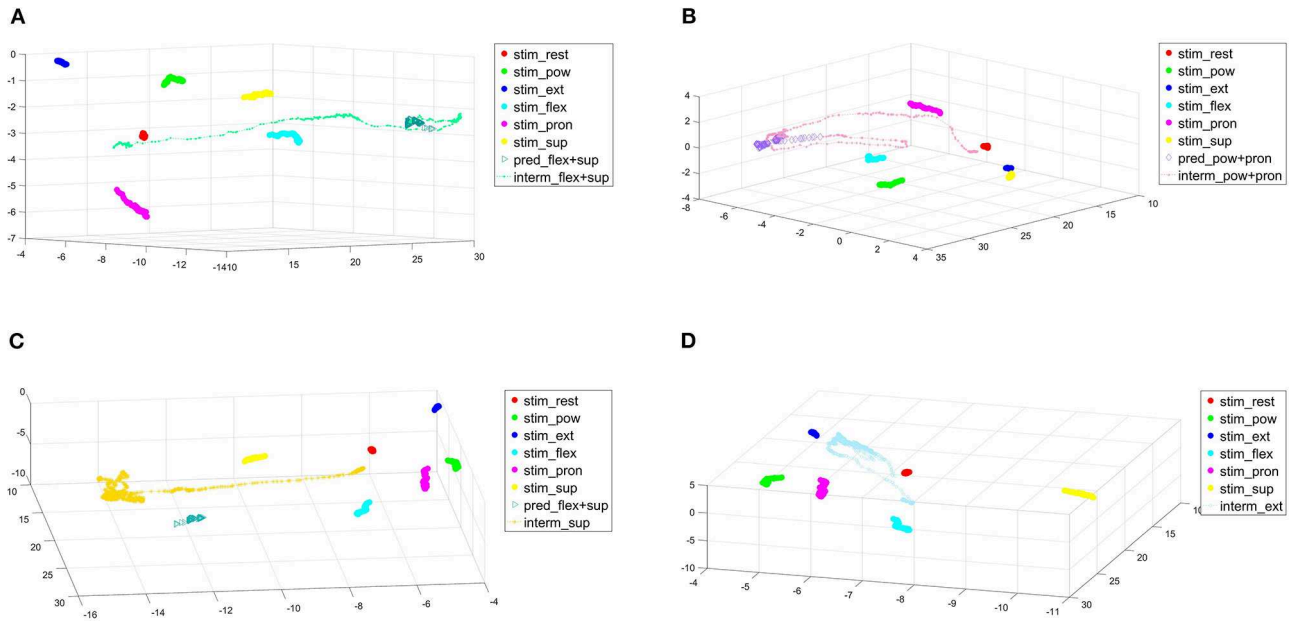

FIGURE 12 | PCA of some actions (failed or non-reachable) performed by the amputee during the first repetition. Legend items starting with "stim," "pred," and "interm" represent respectively the trained action clusters, the samples when the subject is in the target and the intermediate values while trying to reach the target. **(A)** PCA with emphasis on failed flex.+sup. for RR, **(B)** PCA with emphasis on failed pow.+pron. for RR-ROIG, **(C)** PCA with emphasis on non-reachable supination action for RR, and **(D)** PCA with emphasis on non-reachable extension action for RR.

seen in the top right subfigure, we can see that the subject first moved from rest to pronation to then additionally perform a flexion. The subject then reached the target for some time but did not manage to stay in the target for the required amount of time. The subject returned then slightly toward the rest position before trying again (which was also an advised strategy) and reaching the target for new samples, unfortunately not enough to achieve a successful task. The bottom left subfigure shows the subject trying to reach 80% of supination but going too far after the target and never reaching it. We can suppose that he has put too much strength into his muscles while trying to reach the target compared to the strength level he had performed during the training phase. The last subfigure (d) shows the trajectory going in the direction of the wrist extension cluster but slightly off, never reaching the 80% target. This shows, in our opinion, that the subject was able to control the hand but, due to different limitations (hardware, muscle fatigue, or simply not being able to reproduce the trained actions), was not able to perform well into our TAC test with the parameters and timings that we had set (15 s to achieve 1.5 s in task).

To get a better insight, a movie available in the **Supplementary Material** is showing part of the TAC test for the amputated subject.

5. DISCUSSION

In this work we have first thoroughly examined the literature about the physiological limits of the hand/wrist complex, in particular, as far as the maximal combined activations of hand and wrist actions are concerned. This has allowed us to define a set of muscle activation limits for combined actions, which can, and to some extent, we claim, should be reused in similar experiments.

Of course, each amputation results in a different stump with a different muscle remnant configuration, and, to the best of our knowledge, biomechanical relationships among muscles in a stump cannot be estimated. But these findings could be taken as upper limits while designing a TAC test for amputees, since if an intact subject cannot reach a specific activation, reasonably, no amputee will be able to as well. Moreover, amputees usually strain their muscle remnants while activating them, since they lack proprioceptive feedback. Limiting the visual appearance of TAC test targets can only be beneficial.

Having determined this set of limits, we have then engaged a few intact subjects and an amputated person in such a test, aimed at checking how well TMG could be used to detect single and combined hand/wrist actions. The experimental results presented in the previous section indicate that TMG is viable for myocontrol, as it had already been discovered (see, e.g., Radmand et al., 2016; Jaquier et al., 2017; Nissler et al., 2017): The SRs obtained by our subjects are in line with these previous works.

But furthermore, and this may be the main finding of this work, the results denote that, by gathering data while the subjects perform single actions, TMG is able to predict *combinations of them*. This is of valuable interest, considering that it confirms previous results with HD-EMG (Muceli et al., 2014; Ison et al., 2016) and, as far as we know, it had not yet been

discovered using TMG. We can suppose that, a high number of sensors, independent of the sensor type (force or sEMG), gives automatically the combined actions, provided a linear algorithm is used. TMG could detect single *and* combined actions, *with no statistically significant difference in the related success rates.* Notice that the SRs over all actions is slightly lower than the ones found in previous studies with TMG: 59.0% for RR in **Figure 8** vs. 75.6% in Nissler et al. (2017) where no combined motions were tested. However, when we remove the "combined actions including the power grasp" of the picture, results average 69.1% of SR and are in line with previous literature for TAC tests. The action of power-grasping leads to a substantial reduction of the SR when combined with wrist movements. Although still more than one third of the tasks were achieved, this is a problem which needs to be tackled. In the current version of the bracelet, it is due to saturation of most of the taxels, in turn due to the large number of muscles involved in this action. (When combined with other actions, the problem is obviously amplified.) To solve this issue, further versions of the semi-conductive foam and tuning of the pull-up resistors of the controlling boards are being tested.

Although standard metrics were used, a comparison with other studies involving combined motions is difficult considering the different experimental conditions. Considering that offline and online analysis are hardly comparable, we will here only examine our results in contrast with articles including an online test. Muceli et al. (2014) present a very similar work with an online TAC test investigating the control of the 2 wrist DoFs. They show that a reduced version of HD-EMG (16 electrodes) fed to an NMF algorithm results in a successful prediction of combined movements. The tasks are however slightly easier to reach than ours: the required consecutive time in task is 300 ms (while the subjects had to maintain 5 times this duration in our experiment) and the time given to complete the task was 20 s (15 s in our case). In addition, in our experiment, subjects had a simultaneous control over 3 DoFs: the machine learning algorithm was fed with one additional pattern for the power grasp, which can interfere with other actions, and in particular wrist flexion that involves common muscles. Nonetheless, after recalculating our results with 300 ms of required consecutive TIT, we found an increase of more than 10% in the SRs (RR from 58.3 to 68.5% and RR-ROIG from 51.13 to 62.13%), while the TCTs decreased in general of 1.5 s or more and of 2 s in case of "combined actions including the power grasp." Ison et al. (2016) accomplish control over 4 DoFs simultaneously where the participants had to control a 7-DoFs robotic arm in tasks such as grasping a tennis-sized ball and customized clothespins. However, the subjects were free in the sequence or combination of gestures to achieve the tasks. It needs to be noted that all of these articles use a non-intuitive mapping. Therefore, in these studies, the cognitive load of the training phase is supposedly higher than with the direct mapping that we use and the number of simultaneously controlled DoFs is limited in case no advanced surgical technique such as e.g., Targeted Muscle Reinnervation (Farina et al., 2017) is used. Another impressive work, also using non-intuitive mapping, is the one of Hahne et al. (2018), in which they focus on wrist rotation and grasping with 8 EMG and linear regression by involving 5 amputees in a series of prosthesis tests (clothespins and box and blocks tests). It is still a goal that has not yet been achieved by TMG and a limitation of our work, considering we only tested one amputee. However, TMG requires much less electronics for the same resolution, provides more stable signals (Connan et al., 2016) : Indeed force myography signals provide a stable plateau of activation while EMG signals present a peak of activation that decreases over time due to muscular motor-unit recruitment (Merletti et al., 2010a,b). Add in the fact that it is wearable, it could to a certain degree be easily integrated in a prosthesis. The computational burden required to extract the ROIG features is negligible, as already proved in (Sierra González and Castellini, 2013).

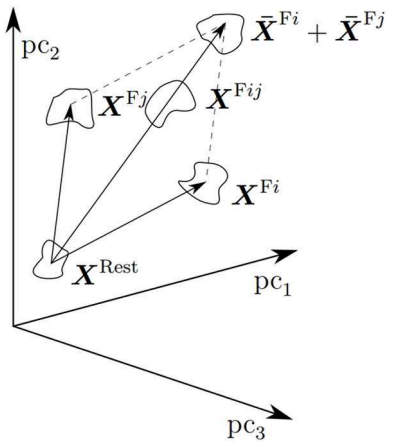

FIGURE 13 | A graphical representation of linear superposition of effects in the input space. A rest cluster X^{Rest}, two single-action clusters X^{Fi} and X^{Fj} and the combination cluster X^{Fij} are depicted. That linear regression can predict combined actions from single actions only, should imply that X^{Fij} largely coincides with $X^{Fi} + X^{Fj}$ (Reproduced with permission from Nowak, 2014).

That combined actions can be correctly detected using single-action data and linear regression indicates that linear superposition of effects might be present in the input space, as already suggested in Muceli et al. (2014). This fact needs be investigated in the future; it is likely that clusters of combined actions X^{Fij} should be to a large extent similar to the linear sum of the single-action clusters X^{Fi} and X^{Fj} they are composed of. A graphical representation of this issue is shown in **Figure 13**.

In this work, we also compared RR with RR-ROIG and showed in **Figure 8** that the success rate of RR is slightly higher than the one of RR-ROIG but the results are comparable. This newly presented online RR-ROIG would thus be valuable when fewer dimensions are required to be fed to the learning algorithm. This would be the case, for instance, in the presence of a high number of sensors and when there would be a CPU limitation. This is clearly advantageous when the software will be transferred to a prosthesis-embedded system in the future.

Our experiment was also tested by one trans-radial amputee. His results in terms of success rate are relatively low compared to the ones of the intact subjects. However, in each subgroup of types of combined movement, half or more of the tasks were

reachable (without achievement of the 1.5 s in task) at least once during the 3 repetitions. Moreover, the TIT for successful tasks was around 2 s, which is comparable to the one for intact subjects (cf. **Figure 11**). As for intact subjects, the time to complete the tasks seems to increase with the complexity of the task, from "single actions" through "combined actions without the power grasp" to "combined actions including the power grasp," indicating that the tasks became harder to achieve for the amputated subject as well as for the intact subjects. The TCT are nonetheless around 1.5 s more for the amputee, the tasks seemingly being harder to complete for him. However, as it can be seen in the complementary video, the subject was able to control the 3D hand model relatively well. Several possibilities could explain his low success rates. The first one being that the foam softness might not have been adapted to the relatively weak muscles of an amputee's stump and the amputated bulge could not create enough depth print on the tactile bracelet. We also speculate that the highly precise tasks of the TAC test were difficult to achieve for the subject. Lastly, we wanted the experiment with the amputee to be as similar as possible as the one with intact subjects. Therefore, we had the same length of familiarization phase. However, considering the impairment of the subject as well as the fact that he was not versed into technology, a longer familiarization phase might have improved the results. We are aware of the limitations of this study considering that we only tested one amputated person and, in the future, we want to test the device on more amputees after improving this prototype version. This study is, however, a first step in showing that this technique of TMG could also be used for the amputees.

One further limitation that we would like to address is the drift of the tactile bracelet, especially considering that it affected the experiment design with the necessity of retraining in between the 3 repetitions of the task reaching phase. Though hypothetically partially based on the elasticity of the skin, we suppose that the main part was coming from the bracelet itself and more specifically the foam that we used over the taxels. We tested several foams to counter this issue, including some harder foams bringing less drift but impairing the detection of the slight changes in the muscle pressure signature. However, we did not yet come to a satisfying definitive solution and are therefore investigating new innovative conductive materials.

6. CONCLUSION

In this study on 12 intact subjects, we demonstrated the feasibility of using a new technology called tactile myography for combined control of 2 combined DoFs in highly complex online TAC-test with simultaneous control of 3 DoFs (6 actions trained including rest), instead of the configuration of 2 DoFs, typically used in the literature. This control was achieved using simple ridge regression and an intuitive mapping. Performance degradation was however observed when including the power grasp into the combined movements. This limitation might yet be due to the tactile bracelet and further work on it will help us clear this point. In this study, we show that TMG is a viable alternative to EMG as a sensing device for gesture recognition. As a first step toward prosthesis control, we tested it on one amputee but the bracelet still needs improvements before further tests on more amputees are reasonable. TMG requires less electronics for the same resolution and is easily wearable, in comparison to the bulky EMG sensors, which additionally are prone to be influenced by sweating and muscle fatigue. For these reasons, TMG is a desirable alternative to the standard sEMG. On another note, by this experiment we show that despite non-linear algorithms being a solution to combined control over multiple DoFs, they might not be the optimal solution and a higher dimensionality of eventually different sensors could be a different path to follow that would be less cumbersome for the machine learning algorithm. Additionally, we proposed a feature selection method, selecting a lower number of sensors, that yields similar results than with the full set of sensors. We can reasonably argue that it could thus be a possible solution for embedding into a prosthesis, where power computation comes into play. Finally, we propose a set of combined motion limitations that can be re-used in similar experiments.

Future Work

In the future, further work has to be done to try to improve the tactile bracelet prototype by increasing its depth resolution and having it adapt to the conic shape of the stumps. Despite already several trials, the thickness and the rigidity of the foam are still not optimal and we are working on fixing these issues by replacing the foam with a different material. Further experiments could include a test on the number of sensors needed to achieve the control of untrained combined actions, as well as a TAC test with three combined actions — since the set of limits previously defined already includes 3-DOF combinations. Moreover, in the advent of deep learning and with the high density of the sensors that we here have, different algorithms could be tested on this bracelet (e.g., de Freitas et al., 2019). Finally, it would be interesting to compare TMG with HD-EMG in terms of single and combined actions.

One last remark about the limitations of the present study: The problem of upper-limb prosthetics is a paradigmatic multi-disciplinary issue and needs focus from such diverse fields as, e.g., material science for the socket, movement science for the ergonomy and physiology of the apparatus as a whole, mathematics and mechatronics for the device and the control systems, and statistics to measure the acceptance in the patient population. In this paper we have focused on a promising device and approach, which lets us foresee a more-than-sEMG myocontrol system embedded in a prosthetic socket. Of course, as already mentioned in, e.g., Cho et al. (2016), tactile myography is subject to different hurdles and problems as sEMG, and they need to be taken into account, too. Moreover, a careful study of further alternatives to tactile myography is required [a promising one being ultrasound A-mode scanning Yang et al. (2020)], as well as a study on how the limb-position effect Betthauser et al. (2018) affects it. In the end, extensive tests on the end-user population are necessary.

DATA AVAILABILITY STATEMENT

The datasets generated for this study are available on request to the corresponding author.

ETHICS STATEMENT

The studies involving human participants were reviewed and approved by Work Ethical Committee of DLR. The patients/participants provided their written informed consent to participate in this study. Written informed consent was obtained from the individual(s) for the publication of any potentially identifiable images or data included in this article.

AUTHOR CONTRIBUTIONS

Conceptualization, methodology, validation, and interpretation of data: CC and MC. System design: RK. Software design, formal analysis, and investigation: MC. Resources, supervision, project administration, and funding acquisition: CC. Writing—original draft, writing—review and editing: MC, RK, and CC. Visualization: MC and RK.

FUNDING

This work was partially supported by the German Research Society project TACT-Hand: improving control of prosthetic hands using tactile sensors and realistic machine learning, DFG Sachbeihilfe CA-1389/1-1.

ACKNOWLEDGMENTS

The authors thank Dr. Bernhard Weber of the DLR for his advice in the data analysis, as well as Christian Nissler for the C# version of the ROI gradient code. This work was partially supported by the German Research Society project *TACT-Hand: improving control of prosthetic hands using tactile sensors and realistic machine learning*, DFG Sachbeihilfe CA-1389/1-1, http://gepris.dfg.de/gepris/projekt/272314643?language=en.

SUPPLEMENTARY MATERIAL

The Supplementary Material for this article can be found online at: https://www.frontiersin.org/articles/10.3389/fnbot.2020.00011/full#supplementary-material

REFERENCES

Amsuss, S., Gobel, P., Graimann, B., and Farina, D. (2014). "Simultaneous, proportional wrist and hand control for natural, dexterous movements of a physical prosthesis by amputees," in *Proceedings of MEC Myoelectric Control Symposium* (New Brunswick, CA), 2–5.

Austin, N. M. (2005). "The wrist and hand complex," in *Joint Structure and Function: a Comprehensive Analysis*, eds P. K. Levangie and C. C. Norkin (Philadelphia, PA: F.A. Davis Co), 305–352.

Betthauser, J. L., Hunt, C. L., Osborn, L. E., Masters, M. R., Lvay, G., Kaliki, R. R., et al. (2018). Limb position tolerant pattern recognition for myoelectric prosthesis control with adaptive sparse representations from extreme learning. *IEEE Trans. Biomed. Eng.* 65, 770–778. doi: 10.1109/TBME.2017.2719400

Bhardwaj, P., Nayak, S. S., Kiswar, A. M., and Sabapathy, S. R. (2011). Effect of static wrist position on grip strength. *Indian J. Plastic Surg.* 44:55–58. doi: 10.4103/0970-0358.81440

Boschmann, A., and Platzner, M. (2014). "A computer vision-based approach to high density emg pattern recognition using structural similarity," in *Proceedings of MyoElectric Controls Symposium (MEC)* (New Brunswick, CA), 36–40.

Brand, P. W., and Hollister, A. (1999). *Clinical Mechanics of the Hand, Vol. 93* (St. Louis: Mosby).

Castellini, C., Artemiadis, P., Wininger, M., Ajoudani, A., Alimusaj, M., Bicchi, A., et al. (2014). Proceedings of the first workshop on peripheral machine interfaces: going beyond traditional surface electromyography. *Front. Neurorobot.* 8:22. doi: 10.3389/fnbot.2014.00022

Castellini, C., Kõiva, R., Pasluosta, C., Viegas, C., and Eskofier, B. M. (2018). Tactile myography: an off-line assessment on able-bodied subjects and one upper-limb amputee. *MDPI Technol.* 6:38. doi: 10.3390/technologies6020038

Castellini, C., Passig, G., and Zarka, E. (2012). Using ultrasound images of the forearm to predict finger positions. *IEEE Trans. Neural Syst. Rehabil. Eng.* 20, 788–797. doi: 10.1109/TNSRE.2012.2207916

Cho, E., Chen, R., Merhi, L.-K., Xiao, Z., Pousett, B., and Menon, C. (2016). Force myography to control robotic upper extremity prostheses: a feasibility study. *Front. Bioeng. Biotechnol.* 4:18. doi: 10.3389/fbioe.2016.00018

Claudon, L. (1998). Evaluation of grip force using electromyograms in isometric isotonic conditions. *Int. J. Occupat. Saf. Ergon.* 4, 169–184. doi: 10.1080/10803548.1998.11076388

Connan, M., Ruiz Ramírez, E., Vodermayer, B., and Castellini, C. (2016). Assessment of a wearable force- and electromyography device and comparison of the related signals for myocontrol. *Front. Neurorobot.* 10:17. doi: 10.3389/fnbot.2016.00017

Craelius, W. (2002). The bionic man: restoring mobility. *Science* 295, 1018–1021. doi: 10.1126/science.295.5557.1018

Curcie, D. J., Flint, J. A., and Craelius, W. (2001). Biomimetic finger control by filtering of distributed forelimb pressures. *IEEE Trans. Neural Syst. Rehabil. Eng.* 9, 69–75. doi: 10.1109/7333.918278

D'Avella, A., Saltiel, P., and Bizzi, E. (2003). Combinations of muscle synergies in the construction of a natural motor behavior. *Nat. Neurosci.* 6, 300–308. doi: 10.1038/nn1010

de Freitas, R. C., Alves, R., da Silva Filho, A. G., de Souza, R. E., Bezerra, B. L., and dos Santos, W. P. (2019). Electromyography-controlled car: A proof of concept based on surface electromyography, extreme learning machines and low-cost open hardware. *Computers Elect. Eng.* 73, 167–179. doi: 10.1016/j.compeleceng.2018.11.012

De Smet, L., Tirez, B., and Stappaerts, K. (1998). Effect of forearm rotation on grip strength. *Acta Orthop. Belg.*. 64, 360–362.

Dempsey, P. G., and Ayoub, M. M. (1996). The influence of gender, grasp type, pinch width and wrist position on sustained pinch strength. *Int. J. Industr. Ergon.* 17, 259–273. doi: 10.1016/0169-8141(94)00108-1

Duque, J., Masset, D., and Malchaire, J. (1995). Evaluation of handgrip force from EMG measurements. *Appl. Ergon.* 26, 61–66. doi: 10.1016/0003-6870(94)00003-H

Fang, Y., Hettiarachchi, N., Zhou, D., and Liu, H. (2015). Multi-modal sensing techniques for interfacing hand prostheses: A review. *IEEE Sens. J.* 15, 6065–6076. doi: 10.1109/JSEN.2015.2450211

Farina, D., Vujaklija, I., Sartori, M., Kapelner, T., Negro, F., Jiang, N., et al. (2017). Man/machine interface based on the discharge timings of spinal motor neurons after targeted muscle reinnervation. *Nat. Biomed. Eng.* 1:0025. doi: 10.1038/s41551-016-0025

Fong, P. W., and Ng, G. Y. (2001). Effect of wrist positioning on the repeatability and strength of power grip. *Am. J. Occupat. Therap.* 55, 212–216. doi: 10.5014/ajot.55.2.212

Fougner, A., Stavdahl, Ø., Kyberd, P. J., Losier, Y. G., and Parker, P. A. (2012). Control of upper limb prostheses: terminology and proportional myoelectric control - a review. *IEEE Trans. Neur. Syst. Rehab. Eng.* 20, 663–677. doi: 10.1109/TNSRE.2012.2196711

Hahne, J. M., Schweisfurth, M. A., Koppe, M., and Farina, D. (2018). Simultaneous control of multiple functions of bionic hand prostheses: performance and robustness in end users. *Sci. Robot.* 3:eaat3630. doi: 10.1126/scirobotics.aat3630

Halpern, C. A., and Fernandez, J. E. (1996). The effect of wrist and arm postures on peak pinch strength. *J. Hum. Ergol.* 25, 115–130. doi: 10.11183/jhe1972.25.115

Haralick, R. M., and Shapiro, L. G. (1992). *Computer and Robot vision* (Reading: Addison-wesley).

Harris, C. G., and Stephens, M. (1988). "A combined corner and edge detector," in *Alvey Vision Conference* (Citeseer), 10–5244.

Hoerl, A. E., and Kennard, R. W. (1970). Ridge regression: Biased estimation for nonorthogonal problems. *Technometrics* 12, 55–67.

Hume, M. C., Gellman, H., McKellop, H., and Brumfield, R. H. (1990). Functional range of motion of the joints of the hand. *J. Hand Surg.* 15, 240–243. doi: 10.1016/0363-5023(90)90102-W

Ison, M., Vujaklija, I., Whitsell, B., Farina, D., and Artemiadis, P. (2016). High-density electromyography and motor skill learning for robust long-term control of a 7-dof robot arm. *IEEE Trans. Neural Syst. Rehabil. Eng.* 24, 424–433. doi: 10.1109/TNSRE.2015.2417775

Jaquier, N., Connan, M., Castellini, C., and Calinon, S. (2017). Combining electro- and tactile myography to improve hand and wrist activity detection in prostheses. *MDPI Technol.* 5:64. doi: 10.3390/technologies5040064

Jiang, N., Dosen, S., Müller, K.-R., and Farina, D. (2012). Myoelectric control of artificial limbs - is there a need to change focus? *IEEE Signal. Process. Mag.* 29, 148–152. doi: 10.1109/MSP.2012.2203480

Jiang, N., Englehart, K. B., and Parker, P. A. (2009). Extracting simultaneous and proportional neural control information for multiple degree of freedom prostheses from the surface electromyographic signal. *IEEE Trans. Biomed. Eng.* 56, 1070–1080. doi: 10.1109/TBME.2008.2007967

Kattel, B. P., Fredericks, T. K., Fernandez, J. E., and Lee, D. C. (1996). The effect of upper-extremity posture on maximum grip strength. *Int. J. Industr. Ergon.* 18, 423–429. doi: 10.1016/0169-8141(95)00105-0

Kent, B. A., and Engeberg, E. D. (2011). "Biomimetic myoelectric control of a dexterous artificial hand for prosthetic applications," in *2011 IEEE International Conference on Robotics and Biomimetics* (IEEE), 1555–1560.

Kõiva, R., Riedenklau, E., Viegas, C., and Castellini, C. (2015). "Shape conformable high spatial resolution tactile bracelet for detecting hand and wrist activity," in *Proceedings of ICORR - International Conference on Rehabilitation Robotics*, 157–162. doi: 10.1109/ICORR.2015.7281192

Marley, R. J., and Wehrman, R. R. (1992). Grip strength as a function of forearm rotation and elbow posture. *Hum. Fact. Ergon. Soc. Ann. Meet.* 36, 791–795.

Merletti, R., Aventaggiato, M., Botter, A., Holobar, A., Marateb, H., and Vieira, T. M. (2010a). Advances in surface emg: recent progress in detection and processing techniques. *Crit. Rev. Biomed. Eng.* 38, 305–345. doi: 10.1615/critrevbiomedeng.v38.i4.10

Merletti, R., Botter, A., Cescon, C., Minetto, M. A., and Vieira, T. M. (2010b). Advances in surface emg: recent progress in clinical research applications. *Crit. Rev. Biomed. Eng.* 38:347–379. doi: 10.1615/critrevbiomedeng.v38.i4.20

Mogk, J. P. M., and Keir, P. J. (2003). The effects of posture on forearm muscle loading during gripping. *Ergonomics* 46, 956–975. doi: 10.1080/0014013031000107595

Muceli, S., Jiang, N., and Farina, D. (2014). Extracting signals robust to electrode number and shift for online simultaneous and proportional myoelectric control by factorization algorithms. *IEEE Trans. Neural Syste. Rehabil. Eng.* 22, 623–633. doi: 10.1109/TNSRE.2013.2282898

Mussa-Ivaldi, F. A., Giszter, S. F., and Bizzi, E. (1994). Linear combinations of primitives in vertebrate motor control. *Proc. Natl. Acad. Sci. U. S.A.* 91, 7534—7538.

Nagata, K., and Magatani, K. (2011). "Basic study on combined motion estimation using multichannel surface emg signals," in *Engineering in Medicine and Biology Society, EMBC, 2011 Annual International Conference of the IEEE* (Boston, MA: IEEE), 7865–7868.

Nissler, C., Connan, M., Nowak, M., and Castellini, C. (2017). "Online tactile myography for simultaneous and proportional hand and wrist myocontrol" in *Proceedings of MEC - Myoelectric Control Symposium* (New Brunswick, CA), 167–170. doi: 10.13140/RG.2.2.11230.54082

Nowak, M. (2014). *Simultaneous and proportional control of hand prostheses with multiple degrees of freedom: a new method of improving the training process* (Master's thesis). Technical University of Munich, Munich, Germany.

Nowak, M., Aretz, B., and Castellini, C. (2016). "Wrist and grasp myocontrol: online validation in a goal-reaching task," in *Proceedings of RO-MAN - IEEE International Symposium on Robot and Human Interactive Communication* (New York, NY), 132–137. doi: 10.1109/ROMAN.2016.7745101

Nowak, M., and Castellini, C. (2015). "Wrist and grasp myocontrol: simplifying the training phase," in *Proceedings of ICORR - International Conference on Rehabilitation Robotics* (Singapore), 339–344. doi: 10.1109/ICORR.2015.7281222

Nowak, M., and Castellini, C. (2016). The LET procedure for prosthetic myocontrol: towards multi-DOF control using single-DOF activations. *PLoS ONE* 11: e0161678. doi: 10.1371/journal.pone.0161678

Ortenzi, V., Tarantino, S., Castellini, C., and Cipriani, C. (2015). "Ultrasound imaging for hand prosthesis control: a comparative study of features and classification methods," in *Proceedings of ICORR - International Conference on Rehabilitation Robotics* (Singapore), 1–6. doi: 10.1109/ICORR.2015.7281166

Ortiz-Catalan, M., and Branemark, R. (2014). "A permanent, bidirectional, osseointegrated interface for the natural control of artificial limbs," in *Proceedings of Myoelectric Controls/Powered Prosthetics Symposium* (Fredericton, NB), 168.

Palmer, A., Werner, F., Murphy, D., and Glisson, R. (1985). Functional wrist motion: a biomechanical study. *J. Hand Surg.* 10, 39–46. doi: 10.1016/S0363-5023(85)80246-X

Parvatikar, V., and Mukkannavar, P. (2009). Comparative study of grip strength in different positions of shoulder and elbow with wrist in neutral and extension positions. *J. Exerc. Sci. Physiother.* 5, 67–75.

Radmand, A., Scheme, E., and Englehart, K. (2016). High-density force myography: a possible alternative for upper-limb prosthetic control. *J. Rehabil. Res. Dev.* 53, 443–456. doi: 10.1682/JRRD.2015.03.0041

Richards, L. G., Olson, B., and Palmiter-Thomas, P. (1996). How forearm position affects grip strength. *Am. J. Occupat. Therap.* 50, 133–138. doi: 10.5014/ajot.50.2.133

Russ, J. C. (1999). *The Image Processing Handbook, 3rd Edn.* Boca Raton, FL: CRC Press, Inc.

Ryu, J., Cooney, W. P., Askew, L. J., An, K.-N., and Chao, E. Y. (1991). Functional ranges of motion of the wrist joint. *J. Hand Surg.* 16, 409–419. doi: 10.1016/0363-5023(91)90006-W

Sierra González, D. and Castellini, C. (2013). A realistic implementation of ultrasound imaging as a human-machine interface for upper-limb amputees. *Front. Neurorobot.* 7:17. doi: 10.3389/fnbot.2013.00017

Simon, A. M., Hargrove, L. J., Lock, B. A., and Kuiken, T. A. (2011). Target achievement control test: Evaluating real-time myoelectric pattern recognition control of multifunctional upper-limb prostheses. *J. Rehabil. Res. Dev.* 48, 619–628. doi: 10.1682/JRRD.2010.08.0149

Terrell, R., and Purswell, J. L. (1976). The influence of forearm and wrist orientation on static grip strength as a design criterion for hand tools. *Proc. Hum. Fact. Ergon. Soc. Ann. Meet.* 20, 28–32. doi: 10.1177/154193127602000115

Yang, X., Yan, J., Chen, Z., Ding, H., and Liu, H. (2020). A proportional pattern recognition control scheme for wearable a-mode ultrasound sensing. *IEEE Trans. Indust. Electron.* 67, 800–808. doi: 10.1109/TIE.2019.2898614

Yatsenko, D., McDonnall, D., and Guillory, K. S. (2007). "Simultaneous, proportional, multi-axis prosthesis control using multichannel surface emg," in *2007 29th Annual International Conference of the IEEE Engineering in Medicine and Biology Society* (IEEE), 6133–6136.

Zellers, K. K., and Hallbeck, M. S. (1995). The effects of gender, wrist and forearm position on maximum isometric power grasp force, wrist force, and their interactions. *Proc. Hum. Fact. Ergon. Soc. Ann. Meet.* 39, 543–547.

Conflict of Interest: The authors declare that the research was conducted in the absence of any commercial or financial relationships that could be construed as a potential conflict of interest.

A.3 "Deep and Surface Sensor Modalities for Myo-intent Detection"

Authors Mathilde Connan, Bingbin Yu, Christian Gibas, Rainer Brück, Elsa Andrea Kirchner and Claudio Castellini

Conference Proceedings of Myoelectric Control Symposium (MEC)

Year 2022

Number of pages 4

Review Peer-reviewed

Abstract Electromyography is the gold-standard among sensors for prosthetic control. However, stable and reliable myocontrol remains an unsolved problem in the community. Amid improvements currently under investigation, one focuses on alternative or complementary sensors. In this study, we compare different techniques, recording surface and deep muscle activity. Ten subjects were involved in an experiment in which three different modalities were attached on their forearm: force myography, electro-impedance tomography and ultrasound. They were asked to perform wrist and grasp movements. For the first time, we evaluate and compare in an offline analysis these three different modalities while recording several hand gestures.

Author contributions Conceptualization; Methodology; Software Design; Test setup and conduction of user surveys; Data Curation; Formal Analysis; Validation; Visualization; Writing-original draft; Writing-review and editing.

Citation M. Connan, B. Yu, C. Gibas, R. Brück, E. A. Kirchner, and C. Castellini, "Deep and surface sensor modalities for myo-intent detection," in *Proceedings of MEC - Myoelectric Control Symposium*, 2022

DEEP AND SURFACE SENSOR MODALITIES FOR MYO-INTENT DETECTION

Mathilde Connan[1], Bingbin Yu[2,3], Christian Gibas[4], Rainer Brück[4],
Elsa Andrea Kirchner[3,5], Claudio Castellini[1,6]

[1]*German Aerospace Center (DLR), Institute of Robotics and Mechatronics, Wessling, Germany*
[2]*University of Bremen, Robotics Research Group, Bremen, Germany*
[3]*German Research Center for Artificial Intelligence (DFKI), Bremen, Germany*
[4]*University of Siegen, Medical Informatics and Microsystems Engineering, Siegen, Germany*
[5]*University of Duisburg, Institute of Medical Technology Systems, Duisburg, Germany*
[6]*Friedrich-Alexander University of Erlangen-Nuremberg, Artificial Intelligence in Biomedical Engineering, Erlangen, Germany*

ABSTRACT

Electromyography is the gold-standard among sensors for prosthetic control. However, stable and reliable myocontrol remains an unsolved problem in the community. Amid improvements currently under investigation, one focuses on alternative or complementary sensors. In this study, we compare different techniques, recording surface and deep muscle activity. Ten subjects were involved in an experiment in which three different modalities were attached on their forearm: force myography, electro-impedance tomography and ultrasound. They were asked to perform wrist and grasp movements. For the first time, we evaluate and compare in an offline analysis these three different modalities while recording several hand gestures.

INTRODUCTION

Although surface electromyography (sEMG) has been used for decades in myoelectric control, it is subject to several drawbacks, such as sweat, electrode shift, muscular fatigue, or cross-talk among others [1]. Possible alternatives are being investigated in order to potentially replace or complement sEMG. For instance, in [2], it was shown that force myography (FMG), which is based on the deformation of the forearm due to muscular contractions, provides a more stable signal compared to electromyography. Although there are of course still some steps to go before integration, FMG showed a higher separateness of clusters and a higher accuracy when compared to sEMG. However, both sEMG and FMG are *surface* techniques, meaning that they record information mostly from surface muscles. Indeed, even though FMG indirectly contains some information about deeper muscle activity, these two techniques are still considered surface modalities. Deeper acquisition sources could therefore potentially provide important missing information. For example, ultrasound (US) imaging has already been evaluated for myocontrol with positive results for single finger movements [3]. Another deep sensing modality has also gained interest in recent years due to the search for alternatives to sEMG: Electrical Impedance Tomography (EIT). In medical EIT, particularly for myocontrol of the hand, a certain number of electrodes are placed around the forearm and a micro non-invasive alternating current is applied to one of them while the others measure bioimpedance. This process is repeated by applying the current in each electrode, in turn, until completion of the circle. The collected measurements can be reconstructed into a tomographic image using a back-projection algorithm [4]. The technique has already shown that it can be used to discriminate different hand movements offline with good classification accuracy using a support vector machine algorithm [5] EIT has also been integrated in an armband together with sEMG [6].

In this paper, we describe an experiment comparing FMG, US and EIT and discuss their potential for myocontrol applications. Ten subjects were fitted with the three modalities simultaneously and asked to perform wrist and grasp movements. To the best of our knowledge, this is the first time these three modalities have been compared in an experiment. The results show that US is always within the first two best performing algorithms for each hand/wrist gesture.

MATERIALS AND METHODS

Experimental setup

The EIT system used in this experiment was developed by the University of Siegen [7]. It consists of 16 electrodes placed around the forearm and provides 256 raw values. Its output frequency was approximately 2.7Hz. Post-filtering and processing to reconstruct the tomographic image were performed using the EIDORS library [4].

FMG data were collected using a custom-made armband with a Velcro strap and 10 force sensitive resistors developed at DLR [2]. The data were filtered with a second-order Butterworth low-pass filter with a cut-off frequency of 1Hz and saved at 94.2Hz. FMG was preferred over EMG due to the potential interference with the EIT system, which would have injected microcurrents into the same area where the EMG sensors would have recorded electrical muscle activity.

The newly developed portable US system was developed by the Fraunhofer IBMT [8] and is one of the smallest systems available for ultrasound imaging, as the probe is flat and circular, unlike the normally bulky probes of medical systems. The 1161px by 162px B-mode displayed image was streamed into our software and stored at a frequency of approximately 5.1Hz. A bird's eye view of the experiment can be seen in Figure 1(A).

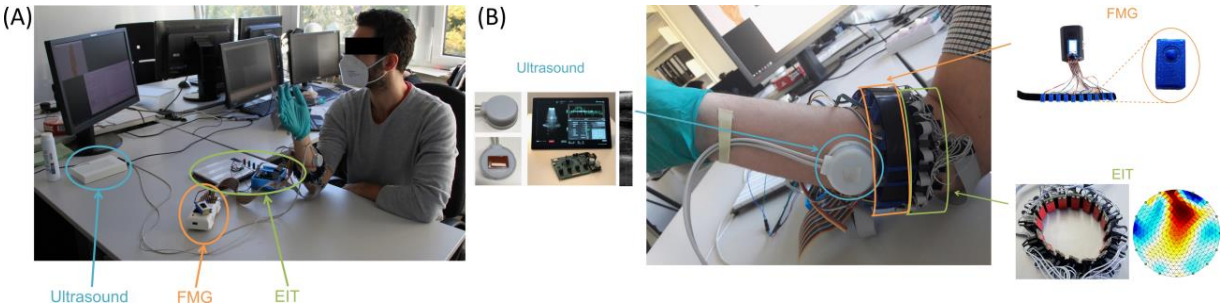

Figure 1: (A) Bird's eye view of the experiment. (B) Zoom on the modalities.

The three devices were placed in the following order from proximal to distal: EIT, FMG and US, as shown in Figure 1(B). Both the EIT and FMG systems were sending the data to our Interactive Myocontrol software via Bluetooth while the US device sent its data via USB.

Subjects and experimental protocol

Ten people (8 men, 2 women, 32.5 +/- 6.3 years old) took part in this experiment. Half of the subjects wore the sensors on their left arm, and the other half on their right arm. A sequence consisted of eight actions: rest, power, point, precision (tridigital), wrist flexion, wrist extension, wrist supination and wrist pronation. After a familiarisation phase, three repetitions of the sequence followed. All subjects signed an inform consent form and the experiment was previously approved by the DLR Work Ethical Committee.

The subjects sat in front of a table and placed their elbow on the table so that the arm was in line with the shoulder and the forearm formed an angle of about 90° to the upper arm, with the palm facing the side of the body. A 3D hand model on a screen indicated which hand movement had to be performed. For each action 2 seconds of data were recorded, with up and down phases lasting 1 second each and a further 2 seconds of non-captured rest between each action. For each subject and each repetition, the order of the actions was randomized.

Data analysis

The machine learning used for the analysis was Ridge Regression (RR), as it has the advantage with high-dimensional (HD) data that combined movements are possible without having to be trained, as was the case with HD-FMG [9]. The hyperparameters were evaluated for each subject using cross-validation.

For each modality, different feature selection methods were chosen for comparison. Each modality was rescaled between 0 and 1. The 255-feature vector of EIT data was compared with restored images from different reconstruction algorithms of the EIDORS library. The first two methods use a basic solver using unfiltered back-projection. This is one of the simplest algorithms for reconstructing an EIT image. The second method uses additional artificially

generated data compared to the first one. The third method is the Gauss-Newton approach with one-step iteration: it is the most commonly used for back projection in clinical and experimental publications. US data cannot be processed directly in the RR algorithm due to its size and must be reduced by feature selection algorithms. The first feature selection algorithm for US is Region of Interest Gradient (ROI-G) [10]. It has already been used successfully in experiments on US [11] and HD-FMG [9]. After some preliminary tests, a square of 40px with a step size of 30px was chosen as ROI. The other feature selection algorithms consisted of rescaling the matrices to a smaller size by selecting one row in *n* with *n* in {14, 20, 25, 30} as the different step sizes. For all methods, the features were amplified by a factor of 10 and filtered through a second-order Butterworth low-pass filter with a cut-off frequency of 1Hz.

In order to compare the accuracy of the individual feature selection method, the normalized root mean square error (nRMSE) was calculated. This was averaged across all subjects, using the first two repetitions as the training samples and the last repetition as the test set. We also performed a comparative analysis of cluster separability for each modality. For each subject and each cluster pair (C_i, C_j), we evaluated a numerical index called the Safety Index [11], which indicates how separated two clusters are in a given input space. The Safety Separateness Index of the clusters was calculated as follows: it is the ratio between the maximum standard deviation of cluster C_i (evaluated over all dimensions) and the Euclidean distance between cluster C_i and C_j, $s_{ij} = \frac{max(\sigma_i)}{||\overline{C_i} - \overline{C_j}||}$ where σ_i is the standard deviation of cluster C_i and $\overline{C}$ is the mean of cluster C. In addition, the average number of principal components to reach 99% of the variance of the input space was calculated across all subjects.

RESULTS

The nRMSE of RR for each modality was calculated action-wise as shown in Figure 2. The results were evaluated statistically across all actions using Friedman test for non-parametric data, showing that the nRMSE was statistically significantly different across the different modalities $X2(9) = 40.8$, $p < 0.0001$, with a moderate effect size $W=0.453$. The post-hoc Wilcoxon paired test could not conclude between which methods after the Holm correction for multiple comparisons.

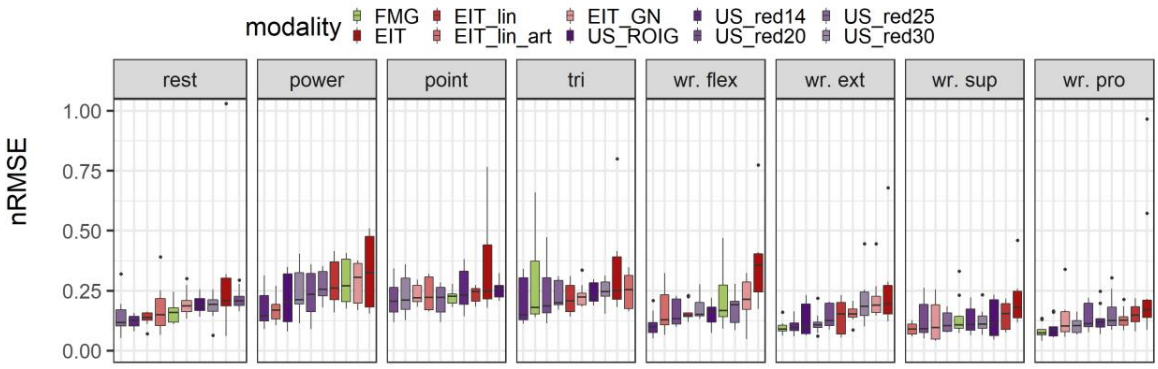

Figure 2: nRMSE on the three modalities and their respective feature selections: FMG in green, EIT in red, US in purple. The modalities are sorted in an increasing order of the median of nRMSE (best performing first) for each action.

The number of principal components (PCs) for reaching 99% of the variance of the input space was calculated for each subject and averaged for each modality in Table 1. This needs to be compared with the actual input space, i.e. the number of features, of each modality, which is also reported in the table.

Table 1: Number of features for each method. Average and standard deviation (SD) of the number of principal components in order to reach 99% of the variance. Separateness index (mean and SD) indicating the separateness of the clusters (the lower the better).

Modality	**EIT**	**EIT_GN**	**EIT_lin**	**EIT_lin_art**	**FMG**	**US_red14**	**US_red20**	**US_red25**	**US_red30**	**US_ROIG**
Number of features	256	740	740	740	10	996	531	329	234	348
Number of PCs (mean)	14.3	3.6	4.1	3.6	6.3	25.7	27.2	24.6	23	51.7
Number of PCs (SD)	2.9	0.7	1	0.7	0.8	6.4	6.5	5.8	5.5	7.4
Separateness index (mean)	0.495	0.098	0.089	0.093	0.181	0.067	0.1	0.111	0.126	0.143
Separateness index (SD)	0.341	0.034	0.025	0.03	0.05	0.015	0.039	0.025	0.029	0.023

The safety index to estimate the separateness of the clusters was evaluated and averaged across all subjects for each modality. Non-reconstructed EIT shows the lowest separability, while US rescaled every 14 rows shows the highest one.

DISCUSSION

Figure 2 shows that, despite no clear method standing out from the others, at least one feature selection algorithm from US is always in the top two according to nRMSE. FMG, with its 10 features, surprisingly performs better than the other algorithms for wrist extension and wrist pronation. The basic solver EIT_lin_art is the best performing for wrist supination. Comparing the number of principal components necessary to reach 99% of the input space, the US-related number of components are the highest ones, but generally exhibits a good cluster separateness index, especially the US_red14, which has the best separateness. Non-reconstructed EIT has the worst overall Safety Index. However, this could be explained by electrodes with high impedance that would negatively affect other measurements and that are filtered in the reconstruction algorithms. The EIT reconstruction algorithms have surprisingly a low number of PCs and better cluster separability than most of US methods. However, the fact that the number of PCs is lower than the number of gestures to be controlled could explain the generally lower nRMSE results compared to US and possibly indicate that important data is lost during reconstruction. This could also be due to the lower sampling rate of EIT.

Several feature selection algorithms were tested here on the different modalities. Unfortunately, none of them has yet been able to clearly outperform the others, with some modalities performing better than others for some movements. This might indicate that sensor fusion could be the ultimate solution. However, US was among the best performing methods according to nRMSE and to some extent cluster separateness index. Further feature selection algorithms should be evaluated to confirm this indication. In addition, the three modalities should be evaluated online and on amputees. However, due to the limited length of the stumps, it might be necessary to reduce the number of modalities to the two best performing ones.

ACKNOWLEDGEMENTS

We would like to thank all the subjects who participated in this experiment. This work was partially supported by the German Research Society project Deep-Hand (DFG Sachbeihilfe CA-1389/1-2).

REFERENCES

[1] J. R. Cram and G. S. Kasman, “Cram's Introduction To Surface Electromyography,” 2nd editio ed., Jones and Bartlett Publishers, 2010, p. 1–163.

[2] M. Connan, E. R. Ramírez, B. Vodermayer and C. Castellini, “Assessment of a Wearable Force- and Electromyography Device and Comparison of the Related Signals for Myocontrol,” *Frontiers in Neurorobotics,* vol. 10, p. 1–13, November 2016.

[3] M. Sagardia, K. Hertkorn, D. Sierra González and C. Castellini, “Ultrapiano: A Novel Human-Machine Interface Applied to Virtual Reality,” in *Proceedings of {ICRA} - International Conference on Robotics and Automation*, 2014.

[4] A. Adler and W. R. B. Lionheart, “Uses and abuses of EIDORS: an extensible software base for EIT,” *Physiological measurement,* vol. 27, p. S25, 2006.

[5] Y. Zhang and C. Harrison, “Tomo: Wearable, low-cost electrical impedance tomography for hand gesture recognition,” in *Proceedings of the 28th Annual ACM Symposium on User Interface Software & Technology*, 2015.

[6] A. Briko, V. Kapravchuk, A. Kobelev, A. Hammoud, S. Leonhardt, C. Ngo, Y. Gulyaev and S. Shchukin, “A Way of Bionic Control Based on EI, EMG, and FMG Signals,” *Sensors,* vol. 22, p. 152, 2022.

[7] C. Gibas, A. Grünewald, S. Büchner and R. Brück, “An EIT system for mobile medical diagnostics,” in *Medical Imaging 2018: Biomedical Applications in Molecular, Structural, and Functional Imaging*, 2018.

[8] M. Fournelle, T. Grün, D. Speicher, S. Weber, M. Yilmaz, D. Schoeb, A. Miernik, G. Reis, S. Tretbar and H. Hewener, “Portable Ultrasound Research System for Use in Automated Bladder Monitoring with Machine-Learning-Based Segmentation,” *Sensors,* vol. 21, p. 6481, 2021.

[9] M. Connan, R. Kõiva and C. Castellini, “Online natural myocontrol of combined hand and wrist actions using tactile myography and the biomechanics of grasping,” *Frontiers in Neurorobotics,* vol. 14, p. 1–16, 2020.

[10] R. M. Haralick and L. G. Shapiro, “Computer and Robot Vision, vol. 1, Addison-Welsey,” *Reading, Mass, USA,* 1992.

[11] D. Sierra González and C. Castellini, “A realistic implementation of ultrasound imaging as a human-machine interface for upper-limb amputees,” *Frontiers in Neurorobotics,* vol. 7, p. 1–11, October 2013.

A.4 "Learning to Teleoperate an Upper-limb Assistive Humanoid Robot for Bimanual Daily-living Tasks"

Authors Mathilde Connan, Marek Sierotowicz, Bernd Henze, Oliver Porges, Alin Albu-Schäffer, Máximo A. Roa and Claudio Castellini

Journal Biomedical Physics & Engineering Express

Year 2021

Number of pages 18 (main article) + 5 (supplementary)

Review Peer-reviewed

Abstract *Objective.* Bimanual humanoid platforms for home assistance are nowadays available, both as academic prototypes and commercially. Although they are usually thought of as daily helpers for nondisabled users, their ability to move around, together with their dexterity, makes them ideal assistive devices for upper-limb disabled persons, too. Indeed, teleoperating a bimanual robotic platform via muscle activation could revolutionize the way stroke survivors, amputees and patients with spinal injuries solve their daily home chores. Moreover, with respect to direct prosthetic control, teleoperation has the advantage of freeing the user from the burden of the prosthesis itself, overpassing several limitations regarding size, weight, or integration, and thus enables a much higher level of functionality. *Approach.* In this study, nine participants, two of whom suffer from severe upper-limb disabilities, teleoperated a humanoid assistive platform, performing complex bimanual tasks requiring high precision and bilateral arm/hand coordination, simulating home/office chores. A wearable body posture tracker was used for position control of the robotic torso and arms, while interactive machine learning applied to electromyography of the forearms helped the robot to build an increasingly accurate model of the participant's intent over time. *Main results.* All participants, irrespective of their disability, were uniformly able to perform the demanded tasks. Completion times, subjective evaluation scores, as well as energy- and time- efficiency show improvement over time on short and long term. *Significance.* This is the first time a hybrid setup, involving myoeletric and inertial measurements, is used by disabled people to teleoperate a bimanual humanoid robot. The proposed setup, taking advantage of interactive machine learning, is simple, non-invasive, and offers a new assistive solution for disabled people in their home environment. Additionally, it has the potential of being used in several other applications in which fine humanoid robot control is required.

Author contributions Conceptualization; Data Curation; Formal Analysis; Investigation; Methodology; Supervision; Validation; Visualization; Writing-original draft; Writing-review and editing.

Video & Supplementary Material https://stacks.iop.org/BPEX/8/015022/mmedia

Citation M. Connan, M. Sierotowicz, B. Henze, O. Porges, A. Albu-Schäffer, M. A. Roa, and C. Castellini, "Learning to teleoperate an upper-limb assistive humanoid robot for bimanual daily-living tasks," *Biomedical Physics & Engineering Express*, vol. 8, no. 1, pp. 1–17, dec 2021, doi: 10.1088/2057-1976/ac3881

IOP Publishing Biomedical Physics & Engineering Express
Biomed. Phys. Eng. Express **8** (2022) 015022 https://doi.org/10.1088/2057-1976/ac3881

Learning to teleoperate an upper-limb assistive humanoid robot for bimanual daily-living tasks

Mathilde Connan[1], Marek Sierotowicz[1], Bernd Henze[1], Oliver Porges[1], Alin Albu-Schäffer[1], Máximo A. Roa[1], Claudio Castellini[1]

[1] *Institute of Robotics and Mechatronics, German Aerospace Center (DLR), Wessling, Germany.*

E-mail: mathilde.connan@dlr.de

Received 3 August 2021
Accepted for publication 10 November 2021
Published 16 December 2021

Abstract

Objective. Bimanual humanoid platforms for home assistance are nowadays available, both as academic prototypes and commercially. Although they are usually thought of as daily helpers for non-disabled users, their ability to move around, together with their dexterity, makes them ideal assistive devices for upper-limb disabled persons, too. Indeed, teleoperating a bimanual robotic platform via muscle activation could revolutionize the way stroke survivors, amputees and patients with spinal injuries solve their daily home chores. Moreover, with respect to direct prosthetic control, teleoperation has the advantage of freeing the user from the burden of the prosthesis itself, overpassing several limitations regarding size, weight, or integration, and thus enables a much higher level of functionality. *Approach.* In this study, nine participants, two of whom suffer from severe upper-limb disabilities, teleoperated a humanoid assistive platform, performing complex bimanual tasks requiring high precision and bilateral arm/hand coordination, simulating home/office chores. A wearable body posture tracker was used for position control of the robotic torso and arms, while interactive machine learning applied to electromyography of the forearms helped the robot to build an increasingly accurate model of the participant's intent over time. *Main results.* All participants, irrespective of their disability, were uniformly able to perform the demanded tasks. Completion times, subjective evaluation scores, as well as energy- and time- efficiency show improvement over time on short and long term. *Significance.* This is the first time a hybrid setup, involving myoeletric and inertial measurements, is used by disabled people to teleoperate a bimanual humanoid robot. The proposed setup, taking advantage of interactive machine learning, is simple, non-invasive, and offers a new assistive solution for disabled people in their home environment. Additionnally, it has the potential of being used in several other applications in which fine humanoid robot control is required.

Keywords: assistive robotics, bimanual tasks, daily-living activities, teleoperation, humanoid robotics, myocontrol, human-machine interaction

1. Introduction

The world around us is shaped to be operated by arms and hands [1]. The loss or impairment of the upper limb leads therefore to a dramatic degradation in the quality of living [2, 3]. A person with an upper-limb disability is prevented from swiftly acting in the world since state-of-the-art prosthetic or assistive solutions cannot usually operate more than one degree of freedom (DoF), or if they can, this happens, in most cases, sequentially, one motion at a time [3]. After an

amputation, however, surprisingly rich residual muscle activity can still be detected from the surface of the residual limb using, e.g., surface electromyography (sEMG) [4]. In controlled conditions, amputees can produce several discernible signal patterns corresponding to the actions intended to be performed with the absent limb [5]. But so far, such techniques have shown little generalization power across participants and when used in practical environments. This is largely due to signal variability, for example when lifting weights or changing body posture [6], as the registered hand gesture patterns are no longer recognized by the machine learning algorithm in these cases. The problem becomes even more complex whenever the device is supposed to help the participant to operate in unstructured home environments while performing complex tasks such as daily-living chores.

So, whereas most research on using and decoding sEMG signals (myocontrol) for assisting impaired patients is naturally focused on controlling prosthetic devices [7, 8], in this work we tackle a new application, using myocontrol to teleoperate a humanoid robot performing bimanual manipulation tasks in a household environment. There are several reasons behind this idea:

i) Service humanoid robots are thought of as flexible and dexterous assistants for elderly or disabled people. Several dual-arm collaborative robots exist in this context [9]. Freed of the manufacturing constraints of prostheses (weight, size, space, etc.), they can be equipped with much more complex electronics, allowing better reaching and manipulation capabilities than current prosthetic arms.

ii) At the same time, the separation of the manipulation device from the participant avoids the hurdles posed by the typical prosthetic system: excessive weight [10] and heat, bad adherence to the skin, low biocompatibility, etc.

iii) To a large extent, teleoperation is irrespective of distances, meaning that the proposed approach could be used for remote maintenance or search-and-rescue tasks as well. Additionally it could provide disabled users with a possibility of teleworking [11].

iv) Lastly, such a setup allows direct comparison of non-disabled and disabled participants using exactly the same hardware, which has not been the case so far as non-disabled participants used bypass sockets [12], while impaired participants used their prosthesis shaft. Hence, the current setup allows to see how close the performance of impaired patients is to that of the non-impaired participants.

The reliability of myocontrol in unstructured environments can be greatly improved using incremental machine learning (iML) [13, 14], i.e., an algorithm that can accommodate for new knowledge on the fly. Degris et. al. [15] have explored the usage of reinforcement learning in the context of participant/prosthesis interaction. In such approaches, a "lazy" data-gathering strategy is enforced, actively recruiting the participant to update the intent-detection model whenever it becomes unstable and/or new patterns (i.e. actions) are required. In [16], the interaction between the participant and a simulated prosthetic system is studied from a psychological point of view in order to maximize the quality of the data produced by the participant. This methodology heavily relies on a carefully designed protocol to involve the participant in an *action / model building / action loop*. Whether this idea works in practice, however, is still controversial [1].

In order to verify the effectiveness of the proposed framework, we have designed an experiment in which participants teleoperated a dexterous assistive humanoid platform using two commercially available sEMG bracelets and a body posture detection device based upon inertial measurement units [17]. iML was employed to account for and correct instabilities of the intent detection system. The trained model was updated whenever the participant deemed the task to be unattainable. Simple verbal feedback with the experimenter was used to ascertain that an update was required. The tasks to be performed consisted of complex daily-living activities resembling kitchen and office chores involving bimanual coordination, such as unscrewing a bottle, dialing numbers on a phone and manipulating a pot and its lid.

As it is well known that, due to the plasticity of the human brain [18], the more a person repeats a task the more she/he learns and improves in performing it. This has already been shown in [19, 20], in which sEMG was used for teleoperating unimanual tasks. In [20], 8 subjects performed one task, with 4 repetitions and 2 sessions over 2 days. The learning, evaluated with TCTs and path efficiency, was visible over the repetitions and continued over the sessions. [19] shows that, even after a week of non-practicing, the learning regresses only slightly. In our case, we have wondered if disabled participants would achieve similar performance levels when compared to non-disabled participants after several repetitions of teleoperated tasks. We hypothesized that such a teleoperation setup and the associated protocol would enable participants to complete all tasks, and that a learning effect would be recognizable, leading, in the end, to uniform results across disabled and non-disabled participants. We also speculated that the performance of disabled participants would not differ statistically from that of non-disabled ones. The experimental results confirm that all participants were able to quickly and efficiently learn to teleoperate the platform and successfully complete all tasks, and that a learning effect was clearly visible, speeding up the execution of the tasks, increasing the efficiency and decreasing energy consumption over time. Learning was uniform across seven non-disabled participants and two upper-limb disabled persons. One disabled participant was born with right-hand trans-radial congenital deficiency and the second participant had bilateral trans-radial traumatic amputation. The learning effect was even stronger in the case of a single non-disabled participant who repeated the same full set of tasks for five consecutive days.

2. Materials and Methods

2.1. Participants

Seven able-bodied (all males, aged 28.4±7.1 years) and two disabled participants were involved in this experiment (cf. **Table S1**): one congenitally missing his right hand (D1) and the other one having been double-amputated (D2) following a trauma (more details about them are described in **Table S2**). All participants were evaluated over a single session and one of the non-disabled participants repeated the experiment over 5 days.

The experimental protocol was thoroughly explained to the participants before the experiment, and each of them signed a written informed consent form. The experiment was performed according to the WMA Declaration of Helsinki and was approved by the Work Ethical Committee of DLR.

2.2. Protocol of the experiment

The participants were asked to teleoperate the humanoid robot TORO [21] with the goal of performing complex bimanual tasks. In order to do so, the participants were equipped with an IMU-based body tracking device for controlling the arms and torso of the robot [17], and with two Myo-armbands from Thalmic Labs[1], recording the EMG data of the forearm muscles to control the robot's hands, and additionally the wrist(s) in the case of the disabled participants.

TABLE 1
DESCRIPTION OF THE TASKS

Task ID	Summary of the task	Detailed description of the task
1a	Take the lid off the pot and place it on the table.	Take the pot handle with the right hand. With the left hand, take the lid off the pot and place it on the table at place 2.
1b	Take an orange ball and put it in the pot.	With the left hand, take the foam ball from place 3 and place it in the pan. Take the pot's lid from place 2 and put it back on the pot in place 1.
2a	Unscrew the cap of the bottle	With the right hand, take the bottle from place 1, lift it, rotate it about 45° and with the left hand, unscrew the cap.
2b	Pour the bottle's contents into the open pot.	With the left hand, take the pot handle. With the right hand, simulate pouring the contents of the bottle into the pot by rotating the wrist. (The bottle is filled with pebbles blocked at the opening with a foam to avoid dangerous spreading in case of task failure) Place back the bottle at place 1.
3	Type numbers on a fixed phone.	With the left hand, with a pointing index, type on the buttons 9, 1, 1. With the right hand, with a pointing index, press on loud speaker.

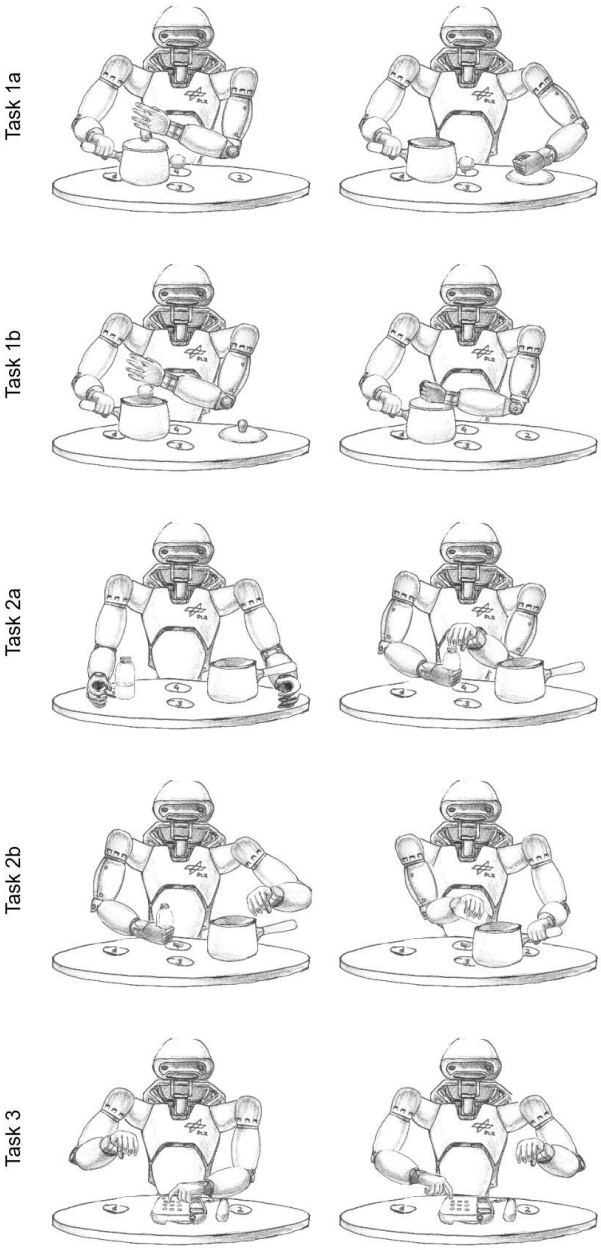

Figure 1. Illustration of the tasks to execute with the assistive robot.

Seven participants performed the experiment, each one in a single session. Additionally, to further investigate the learning effect, one participant was randomly selected from the pool of single-session participants to perform the experiment on 4 additional days for a total of 5 sessions.

The experiment consisted of three tasks, the first two tasks being divided each in two subtasks. These tasks are inspired by those found in assessment protocol for prosthetics users such as the Assessment of Capacity for Myoelectric Control

[1] previously available at www.thalmic.com

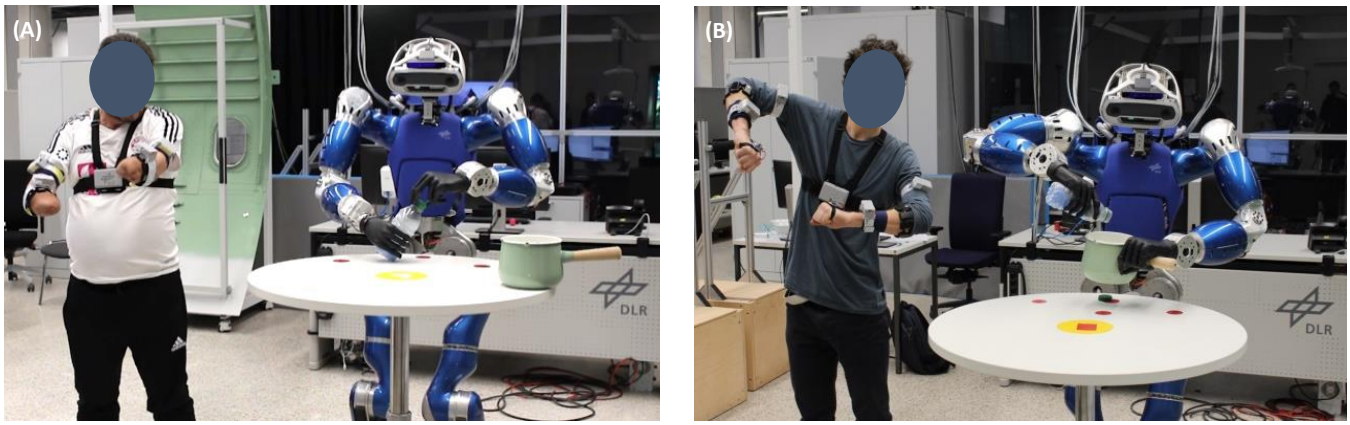

Figure 2. Bird-eye view of the experiment. (A) The double-sided amputee opening a bottle's cap (Task 2A). **(B)** One of the non-disabled participants pouring a bottle's content into a pot (Task 2B).

(ACMC) [22] and from the Chedoke Arm and Hand Activity Inventory (CAHAI) [23, 24], a validated upper-arm functional assessment for stroke recovery, already used in teleoperation experiments [25, 26]. The tasks are explained in detail in **Table 1** and illustrated in **Figure 1**. For the single-session participants, each task had to be repeated four times: the subtasks had to be completed separately before starting a new repetition. As we considered the very first repetition as a familiarization phase, the long-term participant had to perform only three repetitions of the tasks on the remaining days of the experiment after his first session. The familiarization phase was however still kept in the analysis, as it is considered an important phase for the learning effect.

During the experiment, the participants were placed on the right side of the robot at a proper distance from it for safety reasons but so that the table setup was clearly visible to them in order to accomplish the tasks. A bird-eye view of the experiment is shown in **Figures 2A** and **2B**.

Before the first execution of each subtask, the participant was instructed by the experimenter on how to perform that specific subtask. A task was considered as failed by the experimenters if one of the objects fell from the table, if the participant could not retrieve an object, or if it was estimated by the experimenter that the participant could not regain a correct setting of the objects to complete the task. If such a case happened, the teleoperation mode was suspended and the objects would be set back to the initial task setting by the experimenters before the participant could start a new attempt. The participants were not restricted in the number of attempts per repetition. A repetition was considered as completed once the participant achieved the task. Subtasks were achievable separately, meaning, for example, that the participant did not need to restart from task 1a if task 1b failed. A participant could decide to pause or stop the experiment at any moment. If there was a failure from a device, this was also considered as a failed attempt, as the longer the participant took to complete a task, the higher the risk was that a system failure happened. Additionally, if the prediction of the hand action was judged too unstable to perform a task, this was also considered as a failed attempt and the experimenter could decide to collect more samples to train the hand action predictor.

The tasks were performed in the order presented in **Table 1**, except for D2, where, due to a time limitation, and to make sure as many tasks as possible would be completed in this limited time, the experimenters had the participant perform Task 3 before Task 2 as it was considered a shorter task. At the end of the session, the participants were asked to complete a subjective assessment form. Participant D2 was unfortunately not able to complete this form due to a time limitation. The questionnaire was based on the NASA TLX test [27] and different factors were evaluated by the participants on a scale from 0 to 20: mental demand, physical demand, temporal demand, performance, effort and frustration (cf. Supplementary Materials for definitions). When averaging over all criteria, it was decided to transform the only positive criteria 'performance' into a negative one by subtracting the evaluated score to the maximum value of 20 in order to get a global negative index.

As a side note, since the tasks were very different and not designed to be achieved in the same amount of time, we did not compare the TCTs task-wise.

For this experiment, we evaluate the Task Completion Times (TCTs) for each task, the subjective evaluation concordance, the travelled path and the speed of motion for all participants.

2.3. Setup of the teleoperation equipment

The IMU-based upper body tracker system, also called BodyRig [17], was used for transmitting the position and orientation of the participant's hands. It uses the absolute orientation in space of the participant's body segments, gathered via IMUs, to compute the forward kinematics of the participant's body up to the level of the hand using a set of pre-defined link lengths. The difference between these lengths and the link lengths of the participant's actual skeletal frame

causes a divergence between the actual absolute position of the participant's hands and the ones measured by the BodyRig. This factor does not influence the measured orientation of the body segments. A problem, which occurred because of this, is, e.g., the user trying to join the robot's hands, but not being able to, due to their own limbs colliding with each other, while the robot's hands are still separated. This was fixed by introducing translational offsets, which could be adjusted on the fly, that were applied to the commanded pose as transmitted from the BodyRig.

The desired hand pose was computed by a hand movement intention predictor. The predictor utilizes EMG as input, as measured by the two Thalmic Lab's Myo sensors. The setup is depicted in **Figure S1A** of the Supplementary Materials (SM) and uses computers to process the data between the BodyRig and the humanoid robot. The sEMG sensors were sampled at a frequency of 200Hz and filtered through a low-pass 1st order Butterworth filter with 2Hz cut-off frequency, while the BodyRig was sampled at 500Hz and filtered through a low-pass 2nd order Butterworth filter with 5Hz cut-off frequency. The main reason for the relatively low cut-off frequencies is that the participants were directed to perform slow and steady movements, which should allow considering any signal with components of higher frequencies as noise, both on the sEMG and on the BodyRig measurements. In the case of non-disabled participants, IMUs were fitted on chest, humeri, forearms and hands (cf. **Figure S1B** in SM), which allows for direct transmission of the participant's hands' pose and orientation. In the case of amputated participants, it was not possible to fit an IMU directly on the hand, and therefore no direct measurement of the wrist angles was possible. In these cases, the hand movement predictor, trained accordingly, transmitted the desired wrist flexion. For the wrist pronation/supination, the desired angle was measured based on the orientation of the corresponding humerus and forearm IMUs. The relevant vectors are shown in **Figure S1C** in SM. The measured pronation/supination angle θ_{radial} was then multiplied by a magnifying factor and an offset was added so as to guarantee reachability of all operationally necessary hand poses by the participant. These factors were set during a calibration procedure at the beginning of the session and at later points, if the need arose.

2.4. Hand movement intention predictor training protocol

The hand movement intention was predicted by a ridge regressor with a Random Fourier Feature-based Kernel [28, 29]. This characteristic typically guarantees better accuracy, but makes the prediction non-linear with respect to the sEMG samples. Due to this, any hand pose given by the combination of two or more actions had to be separately sampled. For example, if a power grasp with flexed wrist was required to complete a task, it was necessary to create a new target vector (for example power flexed in addition to a normal power grasp) and train the predictor with samples corresponding to this specific position. Using a simple ridge regressor, on the other hand, it is sometimes possible to combine target vectors such as wrist movement and a hand grasp to obtain the combination of the two, provided that a high enough number of sensors is available [30], which was not the case here. It has to be noted that commercially available systems (COAPT and Ottobock) also use machine learning allowing multi-DoF control of upper-limb prostheses.

In the case of non-disabled participants, the hand movement intention predictor was trained on samples for all required hand poses (namely rest, power grasp and pointing), while the desired pose wrist was measured directly based on an IMU coupled to the user's hand.

In the case of amputees, the hand movement intention predictor was required to estimate the desired wrist pose as well, as it was not possible to monitor the desired wrist angles by coupling an IMU to the participant's hand. Therefore, the total number of required hand poses was larger, and accordingly the protocol for the disabled participants was to train the predictor on samples corresponding to only the hand poses specifically needed for the current task. These were defined as shown in **Table S3**.

For the case of the unilateral amputee (D1), the predictor was trained only for the missing right hand, while the wrist pose for the healthy limb was transmitted based on the data of the IMU coupled to the hand, like in the case of non-disabled participants. For D1, as a congenital amputee, a non-intuitive control mapping was applied, which consists in using the signals generated by a group of muscles initially not targeted to produce a specific hand action, to actually control the robotic hand's equivalent pose. For D2, the same mapping was used for the pointing gesture in different wrist positions, as the intuitive signal patterns that D2 was able to produce were too similar to each other.

In all cases, the experimenter could add new samples if the prediction was too unstable, with particular focus on samples acquired with the participant in the specific body poses in which the prediction seemed most unstable. These new samples were acquired in 1 to 2 minutes and this time was not considered in the overall completion times, which were based on the cumulative TCTs for successful and unsuccessful trials. The participants were actively requested to indicate if they thought an update was required. At the beginning of each session, EMG was sampled in two body poses, in order to generalize the prediction over the limb position effect. Typically, each hand pose was sampled twice at session start, with the user holding their arms bent at about 90 degrees, respectively with the elbows in contact with the trunk, and with the elbows held outwards from the body.

2.5. Setup of the humanoid robot

In order to perform the teleoperated bimanual tasks, the test

participant controlled the humanoid robot TORO. This robot was developed by the German Aerospace Center (DLR) for conducting research on walking and multi-contact balancing. A detailed description of the system architecture can be found in [31, 32, 21]. TORO has a height of 1.74 m, and a weight of 76.4 kg. It features 39 DoFs in total. The legs, arms, and hip contain 25 joints that are based on the technology of the DLR-KUKA LBR (Lightweight robot arm), and can be operated both in position and torque-controlled mode [33]. The neck comprises two DoFs, which are locked at all times during the session, as they are not used for conducting the presented experiments. The robot is also equipped with two prosthetic hands from Touch Bionics (i-Limb Ultra Revolution), each hand providing six DoFs, five for individually flexing each finger and one for rotating the thumb. In terms of sensing, the robot features a position and torque sensor in each of the 25 joints based on the LBR. Besides, the ankles are equipped with force-torque sensors to measure the contact forces and torques at the feet. The chest carries an IMU for obtaining the orientation and angular velocity of the torso.

The participant's intention and motion were captured using the equipment above described. The commands of the participant were summarized as desired poses for each hand's frame of reference. Those poses were transmitted via Wi-Fi to the control system of the robot. The architecture of the control framework [34] for the robot (**Figure S1D** in SM) can be summarized as follows: i) In order to maintain balance, the location of the Center of Mass (CoM) and the orientation of the hip are stabilized via a Cartesian compliance in a predefined configuration. ii) The hands are also governed by Cartesian compliance, and their set points (desired poses) are commanded by the operator. iii) The resulting forces required at the CoM (to keep the balance) and at the hands (to perform the desired task) are used as input to compute the required forces at the feet to fulfill both goals (keeping the balance and performing the task). This is achieved via a constrained quadratic optimization problem [34]. iv) As a last step, the computed forces are mapped to the joint torques, which are then commanded to the robot.

To perform the experiments, the humanoid robot TORO was autonomously keeping the balance using suitable forces at the feet, while the hands were free to perform the commanded manipulation tasks. The balance of the robot was ensured via a passivity-based, whole-body control framework [34]. One of the advantages of this control framework is that it enables a compliant and robust behavior, which is crucial for operating the humanoid robot in environments with uncertainties, such as the presented teleoperation scenario. Furthermore, it allows the operator to safely stand close to the robot to get a better view on the manipulation task at hand.

2.6. Statistical methods

We performed a linear mixed effect regression (LMER) analysis over all tasks, using the R package lme4 [35], with log(*var*), to normalize the data, with *var* being respectively the TCT, speed or travelled distance (sumdist), as the dependent variable, the repetition and the amputation condition as independent variables, and participants and tasks as random effects to adapt to the different initial skill level of each participant and the different difficulties of the tasks. The distributions of the residuals were not statistically different from the normal distribution according to Shapiro-Wilk and Jarque-Bera tests. One-way analysis of variance and Tukey's multiple-comparison test were used to analyze the data ($P<.05$). Notice that a slightly different protocol is used for the disabled participants to consider their amputation. For the long-term subject, we only analyzed the data on a descriptive level as the data were not independent due to the learning effect.

3. Results

The participants had five daily-living tasks to accomplish by teleoperating a humanoid platform while their movements and TCTs were registered. The five tasks, which are described more in detail in **Figure 1** and **Table 1**, can be summarized as follows: opening a pot, placing a ball inside the pot and closing

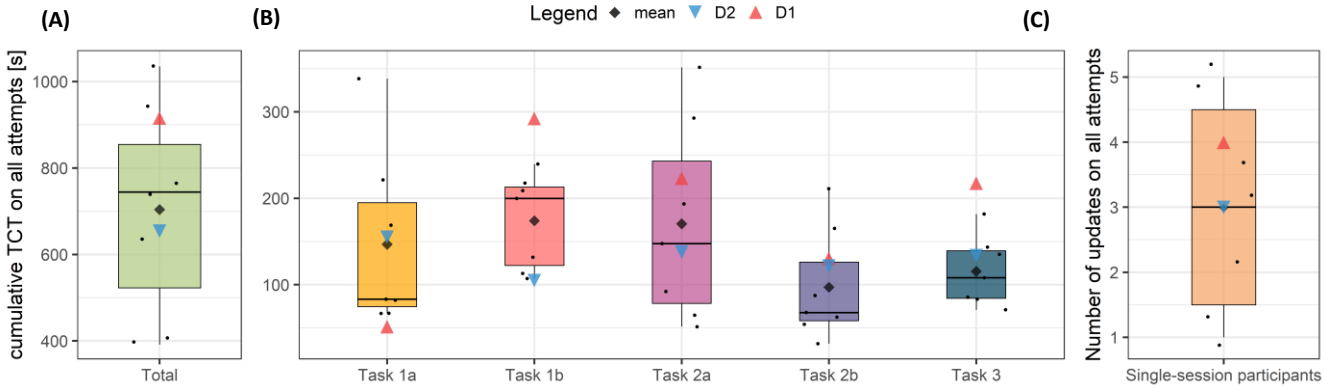

Figure 3. Results of the study on all attempts averaged over the four repetitions. Points indicate the values for each participant. The box limits represent the interquartile range. Error bars indicate 25th and 75th percentile. The bold line represents the median. **(A)** The total task completion time (TCT) on all attempts of all tasks with an average over the 4 repetitions is shown. **(B)** The averaged TCT over the 4 repetitions is shown for each task. **(C)** Number of updates of the iML model during the session, in addition to the initial training.

it, opening a bottle, pouring the content of the bottle, pressing a sequence of buttons on a phone. All details about the design and protocol including the tasks, metrics, setup, and statistical analysis of this experiment can be found in the Materials and Methods section. In the following subsections, we evaluate the TCTs for each task, the subjective evaluation concordance, and the path efficiency for the single-session participants, including disabled participants, and for the long-term participant. In order to better describe the experimental protocol, a video clip in the Supplementary Materials shows exemplary runs of the study with non-disabled participants, as well as with D1 and D2.

3.1. Quantitative evaluation: uniform Task Completion Times

All participants successfully completed all tasks (**Figure 3B**), albeit in some cases the successful attempt (defined in the protocol part of the Materials and Methods section) was preceded by a few failed ones. On average, 1.6 attempts were required to successfully complete each task for the non-disabled participants, 1.95 for D1 and 1.32 for D2 (**Figure 3C**). Total TCTs for all tasks averaged over the 4 repetitions ranged from 392s to 1035s (**Figure 3A**) and the total TCTs of the disabled participants, namely 916s and 655s for D1 and D2 respectively, are comparable to the ones of the non-disabled participants, which averages at 704s. Although in some cases a disabled participant needed more time than the others, e.g., D1 in Task 3, the opposite case also appears, e.g., Task 1a, which D1 accomplished with the shortest TCT of all. D2 also achieved results comparable to the others, with an average TCT for all tasks (131s) slightly better than the mean TCT of non-disabled participants (141s). D1, who has an overall average TCT of 183s, is still comparable to the non-disabled participants. Notice that D1 and D2 obviously used a slightly different setup and protocol to control the robotic wrist (see Materials and Methods for more details). All participants were actively requested to update the intent-detection model whenever it became instable or new patterns were required. The number of updates required per session is visible in **Figure 3C**. On average, during the session, 3 updates were required, ranging from 1 to 5 across the

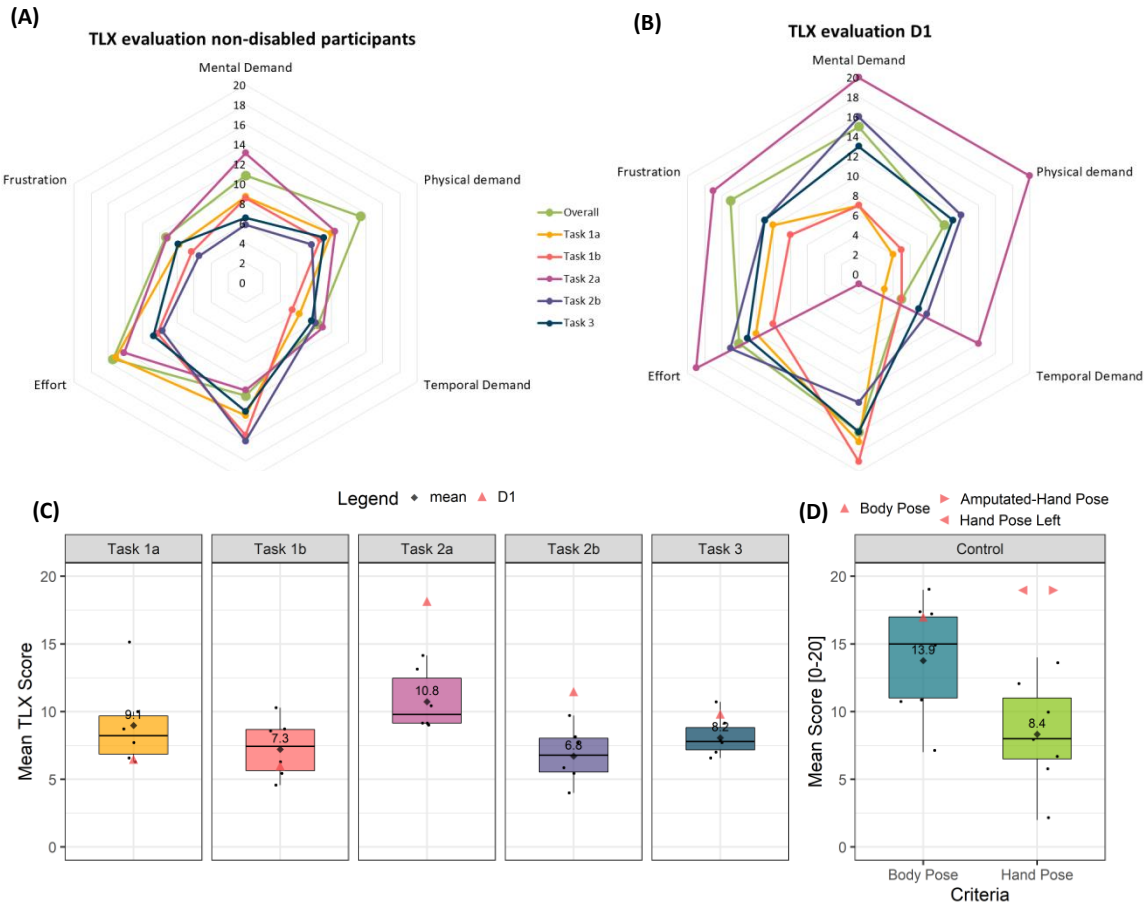

Figure 4. Subjective assessments (based on the NASA TLX evaluation test) for the single-session participants. Subjective scores are between 0 and 20 **(**the lower the better, except for evaluation of Performance and Control). All criteria are based on self-assessment, including 'performance' and 'control'. D2 did not fill the TLX evaluation due to a time limitation. **(A)** Spider plot of the average TLX evaluation on all non-disabled participants for each criterion. **(B)** Spider plot of the TLX evaluation for the disabled participant D1 for each criterion. **(C)** Task-wise average evaluation criteria. For this average, the positive criteria 'performance' was transformed into a negative one by subtracting the evaluated score to the maximum possible (20) in order to get a global negative index. (the lower the better) **(D)** Evaluation of the quality of the body pose control and the hand pose control. (the higher the better)

participants. D1 and D2 respectively needed 4 and 3 updates, including the necessary update for Task 3 as described in Table S3 in the Supplementary Materials.

3.2. Subjective evaluation

Figure 4A shows the outcome of the subjective evaluation based on the NASA TLX questionnaire [27]. Task 2a (unscrewing a bottle) was judged the most complicated one, having the highest scores in terms of mental, physical and temporal demand as well as frustration, the second-highest in terms of effort and the lowest in terms of estimated performance with a total average score of 11.1 out of 20. Task 1a was graded with the highest effort score. The temporal demand of each task of this subjective evaluation qualitatively matches the TCTs found in **Figure 3B** with the exception of Task 2a, which was considered as more time consuming than Task 1b, whereas the mean TCT of the latter is actually slightly higher than the one of the former. As can be seen in **Figure 4C**, both Tasks 1a and 2a were considered more complicated than the tasks which followed them with the same table setup, respectively Tasks 1b and 2b. Quality of control perceived by the participants is shown in **Figure 4C**: out of 20, the body pose control was graded on average at 13.9 while the hand pose control was estimated at 8.4.

Figure 4B shows D1's subjective evaluation. His ratings are comparable to those of all other participants, with the remarkable exception of Task 2a which he rated very difficult on all criteria. Considering the other tasks, overall the mental demand was higher; the temporal demand was judged slightly lower for all tasks compared to the pool of intact participants in **Figure 4A**; the frustration was overall superior, whereas the performance was overall rated similarly higher. When analyzing the mean TLX score of **Figure 4C**, a lower averaged score compared to the pool of intact participants emerges for Tasks 1a and 1b, while the opposite appears for Tasks 2a, 2b and 3. On the other hand, D1 rated control

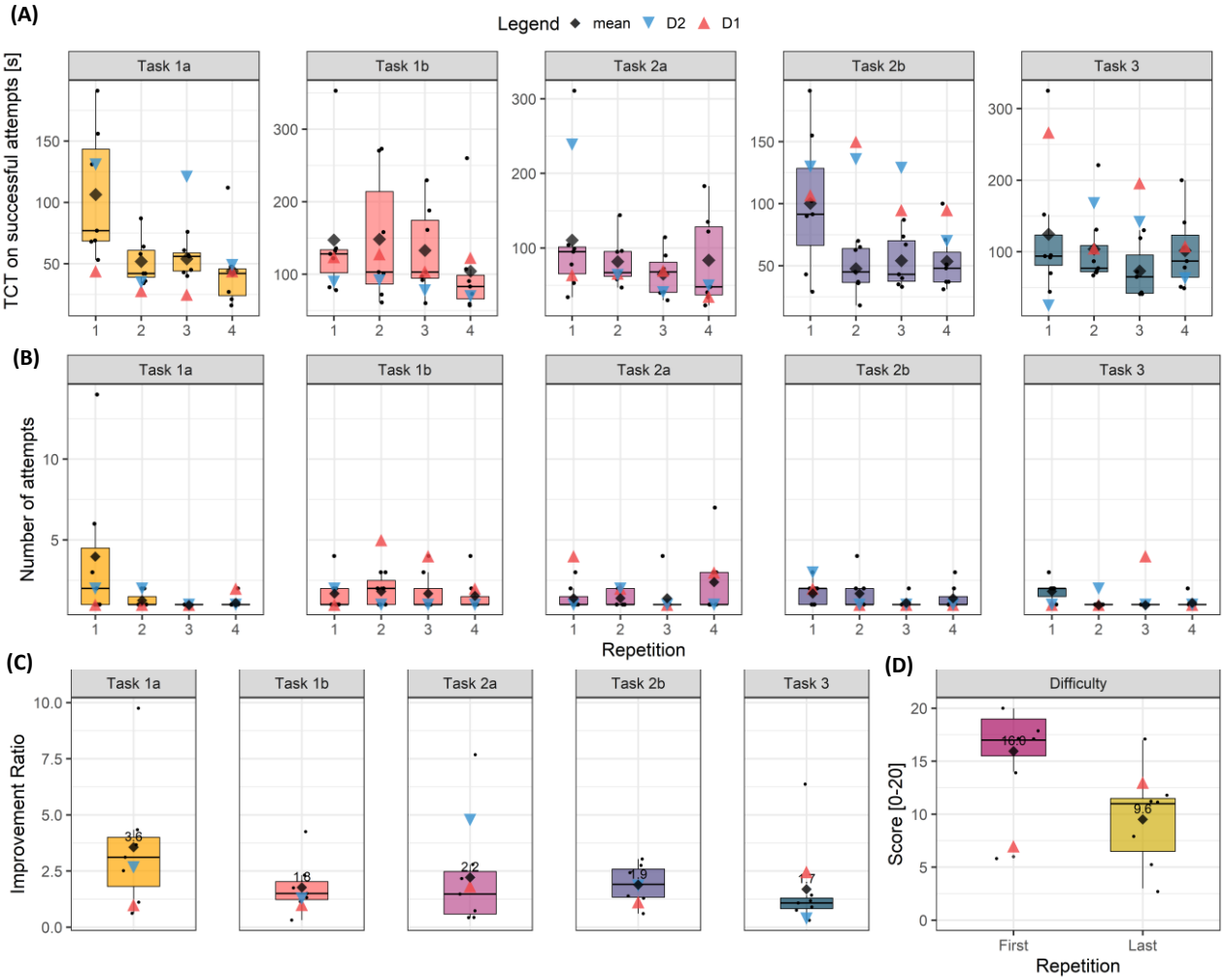

Figure 5. Results of the study on successful attempts for the single-session participants. All criteria are based on self-assessment, including 'performance' and 'control'. D2 did not fill the TLX evaluation due to a time limitation. **(A)** Task-wise TCTs on the successful attempts across repetitions performed by the single-session users (including the disabled ones). **(B)** Task-wise number of attempts per repetition performed by the single-session users. **(C)** Task-wise improvement ratios on the TCTs of the successful attempts between the first and the last repetition for the single-session users (including the disabled ones). (the higher the better) **(D)** Evaluated difficulty on the first and last repetitions for the single-session users and D1 (the lower the better). D2 did not fill the subjective assessment.

(**Figure 4D**) quite in the opposite way with respect to other participants, with a higher rating on the hand pose and a slightly lower one for the body pose. Remarkably, D1 rated similarly control of the left and the right hand. All in all, control scores by D1 are higher (therefore better) than those by non-disabled participants.

3.3. TCTs and number of attempts during single-session experiments

Figure 5 shows the TCTs obtained during single-session experiments, split across single tasks and task repetitions, considering the successful attempts only, and the number of attempts per task and repetition. A decrease in the TCTs while considering each task and the related repetitions is apparent. In all cases, the first repetition has the longest TCTs. While participant D1 had a higher average regarding cumulative TCT on all attempts (293s) for Task 1b, as shown in **Figure 3B**, the averaged TCT for this specific task when considering only the successful attempt (120s) is lower than the average TCT of the pool of participants (133s) as it can be seen in **Figure 5A**. Additionally, D1's TCTs are in line with the non-disabled participants' TCTs, despite being graded with the lowest scores in the TLX evaluation. Considering the data of all single-session participants (with both intact and disabled participants), we performed an LMER analysis, with log(TCT), to normalize the data, as the dependent variable, the repetition and the amputation condition as independent variables, and participants and tasks as random effects to adapt to the different initial skill level of each participant and the different difficulties of the tasks. The analysis showed a significant difference between repetitions 1 and 2 ($p=0.040$), between repetitions 1 and 3 ($p=0.007$), and between repetitions 1 and 4 ($p<0.001$), and no significant difference deriving from the amputation condition.

The number of attempts shown in **Figure 5B**, while also showing a decreasing trend for Task 1a and Task 3, does not follow the same trend for the other tasks. **Figure 5C**, showing the improvement ratio between repetitions 1 and 4 of each task, confirms this statement. The improvement ranged from 3.6 times (Task 1a) to 1.7 times (Task 3), with an average of 2.2 times. A clear improvement is also visible in **Figure 5D** showing that the subjective assessment of difficulty dropped from the first repetition to the last one from 16.0 to 9.6 out of 20.

D1 achieved a very low TCT in Task 1a, therefore his improvement is relatively low in this task. D2 had a higher improvement rate for Task 2a than most of the participants. In the other tasks, both D1 and D2 are in line with the pool of intact participants with the exception of Task 3, in which their improvement rate is higher. The perceived difficulty evaluated in **Figure 5D** by D1 shows an opposite trend compared to the pool, with a higher difficulty during the last repetition than during the first one.

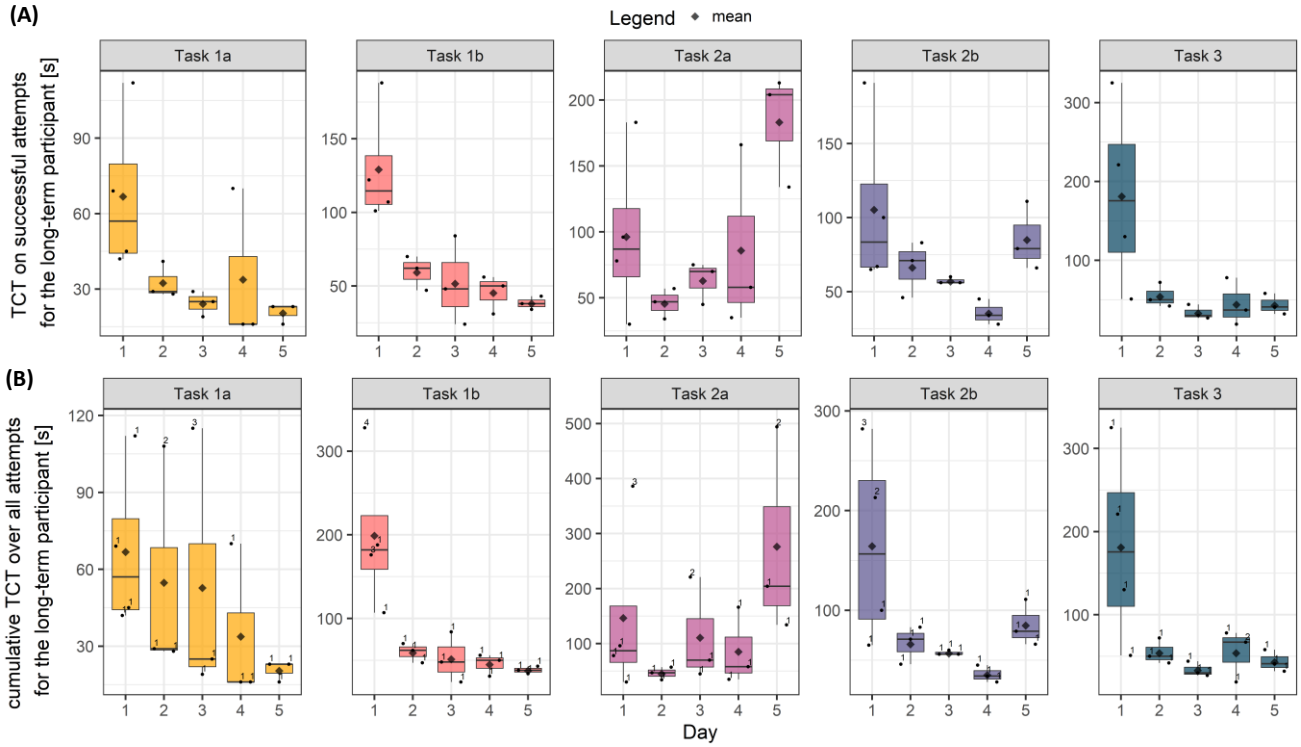

Figure 6. Results of the study for the long-term participant. (A) Task-wise TCTs on the successful attempts performed by the long-term participant across the days. All tasks except Task 2a present a decreasing trend. The points represented in each box plot are placed in the order of the repetition number. **(B)** Task-wise cumulative TCTs over all attempts performed by the long-term participant across the days. All tasks except Task 2a present a decreasing trend. The points represented in each box plot are placed in the order of the repetition number and the number above it indicates the number of attempts.

3.4. TCTs and attempts number during the multi-session experiment

A day-by-day learning effect (decrease in the TCTs on successful attempts), similar to the one previously observed in the single-session users, is apparent in **Figure 6A**, especially for Tasks 1a, 1b and 3. For Task 2b, this decrease is visible over the first 4 days; and on the fifth day, a slight increase can be noted. The tendency over the days for Task 2a is not completely clear. A similar effect is apparent from **Figure 6B**, showing the cumulative TCTs over all attempts. Task 1a shows the highest variance; additionally, the number of attempts between Day 1 and Day 5 is also decreasing with an average of 1.5 attempts on the first day, already decreased to 1.1 on Day 2 maintained until Day 5 with the exception of 1.2 attempts on Day 3. When considering the difference between the TCTs of Day 1 and the other days for all tasks, we notice a strong decrease between Days 1 and 2, Days 1 and 3 and Days 1 and 4 but when considering Day 5, the decrease is not visible for Tasks 2a (being considered as the most difficult task) and 2b.

Figure 7. Results of the NASA TLX test and improvement ratios of the long-term participant. (A) Evaluation of the different TLX criteria over the days for each task and overall. **(B)** Evaluation of the difficulty for the first and last repetitions over the session with a box plot gathering the results over all days. (the lower the easier) **(C)** Evaluation of the quality of the body pose control and the hand pose control over the session with a box plot gathering the results over all days. (the lower the better) **(D)** Task-wise improvement ratios on the TCTs of the successful attempts between the first and the last repetition. One data-point represents the improvement ratio for one day. (the higher the better) **(E)** Improvement ratios averaged over the tasks on the TCTs of the successful attempts between, respectively, Day 1 and Day 2 (RatioD12), Day 1 and Day 5 (RatioD15), and Day 2 and Day 5 (RatioD25). (the higher the better)

Figure 7A, showing the results of the NASA TLX test of the long-term participant, furthermore confirms the effect. While the participant estimated his overall performance at 8/20 on the first session, it rises to 19/20 on the last one. Individual tasks also show a relatively regular growth on this criterion with the exception of Task 2a, which, after a significant increase from 8 to 13 on the second session, seems to decline during the following sessions until finally reaching 12 on the last one. The subjective effort evaluation follows a similar trend with an important increase between the first and second session followed by stabilization. Task 2a's mental demand is relatively high compared to the other tasks and the temporal demand increases over the sessions. Nonetheless, a clear learning curve is visible for all the other tasks as well as for the overall evaluation.

The long-term participant also presents an overall decreasing trend in terms of evaluated difficulty as shown in **Figure 7B**. While the participant evaluated the tasks as being less difficult on the last repetition than on the first one on the first day, it arrives at an equal level for both repetitions on Day 5, indicating a learning effect by the stabilization of the difficulty. Regarding the evaluation of the control (**Figure 7C**), as previously shown in the single-session pool, the body pose control obtains better grades than the hand pose control. Additionally, while the body pose control grading stays relatively stable over the 5 sessions, the hand pose control is increasing over the sessions with a considerably higher increase between Day 1 and Day 2. The improvement ratio of the long-term participant over the sessions shows a similar learning to most tasks as shown in **Figure 7D**. Additionally, as indicated by the improvement ratios over the days (**Figure 7E**), the main part of the learning happened between Day 1 and Day 2 with an improvement ratio of 2.2, while the improvement ratio between Day 2 and 5 was of 1.1. The overall improvement ratio between the first and the last session reached 2.5.

On the first day, 5 updates of the interactive machine learning model were necessary for the long-term participant. This number decreased to 1 for all following days.

3.5. Average speed and travelled path

Both the single-session participants and the long-term participant show an increased hand speed over the repetitions of the different tasks (**Figure 8**). For the single-session participants, all tasks display an increasing trend, except Task 3 (**Figure 8A**). The disabled participants have an average speed (0.071m/s) higher than the non-disabled ones (0.044m/s). Considering the data of all single-session participants (disabled and non-disabled), we performed an LMER analysis, with log(speed), to normalize the data, as the dependent variable, the repetition and the amputation condition as independent variables, and participants and tasks

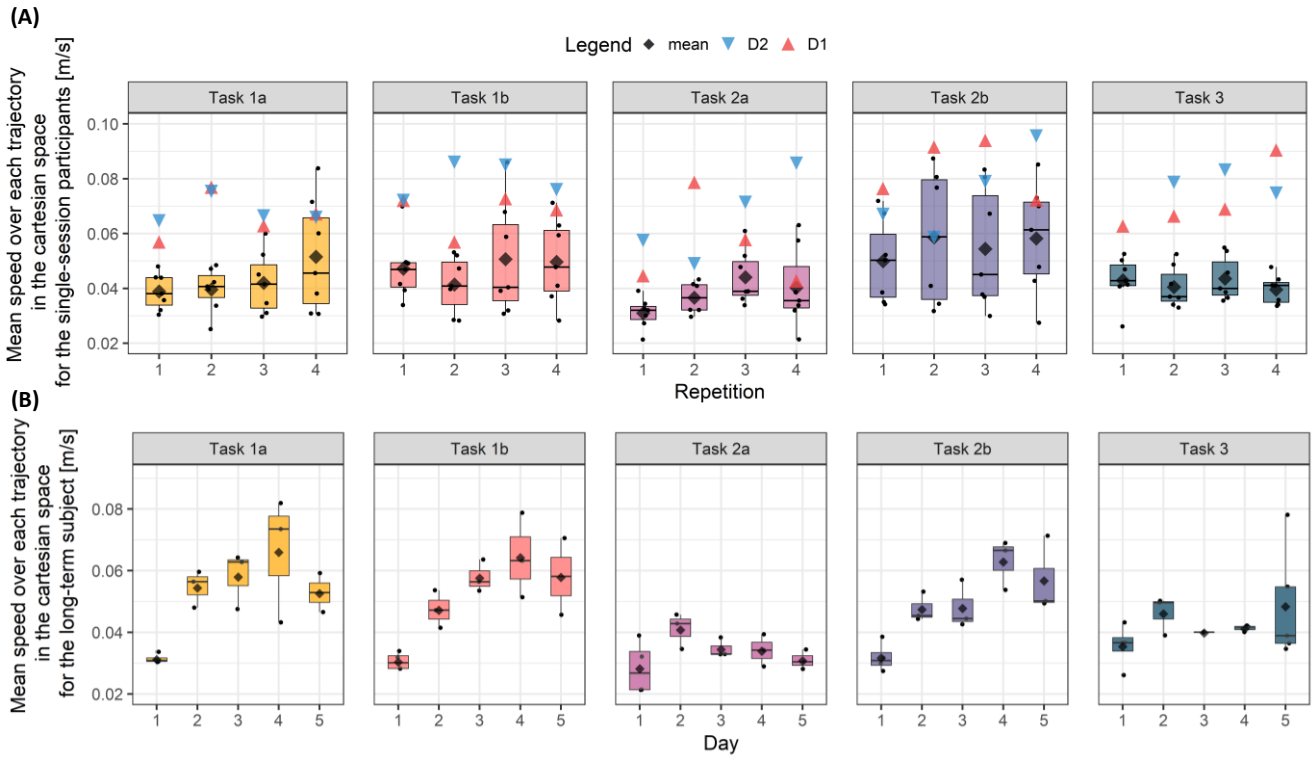

Figure 8. Averaged speed for all participants. The average speed over the trajectories is calculated for the hands of the participants and summed for both hands. **(A)** Task-wise average speed over the trajectories for each repetition for the single-session participants (including the disabled ones) with a generally increasing trend. Outliers of S2, S5 and D2 on respectively, rep. 2 of Task 2b, rep. 2 of Task 2a, and rep.1 of Task 3 were removed due to logging errors. **(B)** Task-wise average speed over the trajectories for each day for the long-term participant with a generally increasing trend. Outliers of the long-term participant on the third repetition of Tasks 1a and 1b of Day 5 were removed due to logging errors.

as random effects. The analysis showed a significant difference between repetitions 1 and 3 (p=0.017) and between repetitions 1 and 4 (p=0.015).

The speed over days (**Figure 8B**) also display a generally increasing trend for all tasks. The trend for Task 2a (evaluated as more difficult) over days is flatter than for the other tasks. On the last day, the long-term participant reached an average speed of 0.053m/s for Tasks 1a, 1b and 2b (compared to the mean of 0.043m/s for intact single-session participants, 0.066m/s for D1, 0.068m/s for D2), and 0.031m/s for the Tasks 2a and 3 (0.042m/s for intact single-session participants, 0.072m/s for D1, 0.079m/s for D2), which require less arm movements.

Additionally, not only the participants gained in speed, but their total travelled path was also reduced over the repetitions and days as shown in **Figure S2** in SM. The cumulated distances over the trajectory of each successful repetition was calculated for each hand and summed together. The total travelled distance of both hands follows a generally decreasing trend over the repetitions for each task.

Considering the data of all single-session participants, we performed an LMER analysis, with log(sumdist), as the dependent variable, the repetition and the amputation condition as independent variables, and participants and tasks as random effects. The analysis showed a significant difference between repetitions 1 and 3 (p=0.035) and between repetitions 1 and 4 (p=0.002).

The hands of the disabled participants travelled distances comparable (albeit higher) to the ones of the non-disabled participants with an average of 6.56m travelled for all tasks over all repetitions for D1 and 7.54m for D2. In comparison, non-disabled participants travelled on average 3.62m. The total distances travelled by the hands of the long-term participant also followed a decreasing trend over the days, except for Tasks 2a and 2b in which the hands travelled longer distances on the last day.

4. Discussion

4.1. Feasibility, TCTs and improvement ratios

The first general remark is that *all participants (disabled or not) were able to complete the 5 tasks*, requesting on average 3 updates of the iML per session; moreover, the disabled participants had overall TCTs comparable to those of non-disabled ones. The tasks were complex bimanual ones requiring fine arm / hand coordination, and involved daily-living non-instrumented objects.

Secondly, *a uniform decreasing trend* in the TCTs was found, with substantially shorter times during the last repetition of each task, in spite of a slight increase in the very last repetition when compared to the previous one, which could be explained by fatigue. From the statistical analysis. A significant difference appeared between repetition 1 and all the other repetitions with no significant effect from the amputation condition. The decreasing trend is consistent across disabled and non-disabled participants and in both the single- and multi-session experiments, and is confirmed by the improvement ratios (2.3 for non-disabled, 1.49 for D1, 2.2 for D2, and 1.54 for multi-session participants). Regarding the multi-session participant, there is a strong decrease of the TCTs between the first and second day but less important between the second and the last days, implying possibly that a large part of the learning happened between Day 1 and Day 2. This is confirmed by the improvement ratios between Day 1 and Day 2 being at 2.2 and the improvement ratios between Day 1 and 5 and Day 2 and 5 being 2.5 and 1.1, respectively.

4.2. Subjective evaluation

4.2.1. TLX Score

This learning effect is further confirmed by the subjective evaluation, with a substantial decrease in the perceived difficulty of 32% between the first and the last repetition for the non-disabled participants. D1 however perceived a higher difficulty for the last repetition, which might be due to the fatigue that could have been increased by two factors in the case of disabled participants, namely the non-intuitive mapping of control patterns inducing a high mental demand (confirmed by the higher scores given overall to the mental demand criterion when compared to non-disabled participants) and the stimulation of usually unused muscle groups causing physical fatigue. This would additionally explain the increasing TCTs of the disabled participants for the last two tasks. This tiredness of the participant could have been further increased by Task 2a, which was considered as the most demanding task, and was the one requiring the highest number of hand-wrist poses to be predicted in the case of disabled subjects. The fatigue induced by such tasks involving precise manipulations would also explain the performance deterioration in the following tasks [36]. The task-wise averaged TLX score would also confirm this hypothesis with a lower (and therefore better) score compared to the non-disabled participants on the first two tasks and a higher one on the last three tasks. Unfortunately, as D2 did not fill the post-experiment subjective form, we could not corroborate this hypothesis with his results.

4.2.2. Hand and body-pose control score

The overall lower grades of the hand pose control when compared to the body pose control are reflecting the fact that the hands were controlled by the prediction of a machine learning algorithm trained on previously registered EMG data while the body pose had a more direct control via the IMUs. Additionally, when looking at the multiple-days experiment, the body-pose control rating remains almost stable over the days while the hand-pose control increases. This could indicate that most of the learning had to be done on the hand-pattern control. *De facto*, this reflects what the experimenters noticed, namely that the participants, being confronted with a

humanoid robot, tended to imitate the hand gesture that they wanted the robotic hand to mimic rather than the ones trained in the initial phase of the experiment. For instance, they actively opened their hand to grasp the ball rather than relaxing their muscles, or made a half-open grasp rather than a closed fist to grasp objects.

On the other hand, D1 rated the control in the opposite way with respect to the non-disabled participants, with a higher rating on the hand pose control and a slightly lower one for the body pose control, which could be determined by the daily use of a 1-DoF prosthesis by the disabled participant as opposed to a 6-DOF one in this experiment. The equally-rated control of the left and right hands by D1 highlights the successful control scheme established for the amputated side with respect to the intact side; this control scheme is further detailed in the Material and Methods section. Finally, the overall higher control scores by D1 compared to non-disabled participants indicates successful usage of the device.

The long-term participant presents the highest improvement ratio in Task 3. The fact that this specific task involved more hand gesture control skills (the pointing gesture being more difficult to reproduce with relation to the trained one) would furthermore confirm that an important part of the learning had to be realized on the hand gesture control.

4.2.3. Particularly challenging task: Task 2a

Task 2a was considered very demanding according to the subjective evaluation of the single-session participants. Its difficulty is confirmed by the evaluation of the long-term participant, the mental demand being considerably higher than the other tasks and the temporal demand even increasing over the sessions. The difficulty of this task can be explained by the high precision required to remove the cap and the vision angle of the subject, which limited the depth perception. The extension of the wrist while maintaining the power grasp did not seem to be a problem for the non-disabled participants but was more complicated for the disabled ones due to the fact that the combined movements depended solely on the prediction of the machine learning algorithm.

4.3. Travelled path and speed of motion

Lastly, given a few exceptions, we found *a uniform decreasing trend in the path travelled by the hands of the participants, together with a similar increasing trend in the speed of motion.* This denotes increased time- and energy-efficiency as the experiments progressed, learning to follow shorter paths with higher speed, thus better controlling the robot. In particular, it indicates that arm movements became more precise over time, and that the subjects became progressively able to avoid most mistakes. Some exceptions can be noticed: the travelled path of Task 3 for the single session participants and Task 2a for the long-term one follows a relatively flat trend compared to the other tasks, which could partially be explained by the fewer hand movements needed in these specific tasks where good hand gesture control and more precise body pose control were required. This could also justify the slower speed that the long-term participant showed for the same two tasks. Additionally, we suppose that the constraints for the pouring of the bottle in Task 2b were not defined strictly enough. This action was performed by shaking the bottle by only some subjects, and this could explain the larger interquartile range shown by the single-session subjects on Task 2b. Additionally, while the specific prediction control of the hands in the case of the disabled participants may have had an influence on their longer travelled path and higher speed, the latter might also be due to the daily experience of using a prosthesis.

4.4. Comparison with the state of the art

The experiment presented in this study is, to the best of our knowledge, unique so far; therefore, the study presents a number of limitations. Firstly, despite the use of standardized performance metrics [37], a proper comparison with any baseline whatsoever is difficult, due to the very peculiar experimental conditions and setup we used. Nonetheless, Herlant et al. [25] have performed similar tasks, also inspired from the CAHAI in a teleoperation setup, involving one robotic arm controlled via a joystick and mode switching. The six participants performed the tasks of unscrewing a jar, pouring water and dialing 911 in an average time of 400s, 460s and 180s respectively, while the average cumulative TCTs for the similar tasks in our study were of 171s, 97s and 115s. Although different objects and instructions were obviously used, the bimanual capability and the intuitive control of our setup would, in all likelihood, be the reason behind the shorter times obtained in our experiment. Although bimanual teleoperation has been widely studied [38, 39, 40, 41, 42, 43], our work was mainly evaluating home tasks, while other bimanual teleoperation experiments focused on field tasks where TCTs, difficulty were also evaluated as well as success rates [44]. The tracking method used is often wired or dependent on external tracking [45, 46], including also the previously published video[2] [47], which has initiated this study (of which initial results were presented in [48]). In this work, we use a wearable, wireless and independent device both for hand movement recognition and upper-body tracking.

4.5. Limitations and future work

Our work is the first one evaluating teleoperation of a bimanual assistive platform by disabled persons. In this case, amputees with two different kinds of amputations were participating in the study. However, we believe that this setup, or a similar one, could eventually be adapted for other kinds of disabilities, such as Parkinson's disease. For people suffering from muscular atrophy, the IMUs in this setup would

[2] https://www.youtube.com/watch?v=M6mQWcLAiko

likely have to be replaced by additional thoughtfully placed sEMG sensors. For instance, in [49], two persons suffering from spinal muscular atrophy (SMA) and equipped with an sEMG-based interface could perform autonomously functional reach and grasp tasks in activities of daily living.

A further limitation of this teleoperation experiment was the viewpoint of the participants with relation to the objects to manipulate: their vision was sometimes occluded by the arm of the robot, thus forcing the participants to take a step forward or backward (as long as the torso stayed aligned, this step was possible without causing an unintended robot motion). This visibility problem is all the more pertinent in a real-world scenario, where it would be common to have the robot placed at a remote location from the user. Valiton et al. [50] have studied this problem in more detail by evaluating camera selection and placement strategies with relation to the time to complete the tasks and the cognitive load. The results are however highly user-dependent, and further studies on the topic are necessary with possible decision support from learned models of camera preference to help the operators. An additional option is to integrate depth perception, which has shown to improve the execution of certain tasks [51], within the visual feedback, which would be feasible in our case by using the 3D cloud of points generated by the robot's cameras and having the user wear a virtual reality headset.

Although embodiment is generally solicited for enhanced teleoperation [52], the higher level of embodiment induced by the headset could also have a counter effect by increasing the problem of mimicking untrained hand gestures that the participants had while performing the tasks. This could be solved in the case of non-disabled users by replacing the prediction-based hand gesture control by a direct mapping of subject-to-robot finger motions using for instance a data-glove[2] [53, 54, 55]. Such data-gloves could be a better alternative to sEMG for non-disabled people to teleoperate such a platform. The complementarity with IMUs if the glove only covers the hand would however remain useful [53] and a comparison study would be interesting with a full data-suit.

At the expense of embodiment, shared control would be another option to evaluate in such a context and it has already been successfully implemented in bimanual humanoid robot manipulation in [56] for non-disabled participants as well as adapted for SMA patients in [57], in which non-disabled participants are involved in a teleoperation experiment of a robotic arm attached to a wheelchair. Additionally, participants could benefit not only from a visual feedback but also from a haptic one, leading towards telepresence rather than teleoperation [58, 59]. For example, a bimanual haptic feedback device has been implemented for teleoperation with non-wireless setups in [60, 44], as well as by the *Shadow Robot Company*[3]. For application to amputees however, a special feedback device should be thought of, e.g. a vibrotactile one [61, 62] or intraneural stimulation [63, 64]. As it is well known in the prosthetic community, feedback is one of the numerous problems still unsolved [2, 5], partly due the lack of space for sensor electronics in the dexterous prostheses currently on the market. These hands have numerous regulations to follow and the size, weight, robustness and electronics integration are problems invariably faced by the manufacturers. There are some notable exceptions involving sometimes targeted muscle reinnervation [65], allowing for instance feedback, multi-DoF wrist (such as in the RIC arm [66] or the Modular Prosthetic Limb [59], only available for trans-humeral amputees so far) or finger abduction/adduction. Yet another problem is the current lack of a 2-DoF active wrist integrated in the multi-dexterous trans-radial prostheses [5]. The presented setup allows the control of these 2 DoFs: flexion/extension by machine learning prediction, and pronation/supination, that no prosthetic companies provides simultaneously to the best of our knowledge. This pronation/supination is added very intuitively as it is simply controlled by the worn IMUs and the user has only to move the arms for the robot to reproduce it. The same is valid for all the additional DoFs of the humanoid platform: as they are controlled from the end-effector position, there is no additional burden to the user and they can possibly allow positions that available prostheses would not. While it needs to be noted that, in most cases, amputees would be able to tackle the task with their own prosthesis as most of our everyday tasks are egocentric, such a setup could come as a complementary help for them when a prosthesis does not bring the required amount of dexterity and complexity, such as with the number of DoFs mentioned above. Of course, the cost of such a platform would need to be taken into consideration as it can vary widely and a dual-arm system could be a viable alternative to a humanoid robot. Moreover, as discussed beforehand, this setup could be adapted to other kind of disabilities in which a prosthesis would not be of help. Notwithstanding the fact that the wearable multimodal sensors presented in this paper could be used when such advanced prostheses, i.e. including a 2-DoF active wrists, will be available (also for trans-radial amputees), the access to teleoperation platforms by disabled persons could open new possibilities of autonomy not available to them as of now, including telework [11].

5. Conclusion

In this study we validated the feasibility of using interactive myocontrol to teleoperate a humanoid robot performing highly complex bimanual tasks, inspired by daily-living activities. Clear learning curves were apparent from the results, demonstrating a decrease in the completion times, an increase in speed, but also a reduction of travelled distance underlining the gain in energy-efficiency for all participants, irrespective of their disability. This setup could potentially be used to teleoperate any other bimanual system in a home

[3] https://www.youtube.com/watch?v=3rZYn62OId8

environment as an assistive platform, and also theoretically in extreme environments in which an operator could teleoperate the robot at very distant locations in order to perform critical tasks.

Appendix

All appendices are attached as supplementary material (stacks.iop.org/BPEX/8/015022/mmedia):

Text. Definition of Task Demand Factors

Figure S1. Setup of the experiment.

Figure S2. Distance travelled by both hands for all participants

Table S1. Participant characteristics.

Table S2. Disability characteristics of the disabled participants.

Table S3. List of task-specific hand poses on which the predictor has to be trained in the case of amputation.

Movie S1. Telemanipulation experiment on a humanoid platform by disabled and non-disabled participants.

Acknowledgements

The authors thank Stephan Haug from the Technical University Munich Statistical Consulting Service TUM|Stat for his help with the statistical analysis, as well as Dr. Aaron Pereira and Dr. Malte Engel for their suggestions on the manuscript.

Funding: This work was partially supported by the German Research Society projects Tact-Hand (DFG Sachbeihilfe CA-1389/1-1) and Deep-Hand (DFG Sachbeihilfe CA-1389/1-2).

Author contributions: Conceptualization MC CC, data curation MS MC CC, formal analysis MC MS, funding acquisition CC MR AA-S, investigation MS BH MC OP, methodology MC CC, project administration CC MR, resources CC MR AA-S, software MS BH OP, supervision MC CC MR AA-S, validation MC CC, visualization MC MS MR, writing – original draft MC CC MS MR BH OP, writing – review & editing MC CC MS BH OP MR AA-S.

Competing interests: The authors declare that they have no competing interests.

Data and materials availability: All data needed to evaluate the conclusions in the paper are present in the manuscript or the Supplementary Materials. Data files are available upon reasonable request.

References

[1] C. Castellini, "Upper Limb Active Prosthetic systems—Overview," in *Wearable Robotics*, Elsevier, 2020, p. 365–376.

[2] B. Peerdeman, D. Boere, H. Witteveen, H. Hermens, S. Stramigioli, H. Rietman, P. Veltink and S. Misra, "Myoelectric forearm prostheses: state of the art from a user-centered perspective.," *Journal of Rehabilitation Research & Development*, vol. 48, no. 6, p. 719–738, 2011.

[3] I. Vujaklija, D. Farina and O. C. Aszmann, "New developments in prosthetic arm systems," *Orthopedic research and reviews*, vol. 8, p. 31–39, 2016.

[4] R. Merletti, M. Aventaggiato, A. Botter, A. Holobar, H. Marateb and T. M. M. Vieira, "Advances in surface EMG: recent progress in detection and processing techniques.," *Critical reviews in biomedical engineering*, vol. 38, p. 305–45, 2010.

[5] C. Castellini, P. Artemiadis, M. Wininger, A. Ajoudani, M. Alimusaj, A. Bicchi, B. Caputo, W. Craelius, S. Dosen, K. Englehart, D. Farina, A. Gijsberts, S. B. Godfrey, L. Hargrove, M. Ison, T. A. Kuiken, M. Marković, P. M. Pilarski, R. Rupp, E. Scheme, M. Markovic, P. M. Pilarski, R. Rupp and E. Scheme, "Proceedings of the first workshop on peripheral machine interfaces: Going beyond traditional surface electromyography," *Frontiers in Neurorobotics*, vol. 8, no. AUG, p. 1–17, 2014.

[6] A. Fougner, E. Scheme, A. D. C. C. Chan, K. Englehart, Ø. Stavdahl and O. Stavdahl, "Resolving the Limb Position Effect in Myoelectric Pattern Recognition," *IEEE Transactions on Neural Systems and Rehabilitation Engineering*, vol. 19, no. 6, p. 644–651, 2011.

[7] A. Fougner, O. Stavdahl, P. J. Kyberd, Y. G. Losier and P. A. Parker, "Control of upper limb prostheses: Terminology and proportional myoelectric controla review," *IEEE Transactions on Neural Systems and Rehabilitation Engineering*, vol. 20, no. 5, p. 663–677, 2012.

[8] N. Jiang, S. Dosen, K.-R. Müller and D. Farina, "Myoelectric Control of Artificial Limbs - Is There a Need to Change Focus?," *IEEE Signal Processing Magazine*, vol. 29, no. 5, p. 148–152, 2012.

[9] U. E. Ogenyi, J. Liu, C. Yang, Z. Ju and H. Liu, *Physical Human–Robot Collaboration: Robotic Systems, Learning Methods, Collaborative Strategies, Sensors, and Actuators*, vol. 51, Institute of Electrical and Electronics Engineers (IEEE), 2021, p. 1888–1901.

[10] C. Cipriani, R. Sassu, M. Controzzi, G. Kanitz and M. C. Carrozza, "Preliminary study on the influence of inertia and weight of the prosthesis on the EMG pattern recognition robustness," in *Myoelectric Controls Symposium (MEC)*, Fredericton, CA, 2011.

[11] K. Takeuchi, Y. Yamazaki and K. Yoshifuji, "Avatar work: Telework for disabled people unable to go outside by using avatar robots," in *Companion of the 2020 ACM/IEEE International Conference on Human-Robot Interaction*, 2020.

[12] M. D. Paskett, N. R. Olsen, J. A. George, D. T. Kluger, M. R. Brinton, T. S. Davis, C. C. Duncan and G. A. Clark, "A Modular Transradial Bypass Socket for Surface Myoelectric Prosthetic Control in Non-Amputees," *IEEE Transactions on Neural Systems and Rehabilitation Engineering*, vol. 27, no. 10, pp. 2070-2076, 2019.

[13] J. M. Hahne, M. A. Schweisfurth, M. Koppe and D. Farina, "Simultaneous control of multiple functions of bionic hand prostheses: Performance and robustness in end users," *Science Robotics,* vol. 3, no. 19, 2018.

[14] I. Strazzulla, M. Nowak, M. Controzzi, C. Cipriani and C. Castellini, "Online bimanual manipulation using surface electromyography and incremental learning," *IEEE Transactions on Neural Systems and Rehabilitation Engineering,* vol. 25, no. 3, p. 227–234, 2016.

[15] T. Degris, P. M. Pilarski and R. S. Sutton, "Model-free reinforcement learning with continuous action in practice," in *IEEE American Control Conference (ACC)*, Montreal, 2012.

[16] M. Nowak, C. Castellini and C. Massironi, "Applying radical constructivism to machine learning: A pilot study in assistive robotics.," *Constructivist Foundations,* vol. 13, no. 2, p. 250–262, 2018.

[17] M. Sierotowicz, M. Connan and C. Castellini, "Human-In-The-Loop Assessment of an Ultralight, Low-Cost Body Posture Tracking Device," *Sensors,* vol. 20, no. 3, p. 890, 2020.

[18] C. S. Green and D. Bavelier, "Exercising your brain: A review of human brain plasticity and training-induced learning.," vol. 23, pp. 692-701.

[19] M. Ison and P. Artemiadis, "Proportional Myoelectric Control of Robots: Muscle Synergy Development Drives Performance Enhancement, Retainment, and Generalization," *IEEE Transactions on Robotics,* vol. 31, p. 259–268, 2015.

[20] M. Ison, I. Vujaklija, B. Whitsell, D. Farina and P. Artemiadis, "High-Density Electromyography and Motor Skill Learning for Robust Long-Term Control of a 7-DoF Robot Arm," *IEEE Transactions on Neural Systems and Rehabilitation,* vol. 24, p. 424–433, 2016.

[21] C. Ott, M. A. Roa, F. Schmidt, W. Friedl, J. Englsberger, R. Burger, A. Werner, A. Dietrich, D. Leidner, B. Henze, O. Eiberger, A. Beyer, B. Bäuml, C. Borst and A. Albu-Schäffer, "Mechanisms and design of DLR humanoid robots," *Humanoid Robotics: A Reference; Goswami, A., Vadakkepat, P., Eds,* p. 1–26, 2016.

[22] L. M. Hermansson, A. G. Fisher, B. Bernspång and A.-C. Eliasson, "Assessment of capacity for myoelectric control: a new Rasch-built measure of prosthetic hand control," *Journal of rehabilitation medicine,* vol. 37, p. 166–71, 2005.

[23] C. Schuster, S. Hahn and T. Ettlin, "Objectively-assessed outcome measures: a translation and cross-cultural adaptation procedure applied to the Chedoke McMaster Arm and Hand Activity Inventory (CAHAI)," *BMC medical research methodology,* vol. 10, p. 1–9, 2010.

[24] S. Barreca, C. Gowland, P. Stratford, M. Huijbregts, J. Griffiths, W. Torresin, M. Dunkley, P. Miller and L. Masters, "Development of the Chedoke Arm and Hand Activity Inventory: theoretical constructs, item generation, and selection," *Topics in stroke rehabilitation,* vol. 11, p. 31–42, 2004.

[25] L. V. Herlant, R. M. Holladay and S. S. Srinivasa, "Assistive teleoperation of robot arms via automatic time-optimal mode switching," in *11th ACM/IEEE International Conference on Human-Robot Interaction (HRI)*, Christchurch, NZ, 2016.

[26] R. Pocius, N. Zamani, H. Culbertson and S. Nikolaidis, "Communicating Robot Goals via Haptic Feedback in Manipulation Tasks," in *Companion of the 2020 ACM/IEEE International Conference on Human-Robot Interaction,* 2020.

[27] S. G. Hart, "NASA Task load Index (TLX). Volume 1.0; Paper and pencil package," 1986.

[28] A. Gijsberts, R. Bohra, D. Sierra González, A. Werner, M. Nowak, B. Caputo, M. A. Roa and C. Castellini, "Stable myoelectric control of a hand prosthesis using non-linear incremental learning," *Frontiers in neurorobotics,* vol. 8, no. 8, 2014.

[29] A. Rahimi and B. Recht, "Uniform approximation of functions with random bases," in *46th Annual Allerton Conference on Communication, Control, and Computing*, Urbana-Champaign, USA, 2008.

[30] M. Connan, R. Kõiva and C. Castellini, "Online natural myocontrol of combined hand and wrist actions using tactile myography and the biomechanics of grasping," *Frontiers in Neurorobotics,* vol. 14, no. 11, pp. 1-16, 2020.

[31] B. Henze, A. Werner, M. A. Roa, G. Garofalo, J. Englsberger and C. Ott, "Control applications of TORO - A Torque controlled humanoid robot," in *IEEE-RAS International Conference on Humanoid Robots*, 2015.

[32] J. Englsberger, A. Werner, C. Ott, B. Henze, M. A. Roa, G. Garofalo, R. Burger, A. Beyer, O. Eiberger, K. Schmid and others, "Overview of the torque-controlled humanoid robot TORO," in *IEEE-RAS International Conference on Humanoid Robots*, Madrid, Spain, 2014.

[33] A. Albu-Schäffer, S. Haddadin, C. Ott, A. Stemmer, T. Wimböck and G. Hirzinger, "The DLR lightweight robot: design and control concepts for robots in human environments," *Industrial Robot: an international journal,* vol. 34, no. 5, p. 376–385, 2007.

[34] B. Henze, M. A. Roa and C. Ott, "Passivity-based whole-body balancing for torque-controlled humanoid robots in multi-contact scenarios," *International Journal of Robotics Research,* vol. 35, no. 12, p. 1522–1543, 2016.

[35] D. Bates, M. Mächler, B. Bolker and S. Walker, *Fitting Linear Mixed-Effects Models using lme4,* 2014.

[36] T.-C. Lin, A. U. Krishnan and Z. Li, "Physical Fatigue Analysis of Assistive Robot Teleoperation via Whole-body Motion Mapping," in *IEEE/RSJ International Conference on Intelligent Robots and Systems (IROS), Macau, China, November 3-8*, 2019.

[37] A. Steinfeld, T. Fong, D. Kaber, M. Lewis, J. Scholtz, A. Schultz and M. Goodrich, "Common metrics for human-robot interaction," in *Proceedings of the 1st ACM SIGCHI/SIGART conference on Human-robot interaction*, 2006.

[38] R. A. Peters, C. L. Campbell, W. J. Bluethmann and E. Huber, "Robonaut task learning through teleoperation," in *IEEE International Conference on Robotics and Automation (Cat. No. 03CH37422)*, Taipei, TW,, 2003.

[39] P. Kremer, T. Wimböck, J. Artigas, S. Schatzle, K. Johl, F. Schmidt, C. Preusche and G. Hirzinger, "Multimodal telepresent control of DLR's Rollin' Justin," in *IEEE*

International Conference on Robotics and Automation, Kobe, JP, 2009.

[40] G. Gorjup, A. Dwivedi, N. Elangovan and M. Liarokapis, "An Intuitive, Affordances Oriented Telemanipulation Framework for a Dual Robot Arm Hand System: On the Execution of Bimanual Tasks," in *IEEE/RSJ International Conference on Intelligent Robots and Systems (IROS)*, Macau, CN, 2019.

[41] K. D. Katyal, C. Y. Brown, S. A. Hechtman, M. P. Para, T. G. McGee, K. C. Wolfe, R. J. Murphy, M. D. M. Kutzer, E. W. Tunstel, M. P. McLoughlin and M. S. Johannes, "Approaches to robotic teleoperation in a disaster scenario: From supervised autonomy to direct control," in *IEEE/RSJ International Conference on Intelligent Robots and Systems*, Chicago, USA, 2014.

[42] P. F. Hokayem and M. W. Spong, "Bilateral teleoperation: An historical survey," *Automatica*, vol. 42, no. 12, pp. 2035-2057, 2006.

[43] D. Sun, Q. Liao and A. Loutfi, "Single Master Bimanual Teleoperation System With Efficient Regulation," *IEEE Transactions on Robotics*, vol. 36, no. 4, pp. 1022-1037, 2020.

[44] T. Klamt, M. Schwarz, C. Lenz, L. Baccelliere, D. Buongiorno, T. Cichon, A. DiGuardo, D. Droeschel, M. Gabardi, M. Kamedula, N. Kashiri, A. Laurenzi, D. Leonardis, L. Muratore, D. Pavlichenko, A. S. Periyasamy, D. Rodriguez, M. Solazzi, A. Frisoli, M. Gustmann, J. Roßmann, U. Süss, N. G. Tsagarakis and S. Behnke, "Remote mobile manipulation with the centauro robot: Full-body telepresence and autonomous operator assistance," *Journal of Field Robotics*, vol. 37, p. 889–919, July 2019.

[45] L. Zhao, Y. Liu, K. Wang, P. Liang and R. Li, "An intuitive human robot interface for tele-operation," in *2016 IEEE International Conference on Real-time Computing and Robotics (RCAR)*, 2016.

[46] C.-Y. Liu, J.-J. Liang, T.-H. S. Li and K.-C. Chang, "Motion Imitation and Augmentation System for a Six Degrees of Freedom Dual-Arm Robot," *IEEE Access*, vol. 7, p. 153986–153998, 2019.

[47] O. Porges, M. Connan, B. Henze, A. Gigli, C. Castellini and M. A. Roa, "A wearable, ultralight interface for bimanual teleoperation of a compliant, whole-body-controlled humanoid robot," in *Proceedings of ICRA-International Conference on Robotics and Automation*, Montreal, CA, 2019.

[48] M. Connan, M. Sierotowicz, B. Henze, O. Porges, A. Albu-Schäffer, M. A. Roa and C. Castellini, "Learning Teleoperation of an Assistive Humanoid Platform by Intact and Upper-Limb Disabled Users," in *Converging Clinical and Engineering Research on Neurorehabilitation IV. ICNR 2020. Biosystems & Biorobotics*, 2020.

[49] A. Hagengruber and J. Vogel, "Functional Tasks Performed by People with Severe Muscular Atrophy Using an sEMG Controlled Robotic Manipulator," in *40th Annual International Conference of the IEEE Engineering in Medicine and Biology Society (EMBC)*, Honolulu, HI, 2018.

[50] A. Valiton and Z. Li, "Perception-Action Coupling in Usage of Telepresence Cameras," in *IEEE International Conference on Robotics and Automation (ICRA)*, Paris, FR, 2020.

[51] M. Mast, Z. Materna, M. Španěl, F. Weisshardt, G. Arbeiter, M. Burmester, P. Smrž and B. Graf, "Semi-Autonomous Domestic Service Robots: Evaluation of a User Interface for Remote Manipulation and Navigation With Focus on Effects of Stereoscopic Display," *International Journal of Social Robotics*, vol. 7, no. 2, pp. 183-202, 2015.

[52] A. Toet, I. A. Kuling, B. N. Krom and J. B. F. van Erp, "Toward Enhanced Teleoperation Through Embodiment," *Front. Robot. AI*, vol. 7, no. 14, pp. 1-22, 2020.

[53] B. Fang, F. Sun, H. Liu, D. Guo, W. Chen and G. Yao, "Robotic teleoperation systems using a wearable multimodal fusion device," *International journal of advanced robotic systems*, vol. 14, no. 4, pp. 1-11, 2017.

[54] H. Hu, X. Gao, J. Li, J. Wang and H. Liu, "Calibrating human hand for teleoperating the HIT/DLR hand," in *IEEE International Conference on Robotics and Automation.*, New Orleans, USA, 2004.

[55] M. V. Liarokapis, P. K. Artemiadis and K. J. Kyriakopoulos, "Telemanipulation with the DLR/HIT II robot hand using a dataglove and a low cost force feedback device," in *21st Mediterranean Conference on Control and Automation*, Chania, GR, 2013.

[56] D. Rakita, B. Mutlu, M. Gleicher and L. M. Hiatt, "Shared control–based bimanual robot manipulation," *Science Robotics*, vol. 4, no. 30, pp. 1-15, 2019.

[57] G. Quere, A. Hagengruber, M. Iskandar, S. Bustamante, D. Leidner and F. Stulp, "Shared Control Templates for Assistive Robotics," in *IEEE International Conference on Robotics and Automation (ICRA)*, Paris, FR, 2020.

[58] P. Salvini, C. Laschi and P. Dario, "From Robotic Tele-Operation to Tele-Presence through Natural Interfaces," in *First IEEE/RAS-EMBS International Conference on Biomedical Robotics and Biomechatronics (BioRob)*, Pisa, IT, 2006.

[59] M. S. Johannes, J. D. Bigelow, J. M. Burck, S. D. Harshbarger, M. V. Kozlowski and T. Van Doren, "An overview of the developmental process for the modular prosthetic limb," *Johns Hopkins APL Technical Digest*, vol. 30, p. 207–216, 2011.

[60] T. Hulin, K. Hertkorn, P. Kremer, S. Schätzle, J. Artigas, M. Sagardia, F. Zacharias and C. Preusche, "The DLR bimanual haptic device with optimized workspace," in *IEEE International Conference on Robotics and Automation*, Shanghai, CN, 2011.

[61] S. Schätzle, T. Ende, T. Wüsthoff and C. Preusche, "VibroTac: An ergonomic and versatile usable vibrotactile feedback device," in *19th International Symposium in Robot and Human Interactive Communication*, 2010.

[62] T. Hulin, P. Kremer, R. Scheibe, S. Schaetzle and C. Preusche, "Evaluating two novel tactile feedback devices," in *4th International Conference on Enactive Interfaces*, Grenoble, France, 2007.

[63] E. D'Anna, G. Valle, A. Mazzoni, I. Strauss, F. Iberite, J. Patton, F. Petrini, S. Raspopovic, G. Granata, R. D. lorio, M. Controzzi, C. Cipriani, T. Stieglitz, P. M. Rossini and S. Micera, "A closed-loop hand prosthesis with simultaneous

intraneural tactile and position feedback," *Science Robotics*, vol. 4, no. 27, p. 1–13, 2019.

[64] F. Clemente, G. Valle, M. Controzzi, I. Strauss, F. Iberite, T. Stieglitz, G. Granata, P. M. Rossini, F. Petrini, S. Micera and C. Cipriani, "Intraneural sensory feedback restores grip force control and motor coordination while using a prosthetic hand," vol. 16, p. 026034, 2019.

[65] J. Cheesborough, L. Smith, T. Kuiken and G. Dumanian, "Targeted Muscle Reinnervation and Advanced Prosthetic Arms," *Seminars in Plastic Surgery,* vol. 29, p. 062–072, 2 2015.

[66] T. Lenzi, J. Lipsey and J. W. Sensinger, "The RIC Arm—a small anthropomorphic transhumeral prosthesis," *IEEE/ASME Transactions on Mechatronics,* vol. 21, p. 2660–2671, 2016.

Appendix B

Further Related Co-Contributed Publications

Table of Contents

B.1 Online tactile myography for simultaneous and proportional hand and wrist myocontrol

Authors Christian Nissler, Mathilde Connan, Markus Nowak and Claudio Castellini

Conference Proceedings of Myoelectric Control Symposium (MEC)

Year 2017

Number of pages 4

Review Peer-reviewed

Abstract Tactile myography is a promising method for dexterous myocontrol. It stems from the idea of detecting muscle activity, and hence the desired actions to be performed by a prosthesis, via the muscle deformations induced by said activity, using a tactile sensor on the stump. Tactile sensing is high-resolution force / pressure sensing; such a technique promises to yield a rich flow of information about an amputated subject's intent.
In this work, we propose a preliminary comparison between tactile myography and surface electromyography enforcing simultaneous and proportional control during an online target-reaching experiment. Six intact subjects and a trans-radial amputee were engaged in repeated hand opening / closing, wrist flexion / extension and wrist pronation / supination, to various degrees of activation. Albeit limited, the results we show indicate that tactile myography enforces an almost uniformly better performance than sEMG.

Author contributions Conceptualization; Methodology; Conduction of experiment; Writing—original draft; Writing—review & editing.

Citation C. Nissler, M. Connan, M. Nowak, and C. Castellini, "Online tactile myography for simultaneous and proportional hand and wrist myocontrol," in *MEC2017 - Myoelectric Control Symposium*, 2017

B.2 Combining electromyography and tactile myography to improve hand and wrist activity detection in prostheses

Authors Noémie Jaquier, Mathilde Connan, Claudio Castellini and Sylvain Calinon

Journal Technologies (MDPI)

Year 2017

Number of pages 16

Review Peer-reviewed

Abstract Despite recent advances in prosthetics and assistive robotics in general, robust simultaneous and proportional control of dexterous prosthetic devices remains an unsolved problem, mainly because of inadequate sensorization. In this paper, we study the application of regression to muscle activity, detected using a flexible tactile sensor recording muscle bulging in the forearm (tactile myography—TMG). The sensor is made of 320 highly sensitive cells organized in an array forming a bracelet. We propose the use of Gaussian process regression to improve the prediction of wrist, hand and single-finger activation, using TMG, surface electromyography (sEMG; the traditional approach in the field), and a combination of the two. We prove the effectiveness of the approach for different levels of activations in a real-time goal-reaching experiment using tactile data. Furthermore, we performed a batch comparison between the different forms of sensorization, using a Gaussian process with different kernel distances.

Author contributions Co-conduction of the first experiment and collection data for the second experiment; Development of the interface used for data acquisition; Experiment Design; Original Draft - Writing.

Videos Video S1: Real-time goal-reaching experiment: hand and wrist movements detection with Gaussian process regression. Video S2: Combining surface electro- and tactile myography for hand and wrist movements detection using Gaussian process regression. https://www.mdpi.com/2227-7080/5/4/64/s1.

Citation N. Jaquier, M. Connan, C. Castellini, and S. Calinon, "Combining electromyography and tactile myography to improve hand and wrist activity detection in prostheses," *Technologies*, vol. 5, no. 4, pp. 1–16, oct 2017, doi: 10.3390/technologies5040064

B.3 A wearable, ultralight interface for bimanual teleoperation of a compliant, whole-body-controlled humanoid robot

Authors Oliver Porges, Mathilde Connan, Bernd Henze, Andrea Gigli, Claudio Castellini and Máximo A. Roa

Conference International Conference on Robotics and Automation (ICRA)

Year 2019

Number of pages 1

Review Peer-reviewed

Abstract Dexterous bimanual manipulation still represents a challenging problem in autonomous robotics. An alternative solution in difficult situations is the teleoperation of a robotic slave. This video presents an unobtrusive bimanual teleoperation setup with very low weight (about 180 grams on each arm), consisting of two Vive virtual reality visual motion trackers and two Myo surface electromyography bracelets. Incremental Ridge Regression with Random Fourier Features is used to robustly enforce multiple hand configurations through simultaneous and proportional control, including power grasp and finger pointing, irrespective of body postural changes and rotation of the wrist; the model can be updated in real time. The video demonstrates complex, dexterous teleoperated bimanual daily-living tasks performed by the torque-controlled humanoid robot TORO. The tasks include unscrewing a lid from a bottle, pouring fluid from the bottle into a pot, grasping, carrying and releasing objects of various sizes, weights and shapes, holding a cordless phone while dialing a number on it, and balancing a ball between the two hands. All tasks require a timely transmission of positions, which are translated into suitable robot torques to let the operator achieve bimanual coordination and high repeatability in the pose of the robotic hands in order to enable fine manipulation.

Author contributions Conceptualization; Methodology; Software Design; Test setup; Writing—original draft; Writing—review & editing.

Video https://www.youtube.com/watch?v=YLEUBFu5qgI

Citation O. Porges, M. Connan, B. Henze, A. Gigli, C. Castellini, and M. A. Roa, "A wearable, ultralight interface for bimanual teleoperation of a compliant, whole-body-controlled humanoid robot," in *Proceedings of ICRA-International Conference on Robotics and Automation*, vol. 35, no. 12, p. 2289, 2019

B.4 VITA — an everyday virtual reality setup for prosthetics and upper-limb rehabilitation

Authors Christian Nissler, Markus Nowak, Mathilde Connan, Stefan Büttner, Jörg Vogel, Ingo Kossyk, Zoltán-Csaba Márton and Claudio Castellini

Journal Journal of neural engineering

Year 2019

Number of pages 11

Review Peer-reviewed

Abstract Objective. Currently, there are some 95 000 people in Europe suffering from upper-limb impairment. Rehabilitation should be undertaken right after the impairment occurs and should be regularly performed thereafter. Moreover, the rehabilitation process should be tailored specifically to both patient and impairment. Approach. To address this, we have developed a low-cost solution that integrates an off-the-shelf virtual reality (VR) setup with our in-house developed arm/hand intent detection system. The resulting system, called VITA, enables an upper-limb disabled person to interact in a virtual world as if her impaired limb were still functional. VITA provides two specific features that we deem essential: proportionality of force control and interactivity between the user and the intent detection core. The usage of relatively cheap commercial components enables VITA to be used in rehabilitation centers, hospitals, or even at home. The applications of VITA range from rehabilitation of patients with musculodegenerative conditions (e.g. ALS), to treating phantom-limb pain of people with limb-loss and prosthetic training. Main results. We present a multifunctional system for upper-limb rehabilitation in VR. We tested the system using a VR implementation of a standard hand assessment tool, the Box and Block test and performed a user study on this standard test with both intact subjects and a prosthetic user. Furthermore, we present additional applications, showing the versatility of the system. Significance. The VITA system shows the applicability of a combination of our experience in intent detection with state-of-the art VR system for rehabilitation purposes. With VITA, we have an easily adaptable experimental tool available, which allows us to quickly and realistically simulate all kind of real-world problems and rehabilitation exercises for upper-limb impaired patients. Additionally, other scenarios such as prostheses simulations and control modes can be quickly implemented and tested.

Author contributions Conceptualization; Methodology; Writing—original draft; Writing—review & editing.

Video https://youtu.be/0nZ5x978kuA

Citation C. Nissler, M. Nowak, M. Connan, S. Büttner, J. Vogel, I. Kossyk, Z.-C. Márton, and C. Castellini, "VITA—An everyday virtual reality setup for prosthetics and upper-limb rehabilitation," *Journal of Neural Engineering*, vol. 16, no. 2, p. 026039, mar 2019, doi: 10.1088/1741-2552/aaf35f

B.5 Human-in-the-loop assessment of an ultralight, low-cost body posture tracking device

Authors Marek Sierotowicz, Mathilde Connan and Claudio Castellini

Journal Sensors (MDPI)

Year 2020

Number of pages 16

Review Peer-reviewed

Abstract In rehabilitation, assistive and space robotics, the capability to track the body posture of a user in real time is highly desirable. In more specific cases, such as teleoperated extra-vehicular activity, prosthetics and home service robotics, the ideal posture-tracking device must also be wearable, light and low-power, while still enforcing the best possible accuracy. Additionally, the device must be targeted at effective human-machine interaction. In this paper, we present and test such a device based upon commercial inertial measurement units: it weighs 575 g in total, lasts up to 10.5 h of continual operation, can be donned and doffed in under a minute and costs less than 290 EUR. We assess the attainable performance in terms of error in an online trajectory-tracking task in Virtual Reality using the device through an experiment involving 10 subjects, showing that an average user can attain a precision of 0.66 cm during a static precision task and 6.33 cm while tracking a moving trajectory, when tested in the full peri-personal space of a user.

Author contributions Conceptualization; Methodology; Supervision; Writing—original draft; Writing—review & editing.

Video https://www.mdpi.com/1424-8220/20/3/890/s1.

Citation M. Sierotowicz, M. Connan, and C. Castellini, "Human-in-the-loop assessment of an ultralight, low-cost body posture tracking device," *Sensors*, vol. 20, no. 3, p. 890, feb 2020, doi: 10.3390/s20030890

B.6 A transradial modular adaptable platform for evaluating prosthetic feedback and control strategies

Authors Ben W. Hallworth, Ahmed W. Shehata, Michael R. Dawson, Florian Sperle, Mathilde Connan, Werner Friedl, Bernhard Vodermayer, Claudio Castellini, Jacqueline S. Hebert and Patrick M. Pilarski

Conference Proceedings of Myoelectric Control Symposium (MEC)

Year 2020

Number of pages 4

Review Peer-reviewed

Abstract Novel multi-modal and closed-loop myoelectric control strategies may yield more robust, capable prostheses which improve quality of life for those affected by upper-limb loss. However, the translation of such systems from an experimental setting towards daily use by persons with limb loss is limited by the cost and complexity of assessing all the possible sensor and feedback configurations. The comparison of different control strategies is further complicated by the use of disparate prosthetic socket and simulated prosthesis designs across experiments. This study aims to address these issues through the development and preliminary assessment of a Modular-Adaptable Prosthetic Platform (MAPP) system for use in experimental control strategy evaluation. The MAPP system is compatible with a variety of commercially available control and feedback devices and can be used in experiments involving participants with either intact or amputated limbs. The modular design enables compatibility with novel devices and quick reconfiguration of components. We compared EMG and FMG data acquired with the MAPP system to a previously characterized transradial simulated prosthesis, using able-bodied subjects. The MAPP was shown to match or exceed the control accuracy achieved using a rigid simulated prosthesis, while providing the added benefits of modularity. This device shows promise as a research tool which can catalyze the deployment of advanced control strategies by enabling comprehensive and standardized assessment of control and feedback strategies.

Author contributions Building of part of the acquisition hardware; advising on the modular hardware building; Writing—original draft; Writing—review.

Citation B. W. Hallworth, A. W. Shehata, M. R. Dawson, F. Sperle, M. Connan, W. Friedl, B. Vodermayer, C. Castellini, J. S. Hebert, and P. M. Pilarski, "A transradial modular adaptable platform for evaluating prosthetic feedback and control strategies," in *MEC-Myoelectric Control Symposium*, pp. 1–4, 2020

B.7 Unobtrusive, natural support control of an adaptive industrial exoskeleton using force myography

Authors Marek Sierotowicz, Donato Brusamento, Benjamin Schirrmeister, Mathilde Connan, Jonas Bornmann, Jose Gonzalez-Vargas and Claudio Castellini

Journal Frontiers in Robotics and AI

Year 2022

Number of pages 14

Review Peer-reviewed

Abstract Repetitive or tiring tasks and movements during manual work can lead to serious musculoskeletal disorders and, consequently, to monetary damage for both the worker and the employer. Among the most common of these tasks is overhead working while operating a heavy tool, such as drilling, painting, and decorating. In such scenarios, it is desirable to provide adaptive support in order to take some of the load off the shoulder joint as needed. However, even to this day, hardly any viable approaches have been tested, which could enable the user to control such assistive devices naturally and in real time. Here, we present and assess the adaptive Paexo Shoulder exoskeleton, an unobtrusive device explicitly designed for this kind of industrial scenario, which can provide a variable amount of support to the shoulders and arms of a user engaged in overhead work. The adaptive Paexo Shoulder exoskeleton is controlled through machine learning applied to force myography. The controller is able to determine the lifted mass and provide the required support in real time. Twelve subjects joined a user study comparing the Paexo driven through this adaptive control to the Paexo locked in a fixed level of support. The results showed that the machine learning algorithm can successfully adapt the level of assistance to the lifted mass. Specifically, adaptive assistance can sensibly reduce the muscle activity's sensitivity to the lifted mass, with an observed relative reduction of up to 31% of the muscular activity observed when lifting 2 kg normalized by the baseline when lifting no mass.

Author contributions Preliminary experiment; Building of parts of the hardware; Collective writing of the manuscript.

Citation M. Sierotowicz, D. Brusamento, B. Schirrmeister, M. Connan, J. Bornmann, J. Gonzalez-Vargas, and C. Castellini, "Unobtrusive, natural support control of an adaptive industrial exoskeleton using force-myography," *Frontiers in Robotics and AI*, vol. 9, p. 223, sep 2022, doi: 10.3389/frobt.2022.919370

B.8 Learning teleoperation of an assistive humanoid platform by intact and upper-limb disabled users

Authors Mathilde Connan, Marek Sierotowicz, Bernd Henze, Oliver Porges, Alin Albu-Schäffer, Máximo A. Roa and Claudio Castellini

Conference Converging Clinical and Engineering Research on Neurorehabilitation IV. ICNR 2020. Biosystems & Robotics

Year 2020

Number of pages 4

Review Peer-reviewed

Abstract With the advent of highly dexterous robotic arms, assistive platforms for home healthcare are gaining increasing attention from the research community. Control of the many degrees of freedom of such platforms, however, must be ensured uniformly, both for non-disabled and disabled users, in order to give them as much autonomy as possible. Nine users, including two upper-limb disabled, were asked to complete highly complex bimanual tasks by teleoperating a humanoid robot with biosignals. The users were equipped with a light and wearable interface consisting of a body tracking device for guiding the torso and arms and two electromyography armbands for controlling the hands by means of interactive machine learning. All users were able to complete the required tasks, and learning curves are visible in completion time metric.

Author contributions Conceptualization; Data Curation; Formal Analysis; Investigation; Methodology; Supervision; Validation; Visualization; Writing-original draft; Writing-review and editing.

Citation M. Connan, M. Sierotowicz, B. Henze, O. Porges, A. Albu-Schäffer, M. A. Roa, and C. Castellini, "Learning teleoperation of an assistive humanoid platform by intact and upper-limb disabled users," in *Converging Clinical and Engineering Research on Neurorehabilitation IV. ICNR 2020. Biosystems & Biorobotics*, vol. 28, pp. 165–169, Springer. Springer International Publishing, oct 2020, doi: 10.1007/978-3-030-70316-5_27

Appendix C

Copyrights

Frontiers Copyright Statement

Frontiers publishes its own journals (referred to here as Frontiers Journals) and journals owned by third parties (referred to here as Hosted Journals). When we refer to Journals, we include both Frontiers Journals and Hosted Journals.

In this Copyright Statement, Websites (with a capitalised W) refers to all Frontiers websites, including those of Hosted Journals. An Owner means Frontiers as owner of all Frontiers Journals, or the respective owner of a Hosted Journal.

All content included on these Websites (including Loop), such as text, graphics, logos, button icons, images, video/audio clips, downloads, data compilations and software, is the property of the person or entity who or which owned it prior to submission to Frontiers or to a Hosted Journal. If not owned by Frontiers or an Owner of a Hosted Journal, it is licensed to Frontiers Media SA ("Frontiers"), such Owner or its or their licensees and/or subcontractors.

The ownership of copyright in the text of individual articles (including research articles, opinion articles, book reviews, conference proceedings and abstracts) is not affected by its submission to or publication by Frontiers, whether for itself or for a Hosted Journal. Frontiers benefits from a general licence over all content submitted. Hosted Journal Owners benefit from a general licence over all content submitted to their respective Hosted Journals. Frontiers, Hosted Journal Owners and all their users benefit from a Creative Commons CC-BY licence over all content, as specified below.

Images and graphics not forming part of user-contributed materials are the property of or are licensed to Frontiers and may not be downloaded or copied without Frontiers' explicit and specific permission or in accordance with any specific copyright notice attached to that material.

IOP Publishing, Ltd Terms and Conditions

These special terms and conditions are in addition to the standard terms and conditions for CCC's Republication Service and, together with those standard terms and conditions, govern the use of the Works. As the User you will make all reasonable efforts to contact the author(s) of the article which the Work is to be reused from, to seek consent for your intended use. Contacting one author who is acting expressly as authorised agent for their coauthor(s) is acceptable. User will reproduce the following wording prominently alongside the Work: the source of the Work, including author, article title, title of journal, volume number, issue number (if relevant), page range (or first page if this is the only information available) and date of first publication; and a link back to the article (via DOI); and if practicable, and IN ALL CASES for new works published under any of the Creative Commons licences, the words "© IOP Publishing. Reproduced with permission. All rights reserved" Without the express permission of the author(s) and the Rightsholder of the article from which the Work is to be reused, User shall not use it in anyway which, in the opinion of the Rightsholder, could: (i) distort or alter the author(s)' original intention(s) and meaning; (ii) be prejudicial to the honour or reputation of the author(s); and/or (iii) imply endorsement by the author(s) and/or the Rightsholder. This licence does not apply to any article which is credited to another source and which does not have the copyright line '© IOP Publishing Ltd'. User must check the copyright line of the article from which the Work is to be reused to check that IOP Publishing Ltd has all the necessary rights to be able to grant permission. User is solely responsible for identifying and obtaining separate licences and permissions from the copyright owner for reuse of any such third party material/figures which the Rightsholder is not the copyright owner of. The Rightsholder shall not reimburse any fees which User pays for a republication license for such third party content. This licence does not apply to any material/figure which is credited to another source in the Rightsholder's publication or has been obtained from a third party. User must check the Version of Record of the article from which the Work is to be reused, to check whether any of the material in the Work is third party material. Third party citations and/or copyright notices and/or permissions statements may not be included in any other version of the article from which the Work is to be reused and so cannot be relied upon by the User. User is solely responsible for identifying and obtaining separate licences and permissions from the copyright owner for reuse of any such third party material/figures where the Rightsholder is not the copyright owner. The Rightsholder shall not reimburse any fees which User pays for a republication license for such third party content. User and CCC acknowledge that the Rightsholder may, from time to time, make changes or additions to these special terms and conditions without express notification, provided that these shall not apply to permissions already secured and paid for by User prior to such change or addition. User acknowledges that the Rightsholder (which includes companies within its group and third parties for whom it publishes its titles) may make use of personal data collected through the service in the course of their business. If User is the author of the Work, User may automatically have the right to reuse it under the rights granted back when User transferred the copyright

Copyrights MEC - Myoelectric Control Symposium